The role of the KDO8PS quaternary structure

A thesis submitted in partial fulfilment
of the requirements for the degree
of
Doctor of Philosophy in Biochemistry
in the Department of Chemistry
by Michael Weusten

March 2021

Abstract

The enzyme 3-deoxy-D-*manno*-octulosonate 8-phosphate synthase (KDO8PS) catalyses the irreversible aldol-like condensation between the five-carbon phosphorylated aldose D-arabinose 5-phosphate (A5P), the three-carbon ester phosphoenolpyruvate (PEP) and water. This is the first committed step in the biosynthesis of 3-deoxy-D-*manno*-octulosonate (KDO), an essential lipopolysaccharide component of all Gram-negative bacteria and plants. KDO8PS is evolutionarily related to the enzyme 3-deoxy-D-*arabino*-heptulosonate 7-phosphate synthase (DAH7PS), which catalyses a similar aldol-like condensation concerning the four-carbon phosphorylated aldose D-erythrose 4-phosphate, PEP and water, in the first step of the shikimate pathway to aromatic compounds in microorganisms and plants. While the family of KDO8PS comprises both metal-independent and metal-dependent enzymes, all DAH7PS are metal-dependent enzymes.

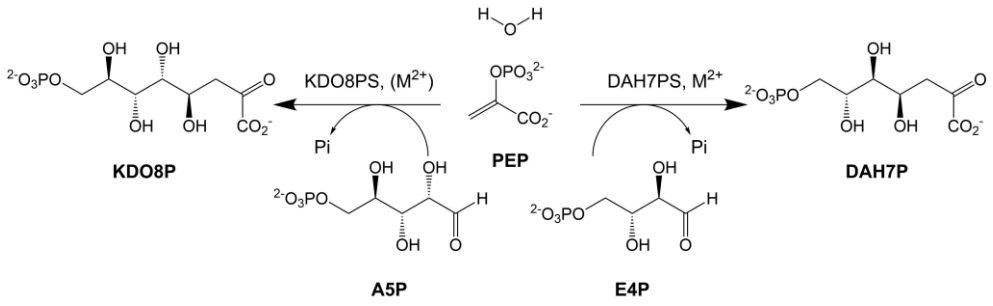

DAH7PS can be categorised into type Iα, Iβ or II enzymes depending on what sequence additions are present, as these additional parts of the enzyme are also responsible for the feedback inhibition of DAH7PS. KDO8PS are suggested to have a common Iβ DAH7PS-like ancestor, with the metal-dependency lost later in time. KDO8PS can be categorised into metal-dependent bacterial, metal-independent bacterial and plant enzymes. All KDO8PS have the quaternary structure of a tetramer, with one plant KDO8PS also reported to be partially dimeric. The KDO8PS tetramer is comprised of the A-C tetramer interface and A-B tetramer interface. Most type Iβ DAH7PS have the quaternary structure of a tetramer, with only those with a C-terminal chorismate mutase domain able to form a unique dimer. The Iβ DAH7PS tetramer is comprised of the A-B tetramer interface and A-C tetramer interface. Little is understood about how role of the quaternary structure may change between metal-dependent bacterial, metal-independent bacterial and plant KDO8PS, and how it relates to the role of the quaternary structure in DAH7PS. This thesis describes the functional and structural studies of KDO8PS and DAH7PS, using the metal-independent bacterial KDO8PS from *Neisseria meningitidis,* the metal-dependent bacterial KDO8PS from *Chlorobium tepidum* the plant KDO8PS from *Chlorela variabilis*, and the type Iβ DAH7PS from *Pyrococcus furiousus*.

Chapter 2 investigates the role of a conserved Asp and Pro in the PEP binding pocket of KDO8PS. In DAH7PS the residues are conserved as a Glu and Gly. Mutational analysis found that in KDO8PS the Pro residue appears to be important for the formation of the A-C tetramer interface. Mutating this Asp and Pro in KDO8PS to Glu and Gly respectively was accommodated by KDO8PS but it was found the changes could potentially be optimised by coupling the change with mutation to other conserved differences.

The work described in Chapter 3 investigates the role of the quaternary structure in the metal-independent *N. meningitidis* KDO8PS. Individual residues of the A-C tetramer interface and A-B tetramer interface were mutated to destabilise the tetramer interfaces. It was found that the β2α2 loop interactions are not significant in the formation of the A-C tetramer interface. The β6α6 and β4α4 loop interactions were significant in the formation of the A-C tetramer interface, as mutation on these loops destabilised the A-C tetramer interface. The A-C tetramer interface was indicated to play an important role in enzyme catalysis and protein stability of metal-independent bacterial KDO8PS. The A-B tetramer interface was suggested to be essential for protein stability at the cost of greater catalytic activity in metal-independent bacterial KDO8PS, as mutation produced either insoluble protein or a more active tetramer.

The role of the quaternary structure in the type Iβ *P. furiousus* DAH7PS is probed in Chapter 4. Individual residues of the A-B tetramer interface and A-C tetramer interface were mutated to destabilise the tetramer interfaces. It was found that one mutation on the A-C tetramer interface destabilised both tetramer interfaces. As the DAH7PS monomer produced was catalytically inactive, the functional unit of DAH7PS is unlikely to be the monomer. The mutation identified that the β6α6 loop interactions were significant in the formation of the A-B tetramer interface. An A-B tetramer interface interaction between a Gln and Arg residue was indicated to be the source of E4P and PEP stabilisation with and without Cd^{2+} in DAH7PS.

In Chapter 5 a metal-dependent *C. tepidum* (*Cte*) KDO8PS and plant *C. variabilis* (*Cvr*) KDO8PS are identified for tetramer interface destabilisation experiments. The complete *Cte*KDO8PS characterisation is achieved and is

found to have similar properties to other characterised KDO8PS. *Cvr*KDO8PS was found to have a unique five residue extension on the β6α6 loop not seen in any other KDO8PS sequence.

Lastly, in Chapter 6 all the chapter results are reviewed, and ideas are discussed for advancing the research presented in this thesis.

Acknowledgements

I am extremely grateful to my supervisor Emily Parker, her steadfast and enthusiastic nature helping me through the good times and the hard times working in the lab and writing this thesis. I would not have managed to get this far without her contributions, which I sincerely appreciate. For the rest of my life, I will look back to this time with great fondness.

I am also grateful to my cosupervisor Renwick Dobson. His advice and constructive criticism during my writing was of great help.

Thank you to all the past and present members of the Parker research group, whose comradery never wavered. Special thanks especially to Gerd Mittelstädt, who provided helpful instruction during my introduction into the lab. Thanks to Tim Allison whose research into KDO8PS, and Ali Nazmi whose research into DAH7PS, is built upon in this thesis. Many thanks to Leyla Bustamante, Nicky Blackmore, Dmitri Joseph, Tammie Cookson, Emma Livingstone, Logan Heyes, Oliver Sterritt and Yu Bai for helpful advice on parts of my thesis throughout the years. Thanks as well to Michael ‘1.0’ Hunter, for his helpful advice on presentations as well as introducing me to a lifelong addiction of Magic: the Gathering.

Thank you to the University of Canterbury for my Ngata Centenary Doctoral Scholarship, whose financial assistance was of great reassurance. Thank you to the Biomolecular Interaction Centre, New Zealand Institute of Chemistry and New Zealand Society of Biochemistry and Molecular Biology for providing access to resources necessary for this thesis to be accomplished. Thank you as well to the New Zealand Synchrotron Group for funding access to the Australian Synchrotron.

Thank you to my family, their support at home allowing me to focus on this thesis.

Lastly, thanks should go out to Ryu Toyama, Tyler Clarke and Mohamad Othman, for the enjoyable conversations during our shared time in the Parker research group.

Contents

Abbreviations

A5P	D-arabinose 5-phosphate.
***Aae*KDO8PS**	*Aquifex aeolicus* KDO8PS.
AEC	anion-exchange chromatography.
***Afe*KDO8PS**	*Acidithiobacillus ferrooxidans* KDO8PS.
***Apy*KDO8PS**	*Aquifex pyrophilus* KDO8PS.
***Ath*KDO8PS**	*Arabidopsis thaliana* KDO8PS.
AUC	analytical ultracentrifugation.
***Bps*KDO8PS**	*Burkholderia pseudomallei* KDO8PS.
BTP	bis[tris(hydroxymethyl)methylamino]propane.
CD	circular dichroism.
CEC	cation-exchange chromatography.
***Cju*KDO8PS**	*Campylobacter jejuni* KDO8PS
CMP	cytidine monophosphate.
***Cte*KDO8PS**	*Chlorobium tepidum* KDO8PS.
CTP	cytidine triphosphate.
***Cvr*KDO8PS**	*Chlorela variabilis* KDO8PS.
DAH7P	3-deoxy-D-*arabino*-heptulosonate 7-phosphate.
DAH7PS	3-Deoxy-D-*arabino*-heptulosonate 7-phosphate synthase.
DNA	deoxyribonucleic acid.

DSF	differential scanning fluorimetry.
DTT	dithiothreitol.
E4P	d-erythrose 4-phosphate.
***Eco*KDO8PS**	*Escherichia coli* KDO8PS.
EDTA	Ethylenediaminetetraacetic acid.
ESI-MS	time-resolved electrospray ionization mass spectrometry.
GALA	galacturonic acid.
HEPES	4-(2-hydroxyethyl)-1-piperazineethanesulfonic acid.
HG	homogalacturonan.
HIC	hydrophobic-interaction chromatography.
***Hpy*KDO8PS**	*Helicobacter pylori* KDO8PS.
IPTG	isopropyl β-d-1-thiogalactopyranoside.
KDO	3-deoxy-D-*manno*-octulosonate.
KDO8P	3-deoxy-D-*manno*-octulosonate 8-phosphate.
KDO8PS	3-deoxy-D-*manno*-octulosonate 8-phosphate synthase.
LB	lysogeny broth.
LPS	lipopolysaccharide.
MWCO	molecular weight cut-off.
***Nme*DAH7PS**	*Neisseria meningitidis* DAH7PS.
***Nme*KDO8PS**	*Neisseria meningitidis* KDO8PS.
NMR	nuclear magnetic resonance.
***Olu*KDO8PS**	*Ostreococcus lucimarinus* KDO8PS.
PCR	polymerase chain reaction.
PDB	Protein Data Bank**.**

***Pe*KDO8PS**	*Phyllostachys edulis* KDO8PS.
PEP	phosphoenolpyruvate.
***Pfu*DAH7PS**	*Pyrococcus furiosus* DAH7PS.
***Pni*DAH7PS**	*Prevotella nigrescens* DAH7PS.
RG-I	rhamnogalacturonan I.
RG-II	rhamnogalacturonan II.
RMSD	root-mean-square deviation.
Ru5P	ribulose 5-phosphate.
SDS-PAGE	sodium dodecyl sulfate polyacrylamide gel electrophoresis.
SEC	size-exclusion chromatography.
SOC	super optimal broth with catabolite repression.
***Sty*KDO8PS**	*Salmonella typhimurium* KDO8PS.
TAE	Tris-acetate-EDTA.
TIM	triose phosphate isomerase.
***Tma*DAH7PS**	*Thermotoga maritima* DAH7PS.

Index of figures

Index of tables

Chapter 1

Introduction

1.1 Cell wall biosynthesis

1.1.1 The Gram-negative bacteria cell wall

Gram-negative bacteria have a layered exterior comprised of an inner cell plasma membrane, surrounded by a cell wall of a peptidoglycan layer which is surrounded by an outer lipid membrane. The outer lipid membrane contains various phospholipids in the interior leaflet, and various polysaccharides on the exterior leaflet.[87] The outer lipid membrane combined with the exterior polysaccharides is known as the lipopolysaccharide (LPS) or endotoxin, and is recognised to be involved in the pathogenicity of various Gram-negative bacteria.[58, 96, 97, 102]

The composition of the endotoxin varies between species and strains, however key regions remain conserved in the majority of Gram-negative bacteria. The endotoxin is comprised of three regions: the lipid A part, a core oligosaccharide region and an O-antigen region (Figure 1.1).

The O-antigen region composition varies drastically; there are 170 different O-antigen structures produced by *Escherichia coli* serotypes alone,[91] which determine the antigenic specificity of bacterial strains. The core oligosaccharide region is comprised of an inner and outer core. While the outer core composition is variable, the inner core has one to three 3-deoxy-D-*manno*-octulosonate (KDO) molecules generally present (Figure 1.2, overleaf).

Loss of these conserved KDO molecules in the inner core oligosaccharide has shown to have a deleterious effect for Gram-negative bacteria: attenuating bacterial cell growth,[43, 48, 68, 78, 93-95] increasing sensitivity to antibiotics, destabilising substances,[43, 78, 89] human sera[78] and in some cases cause cell death.[43, 48, 95] This occurs because without KDO, the Lipid A precursor (IV_A) cannot be built upon by the outer core and O-antigen sugars.

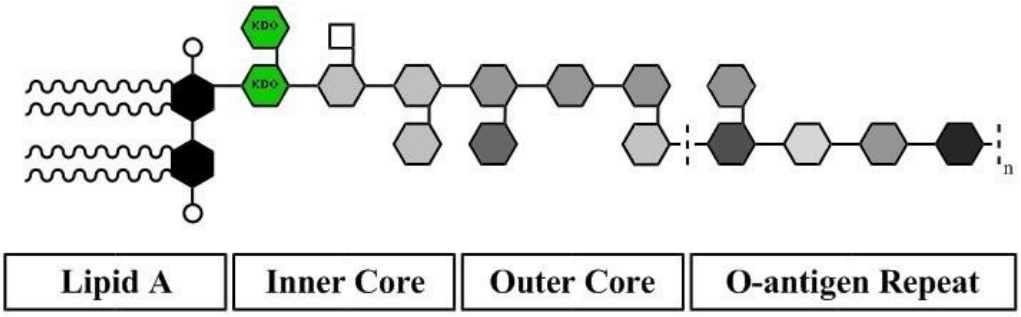

Figure 1.1: General schematic structure of bacterial lipopolysaccharide. The KDO molecules are coloured green. The number of substituents in each section may vary in number, such as the KDO molecules, sugar and phosphoryl residues. Figure recreated from Cipolla *et al*.[20]

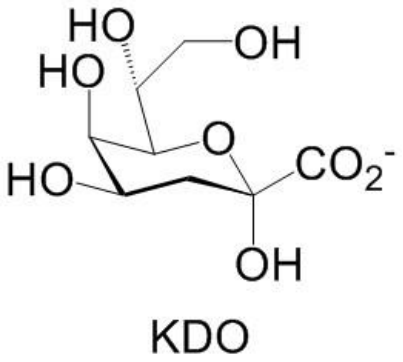

Figure 1.2: Structure of KDO.

These sections aid in bacterial virulence, protecting bacteria from antibiotics and host immune responses. The indispensable role of KDO in cell viability and toxicity, as well as the fact that only bacteria and plants contain the KDO biosynthetic pathway, make this biosynthetic pathway a potential target for antibacterial drug design. Inhibition of this pathway would provide a new class of antibacterial antibiotics.[9, 18, 88, 100]

1.1.2 The plant cell wall

Plants have an exterior comprised of a primary cell membrane, surrounded by a secondary cell wall (primarily made of cellulose), surrounded by a coating known as the middle lamella, which forms a binding interface between neighbouring plant cells. The middle lamella is comprised primarily of heteropolysaccharide pectin.

The composition of the pectin polysaccharides are generally grouped into three main types: the homogalacturonan (HG), rhamnogalacturonan I (RG-I), and rhamnogalacturonan II (RG-II).[8] Ten percent of pectin polysaccharides

are comprised of RG-II, which is largely conserved in plants.[114] RG-II is the only main type of pectin polysaccharide to contain a KDO molecule.[99, 137]

RG-II is comprised of a main chain of at least eight linked galacturonic acids (GALA), with four distinct side chains containing a total of thirteen other saccharides (Figure 1.3).[114] One of the side chains contain a KDO molecule linked to the homopolysaccharide backbone.

KDO is an indispensable component of RG-II, essential for the cell wall integrity of rapidly growing tissues. Loss of the KDO molecule has been shown to have a deleterious effect in pollen grains being unable to develop pollen tubes, thus failing to fertilise.[28]

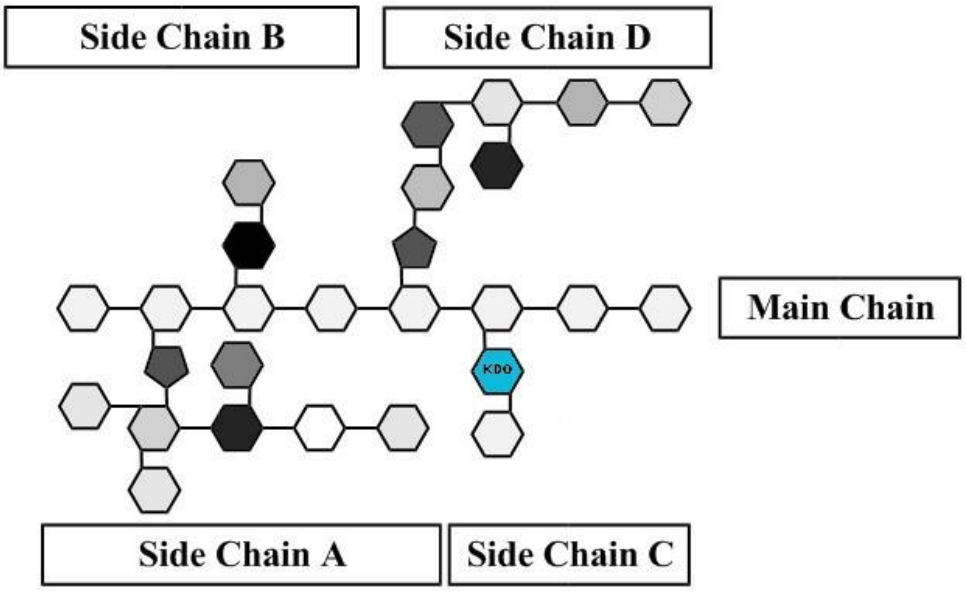

Figure 1.3: General schematic structure of plant rhamnogalacturonan II. The KDO moiety is coloured blue. Also show are various pentose and hexose sugars. Figure recreated from Smyth *et al*.[114]

1.1.3 LPS-KDO and RG-II-KDO biosynthetic pathway

The biosynthesis of KDO is identical in Gram-negative bacteria and plants (Figure 1.4, overleaf).[114] The biosynthesis begins with ribulose 5-phosphate (Ru5P), an end product of the pentose phosphate pathway, as well as an intermediate in the Calvin cycle. Ru5P is isomerised to form aldose D-arabinose 5-phosphate (A5P) by the enzyme A5P isomerase (EC 5.3.1.13). Subsequently, A5P is condensed with phosphoenolpyruvate (PEP) and water to form 3-deoxy-D-*manno*-octulosonate 8-phosphate (KDO8P) by the enzyme 3-deoxy-D-*manno*-octulosonate 8-phosphate synthase (KDO8PS) (EC 2.5.1.55). This is an irreversible step and is the first committed step toward the formation of KDO. KDO8P is then dephosphorylated to form KDO by the enzyme KDO8P phosphatase (EC 3.1.3.45). KDO is then coupled with cytidine triphosphate (CTP) to form cytidine monophosphate (CMP)-KDO by the enzyme CMP-KDO synthetase. This point is where the bacterial LPS-KDO and plant RG-II-KDO biosynthesis pathways diverge.[114]

In the LPS-KDO biosynthesis pathway, the CMP-KDO is transferred to the acceptor lipid IV_A by the enzyme KDO transferase. Subsequently, laurate and myristate are added to the acceptor lipid IV_A, producing the completed KDO_2-Lipid A (Figure 1.4). In the RG-II biosynthesis pathway, the final steps for the formation of RG-II are still unknown.[122] The CMP-KDO is proposed to be transferred to the galacturonic acid backbone by a couple of putative glycosyltransferases (Figure 1.4).[122]

This thesis investigates the enzyme KDO8PS, responsible for catalysing the first committed step in the synthesis of the metabolite KDO.

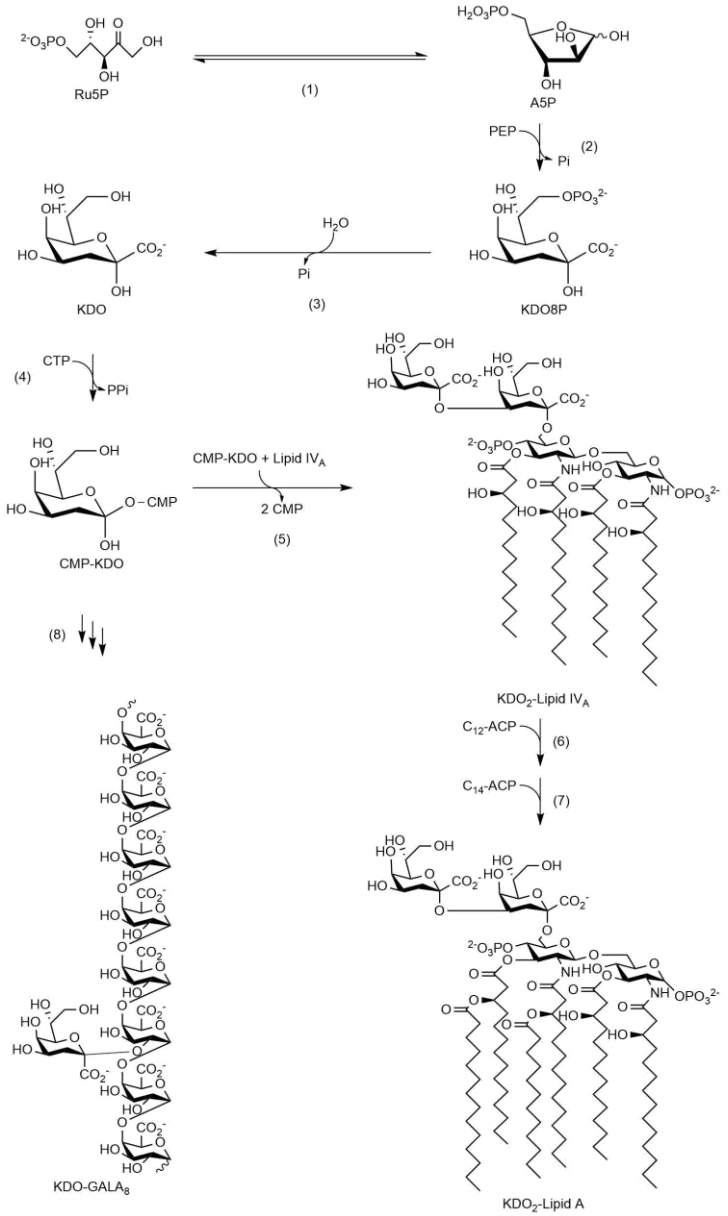

Figure 1.4: The biosynthetic pathway of KDO, the bacterial KDO_2-Lipid A, and the plant KDO-$GALA_8$. Involved in the biosynthesis of KDO are the enzymes (1) A5P isomerase, (2) KDO8PS, (3) KDO8P phosphatase and (4) CMP-KDO synthetase. In bacteria, the KDO_2-Lipid A biosynthesis is continued by (5) KDO transferase, followed by the addition of the acyl chains (6) laurate and (7) myristate. In plants, the (8) enzymes used to attach the KDO molecule to the $GALA_8$ main chain are still unknown. Figure modified from Meredith *et al.*[81]

As the KDO biosynthesis pathway is important to the growth of Gram-negative bacteria and plants, the KDO8PS gene is strongly growth regulated, with increased gene expression in newly divided cells,[27, 115] and decreased expression in growth adverse conditions.[135] The remainder of this introductory chapter focuses on the reaction, structure and function of KDO8PS, and how these features compare to a closely related enzyme.

1.2 KDO8PS catalysed reaction

KDO8PS enzymes that have been purified and characterised in the past derive from a variety of sources, including *Escherichia coli*,[69, 92] *Salmonella typhimurium*,[95, 120] *Neisseria gonorrhoeae*,[116, 134] *Aquifex aeolicus*,[36, 37] *Helicobacter pylori*,[66] *Aquifex pyrophilus*,[110] *Arabidopsis thaliana*,[131, 138] *Neisseria meningitidis*,[2] *Acidithiobacillus ferrooxidans*,[6] *Campylobacter jejuni*[45] and *Phyllostachys edulis*.[140]

Each KDO8PS can be categorised into two groups, depending on the requirement of a metal ion for catalytic activity.[16] Bacterial KDO8PS proteins can be either metal-dependent or metal-independent, whereas all plant KDO8PS proteins are metal-independent.[16]

The KDO8PS catalysed reaction is the irreversible aldol-like condensation of five-carbon phosphorylated aldose A5P with the three-carbon phosphorylated PEP and water (Figure 1.5, overleaf). The C3 of PEP attacks the C1 of A5P, whereas a water molecule attacks the C2 of PEP.

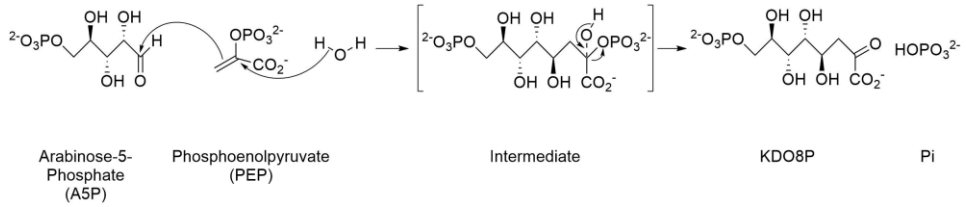

Figure 1.5: The KDO8PS catalysed reaction between PEP and A5P.

An intermediate species is produced which subsequently releases the phosphate derived from PEP, to yield the eight-carbon sugar KDO8P and inorganic phosphate as products.

In the reaction catalysed by KDO8PS, the *si* face of PEP attacks the *re* face of the A5P aldehyde.[7, 32, 35, 36, 44, 60, 118] This has been determined by multiple studies via ^{1}H and ^{19}F nuclear magnetic resonance (NMR) spectroscopy with deuterated or fluorine-substituted PEP.[32, 36, 44, 60] Additional evidence has been obtained via computational studies of *Aquifex aeolicus* (*Aae*) KDO8PS,[118] as well as *Escherichia coli* (*Eco*) KDO8PS crystal structures bound with PEP,[7] and *Aae*KDO8PS bound with PEP and A5P.[35] Kinetic experiments have determined that PEP binds to the KDO8PS enzyme, followed by A5P, in an ordered sequential reaction.[45, 61, 131] A more recent study has also indicated that within metal dependent KDO8PS, the divalent metal ion binds to the KDO8PS enzyme before PEP.[45] A5P binds in the cyclic furanose form and subsequently ring opens to form the acyclic A5P required for the reaction to occur.[56, 57, 61] Product release consists of inorganic phosphate followed by KDO8P.[61, 75] Initial studies utilising pre-steady-state kinetic experiments suggested that product release was the limiting step in the reaction,[44, 76, 109] although the type of metal ion in the metal-dependent KDO8PS can change this. An example of this can be seen in *Helicobacter pylori* (*Hpy*) KDO8PS, where

for Cd^{2+}, Cu^{2+} or Co^{2+} bound *Hpy*KDO8PS the product release is the rate limiting step in the reaction, whereas for Mn^{2+} or Ni^{2+} bound *Hpy*KDO8PS the reaction chemistry is the rate limiting step in the reaction.[101] More recent studies utilising computational approaches on *Aae*KDO8PS, suggest that the formation of the bond between A5P and PEP to be the rate limiting step in the reaction.[118, 119]

The phosphate hemiketal intermediate formed has been identified by ^{31}P NMR spectroscopy,[76] time-resolved electrospray ionization mass spectrometry (ESI-MS),[74, 98] and from X-ray crystallography electron density within the KDO8PS active site.[63] Other mass spectrometry experiments have ruled out the cyclic intermediate possibility, confirming the formation of the acyclic intermediate (Figure 1.6).[26, 75] Inhibitors designed to mimic the acyclic form of the intermediate have greater inhibition,[9, 22, 33, 34, 49] compared to those designed to mimic the cyclic form of the intermediate.[10, 11, 15, 26, 59, 76, 108] The order of the reaction to form the intermediate, as well as whether the new C-C and C-O bonds form stepwise or simultaneously, remains uncertain.[109, 126]

The order which is more probable is the C3 of PEP attacks the C1 of A5P, forming a transient oxocarbenium ion, which water subsequently attacks to form the intermediate (Figure 1.7, Path 1, overleaf).[109, 118, 119] The alternative is the attack of water, on the C2 of PEP to form a transient carbanion, which then attacks the C1 of A5P to form the intermediate (Figure 1.7, Path 2).

Figure 1.6: The two possible KDO8PS phosphate hemiketal intermediates.

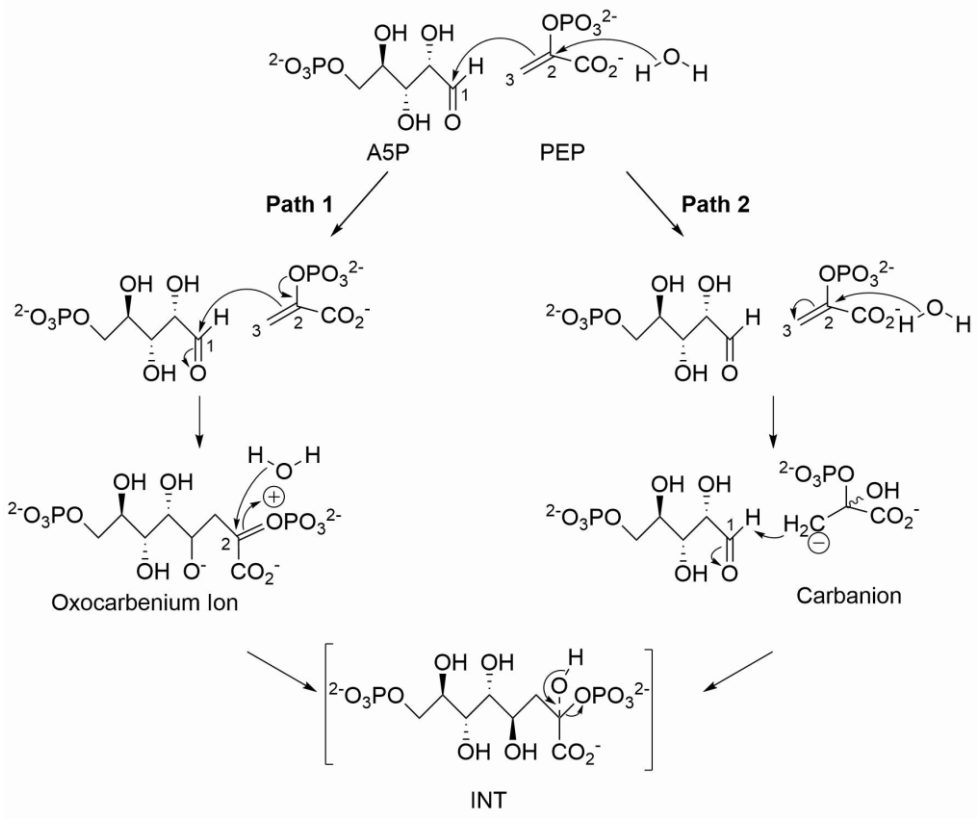

Figure 1.7: The two possible KDO8PS-catalysed reaction pathways. Path 1 is via the transient zwitterionic oxocarbenium ion, and Path 2 is via a transient carbanion.

The transient carbanion would have no delocalisation to stabilise the anionic charge, be highly basic (pK_a > 30), and therefore could just decompose by abstracting a proton from a neighbouring residue or water molecule.[109] Recent

computational studies suggest that the reaction between PEP, A5P and water is partially concerted, with the PEP attack on A5P slightly prior to the water attack on PEP.[118, 119]

Whichever the correct reaction pathway, both will result in the tetrahedral intermediate, which will subsequently break down to form KDO8P and inorganic phosphate as products. The loss of phosphate occurs through the cleavage of the C-O bond of PEP, determined from using ^{18}O labelled specifically on the enolic oxygen of PEP is recovered in the inorganic phosphate product instead of the enolic oxygen on the KDO8P product.[31, 51]

1.3 KDO8PS active site water molecule

While most details of the reaction mechanism for KDO8PS are known, it is still unclear where the water molecule that attacks the C2 of PEP arises from, and whether it attacks the *re* or *si* face of PEP (Figure 1.8, overleaf). Past studies have proposed that the reactive water is the one found on the *si* face of PEP (near the metal-binding site).[63, 118] Computational studies simulating the catalysed reaction within the *Aae*KDO8PS C11N mutant, indicated that the optimum reaction path (with the lowest energy barriers) to the formation of the intermediate is a partially concerted reaction of the *si* face of PEP attacking the *re* face of the A5P aldehyde, alongside attack by a water molecule on the *si* face of PEP.[118]

The crystal structure of an *Aae*KDO8PS mutant exhibits electron density consistent with the computational modelling of the intermediate in a configuration only possible via the transient carbanion path if the reactive

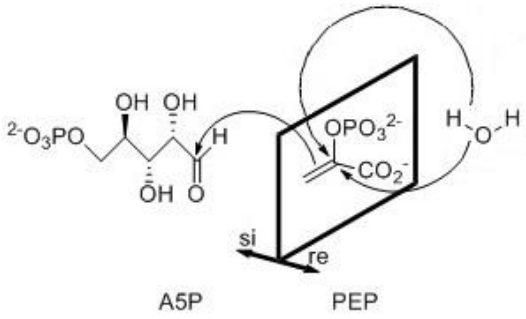

Figure 1.8: The *re* and *si* faces of PEP that the water molecule can attack during the KDO8PS catalysed reaction. Also depicted is the *si* face of PEP attacking A5P.

water attacked from the *si* face of PEP.[63] However, the electron density exhibited is not significant enough to confirm only this specific intermediate is possible. In *Aae*KDO8PS crystallographic models, a water molecule is often seen on the *si* face of PEP,[126] but less often when PEP and A5P are bound.[35, 63] In the only *Burkholderia pseudomallei* (*Bps*) KDO8PS crystallographic model, which has both PEP and A5P bound, no ordered water molecule is seen on the *si* face of PEP.[14] The water molecule may not enter the active site until after the oxocarbenium ion (the more likely possible reaction pathway) is formed, and subsequently attack the C2 of the ion (Figure 1.7, Path 2).[63]

The water molecule on the *si* face of PEP has been suggested to be a metal ligand in metal-dependent KDO8PS, with the metal ion activating the water molecule for attack on the C2 of PEP.[35, 126] The metal-ligand Asp has been suggested to deprotonate the water to enable attack on the C2 of PEP,[62] however this would favour the formation of the carbanion (the less likely possible reaction pathway).

Most recent studies suggest that the role of the metal ion is not involved directly in the reaction chemistry but instead a structural role; enabling the correct orientation of active site residues and substrates.[109, 119] In addition, how

metal-independent KDO8PS would activate the water molecule on the *si* face - of PEP has not been determined.

Attack of a water molecule on the *re* face of PEP is also a possibility, and is suggested to be the more favourable.[63] The water molecule on the *re* face of PEP is seen in many crystallographic models of both metal-dependent and metal-independent KDO8PS proteins.[7, 35, 125, 126] In the crystallographic models of *Aae*KDO8PS with both PEP and A5P bound, this specific water molecule is still present on the *re* face of PEP. In the only *Bps*KDO8PS crystallographic model that has both PEP and A5P bound, this specific water molecule is also still present on the *re* face of PEP (Figure 1.9).[14] The water molecule on the *re* face of PEP could be stabilised by a hydrogen-bonding chain, transferring a proton from the water to a conserved Asp, to a final conserved His residue.[35]

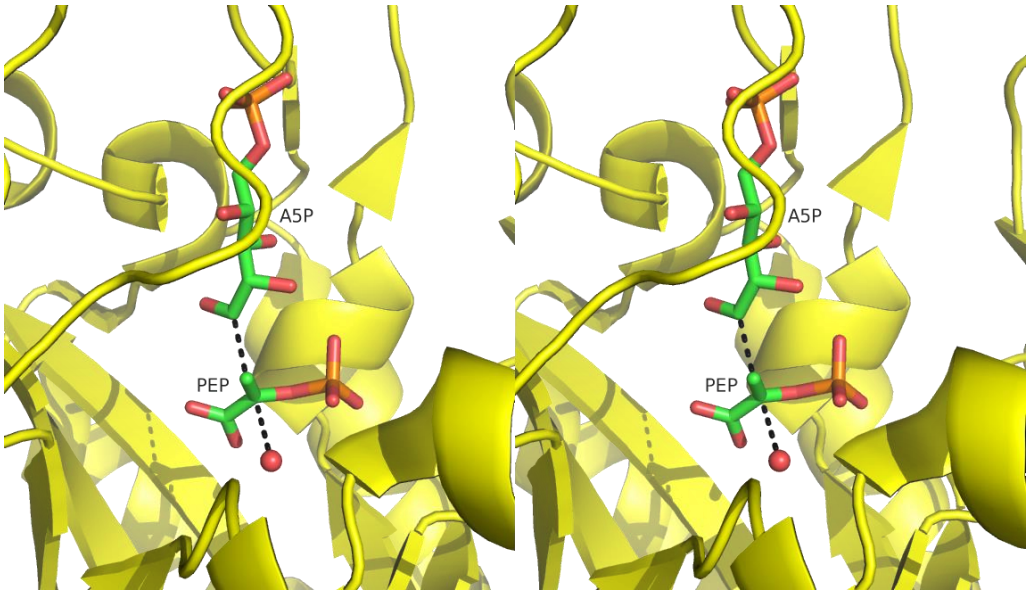

Figure 1.9: Stereoview of *Bps*KDO8PS structure (PDB code 3UND) showing the PEP, A5P and water molecule on the re side of PEP.

1.4 KDO8PS structure

KDO8PS enzymes from various sources have been crystallised: *E. coli*,[90] *A. aeolicus*,[35] *Haemophilus influenzae*,[12] *N. meningitidis*,[21] *Pseudomonas aeruginosa*,[85] *Burkholderia ambifaria*,[14] *Burkholderia cenocepacia*,[14] *Burkholderia pseudomallei*,[14] *A. thaliana*,[138] *H. pylori*,[19] *Bruciella melitensis* and *Vibrio cholerae*. The basic KDO8PS unit structure is a $(\beta/\alpha)_8$ triose phosphate isomerase (TIM) barrel, with extensions to the βα loops on the C-terminal end of the barrel (Figure 1.10).[19, 21, 35, 85, 90] The active site is located on the C-terminal region of the barrel, as is found in other TIM-barrel enzymes.

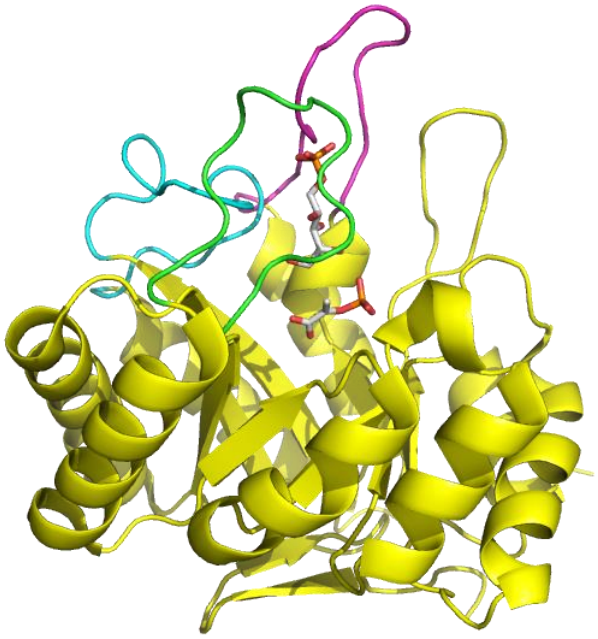

Figure 1.10: The structure of metal-independent *Bps*KDO8PS (PDB code 3UND). A single monomer depicting the two substrates and the three loops that extend from the core barrel over the active site. PEP and A5P are shown with carbon atoms coloured grey. The β2α2 loop is coloured green, β7α7 loop magenta and β8α8 loop cyan.

The ~30 kDa-sized monomers interact to give rise to a homotetramer (see Section 1.6).[6, 31, 36, 92, 130, 131, 138] PEP binds to residues near the end of the core barrel β-strands, while A5P binds further out from the barrel.[35, 90] Three loops which extend from the barrel (β2α2, β7α7 and β8α8) create the A5P binding site. Both metal-dependent and metal-independent KDO8PS proteins have very similar architecture.[35] The metal ion binding site is found near the bound positions of PEP and A5P.

1.5 KDO8PS metal dependency

Each KDO8PS can be categorised into two groups, depending on the requirement of a metal ion for catalytic activity. Metal-dependent KDO8PS contain a divalent metal ion in the active site, interacting with four conserved residues: Asp, Glu, Cys and His (Figure 1.11, overleaf). Different metal ions prefer different coordination geometry with ligands around them; Zn^{2+} prefers a distorted tetrahedral/tetrahedral/trigonal bipyramidal structure, Cd^{2+} and Co^{2+} prefers a distorted octahedral/octahedral structure, and Cu^{2+} Mn^{2+}, and Ni^{2+} preferring a square planar/trigonal bipyramidal/square pyramidal structure.[101] This difference in preferred coordination geometry can alter the actual coordination geometry of the KDO8PS residue ligands around the metal ion. In Cd^{2+} and Zn^{2+} bound *Aae*KDO8PS the metal binding site forms an octahedral arrangement with the KDO8PS residue ligands around it, whereas Cu^{2+} bound *Aae*KDO8PS instead forms a distorted octahedral, with the axial His and Cys ligand interactions notably closer while the remaining equatorial ligands are farther apart.[62]

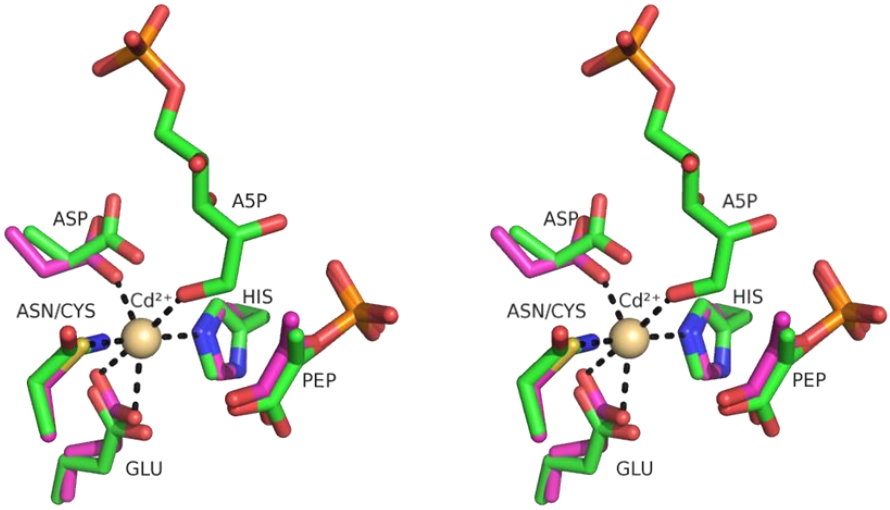

Figure 1.11: Stereoview of the structural superimposition of the metal binding sites of metal-dependent *Aae*KDO8PS with PEP bound (carbon atoms coloured purple, PDB code 1FWW) and the metal-independent *Bps*KDO8PS with PEP and A5P bound (carbon atoms coloured green, PDB code 3UND). The Cd^{2+} in *Aae*KDO8PS is coloured wheat.

In Cd^{2+} bound *Hpy*KDO8PS the metal binding site forms an octahedral arrangement with the KDO8PS residue ligands around it whereas Zn^{2+} bound *Hpy*KDO8PS forms a square pyramidal arrangement instead.[19] Metal-dependent KDO8PS proteins have maximum activity with Cd^{2+}, Mn^{2+}, Co^{2+}, and varying levels for other divalent metal ions.[6, 37, 66, 110]

Metal-independent KDO8PS proteins have conserved three of the four residues located at the metal binding site in metal-dependent KDO8PS, with the fourth metal binding residue Cys replaced with an Asn residue.[16, 53] KDO8PS metal dependency can be reliably predicted by the presence of either a Cys or Asn residue at this particular point in the sequence; for example metal-dependent *Aae*KDO8PS Cys11 and *Hpy*KDO8PS Cys18 compared to

metal-independent *Eco*KDO8PS Asn26, *Nme*KDO8PS Asn23 and *Bps*KDO8PS Asn24.

Past studies have interchanged the metal dependency of KDO8PS, using both metal-dependent and metal-independent KDO8PS proteins.[21, 63, 70, 86, 109] In the metal-independent *Eco*KDO8PS, the N26C mutation was sufficient to allow metal activation, however the single mutant was not sufficient to preserve wild-type enzyme activity.[86] An additional second mutation was added in attempt to retain native activity: M25P, another conserved difference between metal-dependent and metal-independent KDO8PS proteins. Once the N26C mutation was paired with the second mutation M25P, the k_{cat} activity in the presence of the metal Mn^{2+} was restored to equal that of the wild-type enzyme.[86] It should also be noted however that even with either the single or double mutation on *Eco*KDO8PS, there remained some catalytic activity in the absence of divalent metal ions. In other words, the absolute dependency on the presence of a divalent metal ion as exhibited by other characterised metal-dependent enzymes was not created.

In the metal-independent *Neisseria meningitidis* (*Nme*) KDO8PS, the N23C mutation was also sufficient to allow metal activation, and just like with metal-independent *Eco*KDO8PS the single mutant was not sufficient to preserve activity equal to that of the wild-type enzyme, and there remained some catalytic activity in the absence of divalent metal ions.[21] Two additional mutations attempted to restore the k_{cat} of the metal-dependent mutant, in the presence of the metals Mn^{2+} and Cd^{2+};[21] C246S (to avoid creating a disulfide bond in the N23C mutant) and P249A (to reorient a neighbouring Asp which has different conformations in the two KDO8PS groups). The resulting metal-dependent *Nme*KDO8PS triple mutant did display absolute dependency for the

presence of a divalent metal ion for catalytic activity, however the k_{cat} in the presence of a divalent metal ion was only slightly greater than half that of the original metal-independent *Nme*KDO8PS.[21]

In the metal-dependent *Aae*KDO8PS, the C11N mutation successfully removed the absolute dependency on the presence of a divalent metal ion for catalytic activity, as well as decreased the presence of divalent metal ions in the *Aae*KDO8PS single mutant.[70] The metal-independent *Aae*KDO8PS single mutant had less than half the k_{cat} of the original metal-dependent *Aae*KDO8PS.[63] Even the addition of the P10M mutation (another KDO8PS metal-dependent conserved difference) which improved the k_{cat} in the *Aae*KDO8PS double mutant remained less than half that of the original metal-dependent *Aae*KDO8PS.[63]

In the metal-dependent *Aquifex pyrophilus* (*Apy*) KDO8PS, the C11N mutation also successfully removed the absolute dependency on the presence of a divalent metal ion for catalytic activity, as well as decreased the presence of divalent metal ions in the *Apy*KDO8PS single mutant.[109] The metal-independent *Apy*KDO8PS single mutant had less than a quarter of the specific activity of the original metal-dependent *Apy*KDO8PS, which increased in the presence of Cd^{2+}, and was still less effective than the original metal-dependent *Apy*KDO8PS.[109]

The metal-independent KDO8PS proteins are suggested to have evolved from a metal-dependent KDO8PS,[16, 53] and these discoveries suggest that additional compensatory changes were required to optimise metal-independent activity, and that these metal-dependency conversion mutants resemble evolutionary intermediates.

1.6 KDO8PS subunit interfaces

All characterised, crystallised bacterial KDO8PS proteins are tetrameric,[6, 14, 19, 21, 35, 85, 90] suggesting all bacterial KDO8PS proteins are tetrameric. Initial studies suggested that plant KDO8PS proteins form homodimers,[131] however more recent studies involving crystallisation and analytical ultracentrifugation indicate that the tetramer is the more likely quaternary structure.[138] The characterised and crystallised plant KDO8PS from *A. thaliana* (*Ath*), which exhibited interface residues similar to most other plant KDO8PS, forms a tetramer in solution and in the crystal structure.[138] The plant KDO8PS from *P. edulis* (*Pe*) forms both tetrameric and dimeric species in solution due to a unique residue difference compared to other plant KDO8PS proteins.[140]

The KDO8PS tetramer is comprised of two conserved tetramer interfaces, the first comprised of the interaction between subunits A and B (or C and D), and the second of the interaction between subunits A and C (or B and D) (Figure 1.12, overleaf). The A-C tetramer interface is comprised of numerous hydrogen-bonds, salt-bridges and hydrophobic interactions from two α-helices (α4 and α5) and four βα loops (β2α2, β4α4, β5α5 and β6α6).[35, 90] The A-C tetramer interface is closer to the KDO8PS active site, and contains a single conserved Arg able to interact with the neighbouring subunit active site, contributing to the binding of the substrate A5P.[133] The A-B tetramer interface is comprised almost entirely of hydrophobic interactions from three α-helices (α6, α7 and α8), a small part of the β6α6 loop, and the C-terminal.[35, 90]

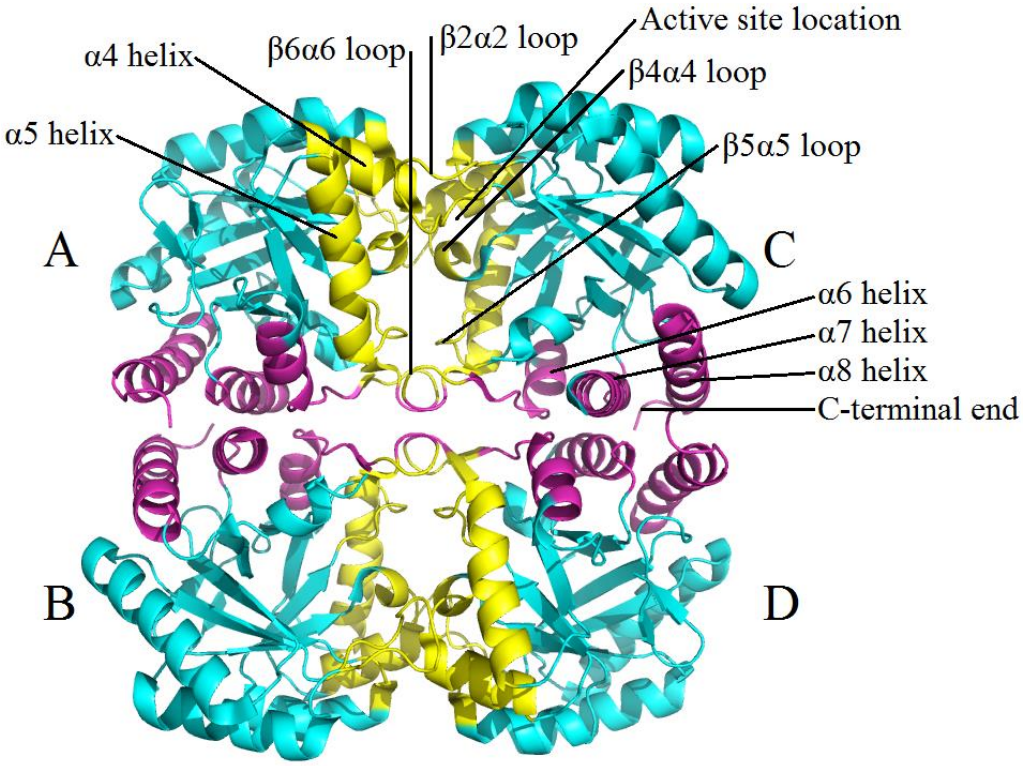

Figure 1.12: The structure of metal-independent *Nme*KDO8PS (PDB code 2QKF). Four monomers are shown depicting the two separate tetramer interfaces. The A-C tetramer interface is coloured in yellow, the A-B tetramer interface magenta, and the non-interface structure in cyan.

1.7 DAH7PS

3-Deoxy-D-*arabino*-heptulosonate 7-phosphate synthase (DAH7PS) (EC 2.5.1.54) is a closely related enzyme to KDO8PS. DAH7PS catalyses a similar aldol-like condensation to KDO8PS, using the four-carbon phosphorylated aldose D-erythrose 4-phosphate (E4P) with PEP and water (Figure 1.13, overleaf).

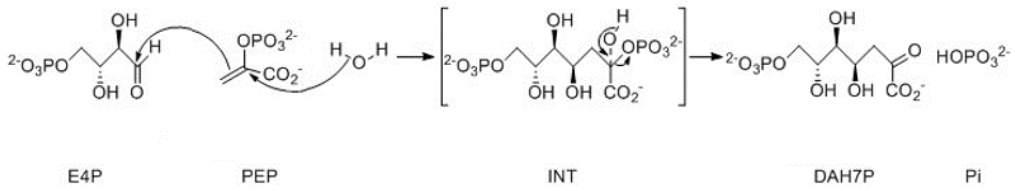

Figure 1.13: The DAH7PS catalysed reaction between PEP and E4P.

Unlike KDO8PS proteins, all DAH7PS proteins are metal-dependent and require a divalent metal ion for catalysis. DAH7PS catalyses the first committed step of the shikimate pathway, whose end products include the aromatic amino acids: phenylalanine, tyrosine and tryptophan. DAH7PS (and the shikimate pathway) is only found in bacteria and plants, enabling DAH7PS to be a potential anti-bacterial drug target. All DAH7PS proteins have a similar core $(\beta/\alpha)_8$ TIM-barrel monomer fold to that of KDO8PS (Figure 1.14, overleaf), however variations can occur with additions to the core barrel at the N- or C-terminal, and to the βα loops. Each DAH7PS can be categorised into three groups (Iα, Iβ or II), depending on what sequence additions are present, as these additional parts of the enzyme are also responsible for the feedback inhibition of DAH7PS.[50, 52, 54, 121, 127, 132]

Type Iα DAH7PS proteins have a two-stranded anti-parallel β-sheet between α5 and β6 as well as an N-terminal extension. The β-sheet insertion interacts with the neighbouring equivalent to create a binding site for phenylalanine and tyrosine.[50] Type II DAH7PS proteins have an N-terminal extension and usually a pair of α-helices between α2 and β3,[128] which create binding sites for aromatic amino acids.[127] Type Iβ DAH7PS proteins usually have an N-terminal extension or an additional N- or C-terminal domain,[23] though are also able to have no additions to the core barrel.[103]

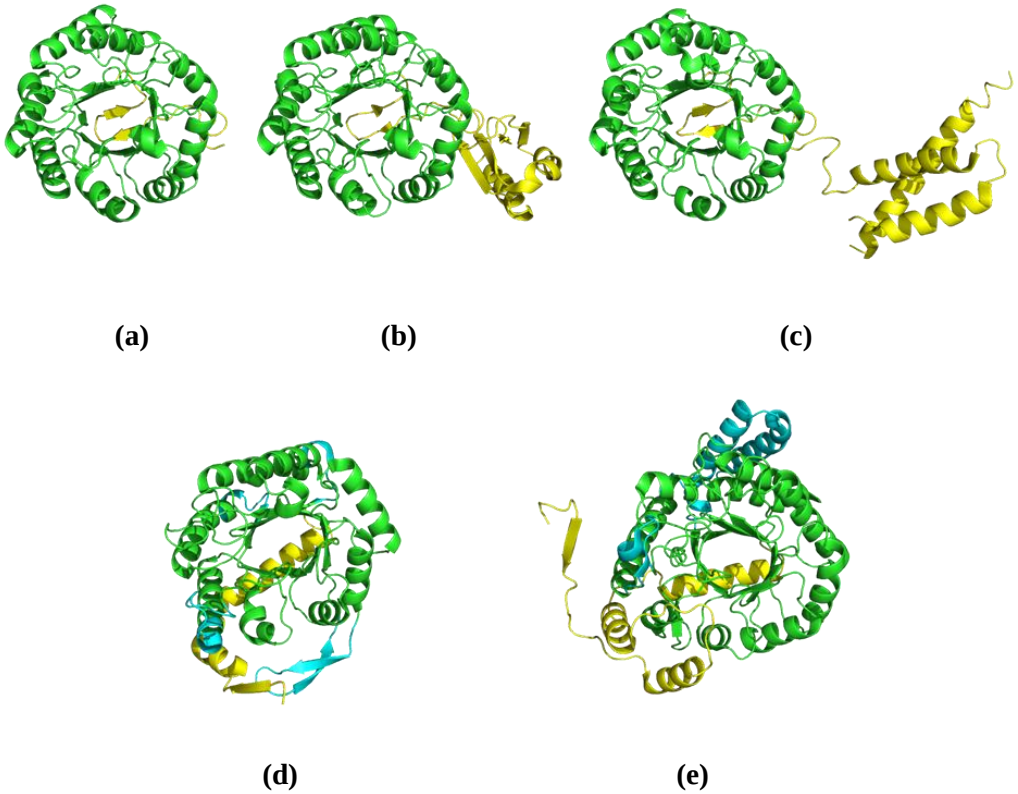

Figure 1.14: The structure of various DAH7PS monomer subunits. The TIM-barrel fold at the core of each structure is coloured green, N-terminal extensions and domains yellow, and other barrel extensions cyan. (a) *Pyrococcus furiosus* DAH7PS (type Iβ, no additional domain, PDB code 1ZCO), (b) *Thermotoga maritima* (*Tma*) DAH7PS (type Iβ, additional N-terminal ACT domain, PDB code 1RZM), (c) *Listeria monocytogenes* DAH7PS (type Iβ, additional N-terminal chorismate mutase domain, PDB code 3NVT), (d) *Neisseria meningitidis* DAH7PS (type Iα, PDB code 4HSN), (e) *Mycobacterium tuberculosis* DAH7PS (type II, PDB code 2B7O).

The N-terminal domain is either a chorismate mutase or ACT domain (a domain found in aspartate kinase, chorismate mutase and TyrA [prephenate dehydrogenase]), while the C-terminal domain is a chorismate mutase domain. These additions to the core barrel play a role in the inhibition of the DAH7PS enzyme,[103] usually by products created further down the shikimate pathway such as chorismate, phenylalanine, tyrosine and tryptophan. KDO8PS proteins

show the most similarity to Iβ DAH7PS proteins,[16, 17, 53] which also have members with no additions and are unregulated by feedback inhibition. The most common quaternary structure arrangement seen in the DAH7PS family is that of a tetramer, with one conserved tetramer interface shared between both type Iα and most Iβ DAH7PS proteins, and none shared with type II DAH7PS proteins.[25, 64, 77, 83, 103, 111, 112] KDO8PS proteins have tetramer interfaces most similar to that of most type Iβ DAH7PS proteins.

The active site architecture of DAH7PS compared to the related KDO8PS has many shared, conserved residues despite the low total sequence identity found between DAH7PS and KDO8PS.[124] The metal binding site is one conserved example,[16, 53] PEP binds in a similar position, and E4P has been modelled to bind in a fashion similar to A5P in KDO8PS (Figure 1.15, overleaf).[90]

In the reaction catalysed by DAH7PS, the *si* face of PEP attacks the *re* face of the E4P aldehyde (similar to KDO8PS). The DAH7PS catalysed reaction is also an ordered sequential reaction, with a reaction mechanism proposed to pass through the equivalent acyclic intermediate breaking down to form 3-deoxy-D-*arabino*-heptulosonate 7-phosphate (DAH7P) and inorganic phosphate as products. The loss of phosphate also occurs through the cleavage of the C-O bond of PEP. In DAH7PS the water molecule on the *re* face of PEP has also been suggested to be the one involved in the catalytic reaction.[64, 111] This water molecule is part of a possible proton relay chain through a conserved Glu (instead of Asp in KDO8PS), and another water molecule, to a final conserved Lys residue (Figure 1.16, overleaf).

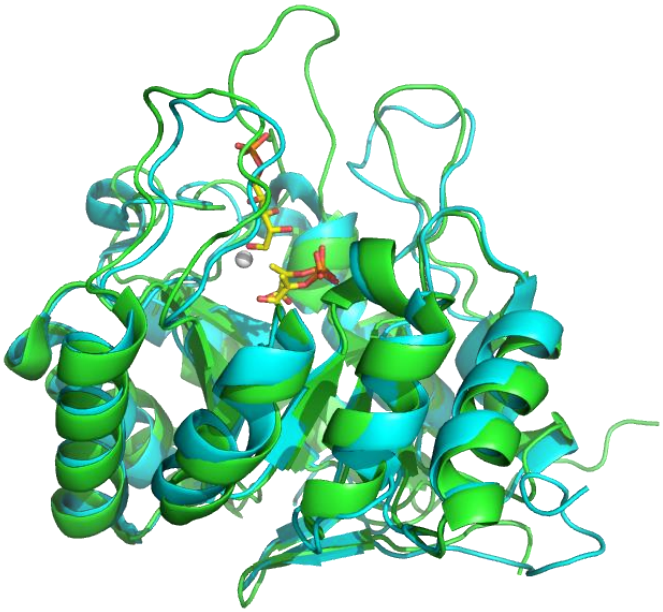

Figure 1.15: The structural superimposition of the *Pfu*DAH7PS monomer (coloured cyan, PDB code 1ZCO) and the *Bps*KDO8PS monomer (green, PDB code 3UND). A5P in *Bps*KDO8PS and PEP in both structures are shown with carbon atoms yellow, and the Mn^{2+} in *Pfu*DAH7PS white.

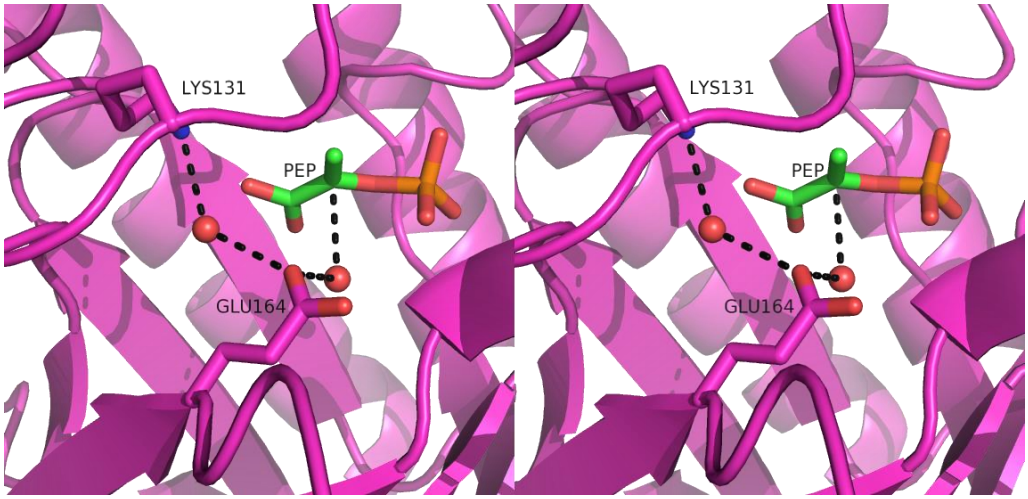

Figure 1.16: Stereoview of *Tma*DAH7PS structure (PDB code 1RZM) showing the proton relay chain comprised of two water molecules, a conserved Glu (Glu164), and a conserved Lys (Lys131).

KDO8PS proteins appear homologous to type Iα and Iβ DAH7PS proteins,[17] with a common Iβ DAH7PS-like ancestor (Figure 1.17).[53, 90] The ancestor is suggested to be metal-dependent, have a wider range of phosphorylated aldose substrates, and a lack of feedback inhibition. The type Iβ DAH7PS from *Pyrococcus furiousus* (*Pfu*) has all these characteristics and has been suggested to bear a resemblance to this ancestor.[103]

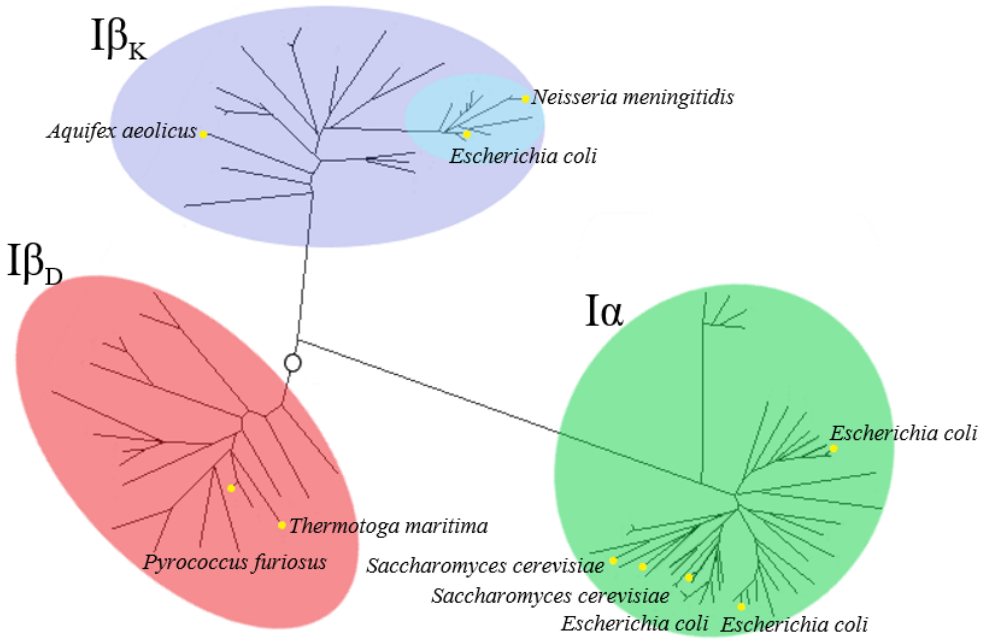

Figure 1.17: Phylogenetic tree displaying the homology between the type Iα (coloured green) and Iβ (coloured red) DAH7PS proteins, and the Iβ-like KDO8PS proteins (coloured purple). The metal-independent bacterial KDO8PS proteins are coloured cyan. The open circle represents the position of the suggested Iβ-like ancestral protein. Figure redrawn from Jensen *et al*.[53]

1.8 Goals of this thesis

The objective of this thesis was to learn the significance of the quaternary structure of metal-independent bacterial KDO8PS on activity and stability. More generally, it was to understand the role the metal-independent bacterial KDO8PS quaternary structure may play in comparison to metal-dependent bacterial KDO8PS, plant KDO8PS and to DAH7PS. These studies also explored the relationship between the catalytic mechanisms of KDO8PS and DAH7PS. This knowledge was utilised to inform rational mutagenesis in an attempt to disrupt the bacterial KDO8PS and DAH7PS quaternary structure into smaller subunits.

The specific goals of this thesis were to:

- To compare KDO8PS and DAH7PS reaction mechanisms to determine the role of conserved active-site Asp and Pro side chains in active-site proton transfer;
- Investigate the significant residues forming the metal-independent bacterial KDO8PS quaternary structure interfaces, as well as the differences in comparison to plant KDO8PS;
- Investigate the significant residues forming the quaternary structure interfaces of a type Iβ DAH7PS;
- Purify and characterise a metal-dependent bacterial KDO8PS;
- Clone a plant KDO8PS.

The experiments were performed using metal-dependent and metal-independent KDO8PS enzymes, as well as a type Iβ DAH7PS enzyme. The metal-dependent bacterial KDO8PS enzyme used in these studies was

*Nme*KDO8PS. It is an enzyme that has been previously characterised in our laboratory, is from a mesophilic organism, and has known crystallisation conditions.[21] The type Iβ DAH7PS enzyme used in these studies was *Pfu*DAH7PS. This is also is an enzyme that has been previously characterised in our laboratory, is from a hyperthermophilic organism, and has known crystallisation conditions.[104] The metal-dependent KDO8PS used in these studies was *Chlorobium tepidum* (*Cte*) KDO8PS. This is an enzyme that has been only partially previously purified and characterised.[136] The plant KDO8PS used in these studies is *Chlorela variabilis* (*Cvr*) KDO8PS. This is an enzyme that has not been previously investigated.

Chapter 2

Investigation into a putative proton relay chain in the KDO8PS active site

2.1 Introduction

While previous studies have identified the reaction mechanism for KDO8PS, several aspects remain unclear about the positioning of the attacking water molecule, whether the *re* or *si* side of the C2 of PEP is attacked by the water molecule, as well as the identification of the significant network of residues that enables this step of the reaction to occur (Figure 2.1, overleaf).

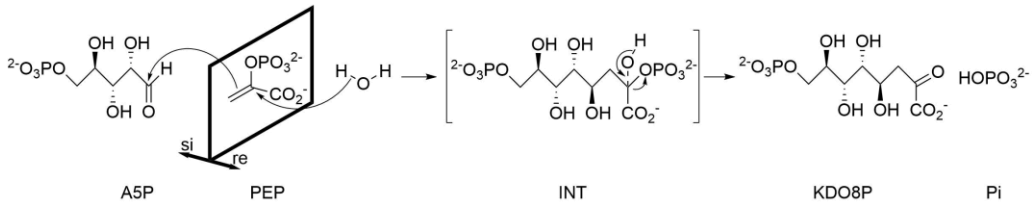

Figure 2.1: The KDO8PS catalysed reaction between PEP and A5P.

In the related DAH7PS enzyme, there is a conserved Glu residue found near the *re* face of PEP. The DAH7PS Glu residue is situated in the PEP binding pocket, on the DAH7PS β3 beta-sheet, and contacts a water molecule that is located between the residue and PEP (Figure 2.2. overleaf). This Glu residue is suggested as part of a putative proton relay chain that would deprotonate a water molecule for attack on the *re* face of PEP, and subsequently, protonate the aldehyde carbon of E4P.[111]

In KDO8PS there is an equivalent well conserved Asp residue in the PEP binding pocket, on the KDO8PS β3 beta-sheet, which contacts a water molecule that is located between the residue and PEP (Figure 2.2). However, it is unclear whether a water molecule attacks the PEP from the *re* or *si* face of PEP, or how the water molecule is activated for attack.[35, 62, 63, 118, 125, 126, 133] In addition, the source of the proton that is donated to the aldehyde carbon of A5P is also unknown, and whether it originates from an active site residue side chain or from one of the substrates themselves. The source of the proton would also be dependent on the position that the A5P molecule takes, which varies in crystal structures (Figure 2.3, overleaf).

If A5P is oriented with its aldehyde closest to the PEP carboxylate (as has been observed in the crystal structure of *Bps*KDO8PS), then water could attack PEP on either face, similarly to DAH7PS.

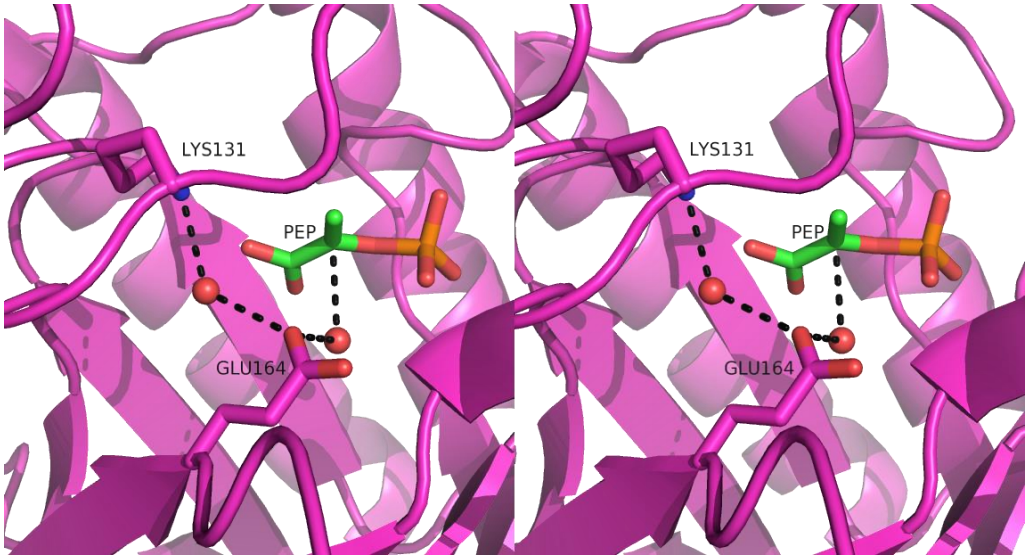

(a)

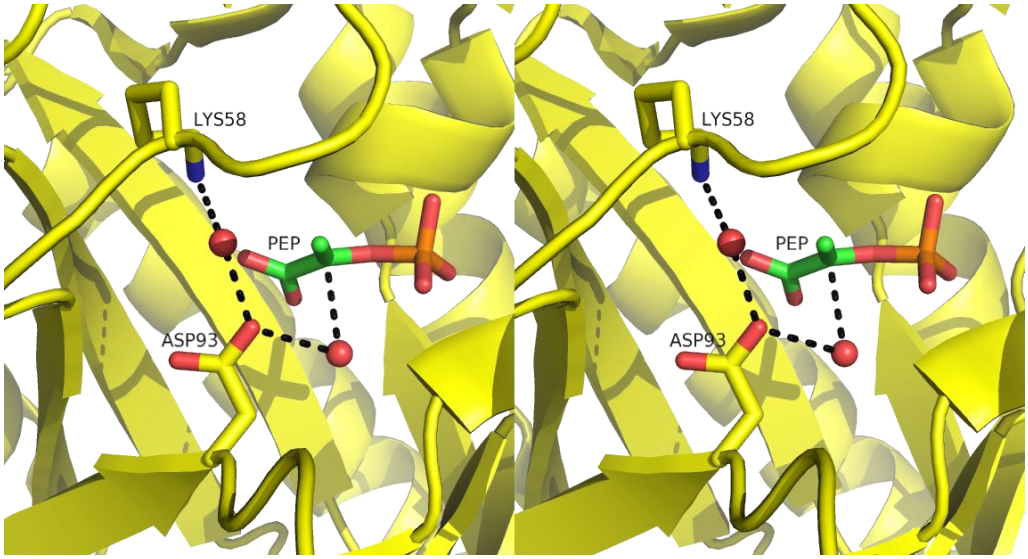

(b)

Figure 2.2: (a) Stereoview of *Tma*DAH7PS structure (PDB code 1RZM) showing the proton relay chain comprised of two water molecules, a conserved Glu (Glu164), and a conserved Lys (Lys131). (b) Stereoview of *Bps*KDO8PS structure (PDB code 3UND) showing the putative proton relay chain comprised of two water molecules, a conserved Asp (Asp93), and a conserved Lys (Lys58). Both structures also depict PEP, with carbon atoms coloured green.

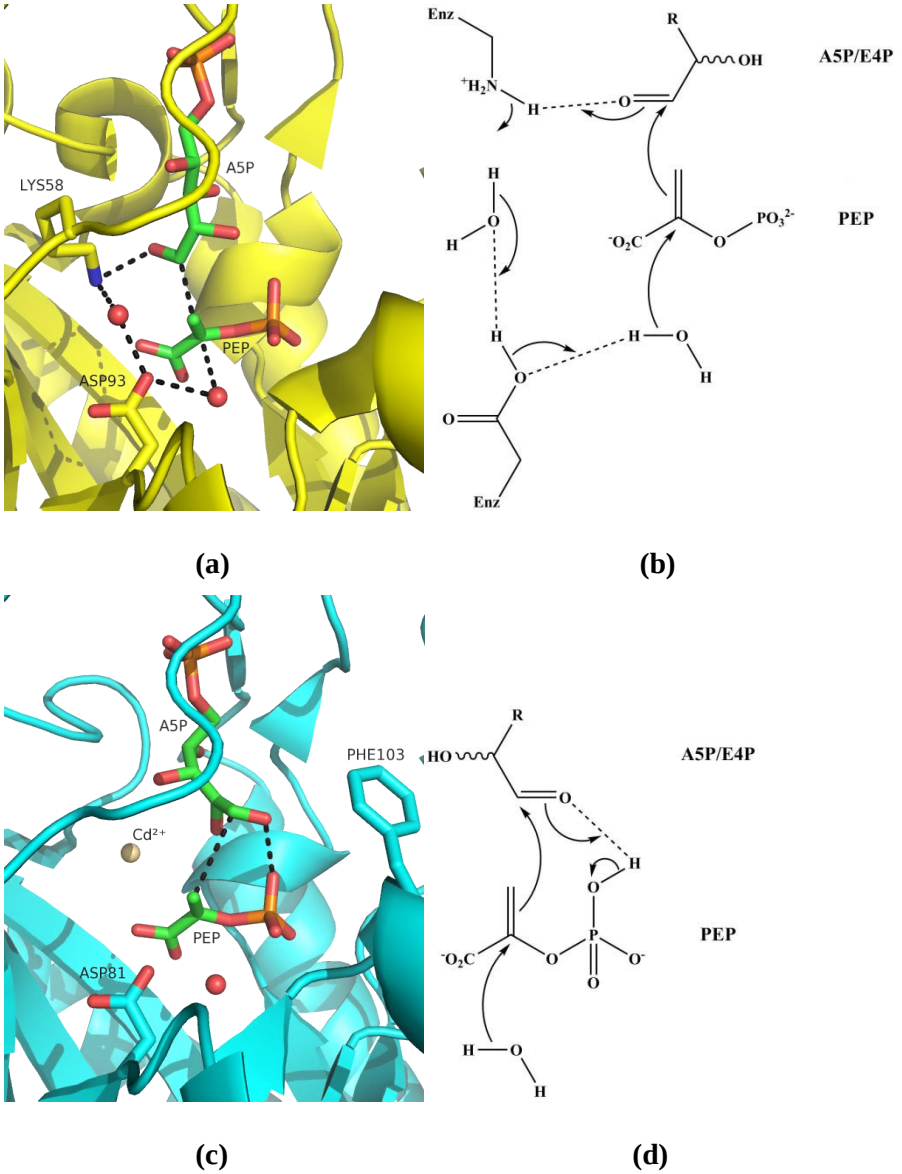

Figure 2.3: The possible proton relay chains for the alternative positions of the A5P aldehyde. (a) The structure of *Bps*KDO8PS (PDB code 3UND) showing A5P with the aldehyde group oxygen pointing towards the PEP carboxylate group, and the putative proton relay chain. (b) Schematic representation of the putative proton relay chain involving the Asp/Glu and Lys residues. (c) The structure of *Aae*KDO8PS (PDB code 1FWW) showing A5P with the aldehyde group oxygen pointing towards the PEP phosphate group, the nearby conserved Phe residue and another possible proton relay chain using substrate assisted catalysis. (d) Schematic representation of another possible proton relay chain involving a monoanionic PEP phosphate group.

This would also allow the same proton relay chain to exist that is suggested in DAH7PS, which would rely on attack of the water molecule on the *re* face of PEP (Figure 2.3a). This proton relay chain would end at a conserved Lys residue in both enzymes, which has been previously found to be essential for catalytic activity.[5] The residues involved in the proton relay chain in both DAH7PS and KDO8PS would be near identical, with the only difference being the conserved Asp in KDO8PS instead of the conserved Glu in DAH7PS (Figure 2.3b). Since both Asp and Glu have a similar carboxylic acid functional group, this residue difference is not significant.

Another possibility is that the A5P is oriented with its aldehyde closest to the PEP phosphate (as has been suggested in the crystal structure of *Aae*KDO8PS)[62] in addition to the phosphate group of PEP being in a monoanionic rather than dianionic state. Though it should be noted that the electron density exhibited in the crystal structure of *Aae*KDO8PS is not significant enough to confirm only this specific orientation of A5P is possible. The proton supplied to the aldehyde carbon of A5P would then be from the PEP phosphate group (Figure 2.3d). A previous study did suggest a nearby conserved Phe residue in KDO8PS, near the PEP phosphate, encouraged the monoanionic state to be present.[1] If the PEP monoanionic phosphate group is the proton source for the A5P aldehyde, then the conserved Asp residue would have no direct role in the catalysed reaction as part of a proton relay chain. In addition, the conserved Asp residue would have little effect on which face of PEP the water molecule attacks. The importance of the conserved Asp residue in KDO8PS as opposed to the conserved Glu in DAH7PS would then become unclear.

A previous study had mutated the conserved Asp residue in the possible proton relay chain to investigate loss of the carboxylic functionality (Ala), replacement with isosteric amide functionality (Asn) and the importance of side chain length (the DAH7PS equivalent residue Glu).[3] The study determined the Asp residue was not important in stability or PEP binding. All three mutations had deleterious effect on KDO8PS catalysis in both metal-independent *Nme*KDO8PS and metal-dependent *Acidithiobacillus ferrooxidans* (*Afe*) KDO8PS, suggesting a catalytic role for the conserved Asp residue. The most deleterious catalytically affected Asn mutation no longer had a water molecule present on the *re* side of PEP; in the PEP bound *Nme*KDO8PS mutant crystal structure. This suggests the water molecule present on the *re* side of PEP may be the water molecule involved in the attack of PEP in catalysis. Interestingly the Glu mutation was the least catalytically affected of the mutants, however it did have the most detrimental effect on the binding of both substrates. The Glu mutation was unable to orient itself correctly, into a similar arrangement to that of the DAH7PS conserved Glu residue, and the possible proton relay chain ending in the Lys residue became impossible. The difference in orientation was suggested to be caused by a nearby conserved KDO8PS Pro residue, the equivalent in DAH7PS is a much smaller, conserved Gly residue (Figure 2.4, overleaf). Mutation of the Pro residue to a Gly residue could allow the Glu mutation to orientate itself into a similar arrangement to DAH7PS, allowing the putative proton relay chain to reform. If this occurs, the resulting mutant may become more catalytically active, with more effective substrate binding than the original single Glu mutant. This would indicate the Asp residue is involved in a proton relay chain similar to that of DAH7PS.

In this chapter the role of the KDO8PS conserved Asp residue, in the putative proton relay chain, is further investigated.

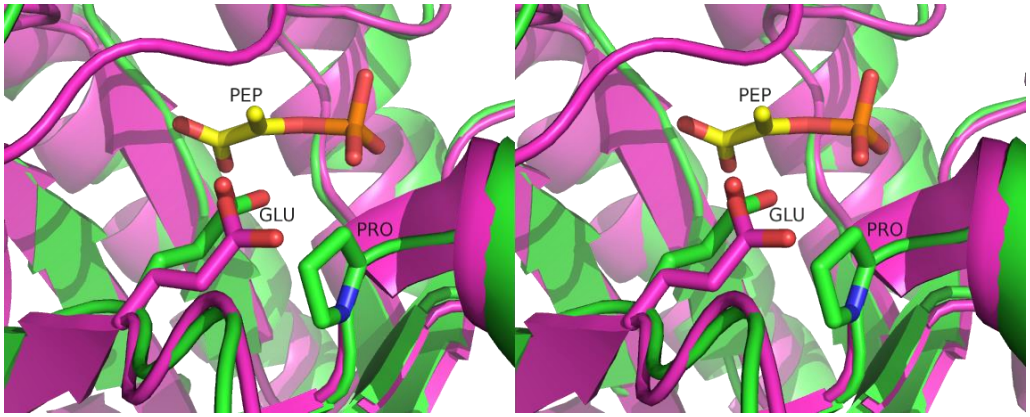

Figure 2.4: Stereoview of the superimposition of *Nme*D92E subunit C (coloured green) onto the structure of *Tma*DAH7PS (PDB code 1RZM, coloured purple). PEP is superimposed from the structure of *Bps*KDO8PS (PDB code 3UND, coloured yellow).

2.2 Preparation and rationale for the mutants

To investigate the role of the conserved Asp residue possibly being involved in a putative proton relay chain, the residue was mutated into Glu in the metal-independent *Nme*KDO8PS. This mutation was combined with the mutation of the nearby conserved Pro residue to Ala and Gly (creating *Nme*D92E/P112A and *Nme*D92E/P112G).

The Pro-to-Ala mutation was generated to remove the geometrically constrained side chain interfering in the positioning of the Asp-to-Glu mutant side chain. The Pro-to-Gly mutation was also generated to remove the side chain interference, as well as insuring the resulting mutant residue was also a helix breaker, as the residue lies between the KDO8PS β4 beta-sheet and an α-helix found on the β4α4 loop.

The *Nme*KDO8PS double mutants were expressed and purified using the same procedures as the wild-type enzyme.[21] After lysing the bacterial cell

cultures, the proteins were purified via anion-exchange chromatography (AEC), followed by hydrophobic-interaction chromatography (HIC), and completed via size-exclusion chromatography (SEC). Both of the *Nme*KDO8PS double mutants after purification were of a similar purity (Figure 2.5). From 1 L of bacterial cell culture, *Nme*D92E/P112A was purified with a yield of 8 mg of protein and *Nme*D92E/P112G a yield of 4.5 mg.

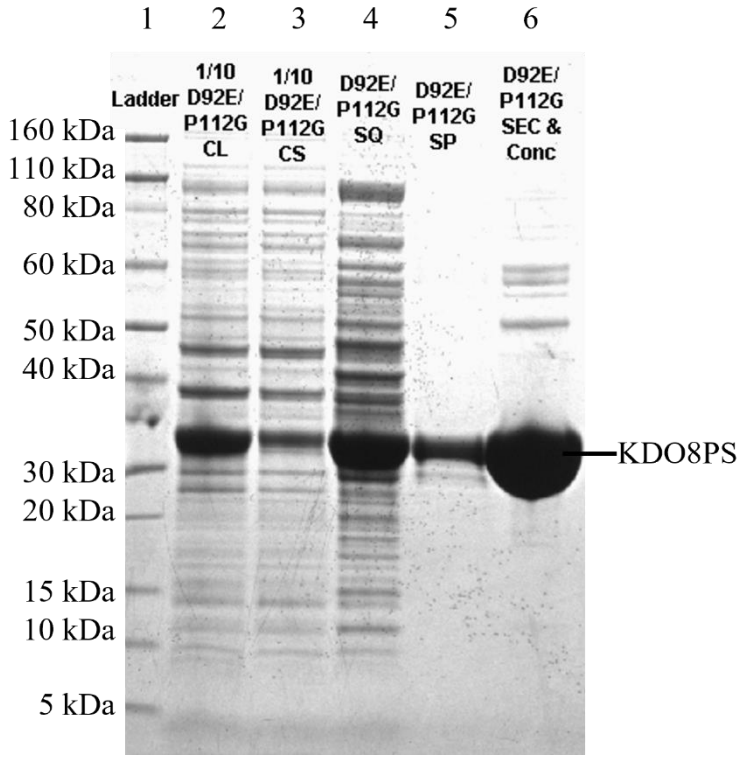

Figure 2.5: The purity of the *Nme*KDO8PS enzyme after each purification step, using *Nme*D92E/P112G. (Column 1) Novex® Sharp Pre-Stained Protein Standards (Thermo Fisher Scientific). (Column 2) Crude lysate after sonication, diluted by a factor of ten. (Column 3) Crude soluble lysate after removal of insoluble lysate, diluted by a factor of ten. (Column 4) The gathered Source™ 15Q fractions after anion-exchange chromatography. (Column 5) The gathered Source™ 15PHE fractions after hydrophobic-interaction chromatography. (Column 6) The gathered HiLoad 26/60 Superdex™ 200 prep grade column fractions after size-exclusion chromatography and spin concentration.

2.3 Structure in solution and stability

Electrospray ionisation mass spectrometry confirmed successful mutation via comparison of the measured mass of the *Nme*KDO8PS wild-type enzyme and double mutants to the calculated mass. *Nme*KDO8PS wild-type enzyme had a resulting size of 30482.8 Da (compared to calculated size 30483.4 Da) *Nme*D92E/P112A had a resulting size of 30472.2 Da (compared to calculated size 30471.3 Da), and *Nme*D92E/P112G had resulting size of 30456.6 Da (compared to calculated size 30457.3 Da).

Circular dichroism (CD) spectrophotometry assessed if any of the introduced mutations produced perturbations in the secondary structure arrangement of the *Nme*KDO8PS double mutants. The spectrum of the *Nme*D92E/P112A was similar to that of the wild-type enzyme, while the spectrum of the *Nme*D92E/P112G showed a notable difference to that of the wild-type enzyme (Figure 2.6, overleaf).

The melting temperatures of the *Nme*KDO8PS double mutants were determined using differential scanning fluorimetry (DSF), with and without the presence of the KDO8PS substrates PEP and A5P (Table 2.1, overleaf), to see if the introduced mutations destabilised the KDO8PS. Both *Nme*KDO8PS double mutants were less stable than the *Nme*D92E mutant and the wild-type enzyme. PEP increased the stability of *Nme*D92E/P112G by 4 °C, similarly to the effect on the wild-type enzyme; PEP does not increase the stability of the *Nme*D92E/P112A, which is similar to the effect on the *Nme*D92E mutant. A5P had no observable effect on the *Nme*KDO8PS double mutants and the wild-type enzyme.

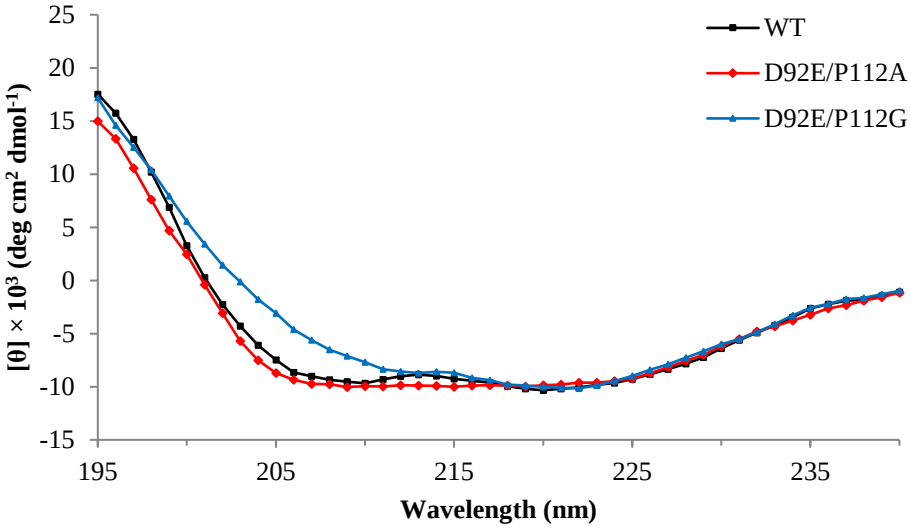

Figure 2.6: CD spectrophotometry of the *Nme*KDO8PS wild-type enzyme and double mutants. *Nme*KDO8PS wild-type enzyme: black squares; *Nme*D92E/P112A: red diamonds; *Nme*D92E/P112G: blue triangles. Every datum point is plotted for the wild-type enzyme and *Nme*D92E/P112G, whereas every fifth datum point is plotted for *Nme*D92E/P112A.

Table 2.1: The effect of additives on the T_m of *Nme*KDO8PS wild-type enzyme, single and double mutants. Those for *Nme*KDO8PS wild-type enzyme and *Nme*D92E were determined by Allison, T. M.[3]

*Nme*KDO8PS	Additives	T_m (°C)	Diff.	Diff. to WT
Wild-type	No additive	58 ± 1		
	PEP	61 ± 1	3	
	A5P	58 ± 1	0	
D92E	No additive	57 ± 1		-1
	PEP	57 ± 1	0	-4
D92E/P112A	No additive	51 ± 1		-7
	PEP	52 ± 1	1	-9
	A5P	51 ± 1	0	-7
D92E/P112G	No additive	47 ± 1		-11
	PEP	51 ± 1	4	-10
	A5P	47 ± 1	0	-11

To see if the introduced mutations destabilised a tetramer interface, the quaternary structure in solution of *Nme*KDO8PS wild-type enzyme and double mutants was determined by analytical SEC, native PAGE and analytical ultracentrifugation (AUC). Both the *Nme*KDO8PS wild-type enzyme and double mutants eluted with similar SEC profiles, at a size corresponding to 130 kDa, identical to the past wild-type enzyme SEC experiments.[21] The native PAGE also showed that both the *Nme*KDO8PS wild-type enzyme and double mutants migrated at a similar size.

AUC, the most reliable technique in the determination of quaternary structure in solution, exposed additional information. Sedimentation velocity experiments determined that *Nme*KDO8PS wild-type enzyme, *Nme*D92E/P112A and *Nme*D92E/P112G all have a similar sedimentation coefficient corresponding to a tetramer (Figure 2.7). There is also another small other peak observed, which is unclear what it can be attributed to and may be a small contaminant in the protein. In addition, *Nme*D92E/P112A also had a

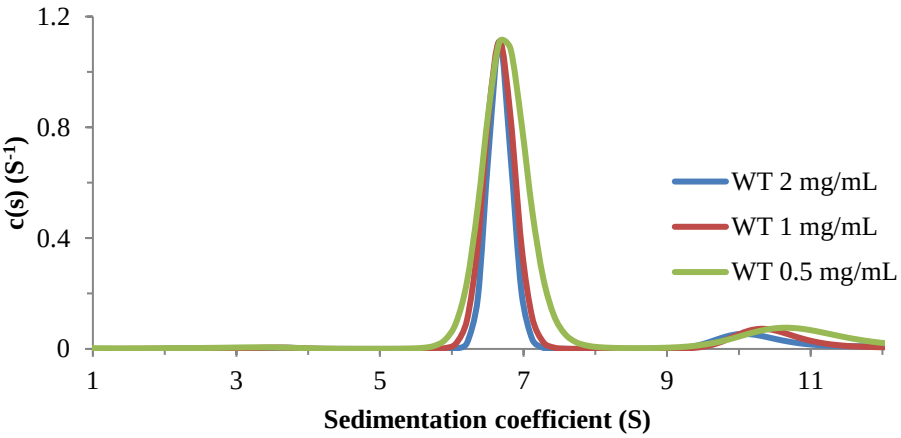

(a)

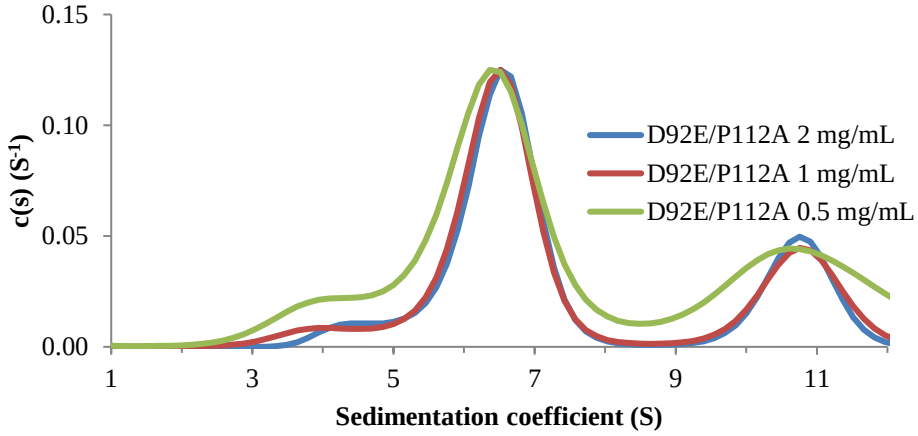

(b)

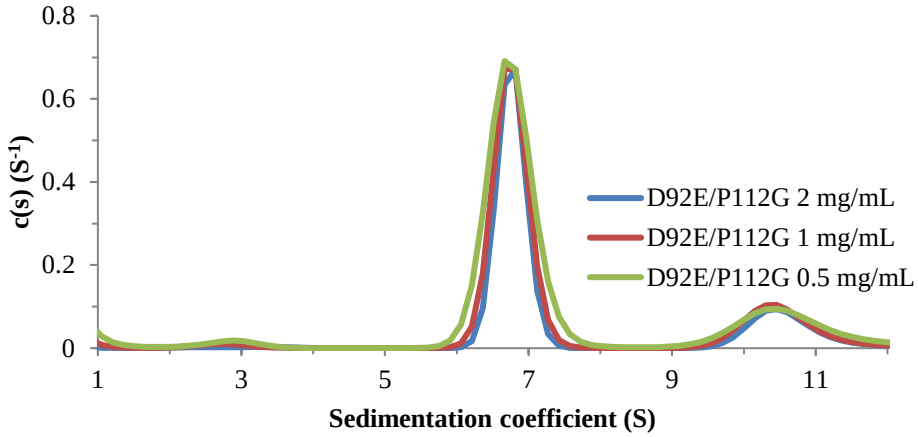

(c)

Figure 2.7: Calculated sedimentation coefficient c(s) distribution plots of *Nme*KDO8PS wild-type enzyme and double mutants. The 1 mg/mL and 0.5 mg/mL results are normalised to the 2 mg/mL result. (a) *Nme*KDO8PS wild-type enzyme. (b) *Nme*D92E/P112A. (c) *Nme*D92E/P112G.

sedimentation coefficient corresponding to dimer (Figure 2.7b).

2.4 Kinetic characterisation

The catalytic activity of both *Nme*KDO8PS double mutants was investigated (Table 2.2). Both of the *Nme*KDO8PS double mutants exhibited catalytic activity. The determined K_m^{PEP}, K_m^{A5P} of both *Nme*KDO8PS double mutants were both significantly higher than the wild-type enzyme, as well as the k_{cat} of both double mutants drastically slower.

In comparison to the *Nme*D92E mutant, the determined K_m^{PEP} and K_m^{A5P} of *Nme*D92E/P112A were both lower (≈4.5 and ≈1.2 times respectively), however the k_{cat} was significantly slower (≈1100 times). In contrast the *Nme*D92E/P112G determined K_m^{PEP} and K_m^{A5P} were both higher (≈4 and ≈17 times respectively), though the k_{cat} was also still slower (≈170 times).

Table 2.2: Kinetic parameters of the *Nme*KDO8PS wild-type enzyme, single and double mutants. Those for wild-type and D92E were determined by Allison, T. M.[3, 4]

*Nme*KDO8PS	K_m^{PEP} (μM)	K_m^{A5P} (μM)	k_{cat} (s^{-1})	k_{cat}/K_m^{PEP} (s^{-1} mM^{-1})	k_{cat}/K_m^{A5P} (s^{-1} mM^{-1})
Wild-type	2.5 ± 0.2	12.0 ± 0.5	8.0 ± 0.1	3200 ± 300	660 ± 40
D92E	83 ± 14	1101 ± 126	0.67 ± 0.04	8 ± 2	0.6 ± 0.1
D92E/P112A	17.7 ± 1.4	910 ± 82	0.0006 ± 0.00001	0.033 ± 0.003	0.0006 ± 0.00007
D92E/P112G	320 ± 30	17500 ± 1200	0.0039 ± 0.0002	0.012 ± 0.002	0.0002 ± 0.00003

2.5 Crystallography

Crystallography was used to discover the structural changes the introduced mutations had on the neighbouring regions around the mutation as well as the putative proton relay chain. Diffraction data was obtained from crystals of *Nme*D92E/P112G (Table 2.3, overleaf). The asymmetric unit of *Nme*D92E/P112G contains one complete tetramer, which is also seen in the previous *Nme*D92E mutant and the wild-type enzyme. The *Nme*D92E/P112G structure is very similar in structure to the *Nme*KDO8PS wild-type enzyme except for the Asp-to-Glu and Pro-to-Gly mutations (RMSD Cα on wild-type is 0.305 Å for 873 atoms). There are two notable changes in the final model in comparison to *Nme*D92E; the truncation of the Pro side chain to Ala (with a water molecule now occupying the new space), and the orientation of the side chain on the other mutation Asp to Glu. No A5P or PEP was found bound to any of the subunits of *Nme*D92E/P112G.

In the *Nme*D92E/P112G chains A, C and D the D92E side chain points towards the site where PEP binds, in a slightly different arrangement compared to the *Nme*D92E chains A and D (Figure 2.8a, overleaf). This D92E side chain arrangement in *Nme*D92E/P112G allows hydrogen bonding to the neighbouring Gln110, which is also seen in the *Nme*D92E chains A and D, but not in the *Nme*KDO8PS wild-type structures (Figure 2.9a, overleaf). These three *Nme*D92E/P112G chains also do not have the *re*-side water that is only present in the wild-type structure, due to the extended length of the D92E side chain.

Table 2.3: Crystal parameters, data collection, and refinement statistics for *Nme*D92E/P112G.

	*Nme*D92E/P112G
Crystal system, space group	orthorhombic, $P2_12_12_1$
Unit cell parameters (Å)	81.88, 85.52, 163.89
Resolution range (Å)	48.00-2.71 (2.84-2.71)
No. of measurements	471847
No. of unique reflections	32054
Redundancy	14.7 (15.0)
Overall CC(1/2)	0.982
Completeness (%)	100 (100)
$I/\sigma(I)$	8.0 (1.4)
R_{merge}	0.475 (2.830)
Wilson B value (Å^2)	45.5
Refinement	
Resolution (Å)	81.94-2.71
R_{cryst}	0.211
R_{free}	0.263
Amino acids (chain length of 280 residues)	253 + 256 + 255 + 254 residues; 7794 atom sites
No. of water molecules	196
No. of chloride molecules	2
No. of others	-
Mean *B* (Å^2)	
Protein	46.24
Water	33.73
Chloride	45.15
Other	-
RMSD from target values	
Bond lengths (Å)	0.018
Bond angles (°)	1.969
Dihedral angles (°)	5.893
Ramachandran	
Most favoured (%)	96.4
Allowed (%)	3.2
Disallowed (%)	0.4

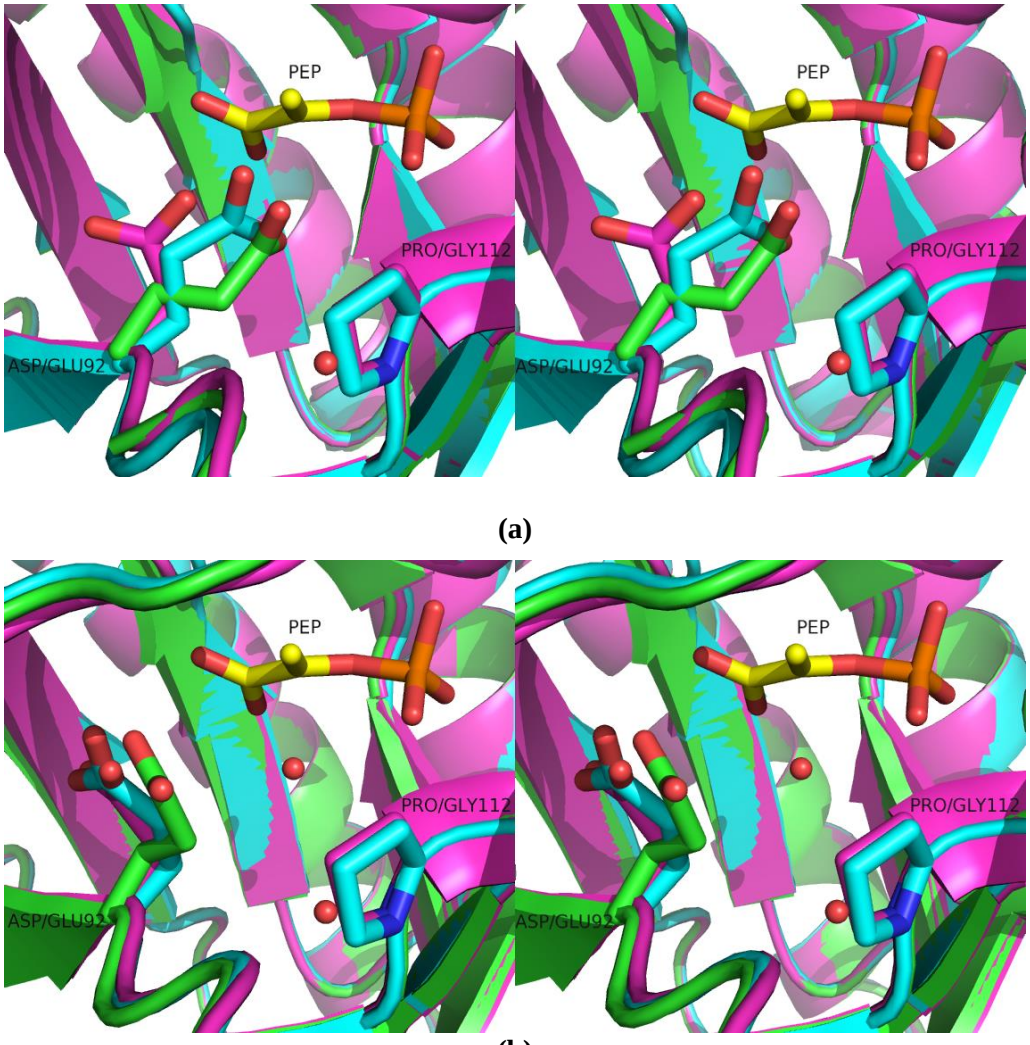

Figure 2.8: Stereoviews of the structure of the *Nme*D92E/P112G (coloured green). (a) Chain D, showing the configuration of D92E and P112G in chains A, C and D. (b) The configuration of D92E and P112G in chain B. The structures of *Nme*D92E/P112G in both subfigures are shown superimposed onto the structures of *Nme*KDO8PS wild-type enzyme (coloured purple) and D92E (coloured cyan). The water molecules shown are from the structure of *Nme*D92E/P112G. PEP (carbon atoms labelled yellow) is from the superimposed structure of *Bsp*KDO8PS (PDB code 3UND).

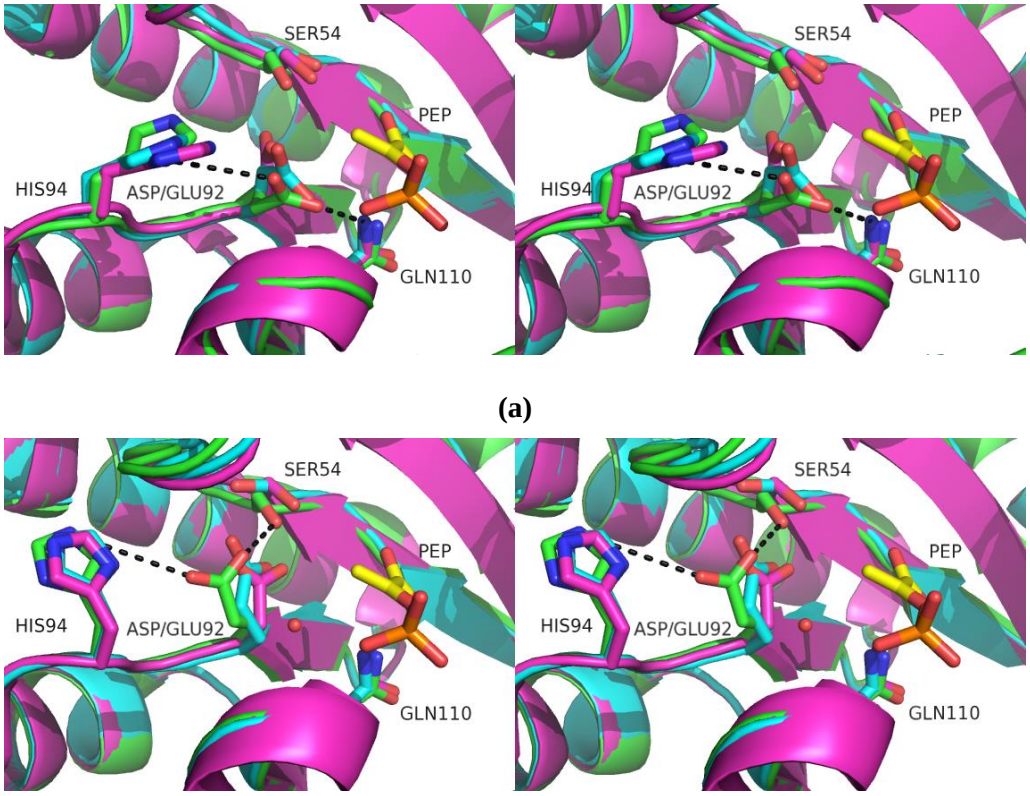

Figure 2.9: Stereoviews of the structure of the *Nme*D92E/P112G (coloured green). (a) Chain D, showing the configuration of D92E in chains A, C and D with hydrogen bonding to His94 and Gln110. (b) The configuration of D92E in chain B with hydrogen bonding to His94 and Ser54. The structures of *Nme*D92E/P112G in both subfigures are shown superimposed onto the structures of *Nme*KDO8PS wild-type enzyme (coloured purple) and D92E (coloured cyan). The water molecule shown is from the structure of *Nme*D92E/P112G. PEP (carbon atoms labelled yellow) is from the superimposed structure of *Bsp*KDO8PS (PDB code 3UND).

In the *Nme*D92E/P112G chain B, the D92E residue forms a unique orientation, where the side chain points away from the site where PEP is expected to bind, allowing the *re*-side water that is lost in the *Nme*D92E structure to return (Figure 2.8b). The *Nme*D92E chain B orientation is allowed due to the movement of the His94 side chain into another position, seen in the

*Nme*KDO8PS wild-type enzyme and *Nme*D92E chain B (Figure 2.9b). The *Nme*D92E chain B orientation hydrogen bonds to Ser54, seen in all the *Nme*KDO8PS wild-type chains, and *Nme*D92E chains A and B.

All four of the *Nme*D92E/P112G chains depict the putative proton relay chain in various stages of completion (Figure 2.10, overleaf). *Nme*D92E/P112G chain B has the only *re*-side water present and close enough to the D92E side chain. While there is no water molecule between the D92E and Lys57 side chains, the longer D92E side chain is close enough to directly form the relay to Lys57. The *Nme*D92E/P112G chain C has a near complete proton relay chain, including a water molecule between the D92E and Lys57 side chains, but no *re*-side water present. *Nme*D92E/P112G chain D has neither of the two water molecules present, and the Lys57 side chain is too distant from the aldehyde carbon of A5P. *Nme*D92E/P112G chain A also has neither of the two water molecules present, as well as the Lys57 side chain position being undefined.

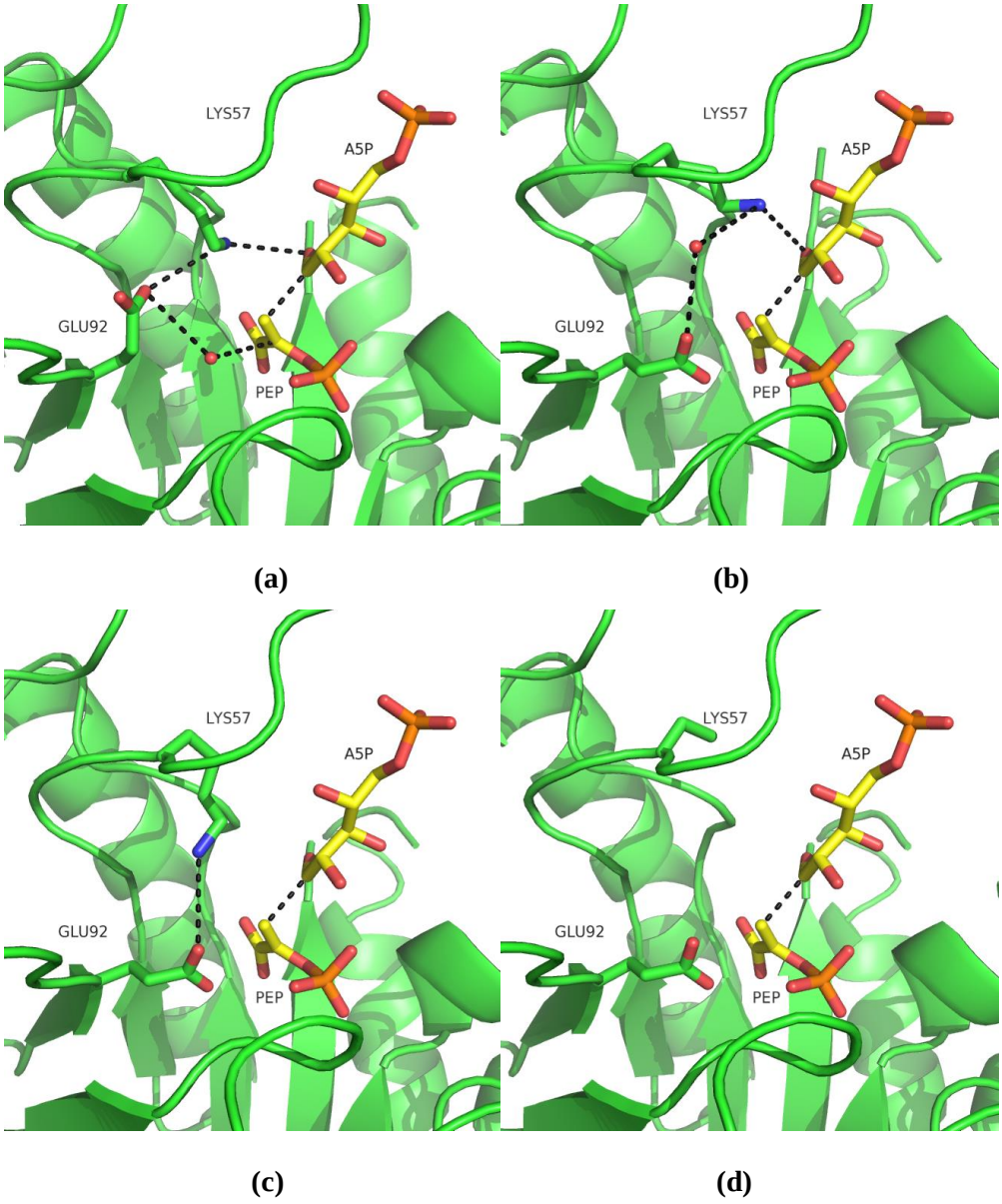

Figure 2.10: The putative proton relay chain in the structure of *Nme*D92E/P112G in decreasing form of completeness. (a) Chain B, showing a complete proton relay chain comprised of a water molecule on the *re* side of PEP, Glu92 and Lys57. (b) Chain C, showing an incomplete proton relay chain comprised of Glu92, a water molecule and Lys57. (c) Chain D, showing a fragmented proton relay chain comprised Glu92 and Lys57. (d) Chain C, showing no proton relay chain. PEP and A5P (carbon atoms labelled yellow) are from the superimposed structure of *Bsp*KDO8PS (PDB code 3UND).

2.6 Discussion

The role of the KDO8PS conserved Asp in the putative proton relay chain, was investigated by mutation to Glu, and coupled with the mutation of the neighbouring Pro to Ala as well as Gly in *Nme*KDO8PS. The mutant proteins were expressed and purified identically to that of the wild-type enzyme.

The *Nme*D92E/P112G mutant quaternary structure in solution and crystal structure was identical to that of the wild-type enzyme and *Nme*D92E. The introduced P112G mutation has completely recovered the PEP stabilisation effect PEP has upon binding the double mutant, which was completely lost in the original D92E mutation. This suggests that the introduced P112G mutation may have opened enough space in the active site to reorient the mutant D92E residue side chain, allowing a change in how the PEP interacts inside *Nme*D92E/P112G, as the P112G mutation is not close enough itself to interact with PEP directly.

There was a noticeable difference in stability and secondary structure in solution of *Nme*D92E/P112G mutant in comparison to that of the wild-type enzyme and *Nme*D92E, most likely caused by the increase in flexibility the introduced P112G mutation provides to the surrounding residues. This increase in flexibility in *Nme*D92E/P112G in comparison to the wild-type enzyme and *Nme*D92E, is also most likely the cause of the drastic reduction in k_{cat} and increase in K_m of both substrates.

The *Nme*D92E/P112G crystal structure shows that the introduced P112G mutation has indeed had an effect on the orientation of the D92E mutation. The *Nme*D92E/P112G chain B depicts a putative proton relay chain

able to perform catalysis, which was not seen in the original D92E mutant crystal structures. This also suggests that the *Nme*D92E/P112G is able to form the putative proton relay chain more easily than the *Nme*D92E mutant, and as a result should have had greater activity if the proton relay chain was involved in catalysis. However, it appears that the increase in flexibility in the active site has suppressed any potential increase in activity the putative proton relay chain could provide. To determine if the formation of the putative proton relay chain does cause an increase in activity, the single mutant *Nme*P112G would be required; to isolate out the effect that the increase in active site flexibility has created.

Intriguingly the D92E residue from the *Nme*D92E/P112G chain B forms an orientation completely different to that of DAH7PS (though the *re*-side water is in a similar location to that of DAH7PS). It is the D92E residues from the *Nme*D92E/P112G chains A, C and D which form an orientation similar to that of DAH7PS, even though they cannot create a complete putative proton relay chain (Figure 2.11, overleaf). However, in comparison to DAH7PS, the end of the *Nme*D92E/P112G D92E residue side chain is rotated around 90 degrees and closer to the PEP molecule, due to hydrogen bonding to different neighbouring residues. In *Nme*D92E/P112G the D92E residue side chain oxygen hydrogen bonds to His94 (DAH7PS proteins usually have a conserved small hydrophobic residue) on the α3 helix, whereas in DAH7PS, the residue hydrogen bonds to Asn187 (KDO8PS proteins have a conserved Leu) on the β4α4 loop. This difference allows a *re*-side water to be present in DAH7PS, while for KDO8PS to not. To encourage a complete DAH7PS-like proton relay chain inside *Nme*KDO8PS, would require the addition of a L115N mutation to go along with the D92E and P112G mutations. This would encourage the D92E residue to orientate similarly to that of DAH7PS. To

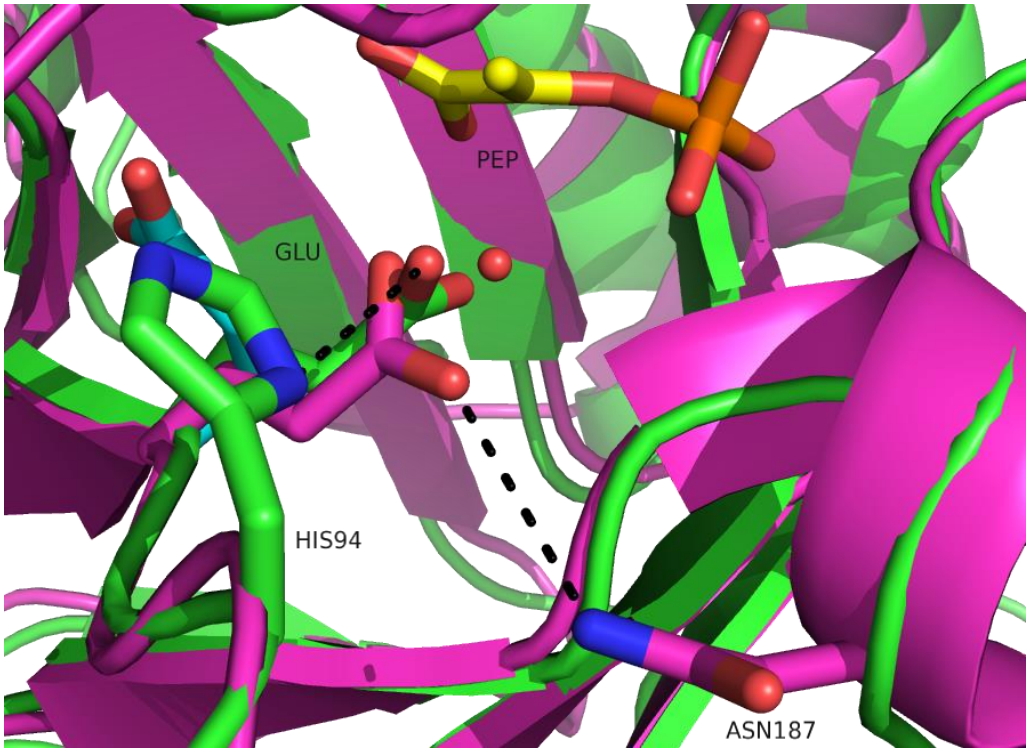

Figure 2.11: Superimposition of the structure of *Nme*D92E/P112G subunit C (coloured green) onto the structure of *Tma*DAH7PS (PDB code 1RZM, coloured purple, with the *re*-side water molecule). An additional Glu92 residue is superimposed from *Nme*D92E/P112G subunit B (coloured cyan). PEP is superimposed from the structure of *Bps*KDO8PS (PDB code 3UND, coloured yellow).

confirm the DAH7PS-like orientation, an additional H94L mutation may also be required. Alternatively, introducing the two mutations N116L and M95H into *Pfu*DAH7PS could encourage the *Pfu*DAH7PS active site Glu93 residue to form an orientation identical to *Nme*D92E/P112G, and provide information on the catalytic impact the unique orientation of *Nme*KDO8PS Glu92 has had.

The comparison of *Nme*D92E/P112A quaternary structure in solution to the wild-type enzyme, indicated the presence of a dimeric species of *Nme*D92E/P112A, non-existent in the wild-type enzyme and *Nme*D92E. No

*Nme*D92E/P112A crystal structure was obtained in the wild-type crystallisation conditions, so the exact dimer formed is not certain. In the *Nme*KDO8PS wild-type crystal structure, the P112A mutation is located right between the β6 beta-sheet and β6α6 loop, with the neighbouring β6α6 loop residues comprising part of the A-C interface of *Nme*KDO8PS. Since the introduced Ala mutation would no longer be a helix breaker, this mutation may have affected the positioning of the residues on the β6α6 loop. This suggests that the introduced Ala mutation disrupts the A-C interface, indicating that the dimeric species present in *Nme*D92E/P112A is comprised of the A-B KDO8PS dimer.

The introduced P112A mutation also had a drastic effect on the activity of *Nme*D92E/P112A. The introduced P112A mutation has mitigated most of the increase in K_m^{PEP} that the original D92E mutation created. This suggests that the introduced P112A mutation may have opened enough space in the active site to reorient the D92E mutation, allowing the PEP substrate to bind with more ease. This reorientation of the D92E mutation is also likely the cause of the partial recovered stabilisation effect PEP has upon binding, which was completely lost in the original D92E mutation. The introduced P112A mutation has a drastically decreased the k_{cat} in comparison to the original D92E mutation. This effect is unlikely to be due to any possible active site rearrangement the introduced P112A mutation caused, instead due to the larger quaternary structure destabilisation that gave rise to an A-B dimeric species of *Nme*D92E/P112A. Past studies on a specific Arg residue in the A-C interface which interacts with the other subunit active site, have determined a drastic reduction in activity when mutated to smaller residues such as Ala and Gly.[4, 133] In addition the *Nme*D92E/P112A double mutant still has a k_{cat} a sixth of that of the double mutant *Nme*D92E/P112G, which has a far more flexible and

disrupted active site but still remains completely tetrameric. To completely clarify which effects are caused by active site rearrangement in comparison to quaternary structure destabilisation, the single mutant *Nme*P112A would need to be generated and characterised. The *Nme*D92E/P112A mutant will also be mentioned again in Chapter 3 of this thesis, which investigates mutations destabilising the quaternary structure of *Nme*KDO8PS.

2.7 Summary

The results in this chapter have identified that the conserved Pro is important structurally for providing rigidity in the KDO8PS active site, as well as being important in the formation of the KDO8PS tetramer. The residue appears to be important for KDOO8PS activity, with mutation (to Ala and Gly) adversely affecting the kinetic parameters of *Nme*KDO8PS. The results do not rule out the conserved Asp residue potentially being part of a proton relay mechanism, in the KDO8PS active site. However, the results also do not eliminate the possibility that the proton supplied to the carbonyl of A5P originates from an alternative source instead. Mutation of the Asp and Pro in KDO8PS for the DAH7PS-conserved Glu and Gly respectively are accommodated, but could be optimised by coupling the changes with mutation to other conserved differences between the two enzymes.

Chapter 3

Investigation into the relationship between KDO8PS quaternary structure, stability and activity

3.1 Introduction

In past studies, the characterisation of bacterial KDO8PS indicated that the quaternary structure of bacterial KDO8PS was tetrameric.[6, 14, 19, 21, 35, 85, 90] In contrast, the few studies which had been performed to characterise plant KDO8PS initially indicated that the quaternary structure of plant KDO8PS was dimeric,[131] before more recent characterisation suggested that the quaternary structure of plant KDO8PS should actually be tetrameric.[138] The characterised

and crystallised plant *Ath*KDO8PS, which exhibits tetramer interface residues similar to most other plant KDO8PS, forms a tetramer in solution and crystal structure.[131] The plant *Pe*KDO8PS however, was reported to form both tetrameric and dimeric species in solution, though which dimer is formed, as well as the reason why the dimer is formed is not given in the paper.[140]

There have been very few studies that have investigated the KDO8PS interfaces, in addition to determining if the optimal functional unit for catalysis in KDO8PS is the tetramer. Electrospray ionisation mass spectrometry determined that the substrates PEP and A5P can have an effect on the stability of the KDO8PS tetramer,[71, 72] as well as the metal ion in metal-dependent KDO8PS.[19, 73]

In a past study involving *S. typhimurium* (*Sty*) KDO8PS, a P145S mutation gave rise to a suspected dimeric species along with the original tetramer.[120] This residue is located on the A-C tetramer interface at the beginning of the α5 helix, so mutation of this helix breaking Pro residue is suspected to have disrupted the area around the α5 helix and the subsequent interactions across the A-C tetramer interface to the β6α6 loop. At 25 °C and 37 °C the *Sty*P145S mutant was less active than that of the *Sty*KDO8PS wild-type enzyme, and while the *Sty*KDO8PS wild-type enzyme became more active when the temperature was increased, the *Sty*P145S mutant activity instead decreased. In addition, as the temperature rose from 15 °C to 35 °C, the *Sty*P145S mutant oligomeric state moved from 70% dimer to completely dimer. This suggested that the increase in dimer from the disruption of the A-C tetramer interface does have a severe effect on the activity of KDO8PS. It should be noted however, that on native PAGE at 35 °C, the *Sty*P145S mutant dimeric species exhibited considerable smearing compared to lower temperatures, which could indicate that the dimer had begun to unravel and

denature. This would suggest that the reduction in the *Sty*P145S mutant activity was not solely due to the increase in dimeric species, but due to denaturing of the dimer at the higher temperature.

In the past study of *Pe*KDO8PS, while the protein is stated to be active, no in-depth kinetic experiments of *Pe*KDO8PS were perfromed, as well as no DSF experiments.[140] So, it is still unknown if disruption of a tetramer interface does have a severe effect on the activity and stability of KDO8PS, as well as if the optimal functional unit for catalysis in KDO8PS is the tetramer and not a possible dimer. An explanation on why the plant *Pe*KDO8PS is partially dimeric would also provide more insight into the destabilisation of the KDO8PS tetramer. The partially dimeric plant *Pe*KDO8PS shares 84% identity with the tetrameric plant *Ath*KDO8PS isozyme 2.[140] None of the residues found on the *Pe*KDO8PS A-B tetramer interface, compared to *Ath*KDO8PS isozyme 2, are truncated or introduce a possible steric or charge clash. On the A-C tetramer interface however, one residue is identified to be of interest. The unique residue is located on the A-C tetramer interface on the β6α6 loop, which is usually a conserved Asn residue in plant KDO8PS, whereas in *Pe*KDO8PS is instead a unique shorter Ser residue. This decrease in length could make the residue no longer able to interact across the A-C tetramer interface with the β5α5 loop and α5 helix. This is also in the area where destabilisation gave rise to the partially dimeric *Sty*P145S mutant.

To investigate the KDO8PS interfaces, a well characterised, easily crystallised KDO8PS would be ideal. In addition, a metal-independent KDO8PS would be preferable, as the metal species present in metal-dependent KDO8PS has been indicated to have an effect on the stability of the KDO8PS tetramer.[19, 73] From these requirements, *Nme*KDO8PS was chosen as the optimum KDO8PS to utilise.

The *Nme*KDO8PS tetramer is comprised of two interfaces, both located in the same regions in all KDO8PS proteins (Figure 3.1). One interface is formed from the interaction between subunits A and C (or B and D). The *Nme*KDO8PS A-C tetramer interface is comprised of numerous hydrogen-bonds, salt-bridges and hydrophobic interactions (Figure 3.2a, overleaf). The A-C tetramer interface is highly conserved over all bacterial and plant KDO8PS, with a small number of residues that only differ depending on if the KDO8PS is a metal-dependent bacterial, metal-dependent bacterial or plant

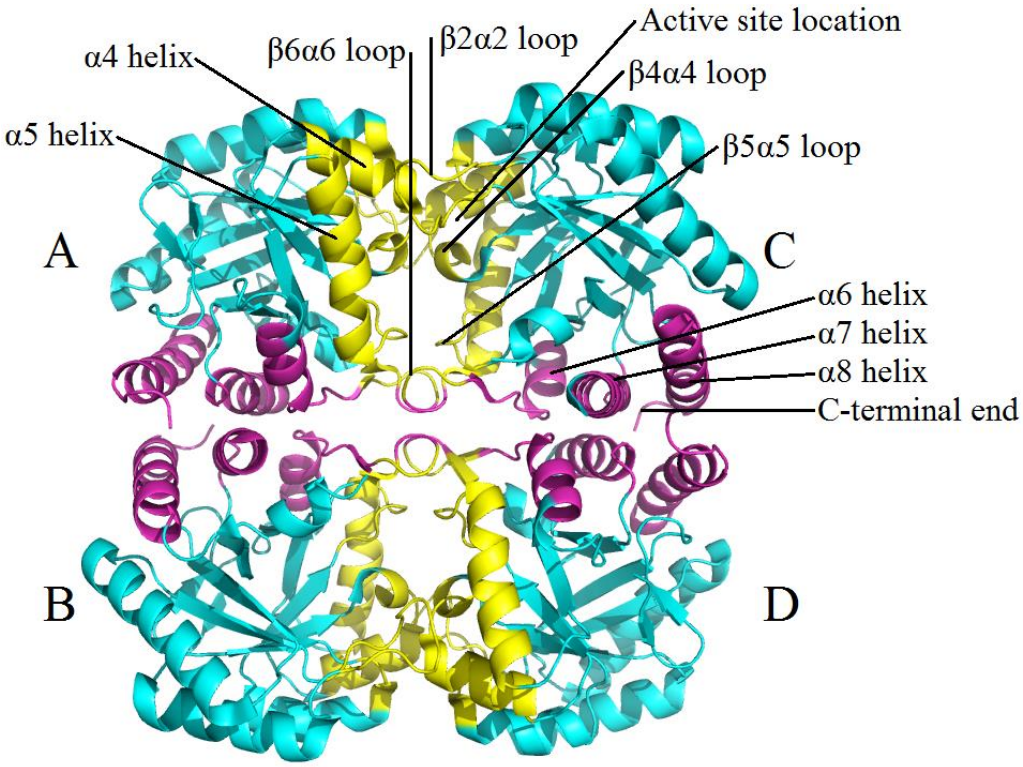

Figure 3.1: The structure of metal-independent *Nme*KDO8PS (PDB code 2QKF). Four monomers are shown depicting the two separate interfaces. The A-C tetramer interface is coloured in yellow, the A-B tetramer interface magenta, and the non-interface structure in cyan.

KDO8PS. When plant KDO8PS were still thought to be dimeric, this was the interface believed not to exist, due to the conserved differences. The other interface is formed from the interaction between subunits A and B (or C and D). The *Nme*KDO8PS A-B tetramer interface is comprised of nearly entirely hydrophobic interactions, as well as a small number of hydrogen-bonds and

(a) **(b)**

Figure 3.2: The *Nme*KDO8PS tetramer interface interactions. (a) *Nme*KDO8PS A-C tetramer interface. (b) *Nme*KDO8PS A-B tetramer interface. Hydrogen bonds are coloured blue, salt-bridges are coloured green and hydrophobic interactions are coloured red. These tetramer interface interactions are constructed from the *Nme*KDO8PS structure (PDB code 2QKF).

salt-bridges (Figure 3.2b). The A-B tetramer interface is also highly conserved over all bacterial and plant KDO8PS.

In this chapter, significant residues in the A-C and A-B tetramer interfaces of *Nme*KDO8PS are identified and mutated in attempt to destabilise a KDO8PS tetramer interface. The results of these mutations on the structure and activity of *Nme*KDO8PS were then used to shed light on the optimal functional unit for catalysis in KDO8PS and the role of the KDO8PS quaternary structure in providing enzymatic function.

3.2 Preparation and rationale for the mutants

To identify significant residues within both the A-C and A-B tetramer interfaces, PDBePISA was utilised.[65] Microsoft Excel was then used to plot the data as tetramer interface interaction diagrams (Figures 3.2a and 3.2b). To destabilise the A-C tetramer interface, six single mutations were chosen, which can be categorised by three separate intentions (Figure 3.3, overleaf).

The first two mutations attempted to destabilise the A-C tetramer interface by creating a more plant-like KDO8PS. The first residue, Ile63 is the most hydrophobic small residue found within the *Nme*KDO8PS A-C tetramer interface and has numerous hydrophobic interactions with many residues across the A-C tetramer interface (Figure 3.4, overleaf). This residue is conserved as a small hydrophobic residue in bacterial KDO8PS, which continue to interact with many residues across the A-C tetramer interface. However, in plant KDO8PS this residue is conserved as a more hydrophilic Ser residue. The mutation I63S would disrupt the numerous hydrophobic interactions across the A-C tetramer interface. The second residue chosen to

mutate was Glu154, one of the residues which Ile63 also shares the same space with (Figure 3.4, overleaf). In metal-independent bacterial KDO8PS this residue is highly conserved as Glu, which interacts with three residues across the A-C tetramer interface, utilising hydrogen bonding for two of the interactions. However, in plant KDO8PS this residue is conserved as a

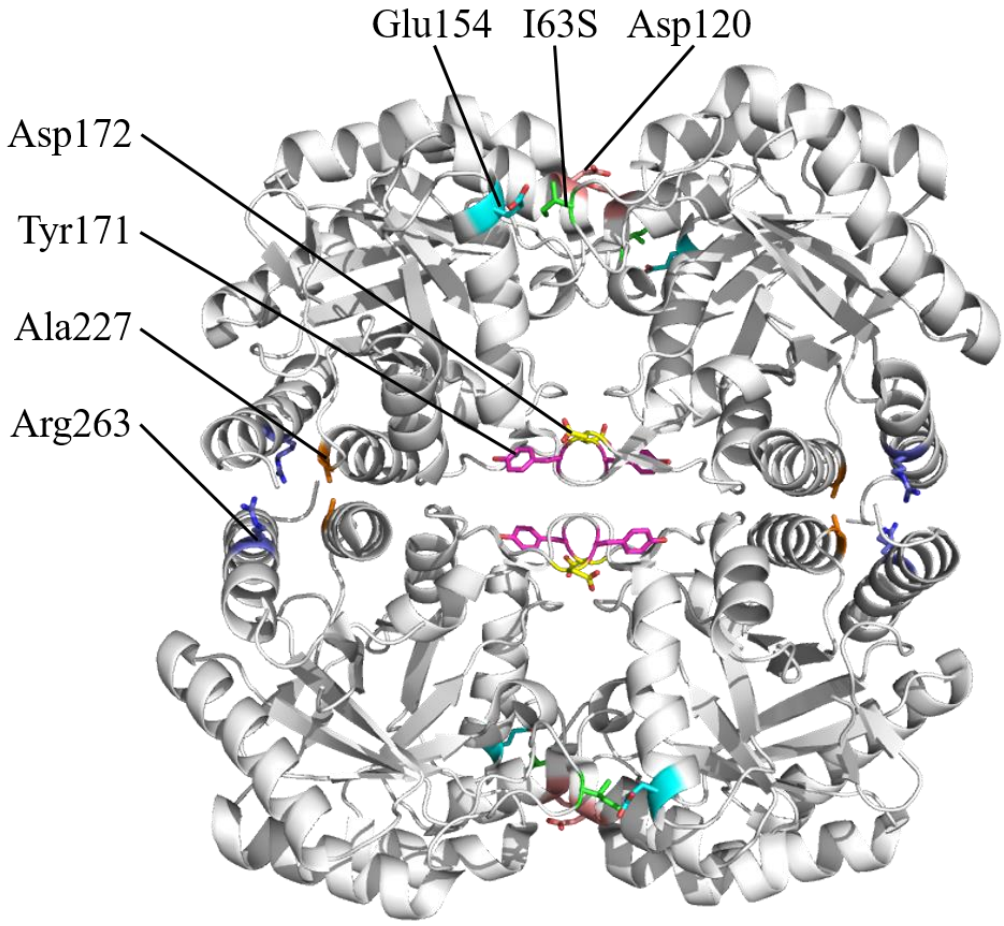

Figure 3.3: The seven total residues of interest on metal-independent *Nme*KDO8PS (PDB code 2QKF). The five residues of interest on the A-C tetramer interface are Ile63 (coloured green), Glu154 (coloured cyan), Tyr171 (coloured magenta), Asp172 (coloured yellow) and Asp120 (coloured salmon). The two residues of interest on the A-B tetramer interface are Ala227 (coloured orange) and Arg263 (coloured dark blue).

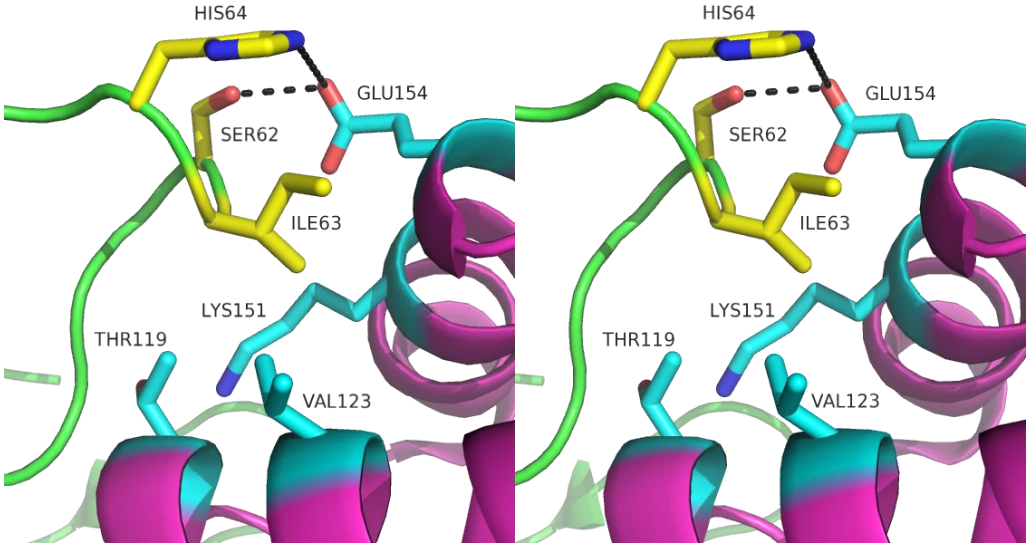

Figure 3.4: Stereoview of *Nme*KDO8PS structure (PDB code 2QKF) showing the A-C tetramer interface interactions residues Ile63 and Glu154 have across the interface. Subunit A is coloured green, subunit A residues of interest coloured yellow, subunit C is coloured magenta, and subunit C residues of interest are coloured cyan.

hydrophobic Leu residue. The mutation E154L would disrupt the two hydrogen bond interactions across the interface. In addition, since both I63S and E154L would be able to interact with each other, the double mutation I63S/E154L was also generated.

The subsequent two mutations attempted to destabilise the A-C tetramer interface by targeting the area where the *Sty*P145S and *Pe*KDO8PS residues of interest are present: the area between the α5 helix and the β6α6 loop. Instead of the mutation of the *Nme*KDO8PS equivalent Pro142, residues that interact with this residue, as well as residues on the β6α6 loop were targeted. The first residue Tyr171 is highly conserved in all KDO8PS and interacts with two separate sections of KDO8PS across the A-C tetramer interface, using hydrophobic interactions and hydrogen bonding (Figure 3.5, overleaf). The mutation Y171A would remove these interactions across the A-C tetramer

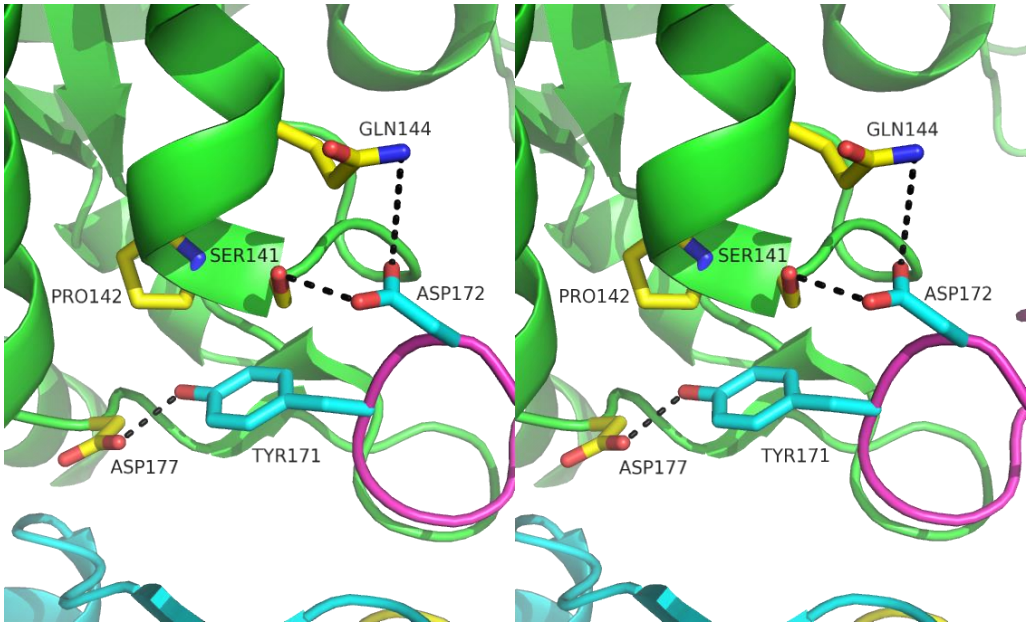

Figure 3.5: Stereoview of *Nme*KDO8PS structure (PDB code 2QKF) showing the A-C tetramer interface interactions residues Tyr171 and Asp172 have across the interface. Subunit A is coloured green, subunit A residues of interest coloured yellow, subunit C is coloured magenta, subunit C residues Tyr171 and Asp172 are coloured cyan, subunit B is coloured cyan and subunit D is coloured yellow.

interface. The second residue Asp172 is highly conserved in metal-independent bacterial KDO8PS, while in plant and metal-dependent bacterial KDO8PS is highly conserved as the residue Asn. In addition, this is the position the residue of interest in the plant *Pe*KDO8PS is located. Asp172 interacts with the area around the α5 helix, via a salt bridge and hydrogen bonding (Figure 3.5). The mutation D172A would remove these interactions across the A-C tetramer interface.

The final two mutations attempted to destabilise the A-C tetramer interface by introducing charge and steric disruptions. The first residue Asp120 is highly conserved in all KDO8PS and forms two of the three possible salt bridges across the A-C tetramer interface (Figure 3.6, overleaf). The mutation

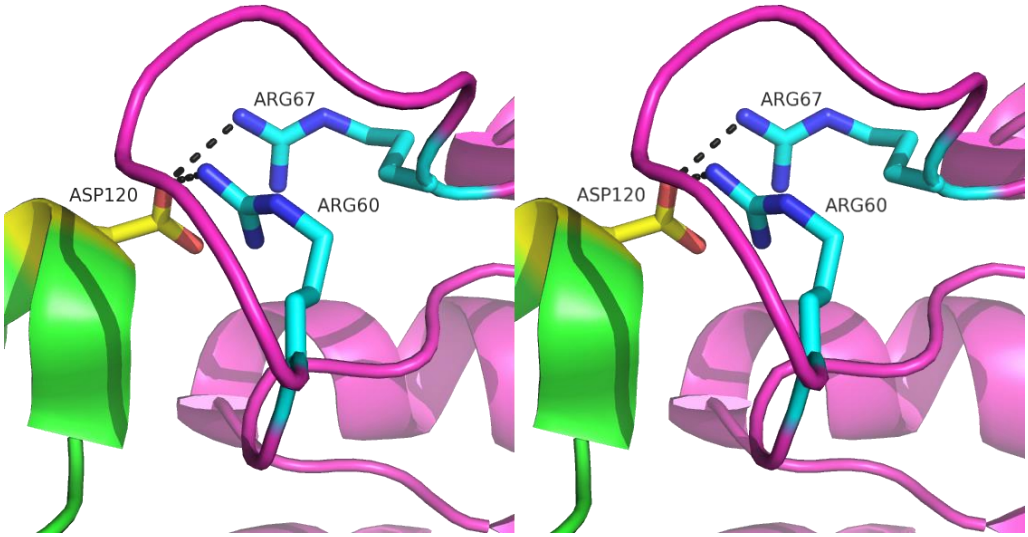

Figure 3.6: Stereoview of *Nme*KDO8PS structure (PDB code 2QKF) showing the A-C tetramer interface interactions residue Asp120 has across the interface. Subunit A is coloured green, subunit A residue Asp120 is coloured yellow, subunit C is coloured magenta, and subunit C residues of interest are coloured cyan.

D120H would introduce charge and steric disruptions. The second mutation revisited Ile63 (Figure 3.4). The mutation I63W would create significant steric disruption around this region.

To destabilise the A-B tetramer interface, three single mutations were chosen. The first mutation attempted to destabilise the A-B tetramer interface by removing the remaining salt-bridges and hydrogen-bonds in this interface. The residue Arg263 was targeted, as it was the sole residue in the A-B tetramer interface to contribute to all these interactions (Figure 3.7, overleaf). The mutation R263A would remove all the salt-bridges and hydrogen-bonds in the A-B tetramer interface. The second mutation utilised charge and steric disruptions to disrupt the A-B tetramer interface. The residue Ala227 is located near the centre of the A-B tetramer interface, is highly conserved as a small Ala or Ser in all KDO8PS and interacts with its equivalent across the interface

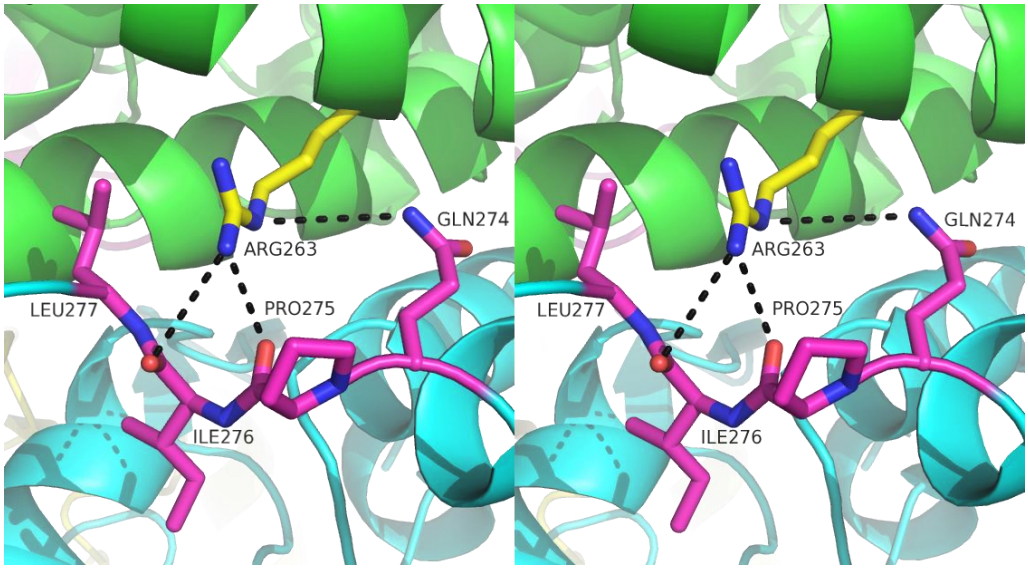

Figure 3.7: Stereoview of *Nme*KDO8PS structure (PDB code 2QKF) showing the A-B tetramer interface interactions residue Arg263 has across the interface. Subunit A is coloured green, subunit A residue Arg263 is coloured yellow, subunit B is coloured cyan, and subunit B residues of interest are coloured magenta.

(Figure 3.8, overleaf). The mutation A227R would force apart the A-B tetramer interface around the tightly packed residue. The third mutation, which was more substantial, would remove half of the entire A-B tetramer interface. The residue Arg263 was again targeted, and the mutation R263term would end the *Nme*KDO8PS earlier in sequence to that of the wild-type enzyme (Figure 3.9). This mutation would expose fewer hydrophobic residues in comparison to the actual intact A-B tetramer interface residue. In an addition, the most drastic of all, the double mutant A227R/R263term was generated.

Once the KDO8PS mutants were generated, they were expressed using the same procedures as the wild-type enzyme.[21] SDS-PAGE was utilised to identify the presence of the mutants in the soluble lysate. All *Nme*KDO8PS A-C tetramer interface single mutants were determined to be soluble, however the

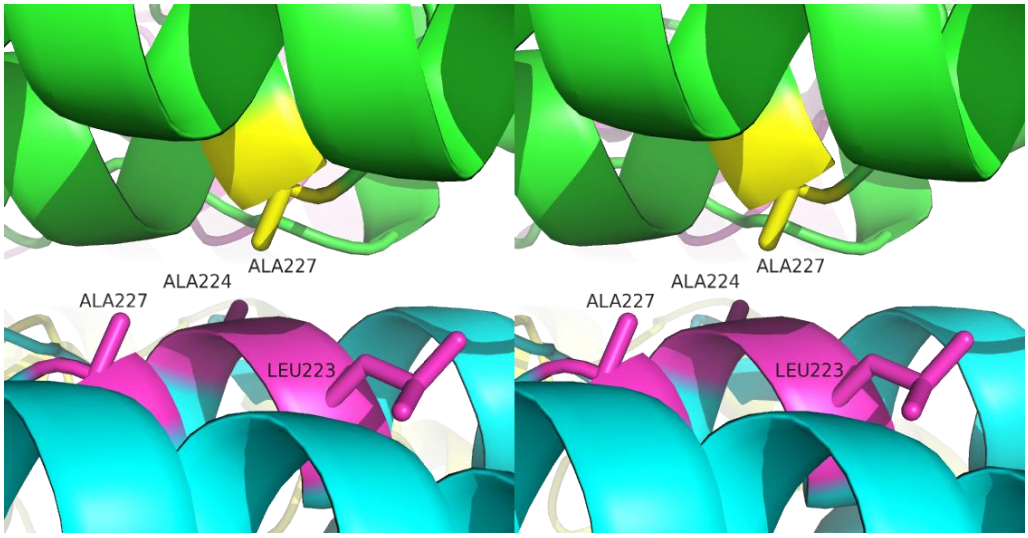

Figure 3.8: Stereoview of *Nme*KDO8PS structure (PDB code 2QKF) showing the A-B tetramer interface interactions residue Ala227 has across the interface. Subunit A is coloured green, subunit A residue Ala227 is coloured yellow, subunit B is coloured cyan, and subunit B residues of interest are coloured magenta.

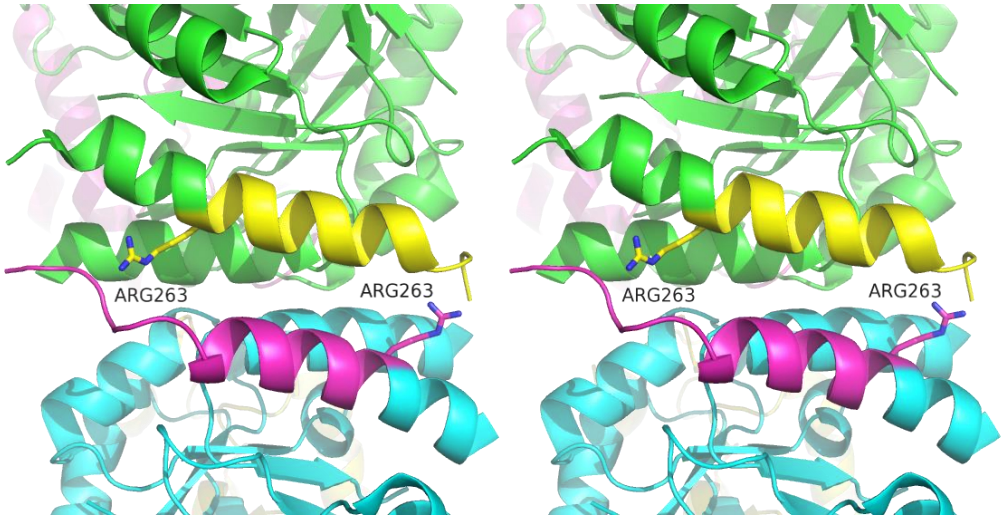

Figure 3.9: Stereoview of *Nme*KDO8PS structure (PDB code 2QKF) showing removal of the A-B tetramer interface section by the mutation R263term. Subunit A is coloured green, subunit A section removed is coloured yellow, subunit B is coloured cyan, and subunit B section removed is coloured magenta.

double mutant *Nme*I63S/E154L was insoluble. Of all the *Nme*KDO8PS A-B tetramer interface single and double mutants, only *Nme*R263A was found to be soluble; *Nme*A227R, *Nme*R263term and *Nme*A227R/R263term were insoluble. Attempts to recover soluble protein from the insoluble *Nme*KDO8PS mutants were all unsuccessful. Attempts include using a lower temperature after cell induction, reducing the sonication duration for lysis, alternative lysis by chemical detergent BugBuster® Protein Extraction Reagent (Merck), and incorporation of 5% glycerol into the lysis buffer.

All soluble *Nme*KDO8PS A-C and A-B tetramer interface single mutants were purified using the same purification procedures as the wild-type enzyme.[21] After lysing the bacterial cell cultures, the proteins were purified via anion-exchange chromatography, followed by hydrophobic-interaction chromatography, and completed via size-exclusion chromatography. All soluble *Nme*KDO8PS A-C and A-B tetramer interface single mutants after purification were of a similar purity (Figure 3.10, overleaf). From 1 L of bacterial cell culture, *Nme*I63S was purified with a varying yield of 2 to 6 mg of protein, *Nme*E154L with a yield of 4 mg, *Nme*Y171A with a varying yield of 2 to 5 mg, N*me*D172A with a varying yield of 2 to 5 mg, *Nme*D120H with a yield of 2.5 mg, *Nme*I63W with a yield of 12 mg and *Nme*R263A with a yield of 5 mg.

3.3 Structure in solution and stability

Electrospray ionisation mass spectrometry was used to confirm successful mutation via comparison of the measured mass of the *Nme*KDO8PS A-C and

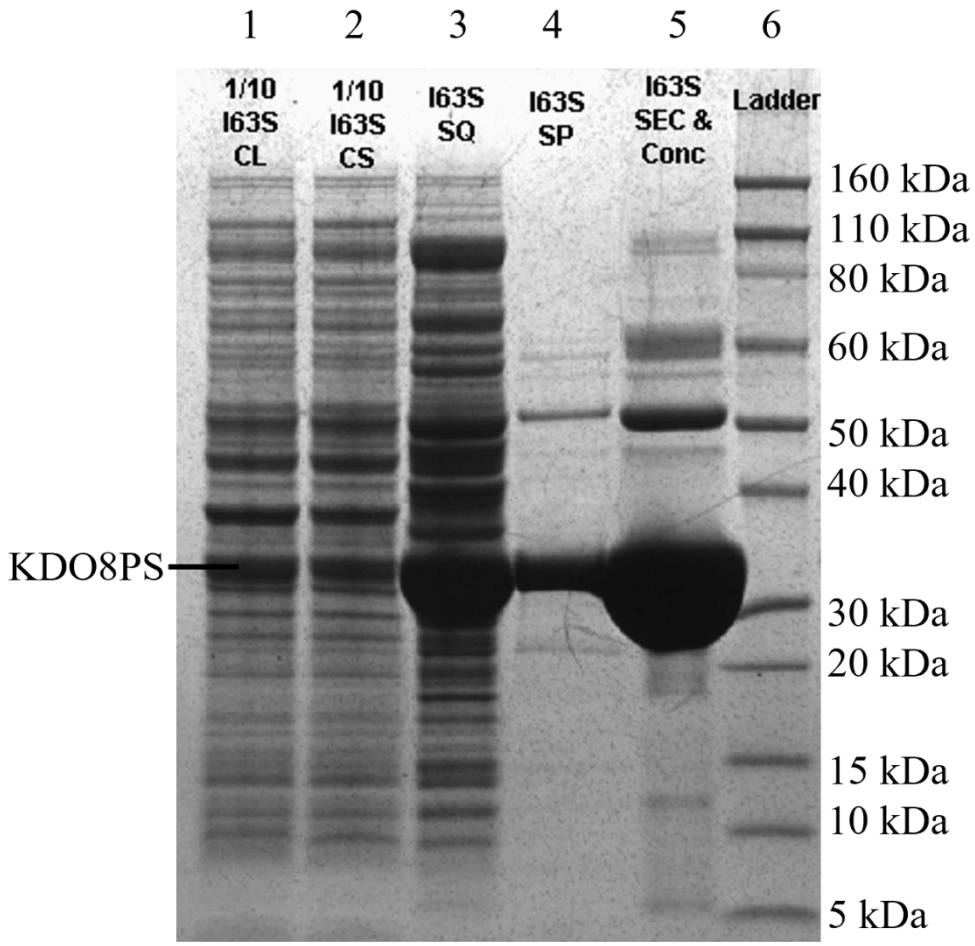

Figure 3.10: The purity of the *Nme*KDO8PS enzyme after each purification step, using *Nme*I63S. (Column 1) Crude lysate after sonication, diluted by a factor of ten. (Column 2) Crude soluble lysate after removal of insoluble lysate, diluted by a factor of ten. (Column 3) The gathered Source™ 15Q fractions after anion-exchange chromatography. (Column 4) The gathered Source™ 15PHE fractions after hydrophobic-interaction chromatography. (Column 5) The gathered HiLoad 26/60 Superdex™ 200 prep grade column fractions after size-exclusion chromatography and spin concentration. (Column 6) Novex® Sharp Pre-Stained Protein Standards (Thermo Fisher Scientific).

A-B tetramer interface mutants to the calculated mass. All *Nme*KDO8PS A-C and A-B tetramer interface mutants have a mass similar to that of their calculated mass. *Nme*I63S had a resulting mass of 30456.6 Da (compared to

calculated mass 30457.3 Da), *Nme*E154L had resulting mass of 30465.8 Da (compared to calculated mass 30467.4 Da), *Nme*Y171A had a resulting mass of 30390.6 Da (compared to calculated mass 30391.2 Da), *Nme*D172A had a resulting mass of 30438.9 Da (compared to calculated mass 30439.3 Da), *Nme*D120H had a resulting mass of 30506.4 Da (compared to calculated mass 30505.4 Da), and *Nme*I63W had a resulting mass of 30557.3 Da (compared to calculated mass 30556.4 Da). The *Nme*KDO8PS A-B tetramer interface mutant *Nme*R263A had a resulting mass of 30397.6 Da (compared to calculated mass 30398.2 Da).

CD spectrophotometry was used to assess if any introduced mutations produced perturbations in the secondary structure arrangement of the *Nme*KDO8PS A-C and A-B tetramer interface mutants. The spectra of five of the *Nme*KDO8PS A-C tetramer interface mutants (*Nme*I63S, *Nme*Y171A, *Nme*D172A, *Nme*D120H and *Nme*I63W), and the A-B tetramer interface mutant *Nme*R263A, were like that of the wild-type enzyme. Only the spectrum of the A-C tetramer interface mutant *Nme*E154L showed some difference to that of the wild-type enzyme (Figure 3.11, overleaf).

The melting temperatures of the *Nme*KDO8PS A-C and A-B tetramer interface mutants were determined using DSF, with and without the presence of the KDO8PS substrates PEP and A5P (Table 3.1, overleaf), to see if the introduced mutations destabilised the KDO8PS. All *Nme*KDO8PS A-C and A-B tetramer interface mutants were less stable than the *Nme*KDO8PS wild-type enzyme. All *Nme*KDO8PS A-C and A-B tetramer interface mutants were stabilised by PEP, and unaffected by A5P, like that of the *Nme*KDO8PS wild-type enzyme.

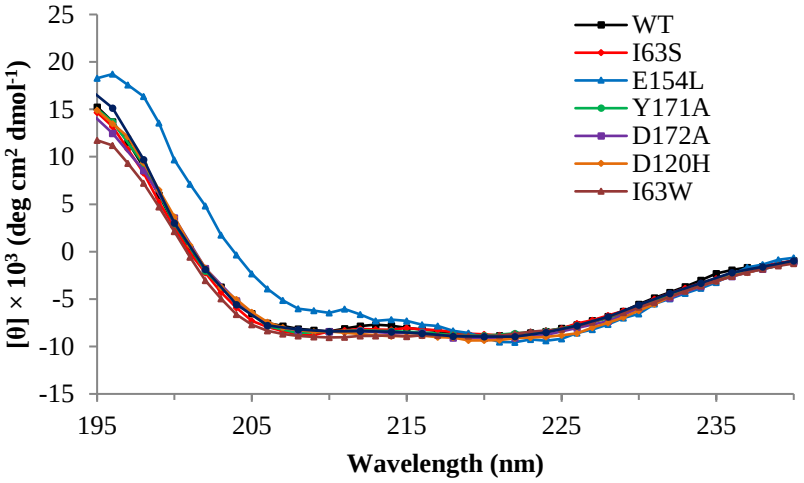

Figure 3.11: CD spectrophotometry of the *Nme*KDO8PS wild-type enzyme, A-C and A-B tetramer interface mutants. *Nme*KDO8PS wild-type enzyme: black squares; *Nme*I63S: red diamonds; *Nme*E154L: blue triangles; *Nme*Y171A: green circles; *Nme*D172A: purple squares; *Nme*D120H: orange diamonds; *Nme*I63W: brown triangles; *Nme*R263A: dark blue circles. Every datum point is plotted for the wild-type enzyme and single-mutants.

To see if the introduced mutations destabilised a tetramer interface, the quaternary structure in solution of the *Nme*KDO8PS A-C and A-B tetramer interface mutants was determined by analytical SEC, native PAGE and AUC. All but one of the *Nme*KDO8PS A-C and A-B tetramer interface mutants eluted with similar SEC profiles, at a mass corresponding to 130 kDa, identical to the previous wild-type enzyme SEC experiments (Table 3.2, overleaf). Native PAGE showed a similar result; with the *Nme*KDO8PS A-C tetramer interface mutant Y171A migrated at a smaller mass compared to all other *Nme*KDO8PS A-C and A-B tetramer interface mutants, which all migrated to a similar mass to the wild-type enzyme.

AUC, the most reliable technique in the determination of quaternary structure in solution, also exhibited a similar result to that of analytical SEC

Table 3.1: The effect of additives on the T_m of *Nme*KDO8PS wild-type enzyme, A-C and A-B tetramer interface mutants. Those for the wild-type enzyme was determined by Allison, T. M.[3]

*Nme*KDO8PS	Additives	T_m (°C)	Diff.	Diff. to WT
Wild-type	No additive	58 ± 1		
	PEP	61 ± 1	3	
	A5P	58 ± 1	0	
I63S	No additive	51 ± 1		-7
	PEP	53 ± 1	2	-8
	A5P	51 ± 1	0	-7
E154L	No additive	52 ± 1		-6
	PEP	55 ± 1	3	-6
	A5P	52 ± 1	0	-6
Y171A	No additive	49 ± 1		-9
	PEP	51 ± 1	2	-10
	A5P	49 ± 1	0	-9
D172A	No additive	47 ± 1		-11
	PEP	52 ± 1	5	-9
	A5P	47 ± 1	0	-11
D120H	No additive	51 ± 1		-7
	PEP	54 ± 1	3	-7
	A5P	51 ± 1	0	-7
I63W	No additive	53 ± 1		-5
	PEP	56 ± 1	3	-5
	A5P	53 ± 1	0	-5
R263A	No additive	53 ± 1		-5
	PEP	58 ± 1	5	-3
	A5P	53 ± 1	0	-5

and native PAGE. Sedimentation velocity experiments determined that all *Nme*KDO8PS A-C and A-B tetramer interface mutants showed a sedimentation coefficient corresponding to a tetramer (Figure 3.12, overleaf). There is also a small other peak observed, which is unclear what it can be attributed to and

Table 3.2: The SEC profiles of the *Nme*KDO8PS wild-type enzyme, A-C and A-B tetramer interface mutants. All proteins were at a concentration of 1 mg mL^{-1}.

*Nme*KDO8PS	Elute (mL)	Calculated Molecular Weight (kDa)
Wild-type	13.6	132
I63S	13.5	140
E154L	13.7	130
Y171A	14.7	78
D172A	13.9	115
D120H	13.7	126
I63W	13.9	116
R263A	13.6	136

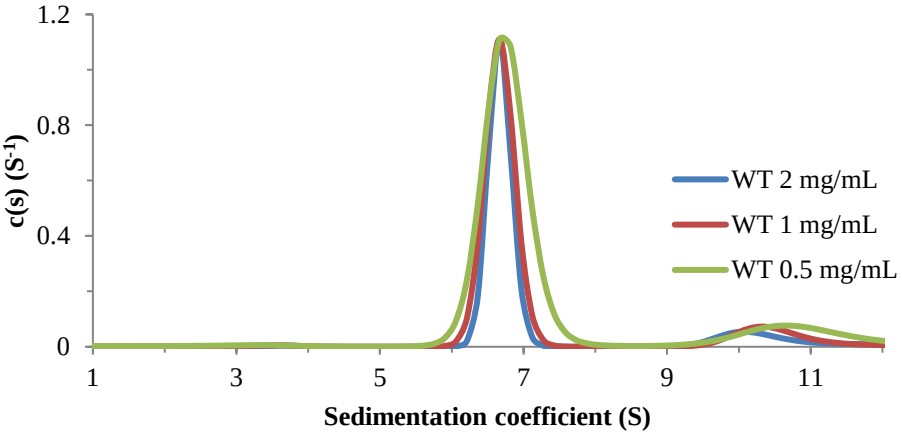

(a)

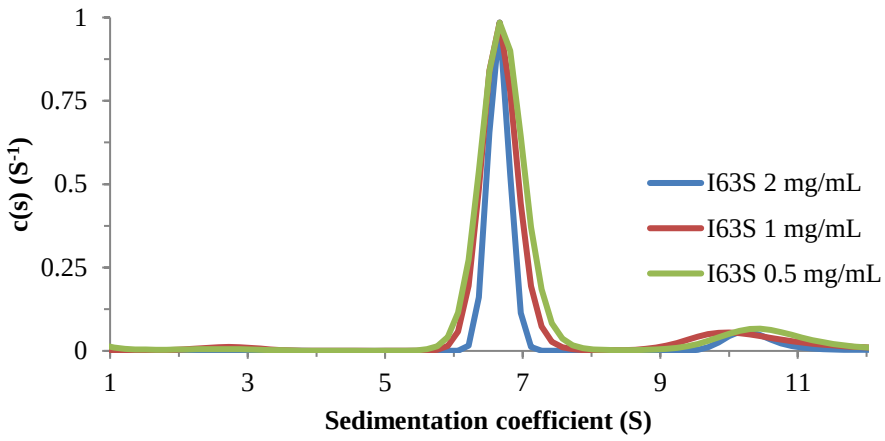
1
0.75
0.5
0.25
0
c(s) (S-1)
1
3
5
7
9
11
Sedimentation coefficient (S)
I63S 2 mg/mL
I63S 1 mg/mL
I63S 0.5 mg/mL

(b)

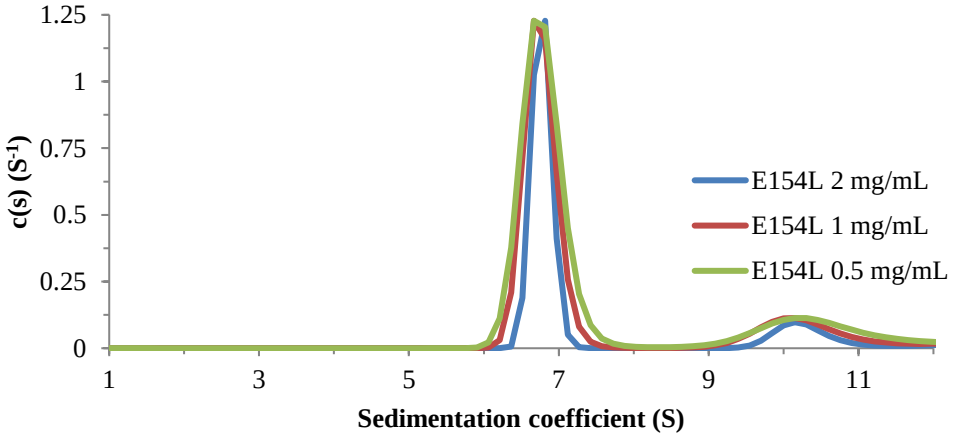
1.25
1
0.75
0.5
0.25
0
c(s) (S-1)
1
3
5
7
9
11
Sedimentation coefficient (S)
E154L 2 mg/mL
E154L 1 mg/mL
E154L 0.5 mg/mL

(c)

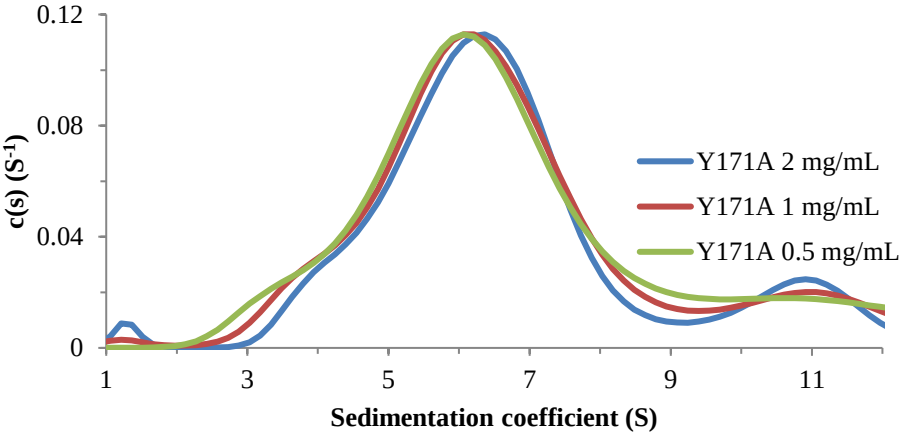
0.12
0.08
0.04
0
c(s) (S-1)
1
3
5
7
9
11
Sedimentation coefficient (S)
Y171A 2 mg/mL
Y171A 1 mg/mL
Y171A 0.5 mg/mL

(d)

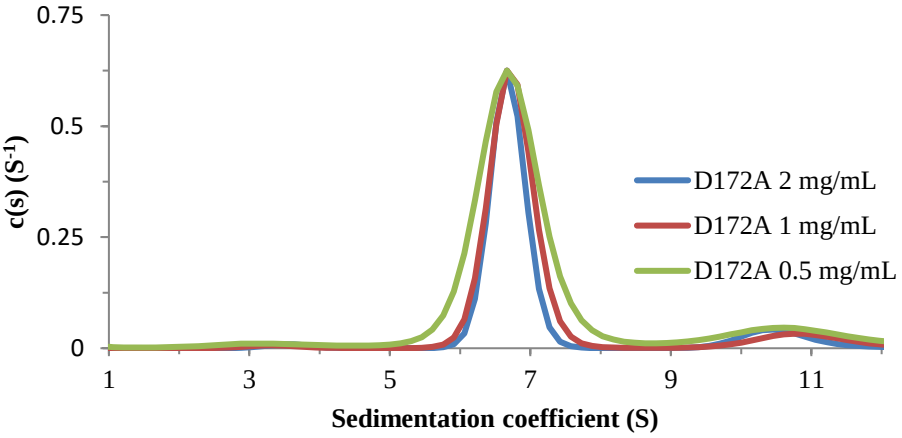
0.75
0.5
0.25
0
c(s) (S-1)
1
3
5
7
9
11
Sedimentation coefficient (S)
D172A 2 mg/mL
D172A 1 mg/mL
D172A 0.5 mg/mL

(e)

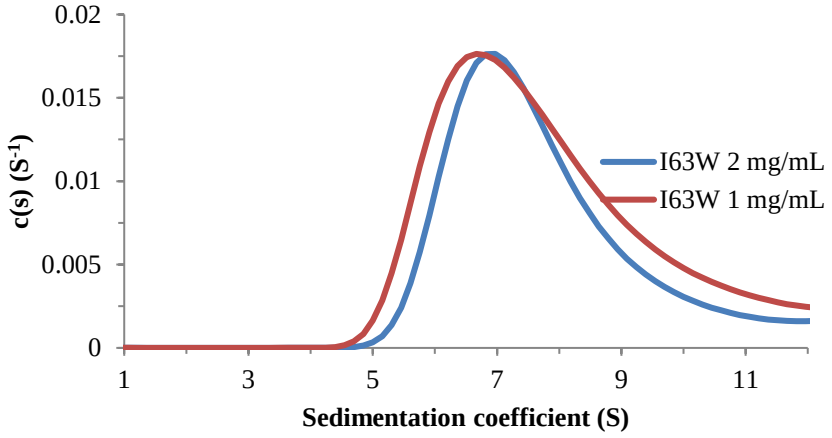

(f)

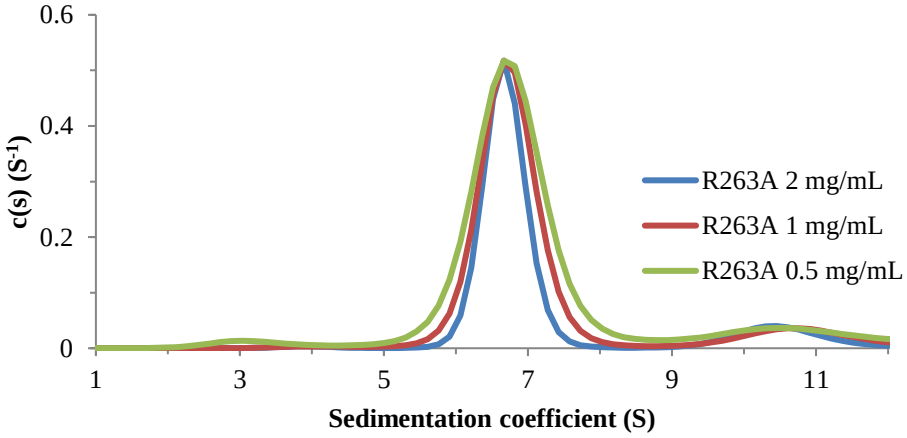

(g)

Figure 3.12: Calculated sedimentation coefficient c(s) distribution plots of the *Nme*KDO8PS wild-type enzyme, A-C and A-B tetramer interface mutants. The 1 mg/mL and 0.5 mg/mL results are normalised to the 2 mg/mL result. (a) *Nme*KDO8PS wild-type enzyme. (b) *Nme*I63S. (c) *Nme*E154L. (d) *Nme*Y171A. (e) *Nme*D172A. (f) *Nme*I63W. (g) *Nme*R263A.

may be a small contaminant in the protein. *Nme*KDO8PS A-C tetramer interface mutant Y171A also which showed a sedimentation coefficient corresponding to a dimer (Figure 3.12d).

Size-exclusion chromatography in line with small angle X-ray scattering (SEC-SAXS) was used to see if the introduced Y171A mutation had disrupted the A-C tetrameric interface in solution. The radius of gyration (R_g), as determined by Guinier analysis, was 36.3 ± 0.3 Å for *Nme*Y171A. The obtained scattering profile was consistent with a tetramer in solution as shown by CRYSOL fit (Figure 3.13). To confirm this result, analytical SEC was done with *Nme*Y171A at 4.9 mg/mL in the presence of 5% glycerol, identical to the loading concentration of the SAX sample. At this high concentration, *Nme*Y171A eluted at 13.7 mL, corresponding to a mass of 130 kDa, which is similar to the wild-type enzyme.

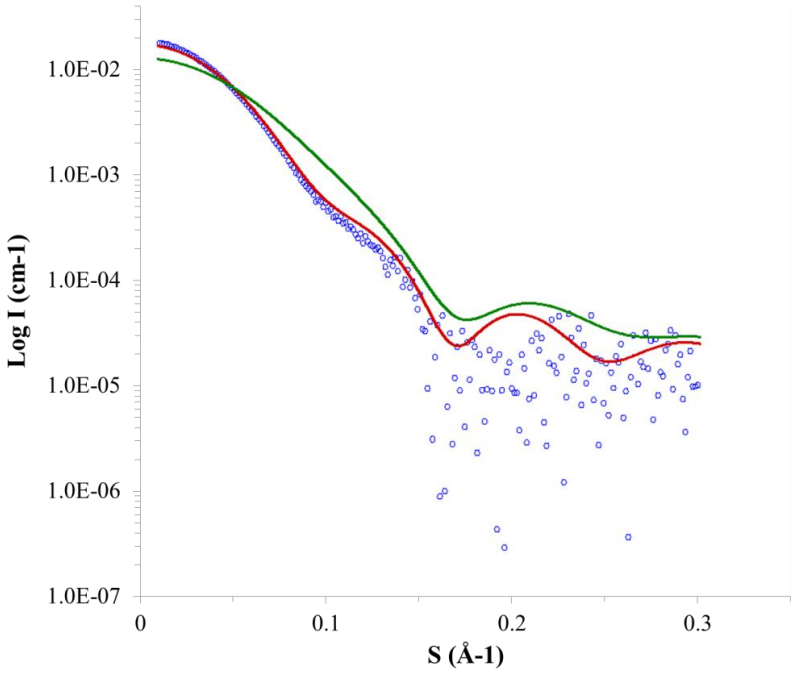

Figure 3.13: SAXS measurement of *Nme*Y171A. Theoretical scattering profiles of the *Nme*Y171A tetramer (red) and A-B dimer (green) derived from the *Nme*Y171A crystal structure, were generated by CRYSOL[117] and compared to the experimentally derived *Nme*Y171A data (blue circles).

3.4 Kinetic characterisation

The kinetic parameters of the *Nme*KDO8PS A-C and A-B tetramer interface mutants were determined by a standard enzyme activity assay to see if the introduced mutations improved or attenuated the catalytic activity (Table 3.3). The A-C tetramer interface mutants were found to have a higher K_m^{PEP} and K_m^{A5P}, as well as a slower k_{cat} than that of the wild-type enzyme. In contrast, the A-B tetramer interface mutant *Nme*R263A had a similar K_m^{PEP} and K_m^{A5P} to that of the wild-type enzyme, in addition to a notably greater k_{cat}.

3.5 Crystallography

Crystallography was used to discover the structural changes the introduced mutations had on the neighbouring regions around the mutation as well as on the tetrameric interfaces.

Table 3.3: Kinetic parameters of the *Nme*KDO8PS wild-type enzyme, A-C and A-B tetramer interface mutants. Those for the wild-type enzyme was determined by Allison.[4]

*Nme*KDO8PS	K_m^{PEP} (μM)	K_m^{A5P} (μM)	k_{cat} (s^{-1})	k_{cat}/K_m^{PEP} (s^{-1} mM^{-1})	k_{cat}/K_m^{A5P} (s^{-1} mM^{-1})
Wild-type	2.5 ± 0.2	12.0 ± 0.5	8.0 ± 0.1	3200 ± 300	660 ± 40
I63S	6.2 ± 0.4	21.0 ± 1.4	8.7 ± 0.2	1400 ± 100	420 ± 40
E154L	4.3 ± 0.4	3.0 ± 0.3	0.67 ± 0.02	160 ± 20	220 ± 30
Y171A	10.0 ± 0.8	15.0 ± 1.2	1.1 ± 0.1	100 ± 10	69 ± 8
D172A	1.3 ± 0.1	72.0 ± 7.0	6.2 ± 0.1	4300 ± 500	74 ± 8
D120H	14.0 ± 1.0	13.0 ± 1.0	5.3 ± 0.2	390 ± 60	400 ± 50
I63W	0.92 ± 0.09	3.2 ± 0.3	1.2 ± 0.1	1300 ± 100	370 ± 40
R263A	4.5 ± 0.4	14.0 ± 0.4	13.0 ± 1.0	2900 ± 400	1000 ± 100

Diffraction data were obtained from crystals of the A-C tetramer interface mutants *Nme*E154L (Table 3.4, overleaf), *Nme*Y171A (Table 3.5, overleaf), *Nme*D172A (Table 3.6, overleaf), and A-B tetramer interface mutant *Nme*R263A (Table 3.7, overleaf). The A-C tetramer interface mutants *Nme*D120H and *Nme*I63W also formed crystals; however, they were too small to be of use. As with the *Nme*KDO8PS wild-type enzyme, the asymmetric unit for all four structures contains one complete tetramer.

The structure of *Nme*E154L is very similar in structure to the *Nme*KDO8PS wild-type enzyme except for the Glu-to-Leu mutation (RMSD Cα on wild-type is 0.185 Å for 847 atoms). However, the β2α2 loop which the E154L residue interacts with across the interface, from Arg60 to Gly68, is no longer discernible within the A and D subunits (Figure 3.14, overleaf). The β2α2 loop within the B and C subunits is still observable, due to being in close proximity to a symmetry mate of the *Nme*KDO8PS tetramer.

The structure of *Nme*Y171A is also very similar to the *Nme*KDO8PS wild-type enzyme, except for the Tyr-to-Ala mutation (RMSD Cα on wild-type is 0.341 Å for 969 atoms). However, there are notable differences, the most notable located near the site of the mutation (Figure 3.15, overleaf). Mutation of the residue Tyr171 to Ala171 has disrupted the interactions across the A-C tetramer interface with the area around the α5 helix. In all four subunits Ala171 no longer interacts across the A-C tetramer interface with Asp177. In addition, the neighbouring residue Asp172 formed a new arrangement; no longer able to interact across the interface with both Gln144 in any of the four subunits, as well as Ser141 in the three A, C and D subunits. The structure of *Nme*D172A is near identical to that of the *Nme*KDO8PS wild-type enzyme other than the Asp-to-Ala mutation (RMSD Cα on wild-type is 0.231 Å for 916 atoms).

Table 3.4: Crystal parameters, data collection, and refinement statistics for *Nme*E154L.

	*Nme*E154L
Crystal system, space group	orthorhombic, $P2_12_12_1$
Unit cell parameters (Å)	81.74, 85.26, 162.52
Resolution range (Å)	47.74-1.60 (1.62-1.60)
No. of measurements	1095501
No. of unique reflections	150433
Redundancy	7.3
Overall CC(1/2)	0.999
Completeness (%)	99.4 (95.1)
$I/\sigma(I)$	13.3 (1.7)
R_{merge}	0.075 (1.099)
Wilson B value (Å^2)	30.8
Refinement	
Resolution (Å)	81.26-1.60
R_{cryst}	0.180
R_{free}	0.202
Amino acids (chain length of 280 residues)	244 + 252 + 257 + 250 residues; 7684 atom sites
No. of water molecules	626
No. of chloride molecules	8
No. of others	5 glycerol
Mean B (Å^2)	
Protein	29.98
Water	38.10
Chloride	42.94
Other	53.58
RMSD from target values	
Bond lengths (Å)	0.019
Bond angles (°)	1.853
Dihedral angles (°)	5.361
Ramachandran	
Most favoured (%)	98.1
Allowed (%)	1.1
Disallowed (%)	0.8

Table 3.5: Crystal parameters, data collection, and refinement statistics for *Nme*Y171A.

	*Nme*Y171A
Crystal system, space group	orthorhombic, $P2_12_12_1$
Unit cell parameters (Å)	81.04, 84.75, 164.18
Resolution range (Å)	47.68-2.22 (2.28-2.22)
No. of measurements	422030
No. of unique reflections	56940
Redundancy	7.4
Overall CC(1/2)	0.998
Completeness (%)	99.9 (98.5)
$I/\sigma(I)$	18.8 (2.6)
R_{merge}	0.102 (0.767)
Wilson B value (Å^2)	37.1
Refinement	
Resolution (Å)	82.09-2.22
R_{cryst}	0.164
R_{free}	0.225
Amino acids (chain length of 280 residues)	254 + 256 + 257 + 254 residues; 7778 atom sites
No. of water molecules	541
No. of chloride molecules	8
No. of others	1 glycerol
Mean B (Å^2)	
Protein	37.63
Water	39.11
Chloride	43.51
Other	71.90
RMSD from target values	
Bond lengths (Å)	0.019
Bond angles (°)	1.873
Dihedral angles (°)	6.533
Ramachandran	
Most favoured (%)	96.7
Allowed (%)	2.5
Disallowed (%)	0.8

Table 3.6: Crystal parameters, data collection, and refinement statistics for *Nme*D172A.

	*Nme*D172A
Crystal system, space group	orthorhombic, $P2_12_12_1$
Unit cell parameters (Å)	81.43, 85.04, 162.77
Resolution range (Å)	47.67-2.03 (2.08-2.03)
No. of measurements	544077
No. of unique reflections	73332
Redundancy	7.4
Overall CC(1/2)	0.999
Completeness (%)	99.9 (98.1)
$I/\sigma(I)$	17.9 (2.8)
R_{merge}	0.093 (0.683)
Wilson B value (Å^2)	30.9
Refinement	
Resolution (Å)	81.39-2.03
R_{cryst}	0.158
R_{free}	0.206
Amino acids (chain length of 280 residues)	254 + 259 + 256 + 256 residues; 7851 atom sites
No. of water molecules	706
No. of chloride molecules	8
No. of others	-
Mean *B* (Å^2)	
Protein	30.64
Water	37.81
Chloride	34.92
Other	-
RMSD from target values	
Bond lengths (Å)	0.019
Bond angles (°)	1.873
Dihedral angles (°)	6.119
Ramachandran	
Most favoured (%)	97.8
Allowed (%)	1.4
Disallowed (%)	0.8

Table 3.7: Crystal parameters, data collection, and refinement statistics for *Nme*R263A.

	*Nme*R263A
Crystal system, space group	orthorhombic, $P2_12_12_1$
Unit cell parameters (Å)	81.78, 85.56, 163.86
Resolution range (Å)	47.94-1.91 (1.94-1.91)
No. of measurements	662345
No. of unique reflections	89689
Redundancy	7.4
Overall CC(1/2)	0.999
Completeness (%)	99.6 (93.3)
$I/\sigma(I)$	19.7 (2.5)
R_{merge}	0.083 (0.767)
Wilson B value (Å^2)	28.9
Refinement	
Resolution (Å)	81.93-1.91
R_{cryst}	0.160
R_{free}	0.203
Amino acids (chain length of 280 residues)	254 + 255 + 258 + 258 residues; 7867 atom sites
No. of water molecules	859
No. of chloride molecules	8
No. of others	2 glycerol
Mean B (Å^2)	
Protein	27.98
Water	37.40
Chloride	35.12
Other	38.88
RMSD from target values	
Bond lengths (Å)	0.018
Bond angles (°)	1.784
Dihedral angles (°)	5.796
Ramachandran	
Most favoured (%)	97.3
Allowed (%)	1.8
Disallowed (%)	0.9

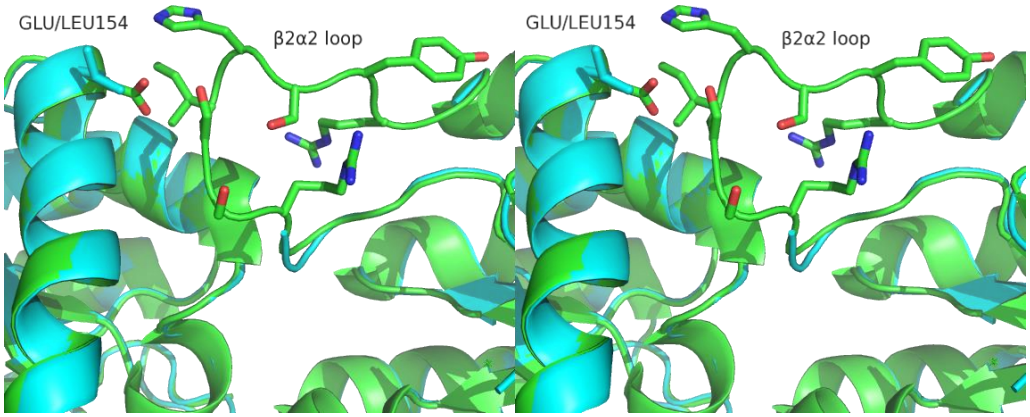

Figure 3.14: Stereoview of the structure of the *Nme*E154L (coloured cyan) superimposed onto the structure of the *Nme*KDO8PS wild-type enzyme (PDB code 2QKF, coloured green). The Glu/Leu154 depicted is from subunit B.

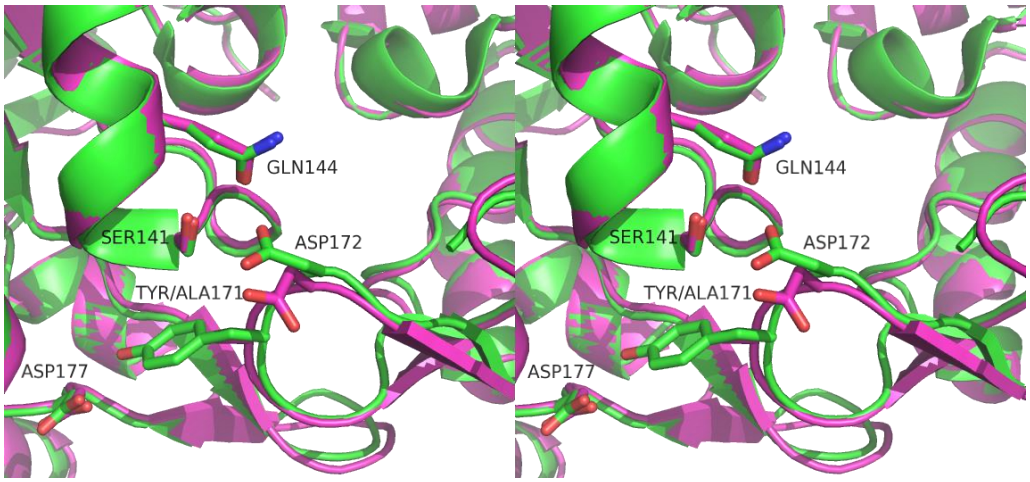

Figure 3.15: Stereoview of the structure of the *Nme*Y171A (coloured magenta) superimposed onto the structure of the *Nme*KDO8PS wild-type enzyme (PDB code 2QKF, coloured green). The Tyr/Ala171 depicted is from subunit D.

Mutation of the residue Asp172 to Ala172 has disrupted the direct interactions across the A-C tetramer interface with both Gln144 and Ser141, though their orientation remains unaffected (Figure 3.16, overleaf).

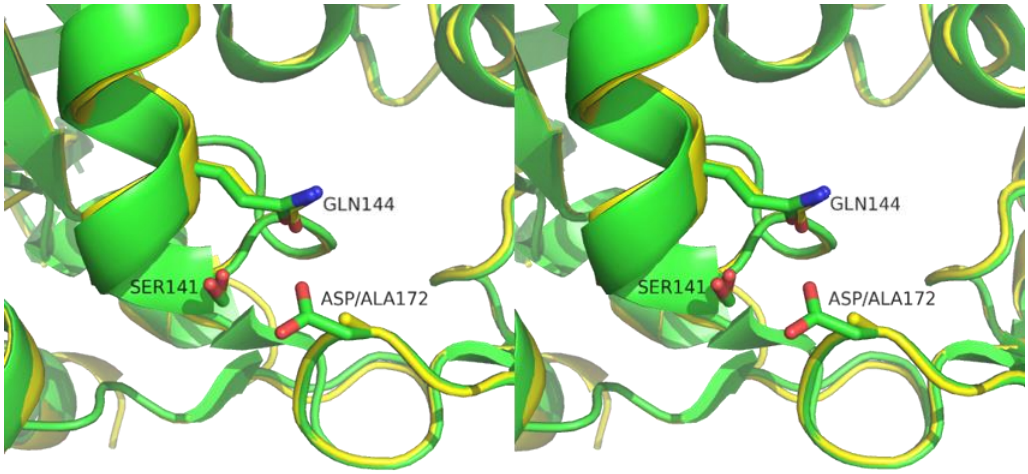

Figure 3.16: Stereoview of the structure of the *Nme*D172A (coloured yellow) superimposed onto the structure of the *Nme*KDO8PS wild-type enzyme (PDB code 2QKF, coloured green). The Asp/Ala172 depicted is from subunit A.

The structure of *Nme*R263A is near identical to that of the *Nme*KDO8PS wild-type enzyme other than the introduced Arg-to-Ala mutation (RMSD Cα on wild-type is 0.200 Å for 917 atoms). Mutation of the residue Arg263 to Ala263 has created a minor effect on the A-B tetramer interface, with the C-terminus end of each subunit slightly closer to the interface, and the side chain of Leu277 now oriented in the space which was occupied by the original Arg263 side chain (Figure 3.17, overleaf).

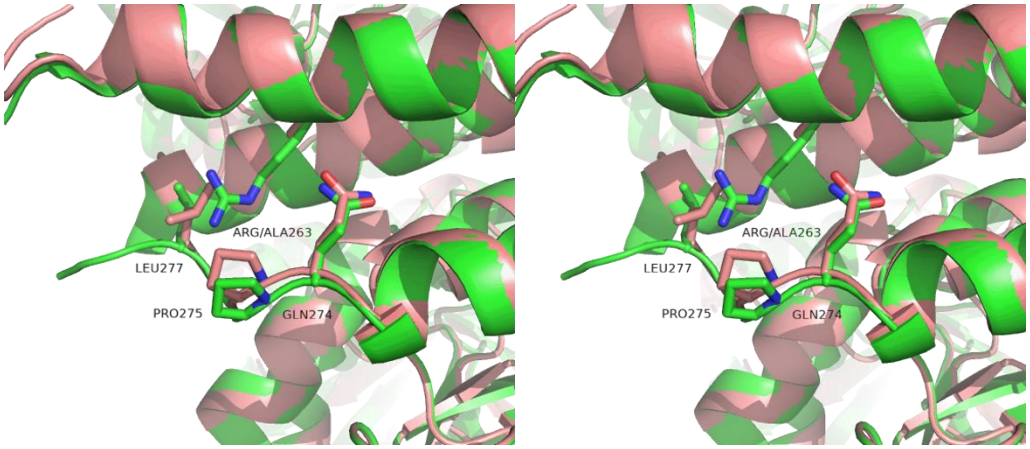

Figure 3.17: Stereoview of the structure of the *Nme*R263A (coloured salmon) superimposed onto the structure of the *Nme*KDO8PS wild-type enzyme (PDB code 2QKF, coloured green). The Arg/Ala263 depicted is from subunit A.

3.6 Discussion

The optimal functional unit for catalysis in KDO8PS was investigated by attempting to destabilise the *Nme*KDO8PS tetramer by mutation of significant residues within the A-B and A-C tetramer interfaces via mutation.

The first two mutations attempted to produce proteins that destabilise the A-C tetramer interface by creating a more plant-like KDO8PS; *Nme*I63S and *Nme*E154L. While both *Nme*I63S and *Nme*E154L target the same area within the *Nme*KDO8PS tetramer, there were some differences that emerged in their properties. *Nme*E154L is noted to be less catalytically active compared to the *Nme*KDO8PS wild-type enzyme and *Nme*I63S. When it came to the quaternary structure of *Nme*I63S and *Nme*E154L, both have very similar profiles in solution from analytical SEC, and AUC; indicative of an *Nme*KDO8PS tetramer, and not a dimer. The crystal structure of *Nme*E154L remained tetrameric, even though the β2α2 loop which the E154L residue

interacts with across the interface is no longer discernible within two of the subunits. The absence of the observable β2α2 loop could suggest that it is more likely to move around more. The absence of the β2α2 loop occurs at the edge of the KANRS motif, with the Serine residue absent. A previous study has identified that the Asp residue is important for catalytic activity, as truncating it to Ala in *Nme*KDO8PS and *Afe*KDO8PS caused a drastic reduction in catalytic activity.[5] So, the increased flexibility of the β2α2 loop could also cause an increase in the flexibility of the KANRS motif Asp residue position, which could be the reason why *Nme*E154L is less catalytically active.

From the *Nme*I63S and *Nme*E154L results, it suggests that a more plant-like KDO8PS would still remain tetrameric. In fact a recent study indicated that this is correct; with the plant KDO8PS from *A. thaliana,* which exhibited tetramer interface residues similar to most other plant KDO8PS being tetrameric, determined by AUC experiments and preliminary crystallisation results.[138]

The subsequent two mutations attempted to create proteins that destabilise the A-C tetramer interface by targeting the area around the α5 helix and β6α6 loop within the *Nme*KDO8PS tetramer; *Nme*Y171A and *Nme*D172A, which the past studies involving *Sty*KDO8PS P145S as well as potentially the plant *Pe*KDO8PS wild-type enzyme, gave rise to a dimeric species.[120, 140] *Nme*Y171A and *Nme*D172A have similar secondary structure to that of the wild-type enzyme, as well as the lowest melting temperatures of all *Nme*KDO8PS mutants; indicative of a decrease in stability of the structure of *Nme*KDO8PS. This is where the similarities of the profiles of *Nme*Y171A and *Nme*D172A end. *Nme*D172A in comparison to that of the wild-type enzyme is more effective at catalysis of PEP, however at the cost of catalysis of A5P; with a lower K_m^{PEP}, higher K_m^{A5P}, and similar k_{cat}. In comparison, *Nme*Y171A

is the least catalytically active out of all A-C tetramer interface mutants generated; with a higher K_m^{PEP}, K_m^{A5P}, and lower k_{cat} than that of the wild-type enzyme. From the analytical SEC and AUC results, and from crystallisation results; *Nme*D172A also remains tetrameric, with little change in the area around the α5 helix and β6α6 loop. Closer investigation into the area around the D172A mutation gives an indication of why; a new water molecule, present in the area where the Asp172 side chain used to occupy can form a hydrogen bond network across the A-C tetramer interface, from the side chains of Ser141 and Glu144 to the main chain nitrogen of D172A (Figure 3.18). The bacterial *Helicobacter pylori* (*Hpy*) KDO8PS also has a uniquely truncated Gly residue instead of the conserved Asp172 residue yet remained a tetramer in solution and in crystal structure for the exact same reason.

In *Hpy*KDO8PS two water molecules occupy the open space around the Gly residue and allow a hydrogen bonding network across the A-C tetramer

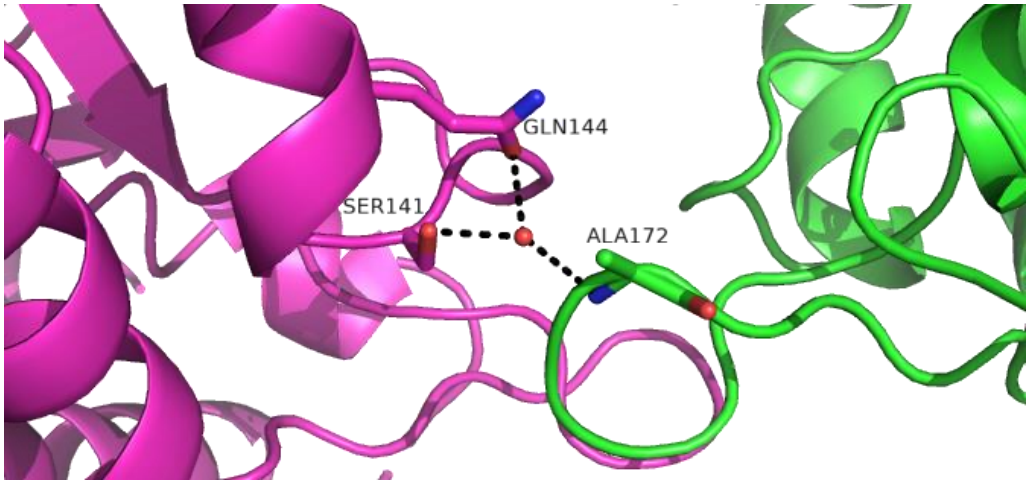

Figure 3.18: The hydrogen bond network involving a water molecule across the A-C tetramer interface of the mutant *Nme*D172A. Subunit A is coloured green and subunit C is coloured magenta.

interface from the side chains of the *Hpy*KDO8PS equivalent Asn136 and Asp139 to the main chain of Gly180. Truncation of the *Nme*KDO8PS Asp172 equivalent residue in the plant *Pe*KDO8PS could result in a dimer due to a select number of different conserved residues in plant KDO8PS. Plant KDO8PS such as *Ath*KDO8PS have conserved Ala and Val residues instead of the conserved Ser141 and Glu144 residues respectively, which removes these specific hydrogen bonding interactions across the A-C tetramer interface, thus weakening it, though not enough to disrupt it. Truncation of the *Nme*KDO8PS Asp172 equivalent, in the case of *Pe*KDO8PS, is then sufficient to finally disrupt the A-C tetramer interface and give rise to a suspected A-B dimer. This would explain why the truncation of the Asp172 in bacterial KDO8PS remains tetrameric, yet for plant KDO8PS gave rise to a suspected A-B dimer.

The Y171A mutation has far greater effects on the *Nme*KDO8PS quaternary structure; analytical SEC showed a significantly later elution of the mutant compared to the wild-type enzyme and all other A-C tetramer interface mutants, as well as being the only A-C tetramer interface mutant to exhibit dimeric species in AUC. The presence of the *Nme*Y171A dimeric species in comparison to tetrameric species is dynamic, notable by SAXS and analytical SEC; lower concentrations of *Nme*Y171A indicate both dimeric and tetrameric species, whereas higher concentrations exhibit only tetrameric species. As these results show that lower concentration of *Nme*Y171A indicates more dimeric species than at higher concentrations, the very low concentration of *Nme*Y171A in kinetic experiments (less than 0.01 mg/mL) would be almost entirely, if not completely, comprised of almost only dimeric species. As *Nme*Y171A has less catalytic activity than that of the wild-type enzyme, this suggests that the dimeric species generated is not the optimal functional unit for catalysis in KDO8PS.

To confirm which dimeric species was generated by the *Nme*Y171A mutation; A-B or A-C dimer, required crystallisation results. *Nme*Y171A crystallised as a tetramer as the Y171A mutation does not introduce any charge or steric disruptions in the A-C tetramer interface, so the artificially high concentration in X-ray experiments would induce tetramer formation. Nevertheless, within the *Nme*Y171A crystal structure were notable changes around the α5 helix and β6α6 loop; interactions across the A-C tetramer interface by Tyr171 were no longer possible, and the neighbouring Asp172 residue formed a new arrangement which also became unable to interact across the A-C tetramer interface. While the Y171A mutation is also near the A-B tetramer interface, there was no observable change in this interface compared to the wild-type enzyme. The *Nme*Y171A crystallisation results indicate destabilising the area around the α5 helix and β6α6 loop successfully destabilises the A-C tetramer interface, and gives rise to an A-B dimer. This indicates that the past study involving the P145S mutation within *Sty*KDO8PS, does give rise specifically to the A-B dimer as well.[120] As both *Nme*Y171A and *Sty*P145S are less catalytically active than their wild-type counterparts, this suggests that the A-B dimer is indeed not the optimal functional unit for catalysis in KDO8PS. In addition, these results would indicate that *Pe*KDO8PS does give rise specifically to the A-B dimer, due to the A-C tetramer interface disruption by the β6α6 loop Asn-to-Ser residue.[140] This Asn-to-Ser residue difference is not unique to *Pe*KDO8PS, as it is also present in one other sequenced plant KDO8PS from *Ostreococcus lucimarinus* (*Olu*). However, *Olu*KDO8PS has not undergone any characterisation, so the quaternary structure is unknown. This Asn-to-Ser residue is the prime target in plant KDO8PS tetramer interface destabilisation experiments, as confirmation of destabilisation would provide a single residue difference that could be used to

identify other dimeric plant KDO8PS wild-type enzymes. As truncation of the Tyr171 residue to Ala successfully destabilised the A-C tetramer interface of *Nme*KDO8PS, it would also be a residue to be targeted for tetramer interface destabilisation experiments in metal-dependent KDO8PS and plant KDO8PS.

The final two mutations attempted to destabilise the A-C tetramer interface by introducing charge and steric disruptions within the *Nme*KDO8PS tetramer: *Nme*D120H and *Nme*I63W. Both *Nme*D120H and *Nme*I63W had similar secondary structure to that of the wild-type enzyme, as well as both having a similar lower melting temperature compared to the wild-type enzyme. From analytical SEC and AUC results, *Nme*D120H and *Nme*I63W are indicated to form a tetramer in solution. Secondarily, from the fact that both *Nme*D120H and *Nme*I63W also formed crystals in similar conditions to that of the wild-type enzyme, this indicates that the introduced mutations did not create sufficient charge and steric disruptions to make formation of the tetrameric species impossible. Thus, the *Nme*D120H and *Nme*I63W attempts to destabilise the A-C tetramer interface around the area of the β2α2 loop were unsuccessful. In addition, two previous mutations around the area of the β2α2 loop were unsuccessful in destabilising the A-C tetramer interface: *Nme*I63S and *Nme*E154L. This suggests that even in the successful disruption of the β2α2 loop interactions across the A-C tetramer, it is not sufficient to destabilise the A-C tetramer interface and generate dimeric species.

While only six mutants were made in an attempt to destabilise the A-C tetramer interface, there was a seventh mutant of interest, generated during the investigation into the putative proton relay chain of *Nme*KDO8PS; in Chapter 2 of this thesis. This seventh mutant was the double mutant *Nme*D92E/P112A; specifically, the P112A mutation being of interest, as it also destabilised the A-C tetramer interface and gave rise to an A-B dimer. The location of the P112A

mutation is not directly part of the A-C tetramer interface, however it is next to a section which is; an alpha helix between the β4 beta-sheet and α4 alpha helix as well as part of the β4 beta-sheet (Figure 3.19a).

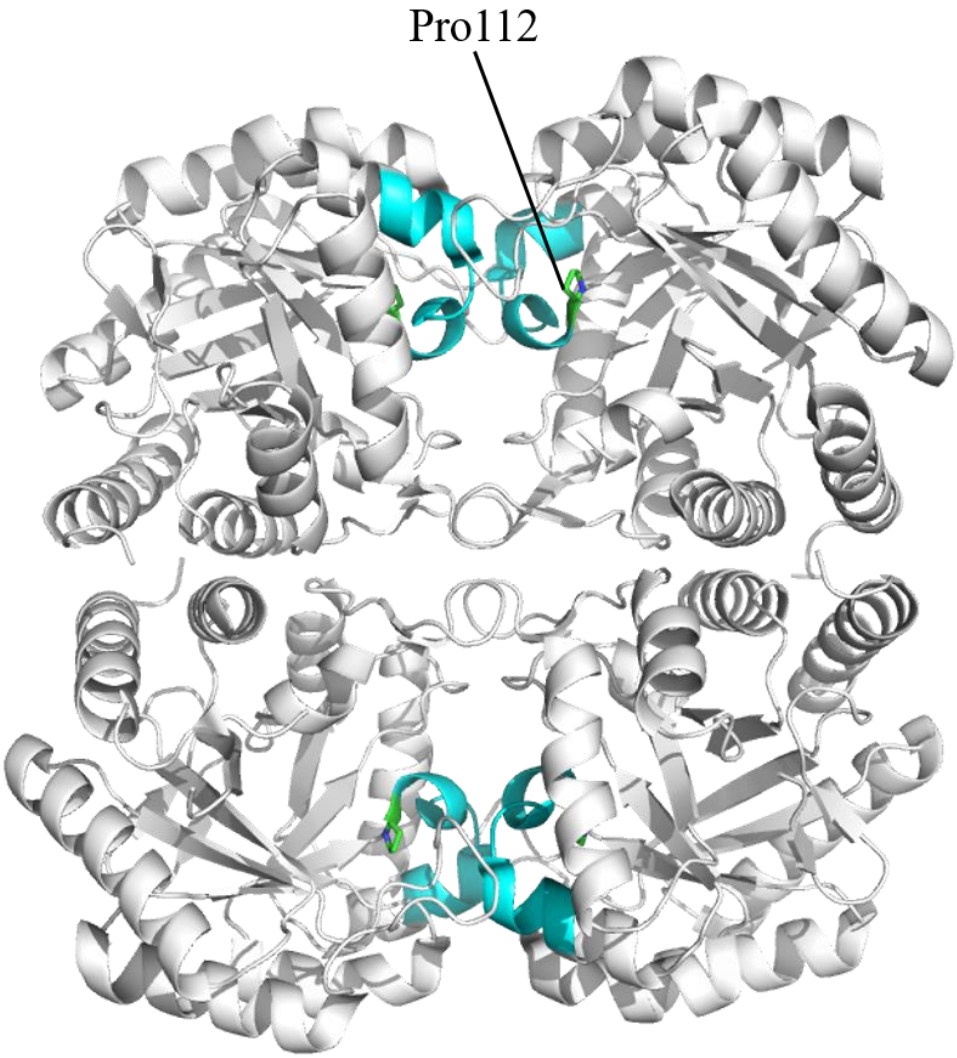

(a)

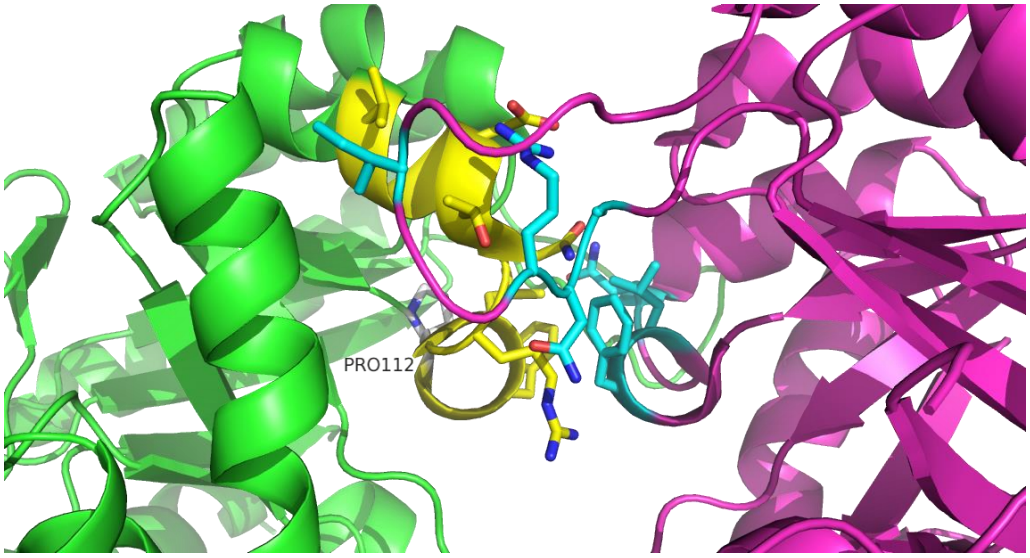

(b)

Figure 3.19: The residue Pro112 and nearby A-C tetramer interface interacting residues. (a) Location of Pro112 (coloured green) and nearby A-C tetramer interface interacting residues (coloured cyan) on *Nme*KDO8PS (PDB code 2QKF). (b) The A-C interface tetramer interactions across the interface near Pro112 on *Nme*KDO8PS (PDB code 2QKF). Subunit A is coloured green, subunit A residue Pro112 is coloured white, other subunit A residues of interest coloured yellow, subunit C is coloured magenta, and subunit C residues of interest are colure cyan.

This section contains the residues from Phe114 to Val123, which interact across the A-C tetramer interface with the equivalent alpha helix between the β4 beta-sheet and α4 alpha helix, equivalent part of the β4 beta-sheet, and the β2α2 loop (Figure 3.2a, Figure 3.19b). Interestingly, none of the other six A-C tetramer interface mutants targeted this area. The P112A mutation ceases to perform the helix breaking role between the β4 beta-sheet and α4 alpha helix, most likely disrupting the organisation of the area around it. This suggestion is strengthened because another Chapter 2 mutation; P112G, which retained the helix breaking role of the residue, remained tetrameric. The double mutant *Nme*D92E/P112A does have a lower melting temperature

compared to the single mutant *Nme*D92E, suggesting that successfully disrupting the A-C tetramer interface does cause a decrease in the stability of KDO8PS. The only other successfully disrupting A-C tetramer interface mutant *Nme*Y171A also exhibits this property, further reinforcing this suggestion. When it comes to the kinetics of the double mutant *Nme*D92E/P112A, it is difficult to clarify which effects are caused by active site rearrangement in comparison to quaternary structure destabilisation. The single-mutant *Nme*P112A would need to be generated and characterised, to be able to provide additional evidence on whether successfully disrupting the A-C tetramer interface does indeed create a A-B dimer with less catalytic activity, which both *Nme*Y171A and *Sty*P145S suggest. As truncation of Pro112 to Ala successfully destabilised the A-C tetramer interface of *Nme*KDO8PS, it would also be a residue to be targeted for tetramer interface destabilisation experiments in metal-dependent KDO8PS and plant KDO8PS.

To destabilise the A-B tetramer interface, three single mutations were generated: *Nme*R263A, *Nme*A227R and *Nme*R263term. Only one of the three mutants; *Nme*R263A, was found to be soluble and able to be characterised. *Nme*R263A had similar secondary structure to that of the wild-type enzyme, as well as having a lower melting temperature compared to the wild-type enzyme. From analytical SEC and AUC results; *Nme*R263A is indicated to form a tetramer in solution, and from crystallisation results; *Nme*R263A also remained tetrameric, with little change in the area around the C-terminus, as well as in the overall KDO8PS structure. The most interesting property about *Nme*R263A, was its kinetic activity. While *Nme*R263A had a slightly higher K_m^{PEP} and K_m^{A5P} compared to the wild-type enzyme, it was the only mutant in all the A-C and A-B tetramer interfaces mutants to have a higher k_{cat}; high enough to indicate that *Nme*R263A was equal, if not superior, to the wild-type enzyme in

catalysis. This could possibly indicate that if the A-B tetramer interface was destabilised, the resulting A-C dimer might be the optimal functional unit for catalysis in KDO8PS. In fact in *Pfu*DAH7PS, which bears a resemblance to the Iβ-like DAH7PS ancient ancestor of KDO8PS, destabilisation of the equivalent A-C tetramer interface gave rise to a catalytically superior mutant; indicating that the optimal functional unit for catalysis in DAH7PS is the A-B dimer, which is the equivalent of the KDO8PS A-C dimer.[84] Addition investigation into the DAH7PS tetramer interfaces occurs in Chapter 4.

The difficulty in destabilising the A-B tetramer interface of KDO8PS should also not be ignored; all generated mutants attempting to destabilise this tetramer interface remained either tetrameric or were insoluble. From the fact that the A-B tetramer interface is comprised of mostly hydrophobic residues (Figure 3.2b), destabilising the A-B tetramer interface may not be sufficient; additional mutations on this interface could be required to ensure the newly exposed surface to be less hydrophobic, to allow the resulting dimeric KDO8PS mutants to remain soluble. In addition, the A-B tetramer interfaces of metal-dependent bacterial as well as plant KDO8PS are not as hydrophobic as that of metal-independent KDO8PS, so successful destabilisation of their A-B tetramer interfaces may not result in an insoluble KDO8PS dimer. An additional investigation into a metal-dependent bacterial KDO8PS as well as plant KDO8PS for potential tetramer interface destabilisation experiments occurs in Chapter 5.

3.7 Summary

The results in this chapter involving the *Nme*I63S, *Nme*E154L, *Nme*I63W and *Nme*D120H mutants have identified that the β2α2 loop does not contribute significant interface interactions across the A-C tetramer interface, as mutation could destabilise the presence of the β2α2 loop, yet the KDO8PS β2α2 loop mutants would remain a tetramer. In addition, the results involving the *Nme*I63S and *Nme*E154L mutants remaining tetrameric provided additional evidence that the β2α2 loop sequence difference in plant KDO8PS is not indicative of a dimer species. The results involving the *Nme*Y171A and *Nme*D92E/P112A mutants have identified that the β6α6 and β4α4 loops are more important in contributing to the A-C tetramer interface, as mutation could destabilise the A-C tetramer interface. In addition, both the Tyr171 and Pro112 are residues to target for tetramer interface destabilisation experiments in metal-dependent bacterial KDO8PS and plant KDO8PS. The results involving the mutant *Nme*D172A indicate that truncation of this residue in bacterial KDO8PS is not sufficient to destabilise the A-C tetramer interface, yet in plant KDO8PS such as *Pe*KDO8PS, it is. In addition, this residue has now been identified to be the prime target in plant KDO8PS tetramer interface destabilisation experiments, as well as possibly being of use to discover other dimeric plant KDO8PS wild-type enzymes. The kinetic experiments of all seven A-C tetramer interface mutants have identified that the A-B dimer is not the optimal functional unit for catalysis in KDO8PS, as all mutants had at least two of three kinetic parameters less effective than the wild-type enzyme: k_{cat}, K_m^{PEP} and K_m^{A5P}, with *Nme*Y171A being the worst of all. The kinetic experiments involving *Nme*R263A have identified that weakening the A-C

tetramer interface can give rise to a more catalytically active mutant than the wild-type enzyme, suggesting that the A-C tetramer could be the optimal functional unit for catalysis in KDO8PS. However, the insolubility of the *Nme*A227R, *Nme*R263term and *Nme*A227R/R263term mutants suggest that successful disruption of the metal-independent bacterial KDO8PS A-B tetramer would require extensive mutations to reduce how hydrophobic the newly exposed areas are to enable a soluble dimer to exist. In addition, the disruption of the metal-dependent bacterial KDO8PS as well as plant KDO8PS A-C tetramer interfaces may be easier due to being comprised of fewer hydrophobic residues.

Chapter 4

Destabilisation of the DAH7PS tetramer and insight into the optimal functional unit for catalysis in DAH7PS

4.1 Introduction

All characterised type Iα, II and most Iβ DAH7PS proteins have a quaternary structure of a tetramer.[25, 64, 77, 83, 103, 111, 112] Only the type Iβ DAH7PS proteins with a C-terminal chorismate mutase domain form a unique dimer.[13] All type II DAH7PS proteins do not share a conserved tetramer interface with either type

Iα and Iβ DAH7PS, whereas one conserved tetramer interface is shared between all type Iα and most Iβ DAH7PS proteins.

Only three past studies have investigated the optimal functional unit for catalysis in DAH7PS, one by disruption of the quaternary structure of a type Iβ DAH7PS tetramer from *Pyrococcus furiosus* (*Pfu*),[84] one from a type Iα DAH7PS tetramer from *Neisseria meningitidis* (*Nme*), and one from a type Iβ DAH7PS dimer from *Prevotella nigrescens* (*Pni*).[24] *Pfu*DAH7PS has been suggested to bear a resemblance to the DAH7PS Iβ-like ancestor that all KDO8PS proteins are suggested to diverge from.[53, 90] This is because *Pfu*DAH7PS has been determined to be metal-dependent, accept a wider range of phosphorylated aldose substrates than most DAH7PS proteins, and, like KDO8PS, has no additions to the core barrel associated with allosteric control.

The type Iβ *Pfu*DAH7PS tetramer is comprised of two interfaces, only one of which is conserved in both type Iα and most Iβ DAH7PS, which is formed from the interaction between subunits A and B (or C and D) (Figure 4.1, overleaf). Only the type Iβ DAH7PS proteins with a C-terminal chorismate mutase domain are suspected to not have this interface, as the only characterised example *Pni*DAH7PS forms a unique dimerization solely via the chorismate mutase domains, determined via analytical ultracentrifugation (AUC) and size-exclusion chromatography in line with small angle X-ray scattering (SEC-SAXS).[13] The *Pfu*DAH7PS A-B tetramer interface is comprised of numerous hydrogen-bonds and hydrophobic interactions, with few salt-bridges also present (Figure 4.2a, overleaf). The second tetramer interface of type Iβ *Pfu*DAH7PS is formed from the interaction between subunits A and C (or B and D), and is identical in all other crystallised type Iβ DAH7PS proteins; with no additions to the core $(\beta/\alpha)_8$ TIM-barrel (*Aeropyrum*

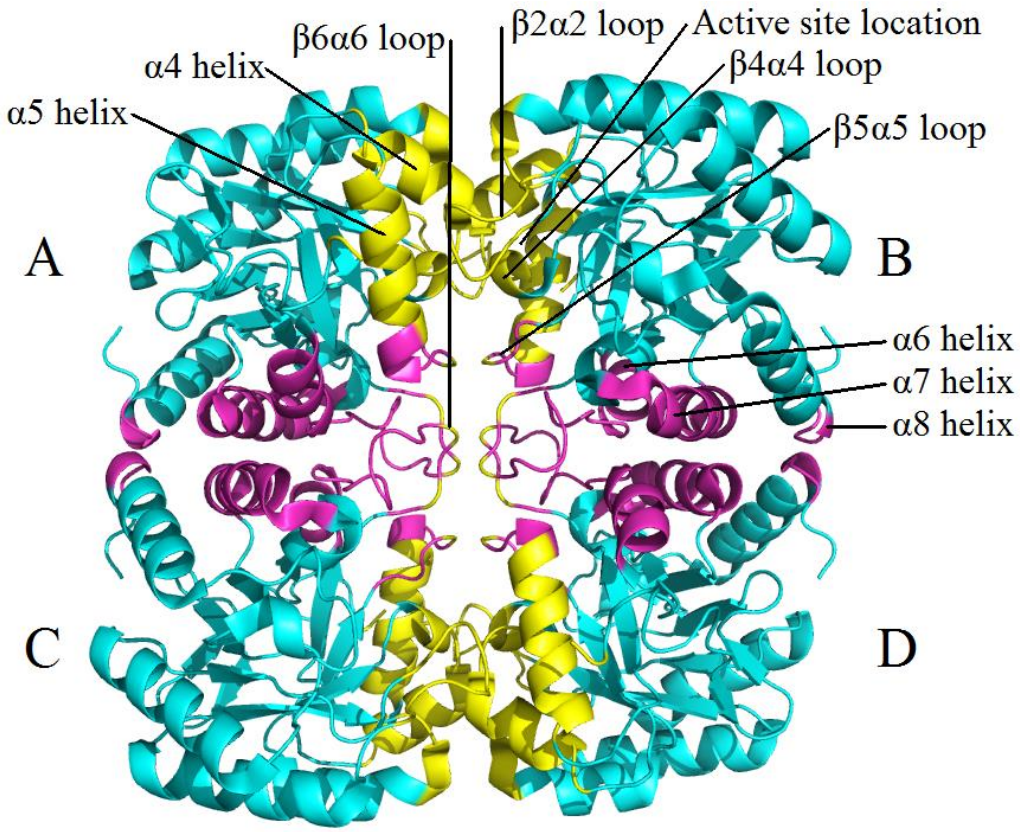

Figure 4.1: The structure of metal-dependent *Pfu*DAH7PS (PDB code 4C1K). Four monomers are shown depicting the two separate interfaces. The conserved A-C tetramer interface is coloured in magenta, the A-B tetramer interface yellow, and the non-interface structure cyan.

pernix),[139] an additional N-terminal ACT domain (*Thermotoga maritima*),[111] or an additional N-terminal chorismate mutase domain (*Listeria monocytogenes* and *Geobacillus sp*.).[77, 83] Interestingly, this second tetramer interface between subunits A and C (or B and D), differs between type Iα and Iβ DAH7PS (Figure 4.3, overleaf), and also does not exist in the characterised Iβ DAH7PS proteins with a C-terminal chorismate mutase domain.[13] The *Pfu*DAH7PS A-C tetramer interface is comprised of mostly hydrophobic interactions, with some hydrogen-bonds and a few salt-bridges also present (Figure 4.2b). The type Iα

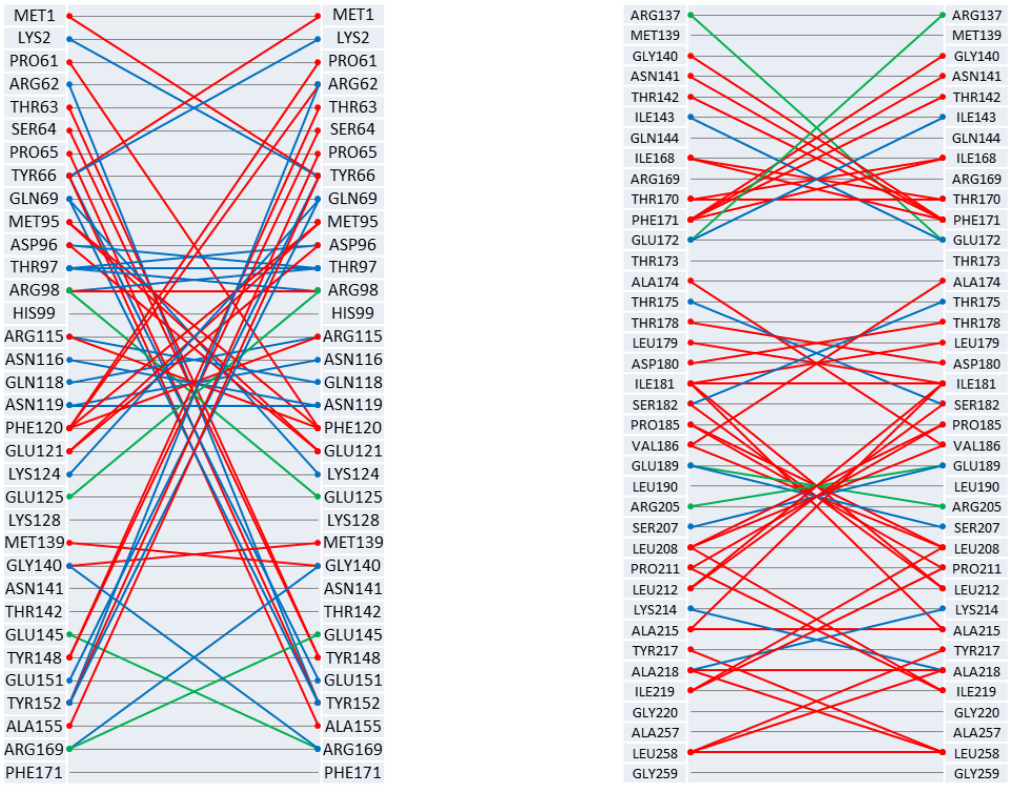

(a) **(b)**

Figure 4.2: The *Pfu*DAH7PS tetramer interface interactions. (a) *Pfu*DAH7PS A-B tetramer interface. (b) *Pfu*DAH7PS A-C tetramer interface. Hydrogen bonds are coloured blue, salt-bridges are coloured green and hydrophobic interactions are coloured red. These tetramer interface interactions are constructed from the *Pfu*DAH7PS structure (PDB code 4C1K).

and Iβ DAH7PS active sites are located near the A-B tetramer interface, suggesting that the A-B dimer is conserved in both to ensure catalytic activity.

In fact, two past studies suggest that the optimal functional unit for catalysis in DAH7PS is indeed the A-B dimer.[24, 84] In the type Iβ *Pfu*DAH7PS, the I181D mutation gave rise to a partially destabilised A-C tetramer interface. The resulting *Pfu*I181D mutant remained in equilibrium between tetrameric

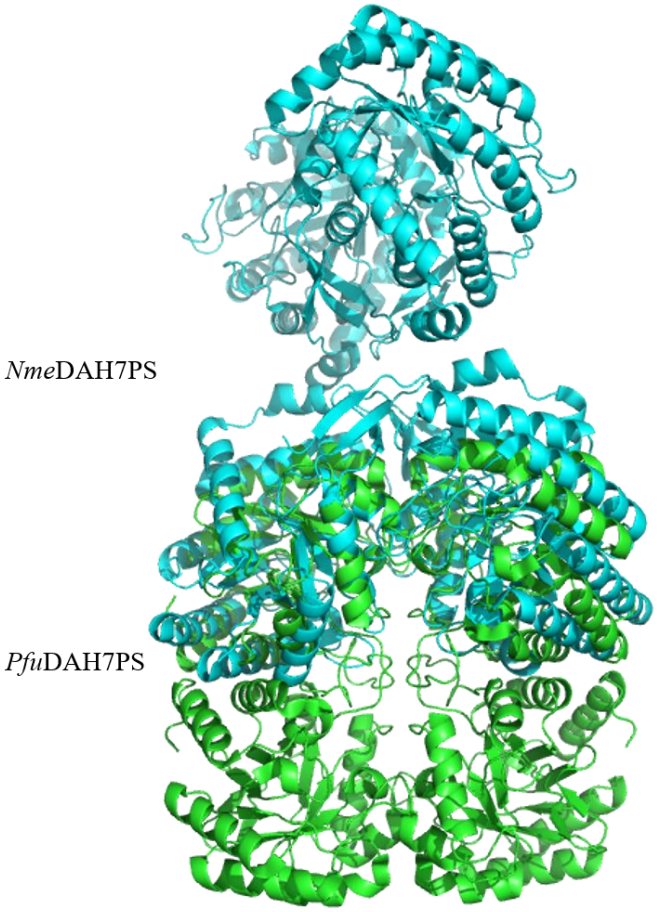

Figure 4.3: The A-B dimer of the type Iα *Nme*DAH7PS tetramer (PDB code 4HSN, coloured cyan) superimposed onto the A-B dimer of the type Iβ *Pfu*DAH7PS tetramer (PDB code 1ZCO, coloured green).

and dimeric forms, crystallised in a tetrameric state, and had greater activity than the wild- type enzyme, however at the notable cost of thermal stability.[84] It has been suggested that for type Iβ DAH7PS, potentially higher activity as a dimer had been compromised for the benefits of greater protein stability as a tetramer instead.[84]

In the type Iα *Nme*DAH7PS, the R126S mutation gave rise to a completely destabilised A-C tetramer interface (Figure 4.4, overleaf). The

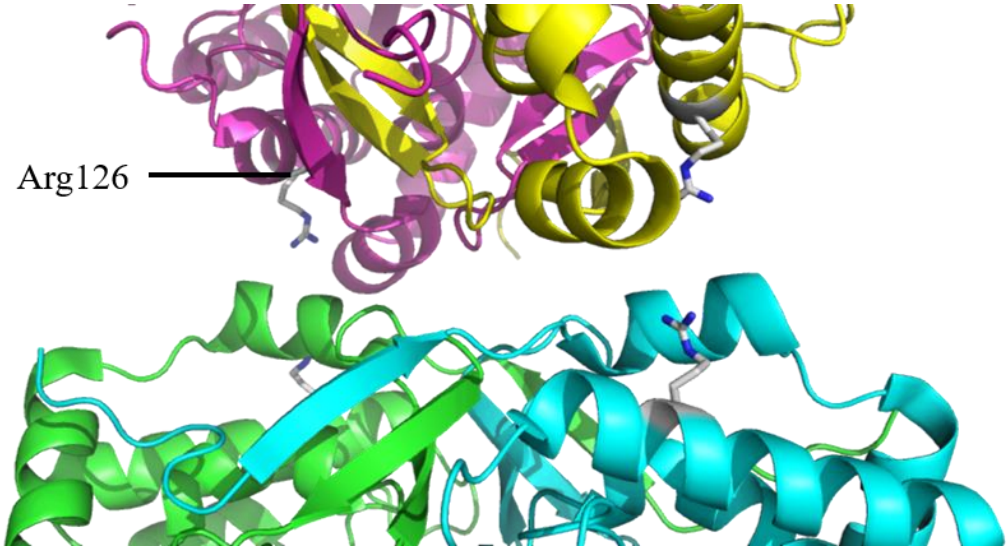

Figure 4.4: The structure of type Iα *Nme*DAH7PS (PDB code 4UC5) showing the A-C tetramer interface residue Arg126 (coloured white). Subunit A is coloured green, subunit B is coloured cyan, subunit C is coloured magenta, and Subunit D is coloured yellow.

resulting *Nme*R126S mutant was completely dimeric in solution although it crystallised in a tetrameric state.[24] The *Nme*R126S mutant did have less catalytic activity compared to the wild-type enzyme, however this may have been caused by the instability of the dimer, as there was a notable decrease in catalytic activity over time compared to the *Nme*DAH7PS wild-type enzyme.[24] This suggests that for type Iα DAH7PS proteins, potentially higher activity as a dimer has been compromised for the benefits of greater protein stability as a tetramer instead, similarly to the type Iβ DAH7PS.[24]

One past study has also generated the DAH7PS monomer, in the *Pni*DAH7PS, a uniquely dimeric type Iβ DAH7PS protein with a C-terminal chorismate mutase domain.[13] The truncation of the *Pni*DAH7PS dimer by removal of the C-terminal chorismate mutase domain gave rise to a DAH7PS monomer.[13] The resulting truncated *Pni*DAH7PS monomer had a drastic

reduction in activity; all three K_m^{PEP}, K_m^{E4P}, and k_{cat} less effective than the wild-type enzyme.[13] This indicates that for type Iβ DAH7PS proteins with a C-terminal chorismate mutase domain, the monomer is not the optimal functional unit for catalysis in DAH7PS, and that the unique dimer interface provided the benefit of greater activity.

No past studies have attempted to destabilise a tetrameric type Iα or Iβ DAH7PS A-B tetramer interface to see if the A-C dimer is catalytically active and assess its thermal stability. In addition, no past studies have attempted to generate the DAH7PS monomer from any of the tetrameric type Iα or Iβ DAH7PS to confirm whether the optimal functional unit for catalysis in DAH7PS is truly the A-B dimer.

To destabilise the DAH7PS interface, a well characterised, easily crystallised DAH7PS would be ideal. In addition, a DAH7PS with no additional domains to the core TIM-barrel would be preferable, to remove any interface influence. A type Iβ DAH7PS would be superior, as the past study only partially destabilised the A-C tetramer interface and still allowed the DAH7PS tetramer to occur in solution,[84] which could have had an influence on the assessment of activity and stability of the mutant.

Finally *Pfu*DAH7PS was selected, due its predicted close resemblance to the DAH7PS Iβ-like ancestor and its relationship to KDO8PS, which would allow the KDO8PS tetramer interface destabilisation experiments (seen in Chapter 3) to also provide insight into the DAH7PS tetramer destabilisation results. In addition, further mutations of the *Pfu*DAH7PS tetramer interface could then be compared to the only previous study involving destabilisation of the type Iβ DAH7PS tetramer interface, that from the *Pfu*I181D mutant.

In this chapter a preliminary investigation into the *Pfu*DAH7PS tetramer interfaces is performed. Significant residues in the A-C and A-B

tetramer interfaces of *Pfu*DAH7PS are identified and mutated in attempt to destabilise a DAH7PS tetramer interface. The result of the mutations on the structure and activity of *Pfu*DAH7PS were then used to shed light on whether the optimal functional unit for catalysis in DAH7PS was indeed the A-B dimer, what influence each tetramer interface performs in the type Iβ DAH7PS tetramer, and to identify additional significant residues in the *Pfu*DAH7PS tetramer interface that could be targeted for disruption in future studies.

4.2 Preparation and rationale for the mutants

To identify significant residues within both the A-C and A-B tetramer interfaces, PDBePISA was utilised.[65] Microsoft Excel was then used to plot the data as tetramer interface interaction diagrams (Figures 4.2a and 4.2b). In each of the two tetramer interfaces one residue was selected with the aim of destabilising the tetramer interface by mutation (Figure 4.5, overleaf).

To destabilise the A-C tetramer interface, the Ile181 residue was selected. Ile181 is located near the centre of the A-C tetramer interface, is the most hydrophobic residue located inside the interface (excluding large hydrophobic residues such as Phe) and interacts with the corresponding Ile181 across the interface (Figure 4.6, overleaf). The past study had mutated this residue to Asp to create a charge disruption on this interface, however the tetrameric form was still able to remain as the Asp mutation side chain was too short to induce any steric disruption on the interface.[84] The Ile-to-Arg mutation was generated, as introducing an Arg residue would retain the unfavourable charge interaction across the interface seen in the past *Pfu*I181D mutant, while

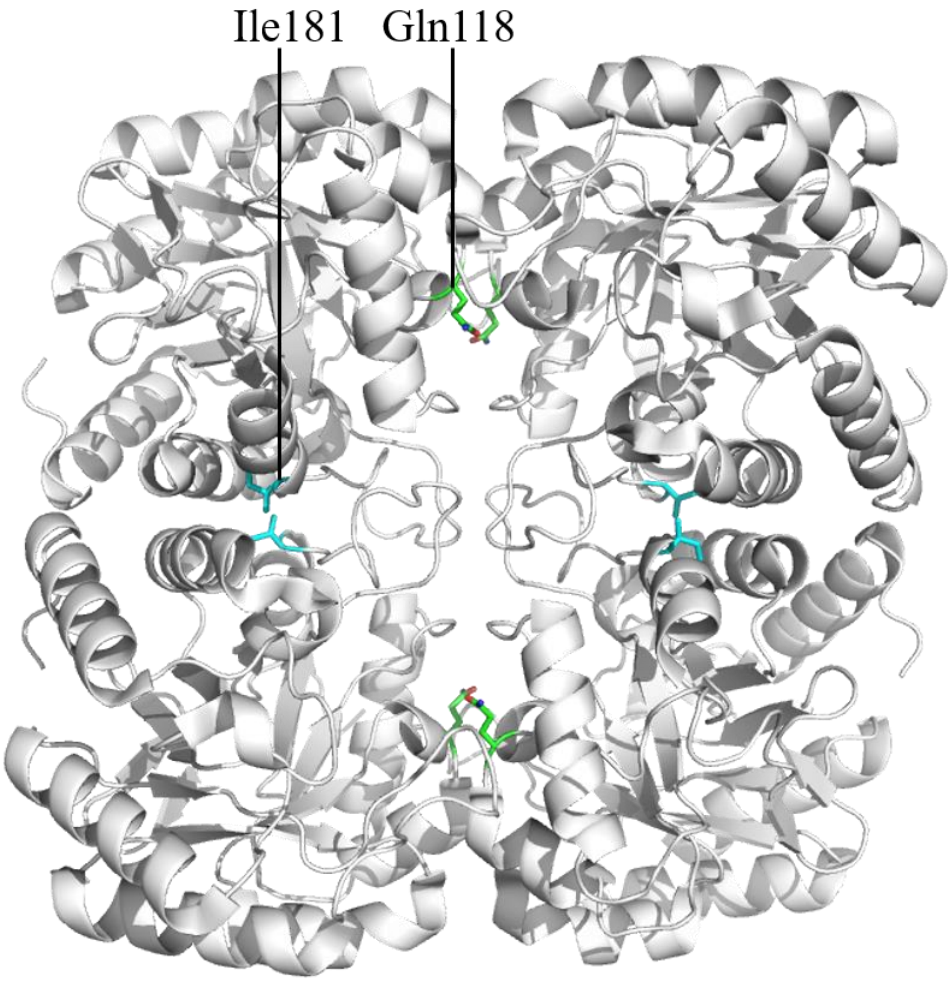

Figure 4.5: The two total residues of interest on metal-dependent *Pfu*DAH7PS (PDB code 4C1K). The residue of interest on the A-C tetramer interface is Ile181 (coloured green). The residue of interest on the A-B tetramer interface is Gln118 (coloured cyan).

also introducing unfavourable steric interactions with numerous neighbouring residues involved in the A-C tetramer interface.

To destabilise the A-B tetramer interface, the residue Gln118 was selected. The Gln118 side chain only interacts with one residue across interface: Arg115, however it is located near the centre of the A-C tetramer

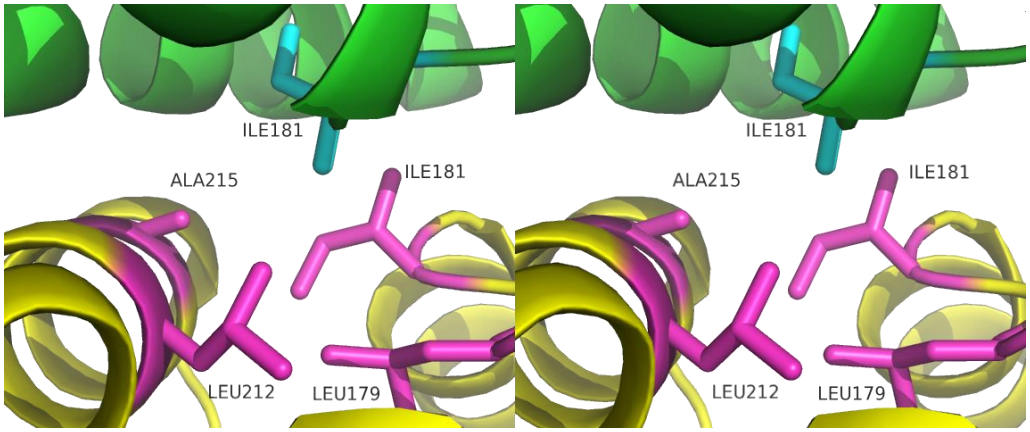

Figure 4.6: Stereoview of *Pfu*DAH7PS structure (PDB code 4C1K) showing the A-C tetramer interface interactions residue Ile181 has across the interface. Subunit A is coloured green, subunit A Ile181 is coloured cyan, subunit C is coloured yellow, and subunit C residues are coloured magenta.

interface. By mutation of Gln118 to the large residue Trp, steric clashes would occur with numerous neighbouring residues involved in the A-B tetramer interface, from both subunits (Figure 4.7, overleaf).

The A-B tetramer interface mutant *Pfu*Q118W was generated, expressed and purified using the same purification procedures as the *Pfu*DAH7PS wild-type enzyme.[104] After lysing the bacterial cell culture, the proteins was purified via heat treatment, followed by hydrophobic-interaction chromatography, and completed via size-exclusion chromatography. The A-C tetramer interface mutant *Pfu*I181R was found to be more problematic in purification, especially during heat treatment and size-exclusion chromatography. Unlike the *Pfu*DAH7PS wild-type enzyme, *Pfu*I181R denatured under heat treatment at 80 °C, and so the step was readjusted to be performed at 60 °C. During size-exclusion chromatography, *Pfu*I181R also tended to elute over a much larger volume compared to the *Pfu*DAH7PS wild-type enzyme. When a HiLoad 26/60 Superdex^{TM} 200 prep grade column (GE

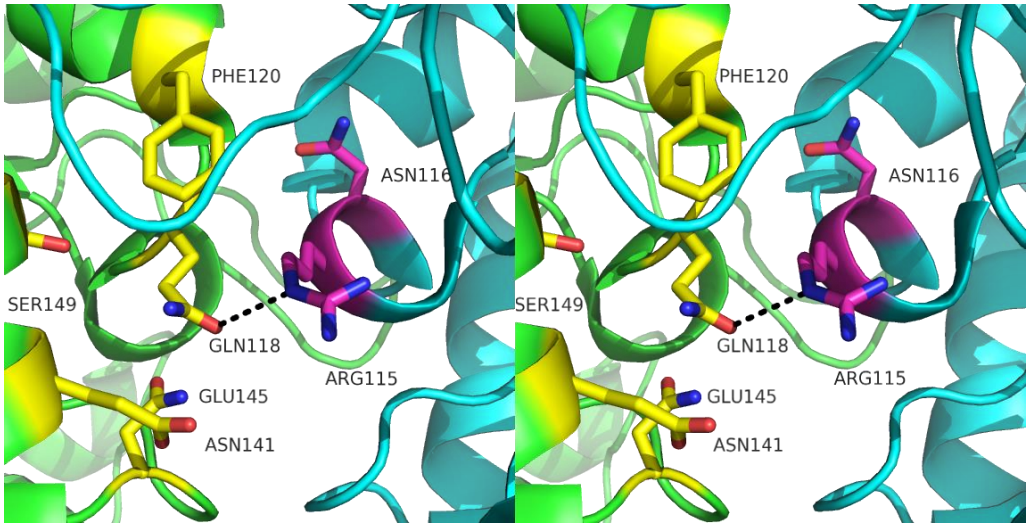

Figure 4.7: Stereoview of *Pfu*DAH7PS structure (PDB code 4C1K) showing the A-B tetramer interface interactions residue Gln118 has across the interface, in addition to the surrounding residues which have steric clashes when Gln118 is modelled as Trp. Subunit A is coloured green, subunit A residues are coloured yellow, subunit B is coloured cyan, and subunit C residues are coloured magenta.

Healthcare) was used (with a bed volume of 320 mL), *Pfu*I181R would elute from 210 to 300 mL. Attempts to then concentrate the large were unsuccessful due to protein aggregation within the spin concentrator. Inclusion of 5% glycerol in the buffer had no change to this aggregation. The A-C tetramer interface mutant *Pfu*I181R was finally purified via heat treatment (at a lower 60 °C), followed by a hydrophobic interaction column, and purification completed via anion-exchange chromatography.

4.3 Structure in solution and stability

Electrospray ionisation mass spectrometry confirmed successful mutation via comparison of the measured mass of the *Pfu*DAH7PS A-C and A-B tetramer

interface mutants to the calculated mass. The A-B tetramer interface mutant *Pfu*Q118W had a resulting mass of 29282.9 Da (compared to calculated mass 29282.8 Da), and the A-C tetramer interface mutant *Pfu*I181R had resulting mass of 29267.5 Da (compared to calculated mass 29267.8 Da).

CD spectrophotometry assessed if any introduced mutations produced perturbations in the secondary structure arrangement of the *Pfu*DAH7PS A-C and A-B tetramer interface mutants. The spectrum of the A-B tetramer interface mutant *Pfu*Q118W showed some difference compared to the wild-type enzyme, while the spectrum of the A-C tetramer interface mutant *Pfu*I181R showed a more notable difference compared to the wild-type enzyme (Figure 4.8, overleaf). This does indicate that the introduced *Pfu*Q118W and *Pfu*I181R mutations have indeed had an effect on the secondary structure, with *Pfu*I181R being the more severe.

The melting temperatures of the *Pfu*DAH7PS wild-type enzyme and single-mutants were determined using DSF, with and without the presence of the DAH7PS substrates PEP and E4P, and the divalent metal ion Cd^{2+} (Table 4.1, overleaf), to see if the introduced mutations destabilised the DAH7PS. The *Pfu*DAH7PS wild-type enzyme is stablised in the presence of Cd^{2+}. PEP and E4P also stabilised the *Pfu*DAH7PS wild-type enzyme, though to a lesser degree in the presence of Cd^{2+}. *Pfu*Q118W retained similar stability to the wild-type enzyme, as well as being more stable in the presence of Cd^{2+}. Interestingly PEP and E4P no longer had an effect on the stability of *Pfu*Q118W, even in the presence of Cd^{2+}. *Pfu*I181R was drastically less stable than the wild-type enzyme, whereas a previous study showed that that the single-mutant *Pfu*I181D only lost 3 °C of stability in comparison to the wild-type enzyme.[84] Cd^{2+} appeared to make *Pfu*I181R more stable in a manner

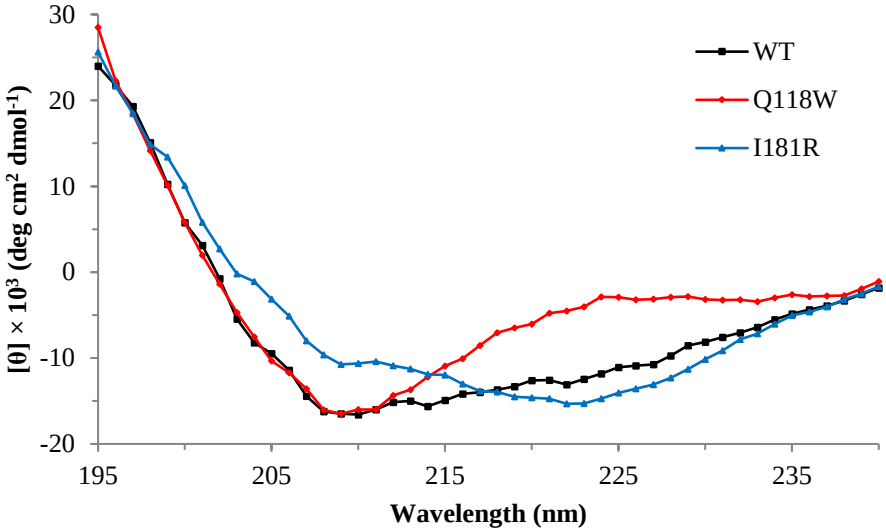

Figure 4.8: CD spectrophotometry of the *Pfu*DAH7PS wild-type enzyme and single-mutants. *Pfu*DAH7PS wild-type enzyme: black squares; *Pfu*Q118W: red diamonds; *Pfu*I181R: blue triangles. Every second datum point is plotted.

similar to that observed by the wild-type enzyme, however there was another inflection point only 2 °C higher compared to PfuI181R in the absence of Cd2+ (Figure 4.9, overleaf). This would indicate that the presence of Cd^{2+} only slightly stabilises the structure of *Pfu*I181R, as one of the two protein unfolding events is only 2 °C higher than the protein unfolding event in the absence of Cd^{2+}. PEP and E4P no longer had an effect on the stability of *Pfu*I181R, even in the presence of Cd^{2+}. Oddly, one of the protein unfolding events found in *Pfu*I181R in the presence of Cd^{2+} disappeared when both substrates PEP and E4P are both present.

To see if the introduced mutations destabilised a tetramer interface, the quaternary structure in solution of the *Pfu*DAH7PS wild-type enzyme, A-C and A-B tetramer interface mutants were determined by analytical SEC, native PAGE and AUC.

Table 4.1: The effect of additives on the T_m of *Pfu*DAH7PS wild-type enzyme and single-mutants. That for *Pfu*I181D was determined by Nazmi.[84]

*Pfu*DAH7PS	Additives	T_m (°C)	Diff. (°C)	Diff. to WT (°C)
Wild-type	No additive	86 ± 1		
	PEP	91 ± 1	5	
	E4P	90 ± 1	4	
	Cd^{2+}	93 ± 1	7	
	Cd^{2+} + PEP	95 ± 1	9	
	Cd^{2+} + E4P	95 ± 1	9	
	Cd^{2+} + PEP + E4P	95 ± 1	9	
I181D	Cd^{2+}	90 ± 1		-3
Q118W	No additive	85 ± 1		-1
	PEP	85 ± 1	0	-6
	E4P	85 ± 1	0	-5
	Cd^{2+}	93 ± 1	8	0
	Cd^{2+} + PEP	93 ± 1	8	-2
	Cd^{2+} + E4P	93 ± 1	8	-2
I181R	No additive	67 ± 1		-19
	PEP	67 ± 1	0	-24
	E4P	67 ± 1	0	-23
	Cd^{2+}	76 ± 1 (69 ± 1)[a]	9 (2)	-17 (-24)
	Cd^{2+} + PEP	76 ± 1 (69 ± 1)[a]	9 (2)	-19 (-26)
	Cd^{2+} + E4P	76 ± 1 (69 ± 1)[a]	9 (2)	-19 (-26)
	Cd^{2+} + PEP + E4P	76 ± 1	9	-19

[a] A significant melting peak was evident at these temperatures.

The *Pfu*DAH7PS wild-type enzyme eluted with a SEC profile at a mass corresponding to 130 kDa, slightly larger than previous studies that performed wild-type SEC experiments (Table 4.2, overleaf).[84] *Pfu*Q118W eluted with a

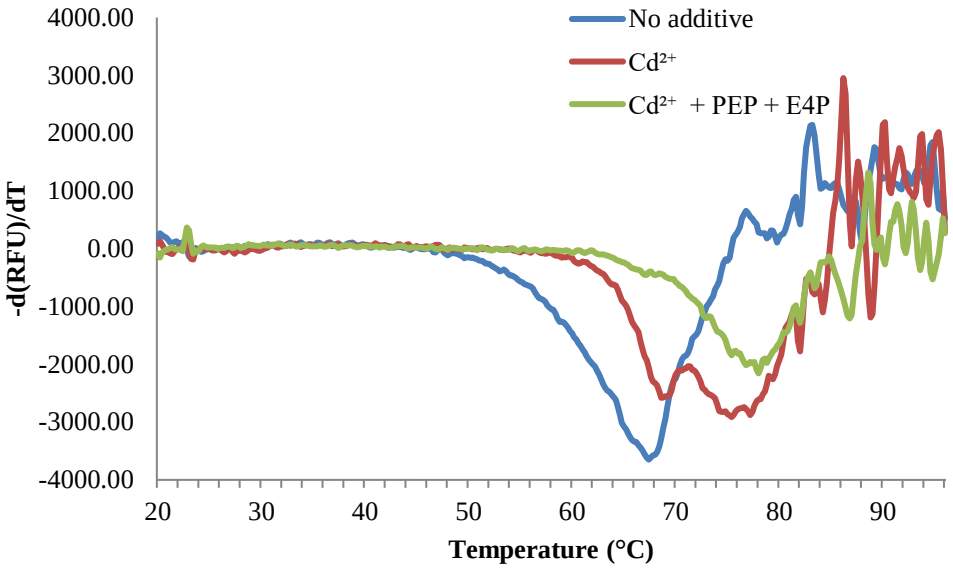

Figure 4.9: DSF of the A-C tetramer interface mutant *Pfu*I181R with various additives. The negative peak indicates the melting temperature of the A-C tetramer interface mutant *Pfu*I181R. RFU stands for relative fluorescence units.

Table 4.2: SEC profiles of the *Pfu*DAH7PS wild-type enzyme and single-mutants. All proteins were at a concentration of 1 mg/mL in solution.

*Pfu*DAH7PS	Elute (mL)	Calculated Molecular Weight (kDa)
Wild-type	13.33	130
Q118W	13.8	104
I181D	14.7	66
I181R	21.4 (10.0 - 21.4)[a]	30 (30-660)

[a] A notable presence was evident at this volume range

SEC profile at a mass corresponding to 104 kDa. The original single-mutant *Pfu*I181D eluted with a SEC profile at a mass corresponding to 66 kDa. *Pfu*I181R exhibited an unexpected SEC profile which was the reason SEC was not used as a purification step. *Pfu*I181R began to elute at a low constant amount from 10.0 mL to 20.0 mL, which then rose into a single steep peak at

21.4 mL (Figure 4.10, overleaf). Agarose gel electrophoresis of the SEC fractions confirmed the presence of *Pfu*I181R in this elution range. The single peak of *Pfu*I181R eluted with a SEC profile at a mass corresponding to 30 kDa, while the wider spread would also indicate the presence of multiple states of aggregation which ranged from 30 to 660 kDa.

Native PAGE also showed both the *Pfu*DAH7PS wild-type enzyme and the A-B tetramer interface mutant *Pfu*Q118W migrated at a similar mass, whereas *Pfu*I181R migrated at two places: one a notably larger mass and the other a notably smaller mass (Figure 4.11, overleaf).

Previous AUC, utilising sedimentation velocity experiments had determined that the *Pfu*DAH7PS wild-type enzyme was a tetramer, and that the original single-mutant *Pfu*I181D had tetrameric and dimeric states.[84] Sedimentation velocity experiments determined that *Pfu*Q118W was a tetramer, having a similar sedimentation coefficient to the *Pfu*DAH7PS wild-type enzyme (Figure 4.12, overleaf). Sedimentation velocity experiments determined that *Pfu*I181R was mostly in a monomeric state, with some dimer at higher concentrations, as well as a large aggregate at higher concentrations.

Size-exclusion chromatography in line with small angle X-ray scattering (SEC-SAXS) was used to see if the introduced I181R mutation had disrupted the A-C tetrameric interface in solution. The 2.5 mg/mL sample showed a rather high R_g of 65.9 ± 8.9 Å, which corresponded to the presence of a large aggregate of *Pfu*I181R. While the introduced Ile-to-Arg mutation would make formation of the tetramer impossible, the scattering profile suggests a *Pfu*I181R large aggregate that would mimic six *Pfu*DAH7PS wild-type tetramers in close contact with one another, as shown by CRYSOL fit (Figure 4.13, overleaf).

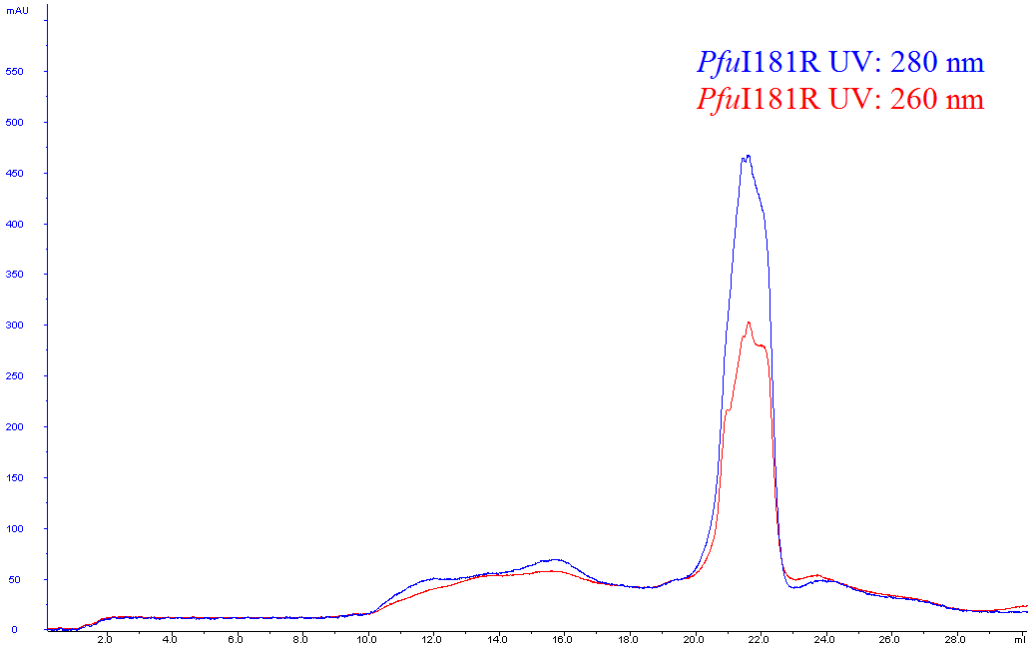

Figure 4.10: Analytical SEC of 1 mg/mL *Pfu*I181R.

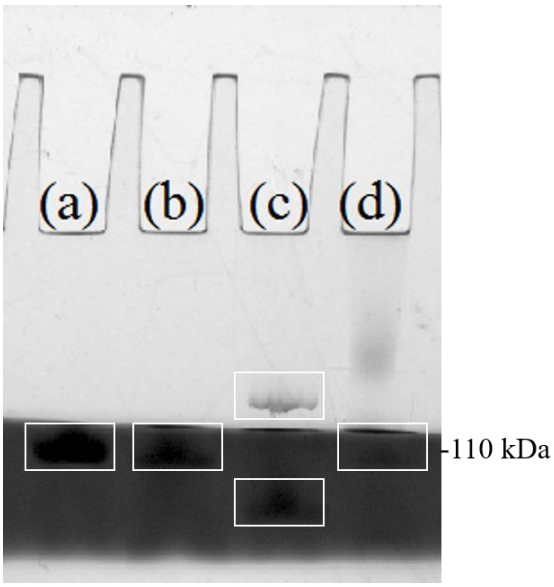

Figure 4.11: Native PAGE of 1 mg/mL *Pfu*DAH7PS wild-type enzyme and single-mutants. (a) *Pfu*DAH7PS wild-type enzyme. (b) *Pfu*Q118W. (c) *Pfu*I181R. (d) Native Mark™ Unstained Protein Standard.

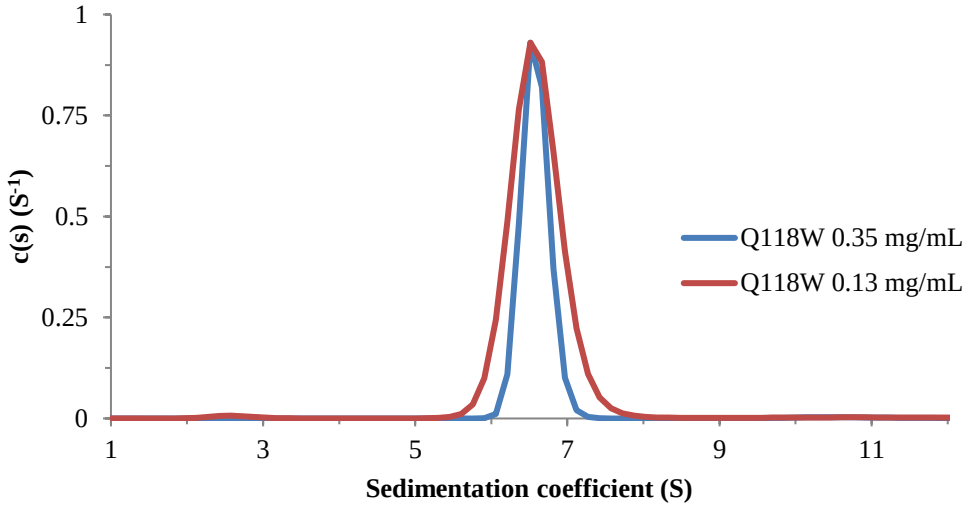

(a)

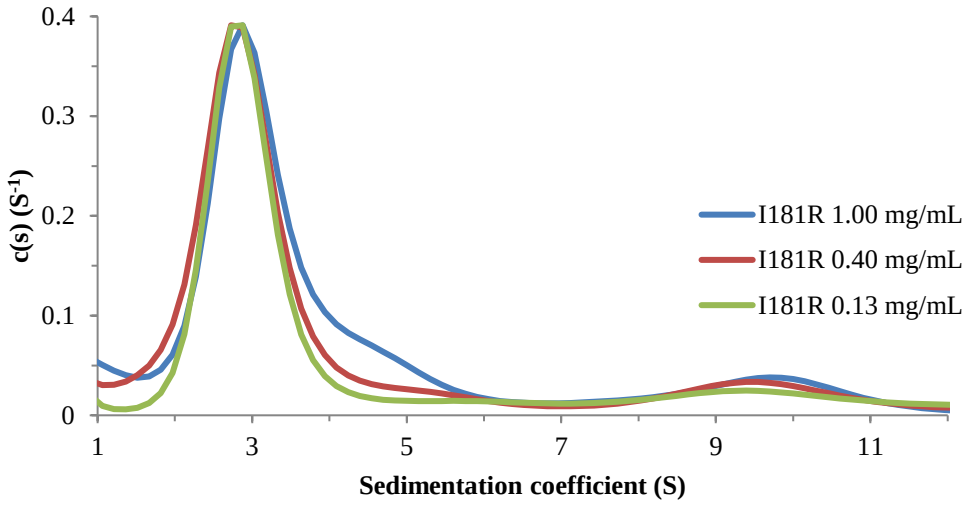

(b)

Figure 4.12: Calculated sedimentation coefficient c(s) distribution plots of *Pfu*DAH7PS single-mutants. The lower concentration results are normalised to the highest concentration result. (a) *Pfu*Q118W. (b) *Pfu*I181R.

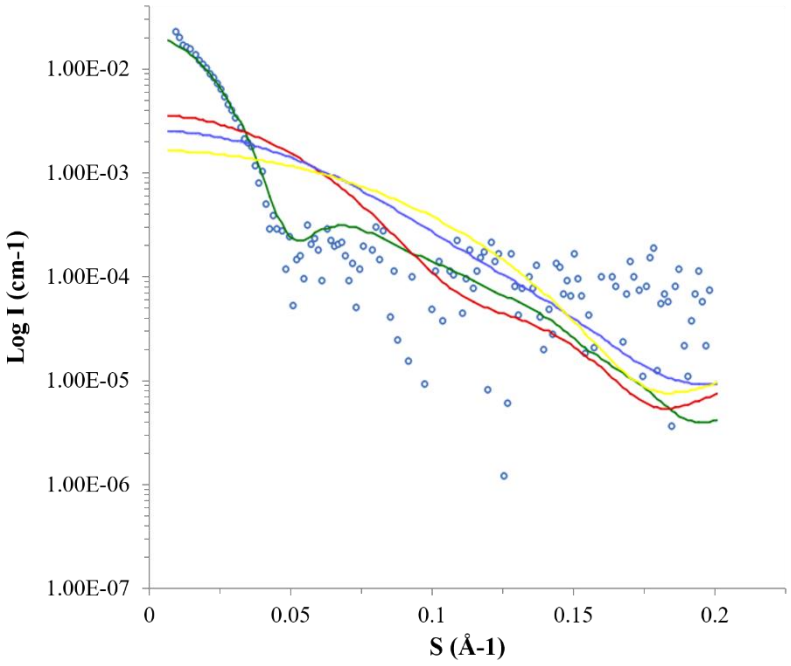

Figure 4.13: SAXS measurement of *Pfu*I181R. Theoretical scattering profiles of the *Pfu*DAH7PS wild-type six close contact tetramers (green), tetramer (red), A-B dimer (blue) and monomer (yellow) derived from the *Pfu*DAH7PS wild-type crystal structure, were generated by CRYSOL[117] and compared to the experimentally derived *Pfu*I181R data (blue circles).

4.4 Kinetic characterisation

The kinetic parameters of both *Pfu*DAH7PS single-mutants were determined by a standard enzyme activity assay to see if the introduced mutations improved or attenuated the catalytic activity (Table 4.3, overleaf). *Pfu*Q118W was found to be catalytically active and have similar characteristics compared to the wild-type enzyme. While the past study determined that *Pfu*I181D was a more active enzyme compared to the wild-type enzyme, the newly created *Pfu*I181R had no measurable activity at all. No measurable activity was

Table 4.3: Kinetic parameters of the *Pfu*DAH7PS wild-type enzyme and single-mutants. Those for the wild-type enzyme and I181D were determined by Nazmi.[84]

*Pfu*DAH7PS	K_m^{PEP} (μM)	K_m^{E4P} (μM)	k_{cat} (s^{-1})	k_{cat}/K_m^{PEP} (s^{-1} mM^{-1})	k_{cat}/K_m^{E4P} (s^{-1} mM^{-1})
Wild-type	112 ± 15	92 ± 9	5.5 ± 0.3	49 ± 9	60 ± 9
I181D	66 ± 5	71 ± 8	14.9 ± 0.5	220 ± 20	210 ± 30
Q118W	55 ± 5	99 ± 10	3.6 ± 0.1	66 ± 8	36 ± 5
I181R[a]	-	-	-	-	-

a No measurable activity

observable at the high *Pfu*I181R concentration of 16.7 μg mL^{-1} while exposed for ten minutes to 200 μM PEP, 300 μM E4P, 100 μM Cd^{2+},10 μM Ethylenediaminetetraacetic acid (EDTA) and 10 mM 1,3-bis[tris(hydroxymethyl)methylamino]propane (BTP) at 60 °C.

4.5 Discussion

The preliminary investigation into the *Pfu*DAH7PS tetramer interfaces was achieved by destabilising the *Pfu*DAH7PS tetramer by mutation of significant residues within the A-B and A-C tetramer interfaces. The A-B tetramer interface mutant *Pfu*Q118W was expressed and purified using the same procedures as the wild-type enzyme. The A-B tetramer interface mutant *Pfu*Q118W quaternary structure in solution remained as a tetramer, as observed by the analytical SEC, native PAGE and AUC results. However, the CD spectrophotometry of *Pfu*Q118W presented a notable change in the secondary structure in solution. This indicates that the change in secondary structure in solution was not due to any quaternary structure change, though could possibly be by the neighbouring regions around the Q118W mutation having to reorient

to enable the introduced larger side chain. The kinetic parameters of *Pfu*Q118W were also similar to the wild-type enzyme, which indicates that the active site around E4P and PEP has not been disturbed. However, the DSF results indicate that the presence of either E4P or PEP in the absence of Cd^{2+} no longer provides a stabilising effect. This is most likely due to the active site interactions with the neighbouring regions having been disrupted instead. As the thermal stability of *Pfu*Q118W with and without Cd^{2+} remained unchanged compared to the *Pfu*DAH7PS wild-type enzyme, the metal-binding site is not expected to be the disrupted neighbouring region. Instead, the suspected neighbouring region of interest is the Q118W region. The original Gln118 residue interacts across the interface with Arg115, a significant conserved residue which interacts with both substrates PEP (Figure 4.14) and E4P. This suggests that the Gln118 interaction with Arg115 is the source of E4P and PEP

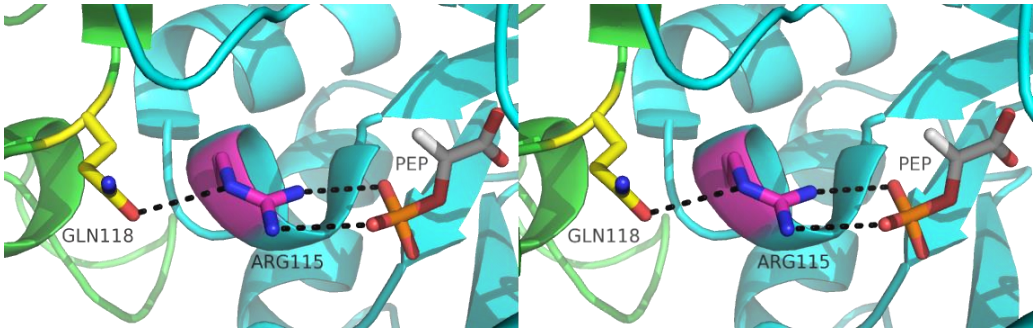

Figure 4.14: Stereoview of *Pfu*DAH7PS structure (PDB code 4C1K) showing the A-B tetramer interface interaction residue Gln118 has across the interface to residue Arg115, which subsequently interacts with the substrate PEP. Subunit A is coloured green, subunit A residue is coloured yellow, subunit B is coloured cyan, subunit C residue is coloured magenta, and PEP is coloured grey.

stabilisation with and without Cd^{2+} in the *Pfu*DAH7PS wild-type. When E4P or PEP bind to the enzyme, the Arg115 side chain would reconfigure to firmly

point towards the nearby substrate phosphate moiety and likely provide a more rigid point of contact for the Gln118 side chain to interact with across the A-B tetramer interface. Thus, additional stabilisation would occur on the A-B tetramer interface and overall protein. The introduced Q118W mutation would disrupt this cross-interface interaction, as the Q118W side chain would no longer form a hydrogen bond across the interface. In the closely related enzyme KDO8PS, the Gln118 residue is instead a conserved Arg residue, which performs the role of both Gln118 and Arg115 residues by directly interacting across the interface with the phosphate moiety of PEP. As no metal-dependent bacterial KDO8PS has had the conserved Arg residue truncated, this could be a residue of interest in a future study to determine if stabilisation via PEP binding in the presence or absence of a divalent metal ion can be disrupted in a metal-dependent bacterial KDO8PS enzyme.

While the A-C tetramer interface mutant *Pfu*I181R was expressed using the same procedures as the wild-type enzyme, the purification protocol was required to be modified due to the lower stability of the mutant. This lower stability was evident in the need to lower the heat treatment temperature from 80 °C to 60 °C, as well as the precipitation of *Pfu*I181R during attempts to concentrate it after size-exclusion chromatography. When it comes to the quaternary structure in solution of the A-C tetramer interface mutant *Pfu*I181R; analytical SEC, native PAGE and AUC all show what appears to be the presence of monomer with additional multiple states of aggregation. Analytical SEC is especially evident of the presence of the monomer; with the extremely late elution of the majority of the *Pfu*I181R mutant in comparison to the tetrameric *Pfu*DAH7PS wild-type enzyme and the partially dimeric *Pfu*I181D. The aggregated mutant is also exhibited in the SEC-SAXS result. The CD

spectrophotometry of *Pfu*I181R has also notably changed, indicating a change in the secondary structure in solution.

The stability of *Pfu*I181R with and without Cd^{2+} is drastically lower compared to the *Pfu*DAH7PS wild-type enzyme or *Pfu*I181D. The lack of additional buttressing subunits could be able to explain this; the *Pfu*I181R monomer would be more exposed and flexible compared to both the *Pfu*DAH7PS wild-type tetramer and *Pfu*I181D partial dimer, and so more vulnerable to unfolding as the mutant is heated. The presence of Cd^{2+} does appear to stabilise *Pfu*I181R, which indicates that the metal binding site does still exist. However, one of the two notable protein unfolding events indicates that the presence of Cd^{2+} does not stabilise *Pfu*I181R as successful as compared to the *Pfu*DAH7PS wild-type enzyme. The stability of *Pfu*I181R with Cd^{2+}, PEP and E4P together does remove the weaker of the two protein unfolding events, producing an increase in *Pfu*I181R stability that matches that of *Pfu*DAH7PS wild-type enzyme in the presence of Cd^{2+}, PEP and E4P together. This indicates that the active site arrangement also still exists. The presence of either PEP or E4P in the absence of Cd^{2+} no longer provided a stabilising effect. This could be due to the same reason as in A-B tetramer interface mutant *Pfu*Q118W; that the Gln118 no longer interacts across the interface with Arg115. This would occur if the A-B tetramer interface has been destabilised, which is to be expected as the *Pfu*I181R mutant is monomeric.

Unlike with the partially dimeric *Pfu*I181D mutant where the destabilisation of the A-C tetramer interface gave rise to a greater catalytic activity at the cost of some stability, the *Pfu*I181R monomer is catalytically inactive as well as drastically less stable. This raises the question of whether the protein is properly folded. The DSF result of *Pfu*I181R in the presence of

Cd^{2+}, PEP and E4P does suggest that at least both the active site and metal binding site are still properly folded. In the related *Pni*DAH7PS enzyme, truncation of the chorismate mutase domain did result in a monomeric DAH7PS that retained some catalytic activity. The DAH7PS domain portion of the *Pni*DAH7PS enzyme is usually completely exposed in the uniquely dimeric wild-type enzyme. So, removal of the chorismate mutase domain does not drastically change the conditions the *Pni*DAH7PS domain is exposed to, and so the *Pni*DAH7PS domain remains properly folded, thus some catalytic activity can be retained. The A-B tetramer interface of *Pfu*DAH7PS wild-type is never exposed, so the destabilisation of the A-B tetramer interface is a much more drastic change in conditions on the *Pfu*DAH7PS monomer, and so the monomer could become catalytically inactive due to improper folding around the exposed A-B tetramer interface.

While experimental data does indicate that the A-C tetramer interface mutant *Pfu*I181R does form a monomer, an explanation is still required to determine how a monomer occurred as opposed to an A-B dimer. The answer involves the β6α6 loop, which is normally located at the centre of where the A-C and A-B tetramer interfaces intersect (Figure 4.15, overleaf). The *Pfu*DAH7PS β6α6 loop is comprised of the residues numbered 168 to 181, which are mostly involved in only the A-C tetramer interface (Figure 4.2b), with one single important distinction; Arg169. Arg169 is the sole β6α6 loop residue which interacts across the A-B tetramer interface, forming a salt bridge with Gln145 and a hydrogen bond with the main chain carboxyl of Gly140

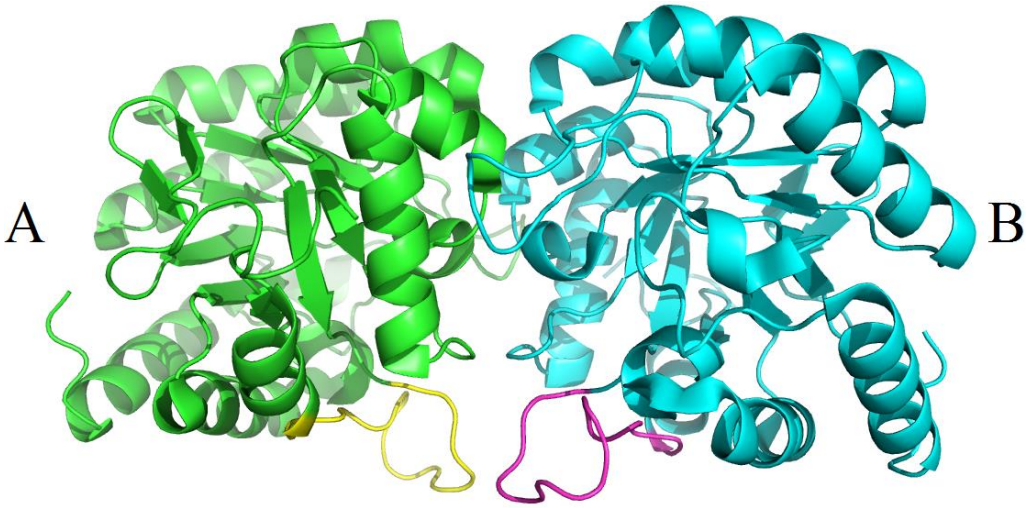

Figure 4.15: The structure of *Pfu*DAH7PS (PDB code 4C1K), with only the A-B dimer shown. Subunit A is coloured green, subunit A β6α6 loop coloured yellow, subunit B coloured cyan, and subunit B β6α6 loop coloured magenta.

(Figure 4.16, overleaf). The Arg169-Gln145 salt bridge comprises half of the salt bridges in the entire A-B tetramer interface (Figure 4.2b). Disrupting the Arg169 interactions across the A-B tetramer interface could disrupt the entire A-B tetramer interface. This is because of research which involved the closely related enzyme KDO8PS, which mutated the β6α6 loop residues performing the identical role in interacting across the same interface (the equivalent KDO8PS A-C tetramer interface). In fact, the research is performed in Chapter 3, where the *Nme*KDO8PS Tyr171 was mutated to Ala, which eliminated all β6α6 loop interactions across the KDO8PS A-C tetramer interface and gave rise to a dimeric species. The β6α6 loop interaction that *Pfu*I181R has which *Pfu*I181D does not is due to the I181R mutation itself (Figure 4.16). The I181R mutation becomes long enough to encourage the flexible β6α6 loop to potentially orient around to enable hydrogen bonding to any of the side chains of Thr170, Thr173, Thr175, and Thr178 as well as an attractive salt bridge with

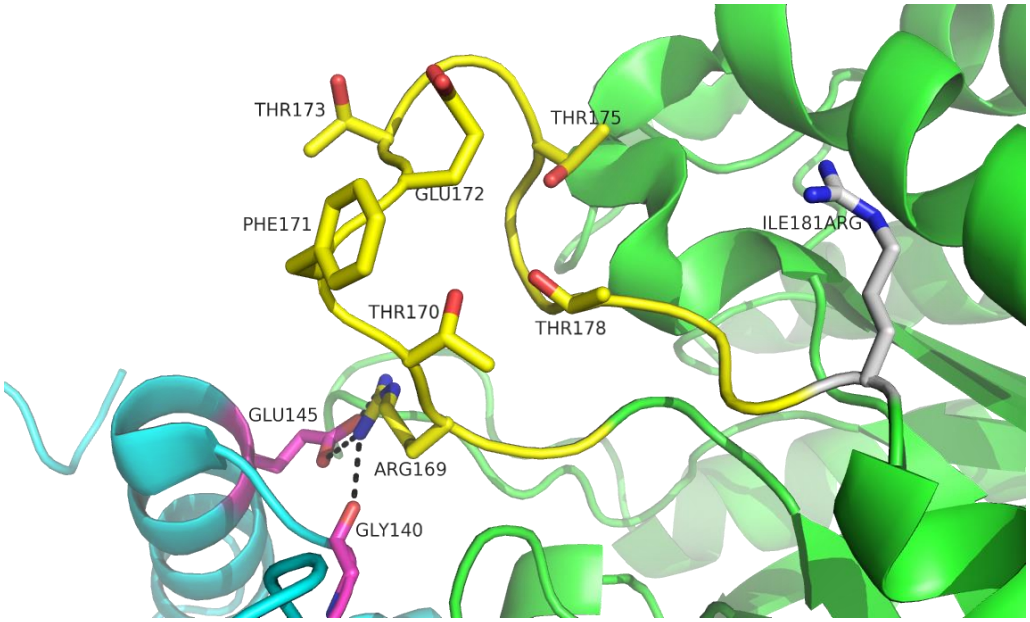

Figure 4.16: The structure of *Pfu*DAH7PS (PDB code 4C1K) depicting the β6α6 loop interactions across the A-B tetramer interface and potential β6α6 loop interactions with the mutated Ile181Arg residue. Subunit A is coloured green, subunit A β6α6 loop coloured yellow, subunit A I181R coloured white, subunit B coloured cyan, and subunit B residues which interact across the A-B tetramer interface coloured magenta.

the side chain of Glu172, in addition to allowing the exposed Phe171 residue to partially bury itself. This changed orientation of the β6α6 loop would disrupt the *Pfu*DAH7PS Arg169 interactions across the A-B tetramer interface, enough to destabilise it and give rise to the monomer. This would not occur in the previously studied *Pfu*I181D as the I181D mutation is too short to interact with any β6α6 loop side chain residues.

From the *Pfu*I181R DSF results and kinetic characterisation, it appears that the role of the A-B tetramer interface is to provide both stability and catalytic activity. As *Pfu*I181R is catalytically inactive, this would indicate that the optimal functional unit for catalysis in DAH7PS is not the monomer, but instead more likely the conserved A-B dimer found within type Iα and most

type Iβ DAH7PS. To further investigate this monomeric *Pfu*I181R, crystallisation would be difficult, as the introduced 181R makes the tetramer seen in the *Pfu*DAH7PS wild-type enzyme physically impossible. However, since *Pfu*I181R is in a monomeric state, it is small enough to enable investigation via nuclear magnetic resonance spectroscopy (NMR) in solution.

To confirm that the optimal functional unit for catalysis in DAH7PS is the conserved A-B dimer interface found within type Iα and most type Iβ DAH7PS, a *Pfu*DAH7PS mutant that forms only the A-C dimer would be ideal. The ideal *Pfu*KDO8PS mutant that could be created to achieve this would be *Pfu*R169A, as this mutant would completely remove the β6α6 loop interactions across the A-B tetramer interface. From the results of *Pfu*I181R, as well as the results from the *Nme*Y171A mutant from Chapter 3, the *Pfu*R169A mutant would likely disrupt the A-B tetramer interface and generate the A-C dimer. In addition, from the kinetics of the *Nme*Y171A mutant, the *Pfu*R169A mutant is also most likely to be less catalytically active compared to the *Pfu*DAH7PS wild-type enzyme.

4.6 Summary

The results in this chapter involving *Pfu*Q118W have identified that the A-B tetramer interface interaction between Gln118 and Arg115 is the source of E4P and PEP stabilisation in the absence of a divalent metal ion in DAH7PS. In addition, an Arg residue is identified in the related metal-dependent bacterial KDO8PS to be of interest in the PEP stabilisation in the absence and presence of a divalent metal ion. The results involving *Pfu*I181R have identified that the β6α6 loop is important in contributing to the DAH7PS A-B tetramer interface,

as the introduced mutation destabilised the A-B tetramer interface via reposition of the β6α6 loop. An Arg residue on the DAH7PS β6α6 loop is identified to be of interest in the formation of the A-B tetramer interface. In addition, the *Pfu*I181R results suggest that the role of the A-B tetramer interface is for providing both stability and catalytic activity, and that the DAH7PS monomer is not the optimal functional unit for catalysis in DAH7PS.

Chapter 5

Characterisation of *Chlorobium tepidum* KDO8PS and cloning of *Chlorella variabilis* KDO8PS

5.1 Introduction

KDO8PS proteins are suggested to have a common Iβ DAH7PS-like ancestor, predicted to have been initially a metal-dependent KDO8PS, with the metal-dependency lost later in time creating metal-independent bacterial KDO8PS and plant KDO8PS.[16, 17, 53, 90] Changes have also occurred within the KDO8PS tetramer interfaces between metal-dependent bacterial KDO8PS, metal-independent bacterial KDO8PS and plant KDO8PS. Metal-independent bacterial KDO8PS have a more hydrophobic A-B tetramer interface than the

metal-dependent bacterial KDO8PS, making disruption of the interface more difficult (as seen in Chapter 3). Performing A-B tetramer interface destabilisation experiments on a metal-dependent bacterial KDO8PS would be more likely to succeed, as the newly exposed interface would be less hydrophobic, and more likely to result in a soluble dimer. These studies would provide insight into the role of the A-B tetramer interface of metal-dependent KDO8PS as well as whether the resulting A-C dimer is the optimal functional unit for catalysis in KDO8PS.

The plant KDO8PS tetramer interface differences compared to metal-dependent bacterial KDO8PS and metal-independent KDO8PS was what led to the initial hypothesis that plant KDO8PS were homodimeric.[131] More recent studies involving crystallisation and analytical ultracentrifugation of a plant *Ath*KDO8PS isozyme have indicated that the tetramer is likely to be the accurate quaternary structure.[138] A recent study has also shown that the plant *Pe*KDO8PS formed both a tetramer and a dimer in solution.[140] The research performed in Chapter 3 of this thesis suggest that the dimeric *Pe*KDO8PS is the A-B dimer, due to a unique residue difference of Asn-to-Ser on the β6α6 loop compared to most other plant KDO8PS proteins. This A-B dimer is not seen in any other characterised KDO8PS, as well as not seen in any characterised type Iβ DAH7PS as the equivalent DAH7PS A-C dimer. However, another plant KDO8PS does exhibit the same Asn-to-Ser residue change: *Olu*KDO8PS. This observation suggests the possibility that the role of the A-C tetramer interface within plant KDO8PS may differ compared to the metal-dependent bacterial KDO8PS, metal-independent bacterial KDO8PS as well as the type Iβ DAH7PS. Performing tetramer interface destabilisation experiments on plant KDO8PS may provide insight into the role of each

tetramer interface of plant KDO8PS, as well as seeing if the A-B dimer is the optimal functional unit for catalysis in plant KDO8PS.

5.1.1 Metal-dependent KDO8PS interface disruption

Only a small number of metal-dependent KDO8PS proteins have been characterised: *A. aeolicus* (*Aae*),[36, 37] *H. pylori* (*Hpy*),[66] *A. pyrophilus* (*Apy*),[110] *A. ferrooxidans* (*Afe*)[6] and *C. jejuni* (*Cju*) KDO8PS.[45] A metal-dependent KDO8PS whose crystal structure has been determined would be an ideal target for interface disruption. For a long time, the only metal-dependent KDO8PS crystallised had been *Aae*KDO8PS,[35] with *Hpy*KDO8PS only recently being crystallised.[19] However, *Aae*KDO8PS is a highly stable metal-dependent bacterial KDO8PS from a hyperthermophile, retaining structure and activity to very high temperatures over a long period of time.[36] Due to the extreme stability of *Aae*KDO8PS, it would not be an ideal metal-dependent KDO8PS target for interface disruption. A new metal-dependent KDO8PS was desirable for tetramer interface disruption experiments.

5.1.2 *Chlorobium tepidum* KDO8PS

Chlorobium tepidum (*Cte*) KDO8PS is a metal-dependent KDO8PS reported to be closely phylogenetically related to the type Iβ DAH7P synthases.[17, 53] *Cte*KDO8PS was identified as the target for metal-dependent KDO8PS interface disruption. *Cte*KDO8PS had been the subject of previous investigation in our laboratory, it was cloned into an expression vector, purification protocol developed, and some initial characterisation was

completed.[136] *Cte*KDO8PS was found to be metal-dependent and to have stability issues after various purification techniques. In this chapter, the characterisation of *Cte*KDO8PS is extended.

5.1.3 Plant KDO8PS interface disruption

All past studies into metal-independent plant KDO8PS proteins have focused on vascular plants including various vegetables,[29] *Pisum sativum L.*,[30] *A. thaliana* (*Ath*),[28, 79, 131, 138] *Lycopersicon esculentum*[27] and *Morus alba L.*[135] Only three plant KDO8PS proteins have been reported to have been characterised: both of the two isozymes of *Ath*KDO8PS,[131, 138] and *Pe*KDO8PS.[140] A plant KDO8PS which has been characterised, as well as having a crystal structure determined, would have been an ideal target for interface disruption. However, none were known until recently from *Ath*KDO8PS isozyme 2.[138] No KDO8PS from a more archaic plant, such as green algae, has ever been studied.

5.1.4 *Chlorela variabilis* KDO8PS

The green algae *Chlorela variabilis* (*Cvr*) KDO8PS was identified for use in tetramer interface disruption experiments. *Cvr*KDO8PS has a high sequence identity to both plants and bacterial KDO8PS and is more closely related to vascular plant KDO8PS sequences compared to bacterial KDO8PS sequences. In addition, *Cvr*KDO8PS contains a unique five residue extension on the β6α6 loop not seen in any other KDO8PS sequence (Figure 5.1, overleaf).

```
HpyKDO8PS       ------MKTSKTKTPKSVLIAGPCVIESLENLRSIATKLQPLANNERLDFYFKASFDKAN
NmeKDO8PS       -MDIKINDITLGNNSPFVLFGGINVLESLDSTLQTCAHYVEVTRKLGIPYIFKASFDKAN
CvrKDO8PS       ----SALFQELKASQPFFLMAGPNVIQSEEHCLKMCRQIKAVTDSLGIKLVFKSSFDKAN
AthKDO8PS       MAATSLLYNQLKAAEPFFLLAGPNVIESEEHILRMAKHIKDISTKVGLPLVFKSSFDKAN
                             .*:.*  *::* :     . :   :: .  :   **:******

HpyKDO8PS       RTSLESYRGPGLEKGLEMLQTIKEEFGYKILTDVHESYQASVAAKVADILQIPAFLCRQT
NmeKDO8PS       RSSIHSYRGVGLEEGLKIFEKVKAEFGIPVITDVHEPHQCQPVAEVCDVIQLPAFLARQT
CvrKDO8PS       RTSAASFRGPGMEEGLRVLKKVKDTFGVPIITDIHESWQAEQVAQVADIIQIPAFLCRQT
AthKDO8PS       RTSSKSFRGPGMAEGLKILEKVKVAYDLPIVTDVHESSQCEAVGKVADIIQIPAFLCRQT
                *:*  *:** *: :**.::::.:*  :.  ::**:**  *.. ..:*.*::*:****.***

HpyKDO8PS       DLIVEVSQTNAIVNIKKGQFMNPKDMQYSVLKALKTRDKSIQSPTYETALKNGVWL--CE
NmeKDO8PS       DLVVAMAKTGNVVNIKKPQFLSPSQMKNIVEKF-------------HEAGNGKLIL--CE
CvrKDO8PS       DLLVAAAKTGKVIQIKKGQFCAASVMRNSAEKC-------------RHAGEAGVWLRVCG
AthKDO8PS       DLLVAAAQTGKIINIKKGQFCAPSVMENSAEKI-------------RLAGNPNVMV--CE
                **:*  ::*. :::*** **   . *.  . *              . * :  : :  *

HpyKDO8PS       R---GSSFGYGNLVVDMRSLKIMRE---FAPVIFDATHSVQMPGGA-----NGKSSGDSS
NmeKDO8PS       R---GSSFGYDNLVVDMLGFGVMKQTCGNLPVIFDVTHSLQTR-----DAGSAASGGRRA
CvrKDO8PS       RLCVGGFVRVDDLVVDPRNFVAMRD--AGCPVTADVTHALQQPAGRPLEGGGVASGGMRD
AthKDO8PS       R---GTMFGYNDLIVDPRNFEWMRE--ANCPVVADITHSLQQPAGKKLDGGGVASGGLRE
                *   *  .  .:*:**  .:  *::     **  * **::*          .  *.*

HpyKDO8PS       FAPILARAAAAVGIDGLFAETHVDPKNALSDGANMLKPDELEQLVTDMLKIQNLF-----
NmeKDO8PS       QALDLALAGMATRLAGLFLESHPDPKLAKCDGPSALPLHLLEDFLIRIKALDDLIKSQPI
CvrKDO8PS       MIPAIARTAVACGVDGLFMEVHDDPTTSPVDGPTQWPLRHLRRLLVELLAIAGASRGKED
AthKDO8PS       LIPCIARTAVAVGVDGIFMEVHDDPLSAPVDGPTQWPLRHLEELLEELIAIARVTKGKQR
                    :* :. *  : *:* * * **  :  ** .      *. ::  :  :

HpyKDO8PS       --------------------
NmeKDO8PS       LTIE----------------
CvrKDO8PS       FHLDLSPIKEEDFDPLAVV
AthKDO8PS       LQIDLTPYRD---------
```

Figure 5.1: Structure-based alignment of KDO8PS proteins. The sequence of green algae *Cvr*KDO8PS was structurally aligned with the structurally characterised bacterial metal-dependent *Hpy*KDO8PS, bacterial metal-independent *Eco*KDO8PS and plant *Ath*KDO8PS. Structural alignment performed using Clustal Omega.[47, 113] The residues involved in the KDO8PS interfaces are colour coded: A-B interface purple and A-C interface green. The 5 unique extra residue in the *Cvr*KDO8PS sequence are colour coded red.

This would likely affect the positioning of the neighbouring Asn residue on the β6α6 loop that has been identified in Chapter 3 to be very significant in allowing the A-C tetramer interface to form in plant KDO8PS. It should be noted that the beginning of the *Cvr*KDO8PS gene sequence (locus tag CHLNCDRAFT_26331) is not complete, however sequence alignments with other KDO8PS proteins indicate less than five residues are missing at the start of the sequence. In addition, there are numerous KDO8PS sequences which are shorter and that begin later compared to the *Cvr*KDO8PS sequence. Due to this, the truncation of the start of the *Cvr*KDO8PS sequence is not expected to affect significantly the activity, stability, and structure of the enzyme. In this chapter, a description of the attempted cloning of *Cvr*KDO8PS is described.

5.2 *Chlorobium tepidum* KDO8PS

5.2.1 Expression, purification and protein characterisation

The *Cte*KDO8PS gene was previously cloned into a pT7-7 expression vector by Yeoman.[136] A putative purification protocol was developed, consisting of anion-exchange chromatography followed by hydrophobic-interaction chromatography. Yeoman also found that the *Cte*KDO8PS protein noticeably denatures over time after concentrating the protein prior to and after hydrophobic-interaction chromatography.

The initial investigation into *Cte*KDO8PS purification was to reduce the number of purification steps. To attempt this, heat treatment was trialled. Temperatures above 50 °C caused noticeable reduction in KDO8PS activity, while below 50 °C created no significant purification of the protein samples.

Cation-exchange chromatography (CEC), in replacement of anion-exchange chromatography was also trialled. As *Cte*KDO8PS has an isoelectric point (pI) of 6.79, CEC was performed at either pH of 4.5 and 5.5. However, *Cte*KDO8PS did not bind sufficiently to the column at both pH 4.5 and 5.5, so CEC was abandoned. Size-exclusion chromatography, added as a third purification step to desalt and increase the purity of the protein samples, was also trialled. However, negligible protein yields arose from size-exclusion chromatography. The use of a desalting column after hydrophobic-interaction chromatography (to desalt the protein samples) was also trialled. Interestingly, *Cte*KDO8PS was found to completely denature after this column, suggesting the presence of salt is important for the stability of the protein.

Other trials in the *Cte*KDO8PS purification were more successful. Protein over-expression by induction using isopropyl β-D-1-thiogalactopyranoside (IPTG) overnight at 23 °C, was found to produce more soluble *Cte*KDO8PS compared to the original 4 hours at 37 °C protocol. Trials of anion-exchange chromatography at a variety of pH comprised of 7.5, 8.25, 8.5 and 9.5, were also investigated. Anion-exchange chromatography at pH 8.25 produced the most soluble *Cte*KDO8PS compared to the original pH 8.5 protocol. Finally, the resulting anion-exchange chromatography product was not concentrated before hydrophobic-interaction chromatography, as this decreased the chance of denaturing of the *Cte*KDO8PS prior to hydrophobic-interaction chromatography. However, these improvements were not sufficient in generating stable *Cte*KDO8PS in consistent sufficient yield. From 1 L of bacterial cell culture, *Cte*KDO8PS was purified with a yield of 0.6 mg/mL.

5.2.2 Buffer and metal activation

The *Cte*KDO8PS activity was tested in a variety of buffers to find the maximum activity in (Figure 5.2). The buffers comprised of tris(hydroxymethyl)aminomethane (Tris), bis[tris(hydroxymethyl)methylamino]propane (BTP), 4-(2-hydroxyethyl)-1-piperazineethanesulfonic acid (HEPES) and Tris-acetate. Tris, BTP and Tris-acetate buffers produced similar *Cte*KDO8PS activity, while HEPES decreased activity. BTP was chosen as it was the only buffer also present in the purification process.

*Cte*KDO8PS had no measurable activity in the presence of 10 µM ethylenediaminetetraacetic acid (EDTA), however in the presence of various divalent metal ions, activity was restored (Figure 5.3, overleaf). The most activating divalent metal ions for *Cte*KDO8PS were Mn^{2+}, followed by a close

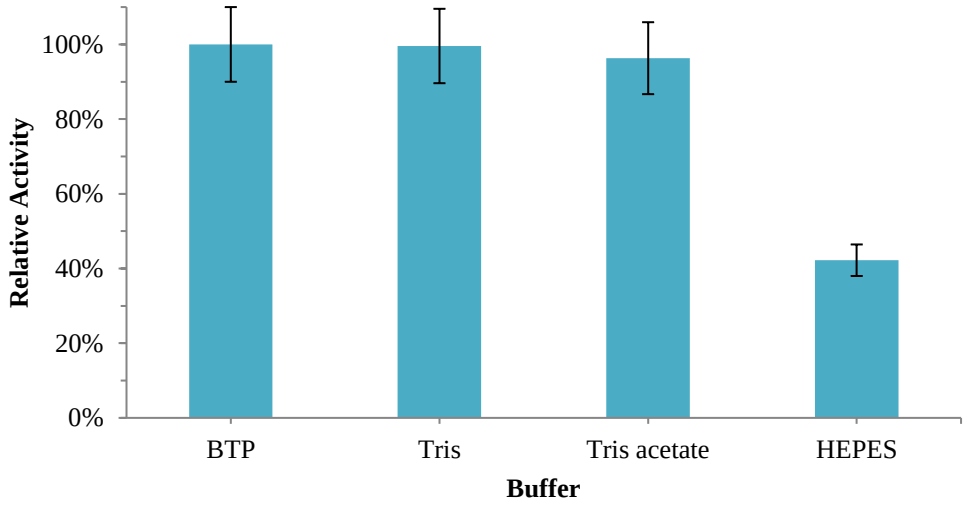

Figure 5.2: The wild-type *Cte*KDO8PS buffer-activity profile. Relative activity has been normalised to the highest activating buffer.

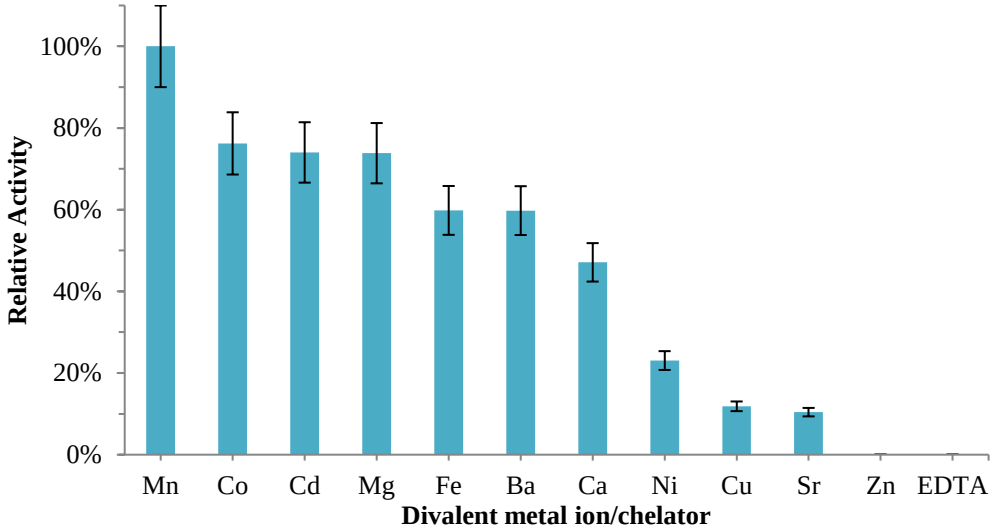

Figure 5.3: The wild-type *Cte*KDO8PS metal-activation profile. Relative activity has been normalised to the highest activating metal ion.

group of Co^{2+}, $Cd^{2+}$and Mg^{2+} (Figure 5.3). As Mn^{2+} was the most activating of the divalent metal ions, it was chosen as the divalent metal ion to be present in the following kinetic experiments. The metal-dependent *Afe*KDO8PS,[6] *Apy*KDO8PS[110] and *Cju*KDO8PS[45] also obtain maximum activity in the presence of Mn^{2+} whereas *Aae*KDO8PS[37] and *Hpj*KDO8PS[66] show maximum activity in the presence of Cd^{2+}.

The *Cte*KDO8PS activity at a variety of temperatures from 25-65 °C was tested in the presence of Mn^{2+} to determine the optimum temperature for *Cte*KDO8PS activity (Figure 5.4, overleaf). *Cte*KDO8PS has maximum activity at 45 °C. This is higher than used in kinetic investigations into *Hpj*KDO8PS (25 °C)[66] and *Afe*KDO8PS (37 °C),[6] and lower than for *Apy*KDO8PS (60 °C),[110] *Cju*KDO8PS (60 °C)[45] and *Aae*KDO8PS (80 °C).[37]

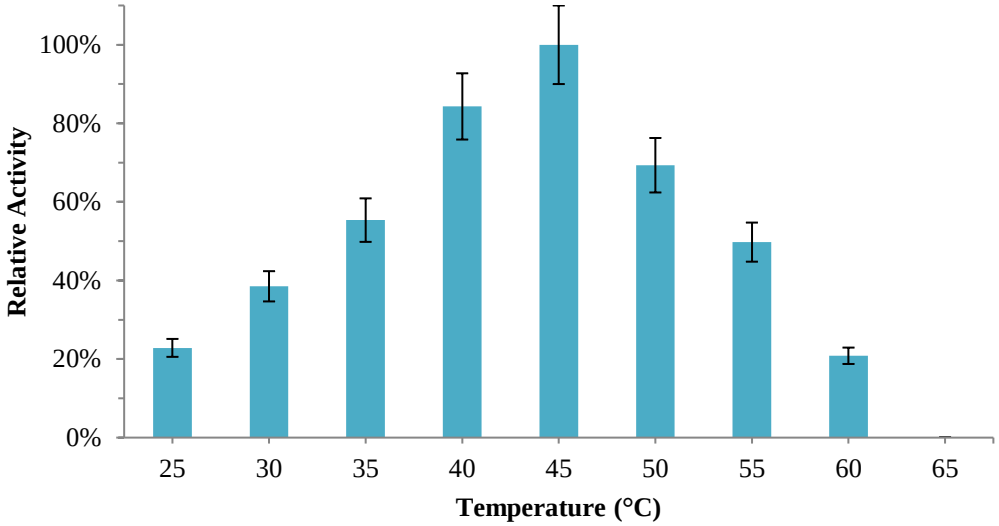

Figure 5.4: The wild-type *Cte*KDO8PS temperature-activation profile. Relative activity has been normalised to the highest activating temperature.

5.2.3 Kinetic properties

The *Cte*KDO8PS kinetic parameters were determined in the presence of the divalent metal Mn^{2+}, BTP buffer and at the optimum temperature of 45 °C. The K_m^{PEP} was 11.9 ± 1.1 µM, the K_m^{A5P} was 18.9 ± 1.8 µM, and the k_{cat} was 3.00 ± 0.01 s^{-1}. The kinetic parameters determined are similar to those observed for KDO8PS enzymes from *E. coli*,[92] *S. typhimurium*,[120] *H. pylori*,[66] *A. thaliana*,[131] *N. meningitidis* (*Nme*),[2] *A. ferrooxidans*[6] and *N. gonorrhoeae*.[134] The k_{cat} value determined is also similar to those observed for KDO8PS enzymes from the hyperthermophilic *Aae*KDO8PS[36] and *Apy*KDO8PS.[110]

5.2.4 Structure in solution and stability

The secondary structure of *Cte*KDO8PS was investigated by circular dichroism CD spectrophotometry and compared to *Nme*KDO8PS to see if *Cte*KDO8PS had any unique secondary structure. The spectrum recorded for *Cte*KDO8PS is similar to the structurally characterised *Nme*KDO8PS (Figure 5.5). This indicates that *Cte*KDO8PS has a similar secondary structure to *Nme*KDO8PS, which would correspond to a similar $(\beta/\alpha)_8$ tertiary structure.

The quaternary structure of *Cte*KDO8PS was investigated by analytical SEC and compared to *Nme*KDO8PS to see if *Cte*KDO8PS had a unique quaternary structure. Data were compared to multiple protein standards of known size and elution volume. The elution volumes correlate to a molar mass of 116 kDa and 130 kDa for *Cte*KDO8PS and *Nme*KDO8PS respectively. Both values indicate tetrameric protein, as the calculated tetramer sizes for

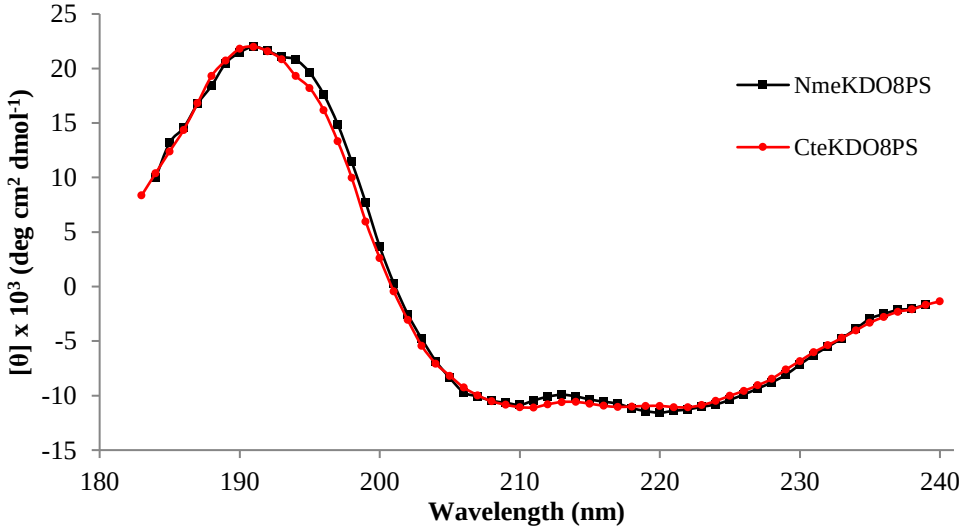

Figure 5.5: The CD spectrophotometry of wild-type and wild-type *Nme*KDO8PS *Cte*KDO8PS (red circles and black squares respectively).

*Cte*KDO8PS and *Nme*KDO8PS are 122 kDa and 121 kDa. This agrees with a previous study into the quaternary structure of *Nme*KDO8PS being tetrameric, from analytical SEC and crystallographic models.[21]

To investigate the thermal stability of wild-type *Cte*KDO8PS, DSF was used. DSF was performed in the presence various divalent metal ions to see if any divalent metal provided a stabilising effect (Table 5.1). In the presence of most divalent metal ions, including the most activating Mn^{2+}, the T_m of *Cte*KDO8PS remained unaffected at 67 °C. Interestingly, in the presence of 80 µM Zn^{2+} and Cd^{2+}, the T_m values dropped by 5 °C and 6 °C respectively. This effect on stability may contribute to why these two divalent metal ions do not

Table 5.1: The effect of divalent metal ions on the T_m of *Cte*KDO8PS wild-type enzyme.

KDO8PS	Additives	T_m (°C)	Difference (°C)
*Cte*KDO8PS	No additive	67 ± 1	
	Mn^{2+}	67 ± 1	0
	Co^{2+}	67 ± 1	0
	Cd^{2+}	62 ± 1	-5
	Mg^{2+}	67 ± 1	0
	Fe^{2+}	65 ± 1	-2
	Ba^{2+}	67 ± 1	0
	Ca^{2+}	67 ± 1	0
	Ni^{2+}	67 ± 1	0
	Cu^{2+}	67 ± 1	0
	Sr^{2+}	67 ± 1	0
	Zn^{2+}	61 ± 1	-6

activate *Cte*KDO8PS, compared to Mn^{2+}.

5.3 *Chlorela variabilis* KDO8PS cloning

The *Cvr*KDO8PS wild-type gene (locus tag CHLNCDRAFT_26331) was ordered within a pBluescript SK vector from Epoch Life Science. The *Cvr*KDO8PS gene contained additional N-terminal residues comprising of Gateway attachment site, a Tobacco Etch Virus (TEV) cleavage site, and a linker region. The C-terminal also had Gateway attachment site.

Gateway cloning was considered, before In-Fusion® cloning was performed to insert the TEV cleavage site, linker region, and *Cvr*KDO8PS gene into the N-terminal polyhistidine tagged pET-28a vector. The restriction enzyme sites used were NdeI and XhoI. Initial cloning attempts inserted the *Cvr*KDO8PS gene in the reverse complement form. Subsequent cloning successfully inserted the *Cvr*KDO8PS gene in the correct forward form, however with a reading frame shift ahead of the inserted *Cvr*KDO8PS gene. This was caused by an additional deoxyribonucleic acid (DNA) base remaining at the NdeI site where the pET-28a vector was cut, ahead of the *Cvr*KDO8PS gene that was inserted. Attempting to remove the unnecessary base via site-directed mutagenesis was unsuccessful. Attempting to use In-Fusion® cloning of the *Cvr*KDO8PS gene, with two additional N-terminal bases after the NdeI site, into the pET-28a vector was unsuccessful. Attempting to use alternative restriction enzyme sites EcoRI and XhoI, with the addition of a base after the EcoRI site to stop the formation of a reading frame shift, was unsuccessful.

5.4 Summary

Wild-type *Cte*KDO8PS was successfully expressed, purified and characterised after considerable trial. In the group of characterised KDO8PS proteins, *Cte*KDO8PS exhibits similar properties, having comparable preferred divalent metal ion, kinetic parameters, a similar fold, and similar tetrameric quaternary structure. However, purification of *Cte*KDO8PS in consistent sufficient yields by modifying the purification protocols and conditions was not achieved. After characterisation of *Cte*KDO8PS, plans to utilise *Cte*KDO8PS as a metal-dependent KDO8PS for tetramer interface destabilisation experiments were not pursued. A metal-dependent KDO8PS that would be ideal for tetramer interface destabilisation experiments would be the *H. pylori* KDO8PS, as it has now been successfully purified, characterised and crystallised.[19]

*Cvr*KDO8PS cloning was only partially successful in inserting the gene into an appropriate plasmid, due to the presence of a reading frameshift that arose from the cloning. After numerous unsuccessful attempts to remove the reading frame shift, plans to characterise and utilise *Cvr*KDO8PS as a plant KDO8PS for interface disruption were not pursued. Cloning, expression, purification, characterisation and crystallisation of *Cvr*KDO8PS would still be an ideal to be pursued in the future, as no archaic plant KDO8PS has yet to undergo such an investigation, as well as due to the unique β6α6 loop extension. A plant KDO8PS that would be ideal for tetramer interface destabilisation experiments would be the *Ath*KDO8PS isozyme 2, as it has now been successfully purified, characterised and crystallised.[138] Another plant KDO8PS that would be of interest for tetramer interface destabilisation experiments would be the plant KDO8PS from *Ostreococcus lucimarinus*, as it

also has the Asn-to-Ser residue difference seen in the plant *Pni*KDO8PS suspected to destabilise the A-B tetramer interface and give rise to a dimeric species.

Chapter 6

Summary of thesis and overall conclusions

In this thesis, the role of the quaternary structure between metal-dependent bacterial, metal-independent bacterial and plant KDO8PS, and how it relates to the role of the quaternary structure in DAH7PS was explored.

The role of the conserved Asp92 and Pro112 residues in the PEP binding pocket of KDO8PS was explored. In type Iβ DAH7PS, the equivalent Asp92 residue is conserved as a Glu, which offers the same functionality but has a side chain one-carbon longer. Previous mutation of Asp-to-Glu in KDO8PS affected the catalytic rate, but not the binding of PEP. However, the inability for the Asp-to-Glu mutant sidechain to form a configuration identical to that found in DAH7PS due to the nearby Pro112 residue disallowed an accurate assessment of the Asp-to-Glu mutant qualities.[3] In type Iβ DAH7PS, the equivalent Pro112 residue is conserved as a Gly, which offers the same helix

breaker functionality but frees space for the equivalent Glu to orient properly. Introduction of the additional mutation of Pro to Gly and Ala in KDO8PS affected the binding of both substrates, the catalytic rate and the quaternary structure. The significance of the conserved Asp92 residue in the putative proton relay chain remained unclear once the Pro112 residue was also mutated, due to the inability of the Asp-to-Glu mutant to form a conformation similar to DAH7PS. In type Iβ DAH7PS, a conserved Asn187 is present on the β4α4 loop which allows the native Glu to be accommodated in a conformation not observed in the Pro-to-Ala mutant KDO8PS, due to conservation as Leu115 instead. A nearby His94 on the KDO8PS α3 helix, which in DAH7PS is conserved as a small hydrophobic residue, may also play a role in the Glu conformational difference. For future studies, producing the *Nme*KDO8PS mutants D92E/P112G/L115N and D92E/ H94L/P112G/L115N could ensure the D92E side chain forms an arrangement similar to that of DAH7PS and help provide more information on the role of the conserved Asp92 and Pro112 residues in the PEP binding pocket of KDO8PS. Producing the *Pfu*DAH7PS double mutant M95H/N116L could encourage the *Pfu*DAH7PS active site Glu93 residue to form an orientation identical to *Nme*D92E/P112G, and provide information on the catalytic impact the unique orientation of *Nme*KDO8PS Glu92 has had. This would also help provide more information on the role of the conserved Asp92 and Pro112 residues in the PEP binding pocket of KDO8PS.

The conserved Pro112 residue exhibits importance in providing rigidity in the KDO8PS active site, as well as being important in the formation of the KDO8PS tetramer due to its nature as a helix breaker. The disruption of the KDO8PS A-C tetramer interface provided additional evidence that the A-B dimer is catalytically less active than the tetramer.

The role of significant residues on the KDO8PS tetramer interfaces was also investigated. Mutation of the metal-independent bacterial *Nme*KDO8PS tetramer interface residues to represent those of plant KDO8PS provided additional evidence that the β2α2 loop sequence difference in plant KDO8PS is not indicative of a dimer species. In addition, the β6α6 and β4α4 loop interactions across the A-C tetramer interface have been identified to be more important compared to the β2α2 loop interactions, as truncation of Tyr171 and Pro112 respectively gave rise to dimeric species. Tyr171 and Pro112 are also identified to be target residues for tetramer interface destabilisation experiments in metal-dependent bacterial KDO8PS and plant KDO8PS. The identification that the β6α6 loop is important for the A-C tetramer interface to form provides another target residue in plant KDO8PS tetramer interface destabilisation experiments, the Asp172 plant equivalent Asn. In the partially dimeric plant *Pe*KDO8PS wild-type enzyme, the main suspected cause of destabilisation is this Asp172 equivalent residue, where instead of being the usual plant Asn residue, it is instead a smaller Ser residue. The same residue could also be used to identify and characterise other dimeric plant KDO8PS wild-type enzymes. The plant *Olu*KDO8PS would be one prime target for a study on the enzyme quaternary structure. The A-C tetramer interface destabilisation experiments indicate that the A-B dimer is not the optimal functional unit for catalysis in KDO8PS, whereas the A-B tetramer interface destabilisation experiments do not rule out that the A-C dimer is. The highly hydrophobic content of the metal-independent bacterial A-B tetramer interface combined with the insolubility of the A-B tetramer interface mutations indicate that extensive mutations would be required to reduce the highly hydrophobic interface to enable a soluble A-C dimer to exist. In addition, A-B tetramer interface destabilisation experiments are suggested to be more successful in the

metal-dependent bacterial KDO8PS and plant KDO8PS A-B tetramer interfaces, as the lower hydrophobic content may enable a soluble A-C dimer to be stable.

The importance of significant residues on the DAH7PS tetramer interfaces was also investigated. Mutation of the DAH7PS A-B tetramer interface has identified a specific Gln118 residue interaction with Arg115 across the A-B tetramer interface important for E4P and PEP stabilisation in the presence or absence of a divalent metal ion in DAH7PS. It also identified a specific residue of interest on the metal-dependent bacterial KDO8PS equivalent A-C tetramer interface that might be important for PEP stabilisation in the presence or absence of a divalent metal ion. Creation of the DAH7PS monomer from mutation of the DAH7PS A-C tetramer interface suggest that the role of the A-C tetramer interface is for providing both stability and catalytic activity as well as indicating that the DAH7PS monomer is not the optimal functional unit for catalysis in DAH7PS. In addition, the β6α6 loop is identified to be important in contributing to the DAH7PS A-C tetramer interface, as well as identifying a specific Arg169 residue that can be targeted to destabilise the DAH7PS A-C tetramer interface.

A metal-dependent bacterial KDO8PS as well as a plant KDO8PS were also investigated as possible targets for tetramer interface destabilisation experiments. The metal-dependent bacterial *Cvr*KDO8PS was characterised and found to have a comparable preferred divalent metal ion, kinetic parameters, a similar fold, and similar tetrameric quaternary structure to other characterised KDO8PSs. *Cvr*KDO8PS was determined to not be an ideal target for tetramer interface destabilisation experiments due to poor purification yields. An alternative metal-dependent bacterial KDO8PS that could be used for tetramer interface destabilisation experiments is *Hpy*KDO8PS. This is due

to being one of only two metal-dependent bacterial KDO8PS that past studies have characterised and crystallised.[19, 66] The other option, *Aae*KDO8PS is a highly stable metal-dependent bacterial KDO8PS from a hyperthermophile, which would make tetramer interface destabilisation experiments extremely difficult. The plant *Cvr*KDO8PS was identified to have a unique five residue extension on the β6α6 loop not seen in any other plant KDO8PS, that could affect the positioning of a very significant residue that allows the A-C tetramer interface to form in plant KDO8PS. An alternative plant KDO8PS that also could be used for tetramer interface destabilisation experiments would be *Ath*KDO8PS isozyme 2, as it is the only plant KDO8PS that has been characterised and crystallised.[131, 138] An additional alternative plant KDO8PS is identified that also could be used for tetramer interface destabilisation experiments, from *Ostreococcus lucimarinus*, which is suspected to be partially dimeric as it shares the β6α6 loop Asn-to-Ser residue seen in *Pe*KDO8PS.

6.1 Significance of the KDO8PS and DAH7PS quaternary structure

All KDO8PSs are suggested to have a common Iβ DAH7PS-like ancestor, are predicted to have been initially a metal-dependent KDO8PS, with the metal-dependency lost later in time creating metal-independent bacterial KDO8PS and plant KDO8PS. The accumulated changes over time from DAH7PS to KDO8PS have changed what substrates are catalysed, the essentiality of a divalent metal for catalysis, and what additional domains are attached to the core TIM barrel for allosteric control.

This thesis shows that even with all these accumulated changes, the core role that the KDO8PS quaternary structure plays in the KDO8PS activity and stability has not changed since their origin in DAH7PS. The *Pfu*DAH7PS tetramer interface destabilisation experiments performed in Chapter 4 of this thesis indicate that the DAH7PS monomer is not the optimal functional unit for catalysis in DAH7PS, and suggests that the A-C dimer is not as well. In addition, the A-B tetramer interface is shown to have an essential role in keeping the DAH7PS catalytically active, as well as providing significant stability. This does provide further evidence that the DAH7PS A-B dimer is indeed the optimal functional unit for catalysis in DAH7PS, with the A-C tetramer interface providing significant stability at the cost of greater catalytic activity.

These DAH7PS discoveries are also shown in the metal-independent bacterial KDO8PS. The *Nme*KDO8PS tetramer interface destabilisation experiments performed in Chapter 3 (as well as unintentionally in Chapter 2) of this thesis show that the KDO8PS A-C tetramer interface (the DAH7PS A-B tetramer interface equivalent) also contributes greater catalytic activity and significant stability. In addition, the KDO8PS A-B tetramer interface (the DAH7PS A-C tetramer interface equivalent) is also suggested to provide significant stability at the cost of greater catalytic activity.

While the core role of the KDO8PS tetrameric structure has on activity and stability has been preserved through evolution from the origin in DAH7PS, some differences have occurred to both tetramer interfaces. While the DAH7PS A-C tetramer interface is not highly hydrophobic, as well as that for the equivalent metal-dependent bacterial KDO8PS and plant KDO8PS A-B tetramer interface, the metal-independent bacterial KDO8PS A-B tetramer

interface is highly hydrophobic. The *Nme*KDO8PS tetramer interface destabilisation experiments performed in Chapter 3 of this thesis show that this increase in hydrophobicity makes disruption of the metal-independent bacterial KDO8PS A-B tetramer interface more difficult, as the result is an insoluble protein. Thus, the KDO8PS A-B tetramer interface is suggested to play an even greater role in the stability of metal-independent KDO8PS compared to DAH7PS, metal-dependent bacterial KDO8PS and plant KDO8PS.

The other tetramer interface also has an interesting difference. The *Pfu*DAH7PS tetramer interface destabilisation experiments performed in Chapter 4 of this thesis suggest that the single β6α6 loop residue Arg169, is essential in the formation of the A-B tetramer interface. In Chapter 3 of this thesis, the equivalent A-C tetramer interface in metal-independent bacterial *Nme*KDO8PS was disrupted by truncation of the β6α6 loop residue Tyr171. As both metal-dependent bacterial KDO8PS and plant KDO8PS also have this Tyr residue, truncation of it would likely destabilise their equivalent A-C tetramer interface as well. Truncation of the β6α6 loop residue Asp172 did not destabilise the equivalent A-C tetramer interface in metal-independent bacterial. This residue truncation is also not expected to destabilise the equivalent A-C tetramer interface in metal-dependent bacterial KDO8PS. Truncation of the equivalent residue in plant KDO8PS however, is suspected to destabilise the equivalent A-C tetramer interface, as it is also the Asn-to-Ser residue of interest identified in dimeric *Pe*KDO8PS wild-type enzyme to destabilise the equivalent A-C tetramer interface. This Asn-to-Ser residue change is also present in the plant *Olu*KDO8PS. Plant KDO8PS also have changes in the β2α2 loop which *Nme*KDO8PS tetramer interface destabilisation experiments performed in Chapter 3 of this thesis show does weakened the A-C tetramer

interface. This plant KDO8PS A-B dimer is not seen in any wild-type metal-independent bacterial KDO8PS, metal-dependent bacterial KDO8PS or the equivalent A-C dimer in DAH7PS. This all suggests that the KDO8PS A-C tetramer interface plays a weaker role in the stability of plant KDO8PS.

To uncover more on the role of the quaternary structure of KDO8PS, tetramer interface destabilisation experiments on a metal-dependent bacterial KDO8PS and plant KDO8PS would be ideal. This thesis has determined that *Hpy*KDO8PS and *Ath*KDO8PS would likely to be suitable candidates for further investigation. The work described in this thesis has also identified two residues that could be targeted to destabilise the A-C tetramer interface in both KDO8PS: the *Nme*KDO8PS Y171 and P112. Mutation of both to Ala is expected to destabilise the tetramer interface. A third residue has been identified that could be targeted to destabilise the plant A-C tetramer interface: the *Nme*KDO8PS Asp172. Mutation of this residue to Ser, would likely destabilise the tetramer interface. To destabilise the A-B tetramer interface, the two mutations that gave rise to insoluble *Nme*KDO8PS: A227R and R262term, could be of use, as they may not result in an insoluble KDO8PS dimer as the less hydrophobic A-B tetramer interface is exposed. To provide additional information on the role of the DAH7PS tetramer interface, as well as the optimal functional unit for catalysis in DAH7PS, this thesis has also found a residue that could destabilise the *Pfu*DAH7PS A-C tetramer interface: Arg169. Mutation to Ala would likely destabilise the tetramer interface. It is apparent that investigation into the proteins generated by these mutations holds promise for discovering more on the role of the quaternary structure of both KDO8PS and DAH7PS.

Chapter 7

Experimental procedures

7.1 General methods

Protein structure figures

Figures of protein structures were created using PyMOL (version 1.5.0.4).[123]

Multiple sequence alignments

Multiple sequence alignments were generated using Muscle[38, 39] and ClustalOmega.[113]

Water

All water used in these experiments was from a Millipore Milli-Q system. This water is referred to as Milli-Q water. Water used for polymerase chain reaction (PCR) work was autoclaved prior to use.

pH measurements

The pH of solutions was measured using a Denver Instruments UB-10 Ultra-Basic pH meter, with either a standard or micro-probe. Solutions were made more acidic by addition of 1 M or 10 M HCl (or when specifically required, glacial acetic acid) and basic by addition of either 1 M or 10 M NaOH.

Removal of metal ions from solutions

Divalent metal ions were removed from solutions by treatment with Chelex® 100 resin (Bio-Rad). The resin was added to a solution and then stirred for at least 1 hour before the resin was removed by filtration (0.2 μm).

Glycerol stocks

All plasmid-containing strains of *E. coli* were stored frozen at -80°C as glycerol stocks. Glycerol stocks were created by mixing 0.4 mL of 50 % (v/v) glycerol with 0.8 mL of an overnight culture in a 1.7 mL micro-centrifuge tube.

Antibiotics

The genes for *Nme*KDO8PS, *Pfu*DAH7PS and *Cte*KDO8PS had previously been cloned into the pT7-7 vector, which confirs resistance to ampicillin. Ampicillin was added to the growth medium to a final concentration of 0.1 mg mL^{-1}. Stock solutions of ampicillin at 100 mg mL^{-1} were created, filter sterilised and stored at -80°C, and freeze-thawed a maximum of two times.

The gene for *Cvr*KDO8PS was ordered in a pBluescript vector, which confers resistance to ampicilin. The gene for *Cvr*KDO8PS was also cloned into the pET-28a vector, which confers resistance to kanamycin. Kanamycin was added to the growth medium to a final concentration of 0.05 mg mL^{-1}. Stock solutions of kanamycin at 50 mg mL^{-1} were created, filter sterilised and stored at -80°C, and freeze-thawed a maximum of two times.

Site-directed mutagenesis

Mutagenesis was performed using either a Quikchange® XL Mutagenesis Kit (Stratagene), GeneArt® Site-Directed Mutagenesis System (Thermo Fisher Scientific), *PfuTurbo* DNA polymerase (Agilent Technologies), with Platinum® Pfx DNA Polymerase (Thermo Fisher Scientific), *PfuUltra* High-Fidelity DNA Polymerase (Agilent Technologies), Phusion® High-Fidelity DNA Polymerase (Thermo Fisher Scientific). PCRs were performed in an Veriti® 96-well Thermal Cycler (Applied Biosystems) or an iCycler (Bio-Rad). Reaction volumes and cycling protocols were those recommended by each kit or polymerase. Primers for mutagenesis were synthesised by Invitrogen or Integrated DNA Technologies and resuspended in sterilised Milli-Q water to a

concentration of 100 μM. Template DNA (which is methylated) was digested by treatment with the restriction enzyme DpnI according to the protocols of the kit or enzyme.

Agarose gel electrophoresis

Separation of DNA was performed by agarose gel electrophoresis using 1 % (w/v) agarose gels. DNA was stained for self-poured gels by inclusion of SYBR® Safe DNA stain.

Agarose gels were created by dissolving 1 % (w/v) agarose in 30 mL of Tris-acetate-ethylenediaminetetraacetic acid (EDTA) [TAE] buffer and heated in a microwave oven until the agarose was dissolved. The hot agarose solution was left to cool in a 60°C oven. Immediately before pouring, SYBR® Safe DNA stain was added. Samples were mixed with a (6×) sample loading dye. Electrophoresis was performed for 50 min at 85 V in TAE buffer using a Mini-Sub® Cell GT (Bio-Rad).

TAE buffer: 50 mM Tris, 1 mM EDTA, 20 mM acetic acid

Sample loading dye (6×): 60 mM Tris-HCl, 60 mM EDTA, 0.2 % (w/v) orange G, 0.05 % (w/v) xylene cyanol ff, 60 % (v/v) glycerol

20 μL from 50 μL PCR reactions were loaded onto the agarose gels for visualisation of amplification products. To one well of each agarose gel, 2 μL of 1 kb Plus DNA Ladder (Invitrogen) was used to estimate DNA size. Stained DNA was visualised and photographed under UV (302 nm).

Plasmid extraction and purification

Plasmids were extracted using a High Pure Plasmid Isolation Kit (Roche), NucleoSpin® Plasmid EasyPure (Macherey-Nagel), or ZR Plasmid Miniprep™ Classic (Zymo Research). Small cultures (5 mL) of plasmid-containing cells were grown overnight with the appropriate antibiotic. The cultures were harvested the following morning and plasmids extracted and purified as per the kit instructions.

The concentration of purified plasmid was measured by absorption at 260 nm using an appropriately blanked Nanodrop™ ND-1 000 spectrophotometer.

DNA sequencing

DNA sequencing was performed by Canterbury Sequencing and Genotyping, Massey Genome Service, or Macrogen Online Sequencing Order System. As *Nme*KDO8PS, *Pfu*DAH7PS and *Cte*KDO8PS genes were in the pT7-7 vector the same forward and reverse primers were used for all sequencing.

Forward: 5’ `TAA TAC GAC TCA CTA TAG GGA GA`

Reverse: 5’ `GTT TAC TCA TAT ATA CTT TAG AT`

Cell lines

The cell line used for plasmid propagation was *E. coli* TOP10 (Invitrogen). For protein expression the *E. coli* BL21 (DE3) Star (Invitrogen) cell line was used.

Transformation

Chemically competent cells (50 µL to 100 µL aliquots) were thawed on ice before addition of 2 µL of either PCR product or purified plasmid. The mixture was left on ice for 30 min then placed in a 42°C water bath for 45 seconds before being placed on ice again for 5 min. Cells were then grown for 1 hour at 37°C while shaking after addition of 250 µL super optimal broth with catabolite repression (SOC) medium.

A portion (50 µL to 100 µL) of the transformed cells was spread directly onto an lysogeny broth (LB)-agar plate containing the appropriate antibiotic and left to grow on the inverted medium overnight at 37°C.

SOC medium: 2 % (w/v) tryptone, 0.5 % (w/v) yeast extract, 10 mM NaCl, 2.5 mM KCl, 10 mM MgSO4, 20 mM glucose. Filter sterilised in aliquots.

Culture media

LB-agar was prepared by dissolving LB (Lennox L) (20 g L^{-1}) and agar (15 g L^{-1}) base in Milli-Q water and sterilised by autoclaving. The LB-agar solution was then heated in a microwave oven until boiling and left to cool in a 60°C oven. The LB-agar solution was then further cooled to <50°C before the

appropriate antibiotic was added immediately prior to pouring into round petri dishes.

LB medium for plasmid extraction, pre-cultures and protein expression cultures were prepared by dissolving 20 g L^{-1} LB (Lennox L) base in Milli-Q water and sterilised by autoclaving. The appropriate antibiotic was added immediately prior to use.

Protein expression cultures

Cultures for protein expression were grown in 2 L to 3 L baffled conical flasks in a shaking incubator at 180 rpm. Expression cultures were inoculated with an overnight culture $\frac{1}{20}$ the volume and grown at 37°C until induction of protein expression.

Transcription of the *Nme*KDO8PS, *Pfu*DAH7PS and *Cte*KDO8PS genes was under the control of an inducible lac operon, therefore protein expression was induced by addition of isopropyl β-d-1-thiogalactopyranoside (IPTG) to a final concentration of either 0.5 or 1 mM, when cultures were at a mid-logarithmic phase (OD_{600} of 0.4 AU to 0.6 AU). After induction cultures were kept shaking at 37°C for 4 hour before being harvested, or were transferred to 23°C and harvested the following morning.

Cell harvesting

Large cultures were harvested via centrifugation in 1 L bottles at 14 000 g for 30 min at 4°C. The supernatant liquid was removed and the cell pellet was either immediately lysed, or was stored at -80°C.

Small volume cultures (≤5 mL) were progressively harvested in 1.6 mL micro-centrifuge tubes at 16 000 g for 10 min.

Cell lysis

Cells were lysed by one of two methods: with a chemical detergent or by sonication. Sonication was performed with an Omni Ruptor 4 000 Ultrasonic Homogenizer (Omni International). Cell pellets were resuspended in chilled lysis buffer (typically 10 mL) on ice, and sonicated in a beaker surrounded by packed ice at 80 % power for 4 multiples of 5 min with 30 percent pulsation and 1 min pauses between bursts.

Lysis by chemical detergent was performed using BugBuster® Protein Extraction Reagent (Merck). Typically, cell pellets were resuspended in lysis buffer containing the BugBuster® reagent to a volume of 5 mL after which 4 μL of Benzonase® Nuclease (Merck) (an engineered promiscuous endonuclease) was added and the solution shaken at 37°C for at least 20 min.

The lysis buffer for *Nme*KDO8PS was 10 mM 1,3-bis[tris(hydroxymethyl)methylamino]propane (BTP), 1 mM dithiothreitol (DTT), 200 mM KCl and 200 μM PEP at pH 7.5.

The lysis buffer for *Pfu*DAH7PS was 50 mM BTP, 2 mM DTT, 200 mM KCl and 200 μM PEP at pH 7.2. A Roche Protease Inhibitor Cocktail Tablet was also added before lysis.

The lysis buffer for *Cte*KDO8PS was 10 mM BTP, 1 mM DTT, 200 mM KCl and 200 μM PEP at pH 8.25.

For *Nme*KDO8PS and *Cte*KDO8PS, after lysis the cellular debris were removed by centrifugation at 21000 g for 30 min at 4°C. For *Pfu*DAH7PS after heat treatment the cellular debris were removed by centrifugation at 16000 g for 10 min at 4°C.

Protein purification

Proteins were purified using various procedures: heat treatment, anion-exchange chromatography, hydrophobic-interaction chromatography and size-exclusion chromatography. The chromatography was performed on GE Healthcare AĖTA purifier^{TM} 10 instruments.

All *Nme*KDO8PS mutants were purified using the same purification procedures as the wild-type.[21] The protein was purified via anion-exchange, followed by a hydrophobic interaction column, and completed via size-exclusion chromatography.

The *Pfu*DAH7PS mutant Q118W was purified using the same purification procedures as the wild-type.[104] After lysing the bacterial cell culture, the protein was purified via heat treatment, followed by a hydrophobic interaction column, and completed via size-exclusion chromatography. *Pfu*I181R was purified via heat treatment, followed by a hydrophobic interaction column, and completed via anion-exchange.

The *Cte*KDO8PS wild-type purification procedure underwent many experimental changes before a final purification procedure was developed. The purification procedures trialled before being discontinued were heat treatment, cation-exchange, desalting column, and size-exclusion chromatography. The final purification procedure was identical to that of Yeoman: the protein was

purified via anion-exchange chromatography, and completed via a hydrophobic interaction column chromatography. [136]

All buffers were filtered (0.2 μm) under vacuum before use. All samples were filtered, before those of volume greater than 5 mL being loaded into either a 10 mL or 50 mL Superloop™ (GE Healthcare), whereas those of volume less than 5 mL being loaded into a static loop. On the AK̈TA purifier™ 10 instrument the flow-through from the injection of the sample onto the column was collected in 50 mL centrifuge tubes, while the eluate was fractionated into 2 mL fractions collected in 96-well plates. Elution from the columns was monitored at 280 nm, 260 nm and 214 nm.

When the fractions corresponding to protein of interest could not be determined from the chromatogram, the suspected fractions containing the protein of interest were analysed by sodium dodecyl sulfate polyacrylamide gel electrophoresis (SDS-PAGE) and/or for activity. Fractions containing the protein of interest were then pooled and prepared for the next chromatographic step.

Heat treatment

HT was performed using a AccuBlock™ Digital Dry Bath.

For the *Pfu*DAH7PS Q118W mutant, after lysis the crude lysate was separated into 600 μL aliquots which subsequently underwent HT at 80°C for 30 min. For the *Pfu*DAH7PS I181R mutant, after lysis the crude lysate was separated into 600 μL aliquots which subsequently underwent HT at 60°C for 30 min.

For the unsuccessful *Cte*KDO8PS wild-type purification step, after lysis the crude lysate was separated into 600 µL aliquots which subsequently underwent HT at 50°C for 30 min. Temperatures greater than 50°C caused a noticeable reduction in KDO8PS activity, while those lower than 50°C created no significant purification of the protein samples, and so this step was discontinued.

Anion-exchange chromatography

AEC was performed using a SOURCE^{TM} 15Q resin packed in a Tricorn 10/100 column (GE Healthcare), at 4°C.

For the *Nme*KDO8PS mutants (pI is 6.25), after lysis and removal of cell debris, the sample was filtered and loaded into a superloop. The no salt buffer used was 10 mM BTP, 1 mM DTT, pH 7.5. Elution from the column was performed using a linear gradient of increasing NaCl concentration up to 1 M at a flow rate of 1.5 mL min^{-1}.

For the *Pfu*DAH7PS I181R mutant (pI is 5.93), the pooled HIC fractions was diluted at a ratio of 1:3 (v/v) with the no salt buffer of 10 mM BTP, pH 7.2. The sample was then filtered and loaded into a superloop. Elution from the column was performed using a linear gradient of increasing NaCl concentration up to 1 M at a flow rate of 1.5 mL min^{-1}.

For *Cte*KDO8PS wild-type (pI is 6.79), after lysis and removal of cell debris, the sample was filtered and loaded into a superloop. The no salt buffer used was 10 mM BTP, 1 mM DTT, pH 8.25. Elution from the column was performed using a linear gradient of increasing NaCl concentration up to 1 M at a flow rate of 1.5 mL min^{-1}.

Cation-exchange chromatography

CEC was performed using a SOURCE^{TM} 15S resin packed in a Tricorn 10/100 column (GE Healthcare), at 4°C.

For the unsuccessful purification of *Cte*KDO8PS wild-type (whose pI is 6.79), after lysis and removal of cell debris, the sample was filtered and loaded into a superloop. The no salt buffer used was 10 mM BTP, 1 mM DTT, pH 4.5 or 5.5. Elution from the column was performed using a linear gradient of increasing NaCl concentration up to 1 M at a flow rate of 1.5 mL min^{-1}. *Cte*KDO8PS wild-type was found not to bind sufficiently to the column at both pH 4.5 and 5.5, and so was discontinued.

Hydrophobic interaction chromatography

HIC was performed using a SOURCE^{TM} 15PHE resin packed in a Tricorn 10/100 column (GE Healthcare), at room temperature.

For the *Nme*KDO8PS mutants, crystalline $(NH_4)_2SO_4$ was added to the pooled AEC fractions to a concentration of 1 M before the sample was filtered and loaded into a superloop. The high salt buffer used was 10 mM BTP, 1 mM DTT, 1 M $(NH_4)_2SO_4$, pH 7.5. Elution from the column was performed using a linear gradient of decreasing $(NH_4)_2SO_4$ down to 0 M at a flow rate of 3 mL min^{-1}.

For the *Pfu*DAH7PS mutants after HT, removal of cell debris and pooling the remaining solution, it was found that addition of crystalline $(NH_4)_2SO_4$ was too destructive. Instead a dilution buffer was added at a ratio 1:1 (v/v), comprised of 10 mM BTP, 2 M $(NH_4)_2SO_4$, pH 7.2, which produces

a final concentration of 1 M $(NH_4)_2SO_4$ before the sample was filtered and loaded into a superloop. The high salt buffer used was 10 mM BTP, 1 M $(NH_4)_2SO_4$, pH 7.2. Elution from the column was performed using a linear gradient of decreasing $(NH_4)_2SO_4$ down to 0 M at a flow rate of 2 mL min^{-1}.

For *Cte*KDO8PS wild-type, crystalline $(NH_4)_2SO_4$ was added to the pooled AEC fractions to a concentration of 1 M before the sample was filtered and loaded into a superloop. The high salt buffer used was 10 mM BTP, 1 mM DTT, 1 M $(NH_4)_2SO_4$, pH 8.25. Elution from the column was performed using a linear gradient of decreasing $(NH_4)_2SO_4$ down to 0 M at a flow rate of 3 mL min^{-1}.

Desalting column

Desalting was performed using a PD-10 Desalting Column, using gravity flow at room temperature.

For the unsuccessful *Cte*KDO8PS wild-type purification step, the pooled HIC fractions were loaded onto the desalting column. Desalting resulted in denaturing of *Cte*KDO8PS wild-type, and so was discontinued.

Size exclusion chromatography

SEC was performed using a HiLoad 26/60 Superdex^{TM} 200 prep grade column (GE Healthcare), at 4°C.

For the *Nme*KDO8PS mutants, the pooled HIC fractions was filtered and loaded into a superloop. The SEC buffer used was 10 mM BTP, pH 7.5. Elution from the column was performed at a flow rate of 0.5-1.0 mL min^{-1}.

For the *Pfu*DAH7PS Q118W mutant, the pooled HIC fractions was filtered and loaded into a superloop. The SEC buffer used was 10 mM BTP, 40 mM KCL, 10 µM EDTA, 200 µM PEP, pH 7.2. Elution from the column was performed at a flow rate of 0.5-1.0 mL min^{-1}.

For the unsuccessful *Cte*KDO8PS wild-type purification step, the pooled HIC fractions was filtered and loaded into a superloop. The SEC buffer used was 10 mM BTP, pH 8.25. Elution from the column was performed at a flow rate of 0.5-1.0 mL min^{-1}. SEC resulted in negligible yields of *Cte*KDO8PS wild-type, and so was discontinued.

Polyacrylamide gel electrophoresis

SDS-PAGE was performed using Bolt™ 4-12% (also 10%) Bis-Tris Plus Gel 1.0 mm × 10 (also 12 or 15)-well pre-cast gels (Thermo Fisher Scientific) in 20X Bolt™ MES SDS Running Buffer (Thermo Fisher Scientific), or NuPAGE™ 10% Bis-Tris Gel 1.0 mm × 12-well pre-cast gels (Thermo Fisher Scientific) in NuPAGE™ MES SDS running Buffer (Thermo Fisher Scientific). Electrophoresis was performed using a XCell SureLock™ Mini-Cell Electrophoresis System (Thermo Fisher Scientific), or Mini Gel Tank (Thermo Fisher Scientific), at 165 V for 35 min. Samples were mixed with Bolt™ or NuPAGE™ LDS Sample Buffer (4×), and sometimes boiled.

Visualisation

All SDS-PAGE gels were stained by coomassie brilliant blue R-250, for at least 20 min before being destained to remove excess dye. Staining and

destaining times were reduced by heating the gel and solution in a microwave oven for 15 seconds until almost boiling.

Stain: 0.1% (w/v) coomassie brilliant blue R-250, 10% (v/v) acetic acid and 40% (v/v) methanol

Destain: 10% (v/v) acetic acid and 40% (v/v) methanol

The molecular weight standard Novex® Sharp Pre-Stained Protein Standards (Thermo Fisher Scientific) was run as the sample in one lane of each gel. Photographs of the gels were taken on a white light transilluminator in a Molecular Imager® Gel Doc™ XR (Bio-Rad).

Protein solution concentration and buffer exchange

Protein solutions were concentrated using 10000 Da molecular weight cut-off (MWCO) devices: Vivaspin 2 (GE Healthcare), Vivaspin 20 (Sartorius Stedim Biotech) and Vivaspin Turbo 15 (Sartorius Stedim Biotech). All filtration units were rinsed with Milli-Q water before use. Protein solutions were buffer exchanged in a MWCO device by repeated concentration and dilution with the desired buffer.

Enzyme storage

Purified protein was divided into aliquots in 0.6 mL micro-centrifuge tubes in 200 μL aliquots, flash-frozen in liquid nitrogen, and stored at -80°C. All protein samples were thawed immediately before use and kept on ice. *Nme*KDO8PS wild-type and mutants was stored at a concentration between 2

mg mL^{-1} and 20 mg mL^{-1}. *Pfu*DAH7PS wild-type and mutants was stored at a concentration between 1 mg mL^{-1} and 3 mg mL^{-1}. *Cte*KDO8PS wild-type was stored at a concentration between 1 mg mL^{-1} and 5 mg mL^{-1}.

Protein concentration determination

The concentration was measured by absorption at 280 nm by an appropriately blanked Nanodrop ND-1000 spectrophotometer, using 2 μL samples of purified protein solution.

For most of the *Nme*KDO8PS mutants the concentration was calculated from the absorption using the *Nme*KDO8PS molar extinction coefficient values of 6335 M^{-1} cm^{-1}. The exceptions with a different molar extinction coefficient values were *Nme*Y171A of 4845 M^{-1} cm^{-1} and *Nme*I63W of 11835 M^{-1} cm^{-1}.

For *Pfu*DAH7PS I181R the concentration was calculated from the absorption using the *Pfu*DAH7PS molar extinction coefficient values of 24535 M^{-1} cm^{-1}. For *Pfu*DAH7PS Q118W had a different molar extinction coefficient value of 30035 M^{-1} cm^{-1}.

For *Cte*KDO8PS the concentration was calculated from the absorption using the *Cte*KDO8PS molar extinction coefficient values of 14565 M^{-1} cm^{-1}.

The coefficient values were calculated from the protein sequence using the ProtParam tool on the ExPASy Proteomics Server.[46]

Standard enzyme activity assay

The standard assay for KDO8PS and DAH7PS activity monitored the consumption of PEP by loss of absorbance at 232 nm, based on the method by Schoner and Herrmann.[105]

All *Nme*KDO8PS mutant kinetic measurements were taken using a Varian Cary 100 UV-visible spectrophotometer stoppered 1 cm pathlength quartz cuvettes and a total assay volume of 1 mL, except *Nme*D92E/P112A and *Nme*D92E/P112G which used a stoppered 1 mm (0.1 cm) pathlength quartz cuvettes and a smaller total assay volume. All measurements were performed in the kinetic buffer of 50 mM BTP and 10 µM EDTA at 37°C, pH 7.2. All reactions were initiated with addition of the *Nme*KDO8PS mutant of interest.

The *Pfu*DAH7PS mutant kinetic measurements were taken using a Varian Cary 100 UV-visible spectrophotometer stoppered 1 cm pathlength quartz cuvettes and a total assay volume of 1 mL. All measurements were performed in the kinetic buffer of 50 mM BTP, 100 µM $CdCl_2$ and 10 µM EDTA at 60°C, pH 7.5. All reactions were initiated with addition of the *Pfu*DAH7PS mutant of interest.

*Cte*KDO8PS wild-type kinetic measurements were taken using a Varian Cary 100 UV-visible spectrophotometer stoppered 1 cm pathlength quartz cuvettes and a total assay volume of 1 mL. All measurements were performed in the kinetic buffer of 50 mM BTP, 100 µM $MnSO_4$ and 10 µM EDTA at 45°C, pH 7.2. All reactions were initiated with addition of the *Cte*KDO8PS wild-type.

Initial rates of reaction were measured as the least-squares fit of the initial rate data using Cary WinUV Kinetics Application (Varian). A unit of

enzyme activity was defined as the loss of 1 μmol min^{-1} of PEP, which could be calculated from the measured loss of absorbance (at 232 nm) using Beer's Law (ε is 2.8×10^3 M^{-1} cm^{-1}). The kinetic parameters were determined by fitting data to the Michaelis-Menten equation using the software GraFit (Erithacus Software Limited).

Determination of substrate concentration

The concentrations of the substrates PEP and A5P in solution were determined using the standard assay system for KDO8PS activity. The concentrations of the substrate E4P in solution was determined using the standard assay system for DAH7PS activity. To measure the concentration of a substrate, a limited amount was used in the presence of an excess of the other not being measured substrate. To confirm the measured substrate was limited, additional amounts of it were added after the reaction had reached completion. The reaction change in absorbance (Δ1) was determined by the difference before the initiation of the reaction with enzyme and that at the completion of the reaction. The enzyme change in absorbance (Δ2) was determined by the initiation of the reaction with enzyme in a control reaction missing one of the substrates. The total change in absorbance (Δ1 + Δ2), was then converted using Beer's Law to the concentration of the limiting substrate in the reaction, and so the stock substrate concentration calculated was obtained.

Protein mass determination

The purified protein masses were measured by electrospray ionisation using a Micromass LCT Classic, Bruker maXis 3G. Protein samples were diluted with water to a final concentration of 1 mg mL^{-1}.

Circular dichroism

All CD experiments were performed using a JASCO J-815 Spectropolarimeter. All measurements were taken in water and the blank spectra of water were recorded before each experiment.

*Nme*KDO8PS wild-type and the mutants I63S, E154L and D92E/P112G were recorded from 240 nm to 180 nm using a 1 nm data pitch, 1 s response, 1 nm bandwidth at 25°C. A 800 µL protein solution at a concentration of 0.05 mg mL^{-1} in a 1 mL quartz cuvette with 1 cm path length was used for each measurement. *Nme*KDO8PS mutants Y171A, D172A and R263A were recorded from 240 nm to 180 nm using a 2 nm data pitch, 1 s response, 1 nm bandwidth at 25°C. A 1 mL protein solution at a concentration of 0.1 mg mL^{-1} in a 1 mL quartz cuvette with 1 cm path length was used for each measurement. *Nme*KDO8PS mutants D120H, I63W and D92E/P112A were recorded from 240 nm to 180 nm using a 0.2 nm data pitch, 1 s response, 1 nm bandwidth at 25°C. A 3 mL protein solution at a concentration of 0.017 mg mL^{-1} in a 1 mL quartz cuvette with 1 cm path length was used for each measurement. All measurements were taken in water and blank spectra of water were recorded before each experiment.

*Pfu*DAH7PS wild-type and mutants Q118W and I181R were recorded from 240 nm to 180 nm using a 0.5 nm data pitch, 1 s response, 1 nm bandwidth at 25°C. A 3 mL protein solution at a concentration of 0.017 mg mL^{-1} in a 1 mL quartz cuvette with 1 cm path length was used for each measurement. All measurements were taken in water and blank spectra of water were recorded before each experiment.

*Cte*KDO8PS wild-type was recorded from 240 nm to 180 nm using a 1 nm data pitch, 1 s response, 1 nm bandwidth at 25°C. An 800 µL protein solution at a concentration of 0.05 mg mL^{-1} in a 1 mL quartz cuvette with 1 cm path length was used for each measurement. All measurements were taken in water and blank spectra of water were recorded before each experiment.

Differential scanning fluorimetry

The melting temperatures of proteins in the presence of different additives were determined by using an iCycler iQ5 Multicolour Real-Time PCR Detection System (Bio-Rad). The method used was based on that of Nordlund *et al*.[41] Triplicate protein samples were added to buffer (containing additives) and SYPRO orange dye (Invitrogen) in a 96-well microplate, which was then sealed. The melt proceeded in 0.2°C increments from 20°C to 95°C, with a 20 seconds dwell time after each temperature rise. Measurements of the fluorescence were made at the end of each dwell time.

For each condition 100 µL of buffer including the desired additive(s) was prepared, to which 5 µL of 250× SYPRO® Orange dye was added. For *Nme*KDO8PS the buffer was 50 mM BTP, pH 7.2. For *Pfu*DAH7PS the buffer was 50 mM BTP, pH 7.0. One fifth of the mixture (21 µL) was added to 4 µL

water, to represent the blank. To the remaining 84 μL mixture, 16 μL of protein (1.0 mg mL^{-1}) was added before 25 μL each were dispersed into three replicate wells followed by the blank in a forth adjacent well in a 96-well plate. After all samples and blanks were loaded the plate was sealed with a self-adhesive transparent seal. For *Nme*KDO8PS the additives were PEP or A5P at a final concentration of 80 μM. For *Pfu*DAH7PS the additives were PEP and/or E4P at a final concentration of 80 μM, and/or $CdCl_2$ with EDTA at a final concentration of 100 μM and 10 μM respectively. For *Cte*KDO8PS the additives were $MnSO_4$, $CoCl_2$, $CdCl_2$, $FeSO_4$, $ZnCl_2$, $CaCl_2$, $BaCl_2$, $SrCl_2$, $NiCl_2$, $MgSO_4$ or $CuSO_4$ at a final concentration of 80 μM.

An Excel spreadsheet with custom VBA-scripted macro was used for data analysis to display melt and derivative curves for each sample. The melt temperatures were calculated as the temperature of maximum inflection of the melting curve after subtracting the reading of the blank well.

Analytical size exclusion chromatography

Analytical SEC was performed using a HiLoad 10/300 Superdex^{TM} 200 prep grade column (GE Healthcare), at 4°C.

Calibration was performed using proteins with known molecular weights, dissolved in the SEC buffer. The proteins were thyroglobin, β-amylase, alcohol dehydrogenase, bovine serum albumin and carbonic anhydrase from bovine erythrocytes. The SEC buffer used was 10 mM BTP, pH 7.5. Elution from the column was performed at a flow rate of 0.2 mL min^{-1}.

The *Nme*KDO8PS wild-type and mutants were diluted with SEC buffer to 500 µL of 1 mg mL^{-1} and loaded into a static loop. Elution from the column was performed at a flow rate of 0.2 mL min^{-1}.

For the *Pfu*DAH7PS wild-type and mutants were diluted with SEC buffer to 500 µL of 1 mg mL^{-1} and loaded into a static loop. Elution from the column was performed at a flow rate of 0.2 mL min^{-1}.

The *Cte*KDO8PS wild-type was diluted with SEC buffer to 500 µL of 1 mg mL^{-1} and loaded into a static loop. Elution from the column was performed at a flow rate of 0.2 mL min^{-1}.

Analytical ultracentrifugation

Sedimentation velocity experiments were performed using a ProteomeLab™ XL-I analytical ultracentrifuge (Beckman Coulter) equipped with UV-visible scanning optics. Protein samples were prepared by dialysis overnight in the reference buffer. For *Nme*KDO8PS wild-type and mutants the reference buffer was 50 mM BTP, 100 mM NaCl, pH 7.2. Each sample was then diluted to three different concentrations of 0.5, 1 and 2 mg mL^{-1} via the identical reference buffer. For *Pfu*DAH7PS mutants the reference buffer was 20 mM BTP, 150 mM NaCl, pH 7.2. The *Pfu*Q118W sample was then diluted to two different concentrations of 0.13 and 0.35 mg mL^{-1} via the identical reference buffer. The *Pfu*I181R sample was then diluted to three different concentrations of 0.13, 0.40 and 1 mg mL^{-1} via the identical reference buffer.

Reference buffer (400 µL) and samples (380 µL) were loaded into 12-mm double-sector cells with quartz windows, which were then mounted into an An-50 Ti eight-hole rotor. *Nme*KDO8PS wild-type and mutants were

centrifuged at 50000 rpm and 20°C, with the radial absorbance data collected at 280 nm wavelength. *Pfu*DAH7PS mutants were centrifuged at 50000 rpm and 20°C, with the radial absorbance data collected at 278 nm wavelength.

AUC data were fitted to a continuous distribution c(s) model using SEDFIT.[106, 107] The partial specific volume of the proteins, buffer density and buffer viscosity were calculated using SEDNTERP.[67]

Small angle X-ray scattering measurements

Measurements were taken by others at the Australian Synchrotron SAXS/WAXS beamline equipped with a Pilatus detector (1 M, 170 × 170 mm, effective pixel size, 172 × 172 μm). The X-ray wavelength was 1.0332 Å. The sample-detector distance was 1.6 m, which provided an s range of 0.01–0.40 $Å^{-1}$. s is defined as the magnitude of the scattering vector, which is related to the scattering angle (2θ) and the wavelength (λ) as: $s = (\frac{4\pi}{\lambda})\sin\theta$.

For *Nme*Y171A (4.90 mg mL^{-1}) and *Pfu*I181R (2.00 mg mL^{-1}), scattering data was collected at 25 °C following elution of the protein sample from a SEC column (Increase 5/150 Superdex^{TM} 200), which was pre-equilibrated with the SEC buffer comprised of 10 mM BTP, 5% (v/v) glycerol, pH 7.5.

The resulting data was processed, and background subtracted using scatterBrain. Scatterings from 280 nm (A280) peaks were summed and averaged. Scattering intensity (I) versus s of each protein was generated via Primus. For *Nme*Y171A the theoretical scattering profiles of the *Nme*Y171A tetramer and A-B dimer (derived from the *Nme*Y171A crystal structure) were

compared and fitted to the experimentally derived *Nme*Y171A scatterings via CRYSOL.[117]

Table 7.1: Reported structural parameters

	Nme KDO8PS Y171A	*Pfu* DAH7PS I181R
Guinier analysis		
$I(0)$ (cm^{-1})	0.019 ± 0.00027	0.021 ± 0.011
R_g (Å)	36.26 ± 0.66	65.89 ± 56.63
$P(r)$ analysis		
R_g (Å)	36.46 ± 0.02	70.68 ± 0.02
Porod Volume ($Å^{-3}$)	272835	2457250

Crystallisation of *Nme*KDO8PS mutants

Crystals of the *Nme*KDO8PS mutants were grown by hanging-drop vapour diffusion in 24-well VDX plates (Hampton Research). Protein solutions (in 10 mM BTP, pH 7.5) were mixed 1:1 (v/v) with a reservoir solution containing a varying concentration of NaCl, 100 mM sodium acetate, pH 4.6 (adjusted using glacial acetic acid). The drop size was 2 μL, and the reservoir solution volume was 500 μL.

The crystallisation trays were left at 20°C until data collection, with crystals being transferred briefly into a cryoprotectant composed of 20% glycerol in the respective reservoir solution.

X-Ray data collection and structure determination

All X-ray diffraction data was collected at the Australian Synchrotron. Pre-grown crystals were mounted on loops, stored in AS Pucks which were stored in a dry shipper (Taylor-Wharton CX100) and transported as checked-in luggage. Data collection at the Australian Synchrotron used either the Macromolecular Crystallography (MX1) or Micro Crystallography (MX2) beamlines[80] and were processed using X-ray Detector Software (XDS),[55] Aimless and Truncate[42] (CCP4 suite).[129]

Structure determination and refinement

*Nme*KDO8PS mutant structures were solved by molecular replacement, using the structure of wild-type *Nme*KDO8PS (PDB code 2QKF) as the starting model via RefMac5,[82] and electron-density maps were analysed with Coot.[40] TLS refinement was also included in the later rounds of refinement. Structures were validated and adjusted using the validation tools of Coot and the wwPDB deposition servers.

7.2 Methods for Chapter 2

Site-directed mutagenesis

The two double mutants mentioned in this chapter *Nme*D92E/P112A and *Nme*D92E/P112G were created by applying the general SDM protocol described previously. The pT7-7 vector carrying the *Nme*KDO8PS D92E mutant gene (created by Allison, T. M.)[3] was used as a template for single-site mutation.

For the primer sequences below, the bases are split into codons and the mismatched bases are in lower-case letters.

*Nme*P112A

For: 5' GAT GTC ATC CAG CTT gCg GCC TTT CTT GCG CG

Rev: 5' CG CGC AAG AAA GGC cGc AAG CTG GAT GAC ATC

*Nme*P112G

For: 5' C GAT GTC ATC CAG CTT ggC GCC TTT CTT GC

Rev: 5' GC AAG AAA GGC Gcc AAG CTG GAT GAC ATC G

Kinetics

To determine the K_m^{PEP} for *Nme*D92E/P112G (135 µg mL^{-1}), the total assay volume was 100 µL, the A5P concentration was 17.5 mM, and the concentration of PEP was varied between 60 µM and 400 µM. To determine the K_m^{A5P} for *Nme*D92E/P112G (135 µg mL^{-1}), the total assay volume was 250 µL, the PEP concentration was 350 µM, and the concentration of A5P was varied between 0.6 mM and 14.0 mM.

To determine the K_m^{PEP} for NmeD92E/P112A (130 µg mL^{-1}), the total assay volume was 250 µL, the A5P concentration was 1.3 mM, and the concentration of PEP was varied between 20 µM and 400 µM. To determine the K_m^{A5P} for NmeD92E/P112A (130 µg mL^{-1}), the total assay volume was 250 µL, the PEP concentration was 360 µM, and the concentration of A5P was varied between 0.8 mM and 7.0 mM.

Crystallisation

*Nme*D92E/P112A (4.1 mg mL^{-1}) was unable to form crystals with a reservoir solution containing 0.6 M to 5.8 M NaCl.

*Nme*D92E/P112G (15.5 mg mL^{-1}) was able to form very small crystals with a reservoir solution containing 1.8 M to 2.6 M NaCl. A single large *Nme*D92E/P112G crystal was crystallised with a reservoir solution containing 2.6 M NaCl, and a 2 µL drop comprised of 1 µL protein, 0.9 µL reservoir solution and 0.1 µL PEP (100 mM). Attempts to create additional large crystals of *Nme*D92E/P112G were unsuccessful. The resulting crystal structure was obtained from the single large *Nme*D92E/P112G crystal.

7.3 Methods for Chapter 3

Site-directed mutagenesis

The *Nme*KDO8PS A-C and A-B tetramer interface mutants in this chapter were created by site-directed mutagenesis using wild-type construct plasmid as the template. The same primers were used to create the double-mutant proteins, for *Nme*I63S/E154L using *Nme*E154L as the template plasmid, and for *Nme*A227R/R263term using *Nme*R263term as the template plasmid, and the respective primers to add the other mutation.

For the primer sequences below, the bases are split into codons and the mismatched bases are in lower-case letters.

*Nme*I63S

For: 5' CA AAC CGT TCC TCC AgC CAT TCT TAT CGC

Rev: 5' GCG ATA AGA ATG GcT GGA GGA ACG GTT TG

*Nme*E154L

For: 5' G GAA AAA TTC CAC ctg GCC GGC AAC GGG AAA CTG

Rev: 5' CAG TTT CCC GTT GCC GGC cag GTG GAA TTT TTC C

*Nme*Y171A

For: 5' GC AGC TTC GGC gcg GAC AAC CTC GTT GTC GAT ATG

Rev: 5' CAT ATC GAC AAC GAG GTT GTC cgc GCC GAA GCT GC

*Nme*D172A

For: 5' C AGC AGC TTC GGC TAC Gcg AAC CTC GTT GTC GAT ATG

Rev: 5' CAT ATC GAC AAC GAG GTT cgC GTA GCC GAA GCT GCT G

*Nme*D120H

For: 5' GCG CGG CAG ACC cAT TTA GTG GTTG

Rev: 5' C AAC CAC TAA ATg GGT CTG CCG CGC

*Nme*I63W

For: 5' GCA AAC CGT TCC TCC tgg CAT TCT TAT CGC GGC

Rev: 5' GCC GCG ATA AGA ATG cca GGA GGA ACG GTT TGC

*Nme*A227R

For: 5' GAT TTG GCA CTT GCA GGC ATG cgt ACC CGC CTT GCC GGT CTG TTC

Rev: 5' GAA CAG ACC GGC AAG GCG GGT acg CAT
GCC TGC AAG TGC CAA ATC

*Nme*R263A

For: 5' CG CTG CAC CTT TTA GAA GAT TTT TTA
ATC gcC ATC AAA GCA TTG G

Rev: 5' C CAA TGC TTT GAT Ggc GAT TAA AAA
ATC TTC TAA AAG GTG CAG CG

*Nme*R263term

For: 5' CAC CTT TTA GAA GAT TTT TTA ATC taa
ATC AAA GCA TTG GAC G

Rev: 5' C GTC CAA TGC TTT GAT tta GAT TAA
AAA ATC TTC TAA AAG GTG

Kinetics

To determine the K_m^{PEP} for *Nme*I63S (1.03 µg mL^{-1}), the A5P concentration was 60 µM, and the concentration of PEP was varied between 5 µM and 50 µM. To determine the K_m^{A5P} for *Nme*I63S (0.965 µg mL^{-1}), the PEP concentration was 70 µM, and the concentration of A5P was varied between 5 µM and 50 µM.

To determine the K_m^{PEP} for *Nme*E154L (1.08 µg mL^{-1}), the A5P concentration was 60 µM, and the concentration of PEP was varied between 5 µM and 50 µM. To determine the K_m^{A5P} for *Nme*E154L (1.08 µg mL^{-1}), the

PEP concentration was 70 µM, and the concentration of A5P was varied between 3 µM and 50 µM. .

To determine the K_m^{PEP} for *Nme*Y171A (7.80 µg mL^{-1}), the A5P concentration was 70 µM, and the concentration of PEP was varied between 6 µM and 60 µM. To determine the K_m^{A5P} for *Nme*Y171A (7.02 µg mL^{-1}), the PEP concentration was 70 µM, and the concentration of A5P was varied between 4 µM and 50 µM.

To determine the K_m^{PEP} for *Nme*D172A (1.01 µg mL^{-1}), the A5P concentration was 70 µM, and the concentration of PEP was varied between 4 µM and 50 µM. To determine the K_m^{A5P} for *Nme*D172A (1.01 µg mL^{-1}), the PEP concentration was 70 µM, and the concentration of A5P was varied between 5 µM and 50 µM.

To determine the K_m^{PEP} for *Nme*D120H (2.15 µg mL^{-1}), the A5P concentration was 70 µM, and the concentration of PEP was varied between 4 µM and 50 µM. To determine the K_m^{A5P} for *Nme*D120H (2.15 µg mL^{-1}), the PEP concentration was 70 µM, and the concentration of A5P was varied between 4 µM and 50 µM.

To determine the K_m^{PEP} for *Nme*I63W (6.84 µg mL^{-1}), the A5P concentration was 70 µM, and the concentration of PEP was varied between 4 µM and 50 µM. To determine the K_m^{A5P} for *Nme*I63W (6.84 µg mL^{-1}), the PEP concentration was 70 µM, and the concentration of A5P was varied between 4 µM and 50 µM.

To determine the K_m^{PEP} for *Nme*R263A (0.99 µg mL^{-1}), the A5P concentration was 70 µM, and the concentration of PEP was varied between 4 µM and 50 µM. To determine the K_m^{A5P} for *Nme*R263A (0.99 µg mL^{-1}), the

PEP concentration was 70 µM, and the concentration of A5P was varied between 5 µM and 60 µM.

Crystallisation

*Nme*I63S (16.5 mg mL^{-1}) was unable to be crystallised with a reservoir solution containing 0.6 M to 2.6 M NaCl. Attempts to crystallise *Nme*I63S with seed crystals of *Nme*E154L was unsuccessful.

*Nme*E154L (19.0 mg mL^{-1}) was able to be crystallised with a reservoir solution containing 1.8 M to 2.6 M NaCl. The resulting crystal structure was obtained from an *Nme*E154L crystal that was crystallised with a reservoir solution containing 2.6 M NaCl.

*Nme*Y171A (6.55 mg mL^{-1}) was able to be crystallised with a reservoir solution containing 1.84 M to 2.6 M NaCl. The resulting crystal structure was obtained from an *Nme*Y171A crystal that was crystallised with a reservoir solution containing 2.16 M NaCl.

*Nme*D172A (7.07 mg mL^{-1}) was able to be crystallised with a reservoir solution containing 2.42 M to 2.68 M NaCl. The resulting crystal structure was obtained from an *Nme*D172A crystal that was crystallised with a reservoir solution containing 2.68 M NaCl.

*Nme*D120H (6.2 mg mL^{-1}) was only able to form very small crystals with a reservoir solution containing 4.24 M NaCl (none from 0.60 M to 3.72 M, 4.76 M to 5.8 M NaCl.

*Nme*I63W (6.8 mg mL^{-1}) was unable to form crystals with a reservoir solution containing 0.6 M to 5.8 M NaCl.

*Nme*R263A (10.9 mg mL^{-1}) was able to be crystallised with a reservoir solution containing 0.6 M to 1.12 M NaCl. The resulting crystal structure was obtained from an *Nme*R263A crystal that was crystallised with a reservoir solution containing 1.12 M NaCl.

7.4 Methods for Chapter 4

Site-directed mutagenesis

The *Pfu*DAH7PS A-C and A-B tetramer interface mutants in this chapter were created by site-directed mutagenesis using wild-type construct plasmid as the template.

For the primer sequences below, the bases are split into codons and the mismatched bases are in lower-case letters.

*Pfu*Q118W

For: 5' GAT AGG AGC CAG AAA TTC Ctg GAA CTT TGA ACT CTT AAA G

Rev: 5' C TTT AAG AGT TCA AAG TTC caG GAA TTT CTG GCT CCT ATC

*Pfu*I181R

For: 5' CG AGA TTT ACA CTT GAT cgT TCT GCA GTC CCA GTG

Rev: 5' CAC TGG GAC TGC AGA Acg ATC AAG TGT AAA TCT CG

Kinetics

To determine the K_m^{PEP} for *Pfu*Q118W (5.70 µg mL^{-1}), the E4P concentration was 300 µM, and the concentration of PEP was varied between 25 µM and 230 µM. To determine the K_m^{E4P} for *Pfu*Q118W (5.70 µg mL^{-1}), the PEP concentration was 320 µM, and the concentration of E4P was varied between 20 µM and 250 µM.

To determine the non-activity of *Pfu*I181R (16.7 µg mL^{-1}), the E4P concentration was 300 µM, the concentration of PEP 200 µM, and the lack of a reaction was observed over ten minutes.

7.5 Methods for Chapter 5

*Cte*KDO8PS wild-type

Standard enzyme activity assay

A number of experiments were performed to create the standard *Cte*KDO8PS activity assay.

To determine the ideal buffer of choice, measurements were performed in a kinetic buffer of choice, 6 µg mL^{-1} *Cte*KDO8PS wild-type, 200 µM PEP, 100 µM $CdCl_2$ and 10 µM EDTA at 47°C, pH 7.5. All reactions were initiated with addition of the 90 µM A5P. The buffers tested were: 100 mM Tris acetate, 20 mM Tris, 50 mM Tris-HCl, 100 mM HEPES, 50 mM BTP and 10 mM BTP.

To determine the ideal divalent metal ion, measurements were performed in a kinetic buffer of 50 mM BTP, 1 µg mL^{-1} *Cte*KDO8PS wild-type, 100 µM PEP, 100 µM divalent metal of interest and 10 µM EDTA at 47°C, pH 7.2. All reactions were initiated with addition of the 100 µM A5P. The divalent metals tested were: $MnSO_4$, $CoCl_2$, $CdCl_2$, $FeSO_4$, $ZnCl_2$, $CaCl_2$, $BaCl_2$, $SrCl_2$, $NiCl_2$, $MgSO_4$, and $CuSO_4$.

To determine the ideal temperature, measurements were performed in a kinetic buffer of 50 mM BTP, 5.3 µg mL^{-1} *Cte*KDO8PS wild-type, 80 µM PEP, 100 µM $MnSO_4$ and 10 µM EDTA at pH 7.2 (pH was adjusted to be exactly 7.2 at each varying temperature). All reactions were initiated with addition of the 37.5 µM A5P. The temperature range tested was from 25°C to 65°C at 5°C intervals.

Kinetics

To determine the K_m^{PEP} for *Cte*KDO8PS wild-type (2.66 µg mL^{-1}), the A5P concentration was 100 µM, and the concentration of PEP was varied between 6 µM and 60 µM. To determine the K_m^{A5P} for *Cte*KDO8PS wild-type (2.66 µg mL^{-1}), the PEP concentration was 70 µM, and the concentration of A5P was varied between 3 µM and 60 µM.

Crystal screening of *Cte*KDO8PS wild-type

Crystal screening of *Cte*KDO8PS wild-type was performed by using a sitting-drop vapour diffusion in a 96-well 2-drop MRC Crystallization Plate. *Cte*KDO8PS wild-type (3.53 mg mL^{-1} in 10 mM BTP, 1 mM DTT, pH 7.5) was mixed 1:1 (v/v) with a reservoir solution. The reservoir solutions screened were the 96 solutions from JCSG-plus™ HT-96 MD1-40 (Molecular Dimensions). The drop size was 2 µL, the reservoir solution volume was 40 µL and the crystallisation trays were left at 4°C. The best reservoir solution to give rise to crystals was the D11 solution (0.14 M calcium chloride dihydrate, 0.07 M sodium acetate, pH 4.6, 14% (v/v) 2-propanol, 30% (v/v) glycerol). Other notable reservoir solutions were the E11, D10 and A5 solutions, with some smaller crystal results from E5, A6 and D9 solutions.

The reservoir solution (0.14 M calcium chloride dihydrate, 0.07 M sodium acetate, pH 4.6, 14% (v/v) 2-propanol, 30% (v/v) glycerol) was further investigated by varying the pH from 3.6 to 6.6 in 1.0 increments, varying the 2-propanol concentration from 8% to 16% in 2% increments (v/v), and varying the glycerol concentration from 15% to 35% in 5% increments (v/v). The best

crystals formed at 0.14 M calcium chloride dihydrate, 0.07 M sodium acetate, pH 3.6, 10% (v/v) 2-propanol, 20% (v/v) glycerol. Using *Cte*KDO8PS wild-type (5.37 mg mL^{-1}) with this reservoir solution, by hanging-drop vapour diffusion in 24-well VDX plates (Hampton Research) and left at 4°C, gave rise to crystal shards.

*Cvr*KDO8PS wild-type

Vector

The gene for *Cvr*KDO8PS wild-type (locus tag CHLNCDRAFT_26331), linked to two small extra gene sections was ordered in a pBluescript SK vector from Epoch Life Science. The first extra gene section was placed at the C-terminal of the *Cvr*KDO8PS gene, comprised of a Gateway® attachment site, Tobacco Etch Virus (TEV) cleavage site and extra linker. The second extra gene section was placed at the N-terminal of the *Cvr*KDO8PS gene, comprised of a Gateway® attachment site.

For the small extra gene section sequences below, the bases are split into codons, with the underlined bases being the Gateway® attachment sites, and the bolded bases are the TEV cleavage site.

First extra gene section

For: 5’ ACA AGT TTG TAC AAA AAA GCA GCG TTC
GAA AAC CTG TAT TTT CAG GGA AGC GGC
GCG C-terminal of the *Cvr*KDO8PS gene

Second extra gene section

For: 5’ N-terminal of the *Cvr*KDO8PS gene TAA AAC CCA GCT TTC TTG TAC AAA GTG GT

In-Fusion® cloning

In-Fusion® cloning is a method that allows directional cloning of sections of deoxyribonucleic acid (DNA) into vectors via enzymatic recognition of a 15-basepair overlap which is engineered at the ends of the target DNA.

The section of DNA utilised was comprised of the *Cvr*KDO8PS gene with the first extra gene section, without either of the Gateway® attachment sites at the N-terminal or C-terminal. This was created via PCR using a forward and reverse primer on the pBluescript vector containing the *Cvr*KDO8PS gene. The vector intended for the *Cvr*KDO8PS gene to be inserted into was the N-terminal polyhistidine tagged pET-28a vector. The restriction enzyme sites used were NdeI and XhoI, or EcoRI and XhoI.

For the In-Fusion® cloning primers used below, the bases are split into codons, with the underlined bases being the section of sequence that is identical to the pET-28a vector.

Inserted reverse complement, XhoI and NdeI

For: 5’ GGT GGT GGT GCT CGA GAA AAC CTG TAT TTT CAG GG

Rev: 5' CGC GCG GCA GCC ATA TTA GAC GAC GGC CAG CGG

Inserted forward complement with one base reading frameshift, NdeI and XhoI

For: 5’ CGC GCG GCA GCC ATA GAA AAC CTG TAT TTT CAG GG

Rev: 5' GGT GGT GGT GCT CGA TTA GAC GAC GGC CAG CGG

Inserted forward complement with two additional bases to fix the reading frame shift (bolded), NdeI and XhoI

For: 5’ CGC GCG GCA GCC ATA **TG**G AAA ACC TGT ATT TTC AGG GAA GCG G

Rev: 5' identical to above Rev: inserted forward complement with one base reading frameshift, NdeI and XhoI

Inserted forward complement with additional base to fix the reading frame shift (bolded), EcoRI and XhoI

For: 5’ TCG CGG ATC CGA ATT **C**GA AAA CCT GTA TTT TCA GGG AAG CGG

Rev: 5' identical to above Rev: inserted forward complement with one base reading frameshift, NdeI and XhoI

Site-directed mutagenesis

The *Cvr*KDO8PS gene was inserted into the pET-28a vector using the In-Fusion® cloning primers: inserted forward complement with one base reading frameshift, NdeI and XhoI. As there was a one base causing a reading frameshift, site-directed mutagenesis was used to attempt remove it.

For the primer sequences below, the bases are split into codons and the deleted base is shown as: del.

*Cvr*KDO8PS del

For: 5' CCG CGC GGC AGC CAT del GAA AAC CTG TAT TTT C

Rev: 5' GAA AAT ACA GGT TTT C del AT GGC TGC CGC GCG G

References

1 M. Ahn, A. L. Pietersma, L. R. Schofield, and E. J. Parker, 'Mechanistic Divergence of Two Closely Related Aldol-Like Enzyme-Catalysed Reactions', *Org. Biomol. Chem.*, 3 (2005), 4046-49.

2 Meekyung Ahn, Fiona C. Cochrane, Mark L. Patchett, and Emily J. Parker, 'Arabinose 5-Phosphate Analogues as Mechanistic Probes for *Neisseria Meningitidis* 3-Deoxy-D-*Manno*-Octulosonate 8-Phosphate Synthase', *Bioorg. Med. Chem.*, 16 (2008), 9830-36.

3 T. M. Allison, 'Substrate Specificity and Mutational Studies of Kdo8ps', *PhD Thesis*, Canterbury University, Christchurch, New Zealand (2012).

4 T. M. Allison, F. C. Cochrane, G. B. Jameson, and E. J. Parker, 'Examining the Role of Intersubunit Contacts in Catalysis by 3-Deoxy-D- *Manno*-Octulosonate 8-Phosphate Synthase', *Biochemistry*, 52 (2013), 4676-86.

5 T. M. Allison, R. D. Hutton, F. C. Cochrane, J. A. Yeoman, G. B. Jameson, and E. J. Parker, 'Targeting the Role of a Key Conserved Motif for Substrate Selection and Catalysis by 3-Deoxy- D - *Manno* -Octulosonate 8-Phosphate Synthase', *Biochemistry*, 50 (2011), 3686-95.

6 T. M. Allison, J. A. Yeoman, R. D. Hutton, F. C. Cochrane, G. B. Jameson, and E. J. Parker, 'Specificity and Mutational Analysis of the Metal-Dependent 3-Deoxy-D-*Manno*-Octulosonate 8-Phosphate Synthase from *Acidithiobacillus Ferrooxidans*', *Biochim. Biophys. Acta*, 1804 (2010), 1526-36.

7 O. Asojo, J. Friedman, N. Adir, V. Belakhov, Y. Shoham, and T. Baasov, 'Crystal Structures of Kdop Synthase in Its Binary Complexes with the Substrate Phosphoenolpyruvate and with a Mechanism-Based Inhibitor', *Biochemistry*, 40 (2001), 6326-34.

8 M. A. Atmodjo, Z. Hao, and D. Mohnen, 'Evolving Views of Pectin Biosynthesis', in *Annu. Rev. Plant Biol.* (2013), pp. 747-79.

9 T. Baasov, and V. Belakhov, 'Towards a New Class of Synthetic Antibacterials Acting on Lipopolysaccharide Biosynthesis', *Drug Dev. Res.*, 50 (2000), 416-24.

10 T. Baasov, and A. Kohen, 'Synthesis, Inhibition, and Acid-Catalyzed Hydrolysis Studies of Model Compounds of the Proposed Intermediate in the

Kdo8p-Synthase-Catalyzed Reaction', *J. Am. Chem. Soc.*, 117 (1995), 6165-72.

11 T. Baasov, S. Sheffer-Dee-Noor, A. Kohen, A. Jakob, and V. Belakhov, 'Catalytic Mechanism of 3-Deoxy-D-*Manno*-2-Octulosonate-8-Phosphate Synthase. The Use of Synthetic Analogues to Probe the Structure of the Putative Reaction Intermediate', *Eur. J. Biochem.*, 217 (1993), 991-99.

12 J. Badger, J. M. Sauder, J. M. Adams, S. Antonysamy, K. Bain, M. G. Bergseid, S. G. Buchanan, M. D. Buchanan, Y. Batiyenko, J. A. Christopher, S. Emtage, A. Eroshkina, I. Feil, E. B. Furlong, K. S. Gajiwala, X. Gao, D. He, J. Hendle, A. Huber, K. Hoda, P. Kearins, C. Kissinger, B. Laubert, H. A. Lewis, J. Lin, K. Loomis, D. Lorimer, G. Louie, M. Maletic, C. D. Marsh, I. Miller, J. Molinari, H. J. Muller-Dieckmann, J. M. Newman, B. W. Noland, B. Pagarigan, F. Park, T. S. Peat, K. W. Post, S. Radojicic, A. Ramos, R. Romero, M. E. Rutter, W. E. Sanderson, K. D. Schwinn, J. Tresser, J. Winhoven, T. A. Wright, L. Wu, J. Xu, and T. J. R. Harris, 'Structural Analysis of a Set of Proteins Resulting from a Bacterial Genomics Project', *Proteins*, 60 (2005), 787-96.

13 Y. Bai, E. J. M. Lang, A. R. Nazmi, and E. J. Parker, 'Domain Cross-Talk within a Bifunctional Enzyme Provides Catalytic and Allosteric Functionality in the Biosynthesis of Aromatic Amino Acids', *J. Biol. Chem.*, 294 (2019), 4828-42.

14 L. Baugh, L. A. Gallagher, R. Patrapuvich, M. C. Clifton, A. S. Gardberg, T. E. Edwards, B. Armour, D. W. Begley, S. H. Dieterich, D. M. Dranow, J. Abendroth, J. W. Fairman, D. Fox Iii, B. L. Staker, I. Phan, A. Gillespie, R. Choi, S. Nakazawa-Hewitt, M. T. Nguyen, A. Napuli, L. Barrett, G. W. Buchko, R. Stacy, P. J. Myler, L. J. Stewart, C. Manoil, and W. C. Van Voorhis, 'Combining Functional and Structural Genomics to Sample the Essential *Burkholderia Structome*', *PLoS ONE*, 8 (2013), e53851.

15 M. R. Birck, A. Husain, G. Y. Sheflyan, B. Ganem, and R. W. Woodard, 'Studies on 3-Deoxy-D-*Manno*-Octulosonic Acid 8-Phosphate Synthase Using Chorismate Mutase Inhibitors', *Bioorg. Med. Chem. Lett.*, 11 (2001), 2795-98.

16 M. R. Birck, and R. W. Woodard, '*Aquifex Aeolicus* 3-Deoxy-D-*Manno*-2-Octulosonic Acid 8-Phosphate Synthase: A New Class of Kdo 8-P Synthase?', *J. Mol. Evol.*, 52 (2001), 205-14.

17 I. G. Bravo, S. García-Vallvé, A. Romeu, and A. Reglero, 'Prokaryotic Origin of Cytidylyltransferases and A-Ketoacid Synthases', *Trends Microbiol.*, 12 (2004), 120-28.

18 M. F. Cesur, B. Siraj, R. Uddin, S. Durmuş, and T. Çakır, 'Network-Based Metabolism-Centered Screening of Potential Drug Targets in *Klebsiella Pneumoniae* at Genome Scale', *Front. Cell. Infect. Microbiol.*, 9:447 (2020).

19 S. Cho, H. Im, K. Y. Lee, J. Chen, H. J. Kang, H. J. Yoon, K. H. Min, K. R. Lee, H. J. Park, and B. J. Lee, 'Identification of Novel Scaffolds for Potential Anti- *Helicobacter Pylori* Agents Based on the Crystal Structure of *H. Pylori*

3-Deoxy- D -*Manno*-Octulosonate 8-Phosphate Synthase (*Hp* Kdo8ps)', *Eur. J. Med. Chem.*, 108 (2016), 188-202.

20 L. Cipolla, L. Gabrielli, D. Bini, L. Russo, and N. Shaikh, 'Kdo: A Critical Monosaccharide for Bacteria Viability', *Nat. Prod. Rep.*, 27 (2010), 1618-29.

21 F. C. Cochrane, T. V. M. Cookson, G. B. Jameson, and E. J. Parker, 'Reversing Evolution: Re-Establishing Obligate Metal Ion Dependence in a Metal-Independent Kdo8p Synthase', *J. Mol. Biol.*, 390 (2009), 646-61.

22 P. Coutrot, S. Dumarçay, Ch Finance, M. Tabyaoui, B. Tabyaoui, and C. Grison, 'Investigation of New Potent Kdo-8-Phosphate Synthetase Inhibitors', *Bioorg. Med. Chem. Lett.*, 9 (1999), 949-52.

23 P. J. Cross, R. C. J. Dobson, M. L. Patchett, and E. J. Parker, 'Tyrosine Latching of a Regulatory Gate Affords Allosteric Control of Aromatic Amino Acid Biosynthesis', *J. Biol. Chem.*, 286 (2011), 10216-24.

24 P. J. Cross, L. C. Heyes, S. Zhang, A. R. Nazmi, and E. J. Parker, 'The Functional Unit of *Neisseria Meningitidis* 3-Deoxy-D-*Arabino*-Heptulosonate 7-Phosphate Synthase Is Dimeric', *PLoS ONE*, 11 (2016), e0145187.

25 P. J. Cross, A. L. Pietersma, T. M. Allison, S. M. Wilson-Coutts, F. C. Cochrane, and E. J. Parker, '*Neisseria Meningitidis* Expresses a Single 3-Deoxy-D-*Arabino*-Heptulosonate 7-Phosphate Synthase That Is Inhibited Primarily by Phenylalanine', *Protein Sci.*, 22 (2013), 1087-99.

26 F. W. D'Souza, Y. Benenson, and T. Baasov, 'Catalytic Mechanism of Kdo8p Synthase: Synthesis and Evaluation of a Putative Reaction Intermediate', *Bioorg. Med. Chem. Lett.*, 7 (1997), 2457-62.

27 F. Delmas, J. Petit, J. Joubès, M. Séveno, T. Paccalet, M. Hernould, P. Lerouge, A. Mouras, and C. Chevalier, 'The Gene Expression and Enzyme Activity of Plant 3-Deoxy-D-*Manno*-2-Octulosonic Acid-8-Phosphate Synthase Are Preferentially Associated with Cell Division in a Cell Cycle-Dependent Manner', *Plant Physiol.*, 133 (2003), 348-60.

28 F. Delmas, M. Séveno, J. G. B. Northey, M. Hernould, P. Lerouge, P. McCourt, and C. Chevalier, 'The Synthesis of the Rhamnogalacturonan Ii Component 3-Deoxy-D-*Manno*-2- Octulosonic Acid (Kdo) Is Required for Pollen Tube Growth and Elongation', *J. Exp. Bot.*, 59 (2008), 2639-47.

29 R. L. Doong, S. Ahmad, and R. A. Jensen, 'Higher Plants Express 3-Deoxy-*D*-*Manno*-Octulosonate 8-Phosphate Synthase', *Plant Cell Environ.*, 14 (1991), 113-20.

30 R. L. Doong, and R. A. Jensen, 'Synonymy of the Three Apparent Isoenzymes of 3-Deoxy-D-*Arabino*- Heptulosonate 7-Phosphate Synthase in Pisum Sativum L. With 3-Deoxy-D- *Manno*-Octulosonate 8-Phosphate Synthase and the Ds-Co/Ds-Mn Isoenzyme Pair', *New Phytol.*, 121 (1992), 165-71.

31 G. D. Dotson, R. K. Dua, J. C. Clemens, E. W. Wooten, and R. W. Woodard, 'Overproduction and One-Step Purification of *Escherichia Coli* 3-Deoxy-D-*Manno*-Octulosonic Acid 8-Phosphate Synthase and Oxygen Transfer Studies During Catalysis Using Isotopic-Shifted Heteronuclear Nmr', *J. Biol. Chem.*, 270 (1995), 13698-705.

32 G. D. Dotson, P. Nanjappan, M. D. Reily, and R. W. Woodard, 'Stereochemistry of 3-Deoxyoctulosonate 8-Phosphate Synthase', *Biochemistry*, 32 (1993), 12392-97.

33 S. Du, H. Faiger, V. Belakhov, and T. Baasov, 'Towards the Development of Novel Antibiotics: Synthesis and Evaluation of a Mechanism-Based Inhibitor of Kdo8p Synthase', *Bioorg. Med. Chem.*, 7 (1999), 2671-82.

34 S. Du, H. Tsipori, and T. Baasov, 'Synthesis and Evaluation of Putative Oxocarbenium Intermediate Mimic in the Kdo8p Synthase Catalyzed Reaction as a Tool for the Design of Potent Inhibitors for Lipopolysaccharide Biosynthesis', *Bioorg. Med. Chem. Lett.*, 7 (1997), 2469-72.

35 H. S. Duewel, S. Radaev, J. Wang, R. W. Woodard, and D. L. Gatti, 'Substrate and Metal Complexes of 3-Deoxy-D-*Manno*-Octulosonate-8-Phosphate Synthase from *Aquifex Aeolicus* at 1.9-Å Resolution: Implications for the Condensation Mechanism', *J. Biol. Chem.*, 276 (2001), 8393-402.

36 H. S. Duewel, G. Y. Sheflyan, and R. W. Woodard, 'Functional and Biochemical Characterization of a Recombinant 3-Deoxy-D-*Manno*-Octulosonic Acid 8-Phosphate Synthase from the Hyperthermophilic Bacterium *Aquifex Aeolicus*', *Biochem. Biophys. Res. Commun.*, 263 (1999), 346-51.

37 H. S. Duewel, and R. W. Woodard, 'A Metal Bridge between Two Enzyme Families: 3-Deoxy-D-*Manno*-Octulosonate-8-Phosphate Synthase from *Aquifex Aeolicus* Requires a Divalent Metal for Activity', *J. Biol. Chem.*, 275 (2000), 22824-31.

38 R.C. Edgar, 'Muscle: A Multiple Sequence Alignment Method with Reduced Time and Space Complexity', *BMC Bioinformatics*, 5 (2004), 113.

39 R.C. Edgar, 'Muscle: Multiple Sequence Alignment with High Accuracy and High Throughput', *Nucleic Acids Res.*, 32(5) (2004), 1792-97.

40 P. Emsley, and K. Cowtan, 'Coot: Model-Building Tools for Molecular Graphics', *Acta Cryst.*, D60 (2004), 2126-32.

41 U. B. Ericsson, B. M. Hallberg, G. T. DeTitta, N. Dekker, and P. Nordlund, 'Thermofluor-Based High-Throughput Stability Optimization of Proteins for Structural Studies', *Anal. Biolchem.* , 357 (2006), 289-98.

42 G. S. French, and K. S. Wilson, 'On the Treatment of Negative Intensity Observations', *Acta Cryst.*, A34 (1978), 517-25.

43 H. Fujishima, A. Nishimura, M. Wachi, H. Takagi, T. Hirasawa, H. Teraoka, K. Nishimori, T. Kawabata, K. Nishikawa, and K. Nagai, '*Kdsa* Mutations Affect Ftsz-Ring Formation in *Escherichia Coli* K-12', *Microbiology*, 148 (2002), 103-12.

44 C. M. Furdui, A. K. Sau, O. Yaniv, V. Belakhov, R. W. Woodard, T. Baasov, and K. S. Anderson, 'The Use of (*E*)- and (*Z*)-Phosphoenol-3-Fluoropyruvate as Mechanistic Probes Reveals Significant Differences between the Active Sites of Kdo8p and Dahp Synthases', *Biochemistry*, 44 (2005), 7326-35.

45 S. R. Gama, N. Balachandran, and P. J. Berti, '*Campylobacter Jejuni* Kdo8p Synthase, Its Inhibition by Kdo8p Oxime, and Control of the Residence Time of Slow-Binding Inhibition', *Biochemistry*, 57 (2018), 5327-38.

46 E. Gasteiger, C. Hoogland, A. Gattiker, S. Duvaud, M. Wilkins, R. Appel, and A. Bairoch, 'Protein Identification and Analysis Tools on the Expasy Server', *The proteomics protocols handbook* (2005), 571-607.

47 M. Goujon, H. McWilliam, W. Li, F. Valentin, S. Squizzato, J. Paern, and R. Lopez, 'A New Bioinformatics Analysis Tools Framework at Embl-Ebi', *Nucleic Acids Res.*, 38 (2010), W695-W99.

48 T. Hansen-Hagge, V. Lehmann, and O. Luderitz, 'Free Flow Electrophoresis as a Tool for Enrichment of Mutants with Temperature-Dependent Lethal Mutations in Lipid a Synthesis', *Eur. J. Biochem.*, 148 (1985), 21-27.

49 A. N. Harrison, S. Reichau, and E. J. Parker, 'Synthesis and Evaluation of Tetrahedral Intermediate Mimic Inhibitors of 3-Deoxy-D-*Manno*-Octulosonate 8-Phosphate Synthase', *Bioorg. Med. Chem. Lett.*, 22 (2012), 907-11.

50 M. Hartmann, T. R. Schneider, A. Pfeil, G. Heinrich, W. N. Lipscomb, and G. H. Braus, 'Evolution of Feedback-Inhibited B/A Barrel Isoenzymes by Gene Duplication and a Single Mutation', *Proc. Natl. Acad. Sci. U.S.A.*, 100 (2003), 862-67.

51 L. Hedstrom, and R. Abeles, '3-Deoxy-D-*Manno*-Octulosonate-8-Phosphate Synthase Catalyzes the C-O Bond Cleavage of Phosphoenolpyruvate', *Biochem. Biophys. Res. Commun.*, 157 (1988), 816-20.

52 P. J. Hoffmann, C. H. Doy, and D. E. A. Catcheside, 'The Separation of Three Allosterically Inhibitable 3-Deoxy-D-*Arabino*-Heptulosonate 7-Phosphate Synthases from Extracts of *Neurospora Crassa* and the Purification of the Tyrosine Inhibitable Isoenzyme', *Biochim. Biophys. Acta*, 268 (1972), 550-61.

53 R. A. Jensen, G. Xie, D. H. Calhoun, and C. A. Bonner, 'The Correct Phylogenetic Relationship of *Kdsa* (3-Deoxy-D-*Manno*-Octulosonate 8-Phosphate Synthase) with One of Two Independently Evolved Classes of *Aroa* (3-Deoxy-D-*Arabino*-Heptulosonate 7-Phosphate Synthase) [2]', *J. Mol. Evol.*, 54 (2002), 416-23.

54 W. Jiao, R. D. Hutton, P. J. Cross, G. B. Jameson, and E. J. Parker, 'Dynamic Cross-Talk among Remote Binding Sites: The Molecular Basis for Unusual Synergistic Allostery', *J. Mol. Biol.*, 415 (2012), 716-26.

55 W. Kabsch, 'Xds', *Acta Cryst.*, D66 (2010), 125-32.

56 L. Kaustov, T. Baasov, and A. Schmidt, 'Binding of the Natural Substrates and Products to Kdo8p Synthase: 31p and 13c Solution Nmr Characterization', *Bioorg. Chem.*, 31 (2003), 306-21.

57 L. Kaustov, S. Kababya, S. Du, T. Baasov, S. Gropper, Y. Shoham, and A. Schmidt, 'Structural and Mechanistic Investigation of 3-Deoxy-D-*Manno*-Octulosonate-8-Phosphate Synthase by Solid-State Redor Nmr', *Biochemistry*, 39 (2000), 14865-76.

58 S. A. Khan, P. Everest, S Servos, N. Foxwell, U. Zähringer, H. Brade, E. T Rietschel, G. Dougan, I. G. Charles, and D. J. Maskell, 'A Lethal Role for Lipid a in *Salmonella* Infections ', *Mol. Microbiol.*, 29 (1998), 571-79.

59 A. Kohen, V. Belakhov, and T. Baasov, 'Towards the Synthesis of the Putative Reaction Intermediate in the Kdo8p Synthase-Catalyzed Reaction. Synthesis and Evaluation of 3-Deoxy-D-*Manno*-2-Octulosonate-2-Phosphate', *Tetrahedron Lett.*, 35 (1994), 3179-82.

60 A. Kohen, R. Berkovich, V. Belakhov, and T. Baasov, 'Stereochemistry of the Kdo8p Synthase. An Efficient Synthesis of the 3-Fluoro Analogues of Kdo8p', *Bioorg. Med. Chem. Lett.*, 3 (1993), 1577-82.

61 A. Kohen, A. Jakob, and T. Baasov, 'Mechanistic Studies of 3-Deoxy-D-*Manno*-2-Octulosonate-8-Phosphate Synthase from *Escherichia Coli*', *Eur. J. Biochem.*, 208 (1992), 443-49.

62 F. Kona, P. Tao, P. Martin, X. Xu, and D. L. Gatti, 'Electronic Structure of the Metal Center in the Cd^{2+}, Zn^{2+}, and Cu^{2+} Substituted Forms of Kdo8p Synthase: Implications for Catalysis', *Biochemistry*, 48 (2009), 3610-30.

63 F. Kona, X. Xu, P. Martin, P. Kuzmic, and D. L. Gatti, 'Structural and Mechanistic Changes Along an Engineered Path from Metallo to Nonmetallo 3-Deoxy-D-*Manno*-Octulosonate 8-Phosphate Synthases', *Biochemistry*, 46 (2007), 4532-44.

64 V. König, A. Pfeil, G. H. Braus, and T. R. Schneider, 'Substrate and Metal Complexes of 3-Deoxy-D-*Arabino*-Heptulosonate-7- Phosphate Synthase from *Saccharomyces Cerevisiae* Provide New Insights into the Catalytic Mechanism', *J. Mol. Biol.*, 337 (2004), 675-90.

65 E. Krissinel, and K. Henrick, 'Inference of Macromolecular Assemblies from Crystalline State', *J. Mol. Biol.*, 372 (2007), 774-97.

66 D. J. Krosky, R. Alm, M. Berg, G. Carmel, P. J. Tummino, B. Xu, and W. Yang, '*Helicobacter Pylori* 3-Deoxy-D-*Manno*-Octulosonate-8-Phosphate (Kdo-8-P) Synthase Is a Zinc-Metalloenzyme', *Biochim. Biophys. Acta*, 1594 (2002), 297-306.

67 T. M. Laue, B. D. Shah, T. M. Ridgeway, and S. L. Pelletier, 'Computer-Aided Interpretation of Analytical Sedimentation Data for Proteins', *In Analytical Ultracentrifugation in Biochemistry and Polymer Science* (1992), S. E. Harding, A. J. Rowe, and J. C. Horton, eds. (Cambridge: Royal Society of Chemistry), pp. 90-125.

68 V. Lehmann, E. Rupprecht, and M. J. Osborn, 'Isolation of Mutants Conditionally Blocked in the Biosynthesis of the 3 Deoxy D *Manno* Octulosonic Acid - Lipid a Part of Lipopolysaccharides Derived from Salmonella Typhimurium', *Eur. J. Biochem.*, 76 (1977), 41-49.

69 D. H. Levin, and E. Racker, 'Condensation of Arabinose 5-Phosphate and Phosphorylenol Pyruvate by 2-Keto-3-Deoxy-8-Phosphooctonic Acid Synthetase', *J. Biol. Chem.*, 234 (1959), 2532-39.

70 J. Li, J. Wu, A. S. Fleischhacker, and R. W. Woodard, 'Conversion of Aquifex Aeolicus 3-Deoxy-D-*Manno*-Octulosonate 8-Phosphate Synthase, a

Metalloenzyme, into a Nonmetalloenzyme', *J. Am. Chem. Soc.*, 126 (2004), 7448-49.

71 Z. l Li, 'Effects of Temperature and Energy on Stability of Oligomeric Enzyme Probed on Electrospray Ionization Mass Spectrometry', *Chem. Res. Chin. Univ.*, 24 (2008), 771-77.

72 Z. Li, and A. K. Sau, 'Probing the Subunit-Subunit Interaction of the Tetramer of E. Coli Kdo8p Synthase by Electrospray Ionization Mass Spectrometry', *Chin. J. Chem.*, 27 (2009), 111-16.

73 Z. Li, and A. K. Sau, 'Structural Studies on Helicobacter Pylori 3-Deoxy-D-*Manno*-2-Octulosonate-8-Phosphate Synthase Using Electrospray Ionization Mass Spectrometry: A Tetrameric Complex Composed of Dimeric Dimers', *Rapid Commun. Mass Spectrom.*, 23 (2009), 1573-78.

74 Z. Li, A. K. Sau, S. Shen, C. Whitehouse, T. Baasov, and K. S. Anderson, 'A Snapshot of Enzyme Catalysis Using Electrospray Ionization Mass Spectrometry', *J. Am. Chem. Soc.*, 125 (2003), 9938-39.

75 P. H. Liang, A. Kohen, T. Baasov, and K. S. Anderson, 'Catalytic Mechanism of Kdo8p Synthase. Pre-Steady-State Kinetic Analysis Using Rapid Chemical Quench Flow Methods', *Bioorg. Med. Chem. Lett.*, 7 (1997), 2463-68.

76 P. H. Liang, J. Lewis, K. S. Anderson, A. Kohen, F. W. D'Souza, Y. Benenson, and T. Baasov, 'Catalytic Mechanism of Kdo8p Synthase: Transient Kinetic Studies and Evaluation of a Putative Reaction Intermediate', *Biochemistry*, 37 (1998), 16390-99.

77 S. H. Light, A. S. Halavaty, G. Minasov, L. Shuvalova, and W. F. Anderson, 'Structural Analysis of a 3-Deoxy-D-*Arabino*-Heptulosonate 7-Phosphate Synthase with an N-Terminal Chorismate Mutase-Like Regulatory Domain', *Protein Sci.*, 21 (2012), 887-95.

78 N. R. Luke, S. Allen, B. W. Gibson, and A. A. Campagnari, 'Identification of a 3-Deoxy-D-*Manno*-Octulosonic Acid Biosynthetic Operon in Moraxella Catarrhalis and Analysis of a *Kdsa*-Deficient Isogenic Mutant', *Infect. Immun.*, 71 (2003), 6426-34.

79 K. Matsuura, I. Miyagawa, M. Kobayashi, D. Ohta, and T. Matoh, 'Arabidopsis 3-Deoxy-D-*Manno*-Oct-2-Ulosonate-8-Phosphate Synthase: Cdna Cloning and Expression Analyses', *J. Exp. Bot.*, 54 (2003), 1785-87.

80 T. M. McPhillips, S. E. McPhillips, H. J. Chiu, A. E. Cohen, A. M. Deacon, P. J. Ellis, E. Garman, A. Gonzalez, N. K. Sauter, R. P. Phizackerley, S. M. Soltis, and P. Kuhn, 'Blu-Ice and the Distributed Control System: Software for Data Acquisition and Instrument Control at Macromolecular Crystallography Beamlines', *J. Synchrotron Radiat.*, 9 (2002), 401-06.

81 T. C. Meredith, P. Aggarwal, U. Mamat, B. Lindner, and R. W. Woodard, 'Redefining the Requisite Lipopolysaccharide Structure in *Escherichia Coli*', *ACS Chem. Biol.*, 1 (2006), 33-42.

82 G. Murshudov, A. Vagin, and E. Dodson, 'Refinement of Macromolecular Structures by the Maximum-Likelihood Method', *Acta Cryst.*, D53 (1997), 240-55.

83 A. R. Nazmi, E. J. M. Lang, Y. Bai, T. M. Allison, M. H. Othman, S. Panjikar, V. L. Arcus, and E. J. Parker, 'Interdomain Conformational Changes Provide Allosteric Regulation En Route to Chorismate', *J. Biol. Chem.*, 291 (2016), 21836-47.

84 A. R. Nazmi, L. R. Schofield, R. C. J. Dobson, G. B. Jameson, and E. J. Parker, 'Destabilization of the Homotetrameric Assembly of 3-Deoxy-D-*Arabino*- Heptulosonate-7-Phosphate Synthase from the Hyperthermophile *Pyrococcus Furiosus* Enhances Enzymatic Activity', *J. Mol. Biol.*, 426 (2014), 656-73.

85 S. K. Nelson, A. Kelleher, G. Robinson, S. Reiling, and O. A. Asojo, 'Structure of 2-Keto-3-Deoxy-D-*Manno*-Octulosonate-8-Phosphate Synthase from *Pseudomonas Aeruginosa*', *Acta Crystallogr. Sect. F Struct. Biol. Cryst. Commun.*, 69 (2013), 1084-88.

86 Z. Oliynyk, L. Briseño-Roa, T. Janowitz, P. Sondergeld, and A. R. Fersht, 'Designing a Metal-Binding Site in the Scaffold of *Escherichia Coli* Kdo8ps', *Protein Eng. Des. Sel.*, 17 (2004), 383-90.

87 M. J. Osborn, 'Structure and Biosynthesis of the Bacterial Cell Wall', *Annu. Rev. Biochem.*, 38 (1969), 501-38.

88 D. Perumal, C. S. Lim, and M. K. Sakharkar, 'In Silico Identification of Putative Drug Targets in *Pseudomonas Aeruginosa* through Metabolic Pathway Analysis', in *Lecture Notes Bioinform.* (2007), pp. 323-36.

89 D. Perumal, K. R. Sakharkar, T. H. Tang, V. T. K. Chow, C. S. Lim, A. Samal, N. Sugiura, and M. K. Sakharkar, 'Cloning and Targeted Disruption of Two Lipopolysaccharide Biosynthesis Genes, *Kdsa* and *Waag*, of *Pseudomonas Aeruginosa* Pao1 by Site-Directed Mutagenesis', *J. Mol. Microbiol. Biotechnol.*, 19 (2011), 169-79.

90 S. Radaev, P. Dastidar, M. Patel, R. W. Woodard, and D. L. Gatti, 'Structure and Mechanism of 3-Deoxy-D-*Manno*-Octulosonate 8-Phosphate Synthase', *J. Biol. Chem.*, 275 (2000), 9476-84.

91 C. R. H. Raetz, and C. Whitfield, 'Lipopolysaccharide Endotoxins', in *Annu. Rev. Biochem.* (2002), pp. 635-700.

92 P. H. Ray, 'Purification and Characterization of 3-Deoxy-D-*Manno*-Octulosonate 8-Phosphate Synthetase from *Escherichia Coli*', *J. Bacteriol.*, 141 (1980), 635-44.

93 P. D. Rick, and M. J. Osborn, 'Isolation of a Mutant of *Salmonella Typhimurium* Dependent on D-Arabinose-5-Phosphate for Growth and Synthesis of 3-Deoxy-D-Mannoctulosonate (Ketodeoxyoctonate)', *Proc. Natl. Acad. Sci. U.S.A.*, 69 (1972), 3756-60.

94 P. D. Rick, and M. J. Osborn, 'Lipid a Mutants of *Salmonella Typhimurium*. Characterization of a Conditional Lethal Mutant in 3 Deoxy D Mannooctulosonate 8 Phosphate Synthetase', *J. Biol. Chem.*, 252 (1977), 4895-903.

95 P. D. Rick, and D. A. Young, 'Isolation and Characterization of a Temperature-Sensitive Lethal Mutant of *Salmonella Typhimurium* That Is

Conditionally Defective in 3-Deoxy-D-*Manno*-Octulosonate-8-Phosphate Synthesis', *J. Bacteriol.*, 150 (1982), 447-55.

96 E. T. Rietschel, and H. Brade, 'Bacterial Endotoxins', *Sci. Am.*, 267 (1992), 54-61.

97 E. T. Rietschel, T. Kirikae, F. U. Schade, U. Mamat, G. Schmidt, H. Loppnow, A. J. Ulmer, U. Zahringer, U. Seydel, F. Di Padova, M. Schreier, and H. Brade, 'Bacterial Endotoxin: Molecular Relationships of Structure to Activity and Function', *FASEB J.*, 8 (1994), 217-25.

98 A. Roberts, C. Furdui, and K. S. Anderson, 'Observation of a Chemically Labile, Noncovalent Enzyme Intermediate in the Reaction of Metal-Dependent *Aquifex Pyrophilus* Kdo8ps by Time-Resolved Mass Spectrometry', *Rapid Commun. Mass Spectrom.*, 24 (2010), 1919-24.

99 C. L. Royce, and R. L. Pardy, 'Endotoxin-Like Properties of an Extract from a Symbiotic, Eukaryotic Chlorella-Like Green Alga', *J. Endotoxin Res.*, 3 (1996), 437-44.

100 M. Sarkar, L. Maganti, N. Ghoshal, and C. Dutta, 'In Silico Quest for Putative Drug Targets in *Helicobacter Pylori* Hpag1: Molecular Modeling of Candidate Enzymes from Lipopolysaccharide Biosynthesis Pathway', *J. Mol. Model.*, 18 (2012), 1855-65.

101 A. K. Sau, Z. Li, and K. S. Anderson, 'Probing the Role of Metal Ions in the Catalysis of *Helicobacter Pylori* 3-Deoxy-D-*Manno*-Octulosonate-8-Phosphate Synthase Using a Transient Kinetic Analysis', *J. Biol. Chem.*, 279 (2004), 15787-94.

102 J. Schletter, H. Heine, A. J. Ulmer, and Rietschel E. T., 'Molecular Mechanisms of Endotoxin Activity', *Arch. Microbiol.*, 164 (1994), 383-89.

103 L. R. Schofield, B. F. Anderson, M. L. Patchett, G. E. Norris, G. B. Jameson, and E. J. Parker, 'Substrate Ambiguity and Crystal Structure of *Pyrococcus Furiosus* 3-Deoxy-D-*Arabino*-Heptulosonate-7-Phosphate Synthase: An Ancestral 3-Deoxyald-2-Ulosonate-Phosphate Synthase?', *Biochemistry*, 44 (2005), 11950-62.

104 L. R. Schofield, M. L. Patchett, and E. J. Parker, 'Expression, Purification, and Characterization of 3-Deoxy-D-*Arabino*- Heptulosonate 7-Phosphate Synthase from *Pyrococcus Furiosus*', *Protein Expr. Purif.*, 34 (2004), 17-27.

105 R. Schoner, and K. M. Herrmann, '3-Deoxy-D-*Arabino* Heptulosonate 7-Phosphate Synthase. Purification, Properties, and Kinetics of the Tyrosine-Sensitive Isoenzyme from *Escherichia Coli*.', *J. Biol. Chem.*, 251 (1976), 5440–47.

106 P. Schuck, 'Size-Distribution Analysis of Macromolecules by Sedimentation Velocity Ultracentrifugation and Lamm Equation Modeling', *Biophys. J.*, 78 (2000), 1606-19.

107 P. Schuck, Perugini. M. A., N. R. Gonzales, Howlett G.J., and D. Schubert, 'Size-Distribution Analysis of Proteins by Analytical Ultracentrifugation: Strategies and Application to Model Systems', *Biophys. J.*, 82 (2002), 1096-111.

108 S. Sheffer-Dee-Noor, V. Belakhov, and T. Baasov, 'Insight into the Catalytic Mechanism of Kdo8p Synthase. Synthesis and Evaluation of the Isosteric Phosphonate Mimic of the Putative Cyclic Intermediate', *Bioorg. Med. Chem. Lett.*, 3 (1993), 1583-88.

109 S. Shulami, C. Furdui, N. Adir, Y. Shoham, K. S. Anderson, and T. Baasov, 'A Reciprocal Single Mutation Affects the Metal Requirement of 3-Deoxy-D-*Manno*-2-Octulosonate-8-Phosphate (Kdo8p) Synthases from *Aquifex Pyrophilus* and *Escherichia Coli*', *J. Biol. Chem.*, 279 (2004), 45110-20.

110 S. Shulami, O. Yaniv, E. Rabkin, Y. Shoham, and T. Baasov, 'Cloning, Expression, and Biochemical Characterization of 3-Deoxy-D-*Manno*-2-Octulosonate-8-Phosphate (Kdo8p) Synthase from the Hyperthermophilic Bacterium *Aquifex Pyrophilus*', *Extremophiles*, 7 (2003), 471-81.

111 I. A. Shumilin, R. Bauerle, J. Wu, R. W. Woodard, and R. H. Kretsinger, 'Crystal Structure of the Reaction Complex of 3-Deoxy-D-*Arabino*-Heptulosonate-7-Phosphate Synthase from *Thermotoga Maritima* Refines the Catalytic Mechanism and Indicates a New Mechanism of Allosteric Regulation', *J. Mol. Biol.*, 341 (2004), 455-66.

112 I. A. Shumilin, R. H. Kretsinger, and R. H. Bauerle, 'Crystal Structure of Phenylalanine-Regulated 3-Deoxy-D-*Arabino*- Heptulosonate-7-Phosphate Synthase from *Escherichia Coli*', *Structure*, 7 (1999), 865-75.

113 F. Sievers, A. Wilm, D. Dineen, T. J. Gibson, K. Karplus, W. Li, R. Lopez, H. McWilliam, M. Remmert, J. Söding, J. D. Thompson, and D. G. Higgins, 'Fast, Scalable Generation of High-Quality Protein Multiple Sequence Alignments Using Clustal Omega', *Mol. Syst. Biol.*, 7 (2011), 539.

114 K. M. Smyth, and A. Marchant, 'Conservation of the 2-Keto-3-Deoxymanno-Octulosonic Acid (Kdo) Biosynthesis Pathway between Plants and Bacteria', *Carbohydr. Res.*, 380 (2013), 70-75.

115 H. Strohmaier, P. Remler, W. Renner, and G. Hogenauer, 'Expression of Genes *Kdsa* and *Kdsb* Involved in 3-Deoxy-D-*Manno*-Octulosonic Acid Metabolism and Biosynthesis of Enterobacterial Lipopolysaccharide Is Growth Phase Regulated Primarily at the Transcriptional Level in *Escherichia Coli* K-12', *J. Bacteriol.*, 177 (1995), 4488-500.

116 P. S. Subramaniam, G. Xie, T. Xia, and R. A. Jensen, 'Substrate Ambiguity of 3-Deoxy-D-*Manno*-Octulosonate 8-Phosphate Synthase from *Neisseria Gonorrhoeae* in the Context of Its Membership in a Protein Family Containing a Subset of 3-Deoxy-D-*Arabino*-Heptulosonate 7-Phosphate Synthases', *J. Bacteriol.*, 180 (1998), 119-27.

117 D.I. Svergun, C. Barberato, and M. H. J. Koch, 'Crysol - a Program to Evaluate X-Ray Solution Scattering of Biological Macromolecules from Atomic Coordinates', *J. Appl. Crystallogr.*, 28 (1995), 768-73.

118 P. Tao, D. L. Gatti, and H. Bernhard Schlegel, 'The Energy Landscape of 3-Deoxy-D-*Manno*-Octulosonate 8-Phosphate Synthase', *Biochemistry*, 48 (2009), 11706-14.

119 P. Tao, H. B. Schlegel, and D. L. Gatti, 'Common Basis for the Mechanism of Metallo and Non-Metallo Kdo8p Synthases', *J. Inorg. Biochem.*, 104 (2010), 1267-75.

120 W. P. Taylor, G. Ya Sheflyan, and R. W. Woodard, 'A Single Point Mutation in 3-Deoxy-D-*Manno*-Octulosonate-8-Phosphate Synthase Is Responsible for Temperature Sensitivity in a Mutant Strain of *Salmonella Typhimurium*', *J. Biol. Chem.*, 275 (2000), 32141-46.

121 D. E. Tribe, H. Camakaris, and J. Pittard, 'Constitutive and Repressible Enzymes of the Common Pathway of Aromatic Biosynthesis in *Escherichia Coli* K-12: Regulation of Enzyme Synthesis at Different Growth Rates', *J. Bacteriol.*, 127 (1976), 1085-97.

122 A. Voxeur, A. André, C. Breton, and P. Lerouge, 'Identification of Putative Rhamnogalacturonan-Ii Specific Glycosyltransferases in *Arabidopsis* Using a Combination of Bioinformatics Approaches', *PLoS ONE*, 7 (2012), e51129.

123 DeLano W., 'The Pymol Molecular Graphics System, Version 1.5.0.4 Schrödinger, Llc', (2002).

124 T. Wagner, R. H. Kretsinger, R. Bauerle, and W. D. Tolbert, '3-Deoxy-D-*Manno*-Octulosonate-8-Phosphate Synthase from *Escherichia Coli*. Model of Binding of Phosphoenolpyruvate and D-Arabinose-5-Phosphate', *J. Mol. Biol.*, 301 (2000), 233-38.

125 J. Wang, H. S. Duewel, J. A. Stuckey, R. W. Woodard, and D. L. Gatti, 'Function of His185 in *Aquifex Aeolicus* 3-Deoxy-D-*Manno*-Octulosonate 8-Phosphate Synthase', *J. Mol. Biol.*, 324 (2002), 205-14.

126 J. Wang, H. S. Duewel, R. W. Woodard, and D. L. Gatti, 'Structures of *Aquifex Aeolicus* Kdo8p Synthase in Complex with R5p and Pep, and with a Bisubstrate Inhibitor: Role of Active Site Water in Catalysis', *Biochemistry*, 40 (2001), 15676-83.

127 C. J. Webby, W. Jiao, R. D. Hutton, N. J. Blackmore, H. M. Baker, E. N. Baker, G. B. Jameson, and E. J. Parker, 'Synergistic Allostery, a Sophisticated Regulatory Network for the Control of Aromatic Amino Acid Biosynthesis in *Mycobacterium Tuberculosis*', *J. Biol. Chem.*, 285 (2010), 30567-76.

128 C. J. Webby, M. L. Patchett, and E. J. Parker, 'Characterization of a Recombinant Type Ii 3-Deoxy-D-*Arabino*-Heptulosonate- 7-Phosphate Synthase from *Helicobacter Pylori*', *Biochem. J.*, 390 (2005), 223-30.

129 M. D. Winn, C. C. Ballard, K. D. Cowtan, E. J. Dodson, P. Emsley, P. R. Evans, R. M. Keegan, E. B. Krissinel, A. G. W. Leslie, A. McCoy, S. J. McNicholas, G. N. Murshudov, N. S. Pannu, E. A. Potterton, H. R. Powell, R. J. Read, A. Vagin, and K. S. Wilson, 'Overview of the Ccp4 Suite and Current Developments', *Acta Cryst.*, D67 (2011), 235-42.

130 M. Woisetschlager, and G. Hogenauer, 'Cloning and Characterization of the Gene Encoding 3-Deoxy-D-*Manno*-Octulosonate 8-Phosphate Synthetase from *Escherichia Coli*', *J. Bacteriol.*, 168 (1986), 437-39.

131 J. Wu, M. A. Patel, A. K. Sundaram, and R. W. Woodard, 'Functional and Biochemical Characterization of a Recombinant *Arabidopsis Thaliana* 3-

Deoxy-D-*Manno*-Octulosonate 8-Phosphate Synthase', *Biochem. J.*, 381 (2004), 185-93.

132 J. Wu, and R. W. Woodard, 'New Insights into the Evolutionary Links Relating to the 3-Deoxy-D-*Arabino*-Heptulosonate 7-Phosphate Synthase Subfamilies', *J. Biol. Chem.*, 281 (2006), 4042-48.

133 X. Xu, F. Kona, J. Wang, J. Lu, T. Stemmler, and D. L. Gatti, 'The Catalytic and Conformational Cycle of *Aquifex Aeolicus* Kdo8p Synthase: Role of the L7 Loop', *Biochemistry*, 44 (2005), 12434-44.

134 G. Ya Sheflyan, A. K. Sundaram, W. P. Taylor, and R. W. Woodard, 'Substrate Ambiguity of 3-Deoxy-D-*Manno*-Octulosonate 8-Phosphate Synthase from *Neisseria Gonorrhoeae* Revisited', *J. Bacteriol.*, 182 (2000), 5005-08.

135 X. B. Yang, S. L. Wu, D. P. Zhu, H. Wu, T. Jiang, Y. H. Qian, and F. Jiao, 'Expression of the 2-Dehydro-3-Deoxyphosphooctonate Aldolase (*Kdsa*) Gene in Mulberry Leaves (*Morus Alba* L.) Is Down-Regulated under High Salt and Drought Stress', *Genet. Mol. Res.*, 14 (2015), 11955-64.

136 J. A. Yeoman, 'Biochemical Characterization of Metal-Dependent 3-Deoxy-D-*Manno*-Octulosonate 8-Phosphate Synthases from *Chlorobium Tepidum* & *Acidithiobacillus Ferrooxidans*', *Master's Thesis* (2007), Massey University, Turitea, Palmerston North, New Zealand.

137 W. S. York, A. G. Darvill, M. McNeil, and P. Albersheim, '3-Deoxy-D-*Manno*-2-Octulosonic Acid (Kdo) Is a Component of Rhamnogalacturonan Ii, a Pectic Polysaccharide in the Primary Cell Walls of Plants', *Carbohydr. Res.*, 138 (1985), 109-26.

138 F. Zhang, Y. Xu, and Z. Zhang, 'Heterologous Expression, Purification, Crystallization and Preliminary X-Ray Diffraction Analysis of Kdo8p Synthase from Arabidopsis Thaliana', *Protein Expr. Purif.*, 101 (2014), 133-37.

139 L. Zhou, J. Wu, V. Janakiraman, I. A. Shumilin, R. Bauerle, R. H. Kretsinger, and R. W. Woodard, 'Structure and Characterization of the 3-Deoxy-D-*Arabino*-Heptulosonate 7-Phosphate Synthase from *Aeropyrum Pernix*', *Bioorg. Chem.*, 40 (2012), 79-86.

140 F. Zhu, F. Zhang, Z. Zhang, and L. Wu, 'Expression, Purification and Characterization of 3-Deoxy-D-*Manno*-Octulosonate 8-Phosphate Synthase from *Phyllostachys Edulis*', *Chin. J. Biotech.*, 33 (2017), 1989-98.